HYDRAULIC GEOMETRY OF SECONDARY CHANNELS OF LOWER FRASER RIVER, BRITISH COLUMBIA, FROM ACOUSTIC DOPPLER VELOCIMETRY

by

ERICA R. ELLIS

B.Sc., The University of British Columbia, 2000

A THESIS SUBMITTED IN PARTIAL FULFILLMENT OF THE REQUIREMENTS FOR THE DEGREE OF

MASTER OF SCIENCE

in

THE FACULTY OF GRADUATE STUDIES

(Department of Geography)

We accept this thesis as conforming to the required standard

THE UNIVERSITY OF BRITISH COLUMBIA

February 2004

Library Authorization

In presenting this thesis in partial fulfillment of the requirements for an advanced degree at the University of British Columbia, I agree that the Library shall make it freely available for reference and study. I further agree that permission for extensive copying of this thesis for scholarly purposes may be granted by the head of my department or by his or her representatives. It is understood that copying or publication of this thesis for financial gain shall not be allowed without my written permission.

Erica R. Ellis
Name of Author *(please print)*

25-03-2004
Date (dd/mm/yyyy)

Title of Thesis: Hydraulic geometry of secondary channels of Lower Fraser River, British Columbia, from acoustic Doppler velocimetry

Degree: MSc Year: 2004

Department of Geography
The University of British Columbia
Vancouver, BC Canada

Abstract

The hydraulics and morphology of secondary channels within the lower Fraser River gravel reach have been examined using data collected during the 2002 freshet utilising an acoustic Doppler current profiler with integrated GPS. A range of sub-reach types was sampled, corresponding to position within an individual secondary channel. Surface and sub-surface grain size distribution data were collected as well. Sub-reach averaged water surface width, mean hydraulic depth and mean velocity data generally conformed well ($R^2 \geq 0.9$) to the form of classical at-a-station hydraulic geometry relations, at higher flow. Spatial and frequency distributions of near-bottom velocity and channel depth were examined. In general, sub-reach types stratified along gradients of width, depth, velocity and sedimentology, although there were exceptions. Additional data collected at high flow were used to generate bankfull scaling relations for secondary channels in the gravel reach. Again, the data conform well to a simple power law, up to and including data points from the main channel. The water surface width to discharge relation agrees with work by Bray (1973) in Alberta gravel bed rivers and with the more general trend of a one-half power relation. However, the mean hydraulic depth to discharge relation (and by continuity, the mean velocity to discharge relation) deviate from previous results. Data collection in the field was somewhat facilitated by the use of the acoustic Doppler current profiler but post-processing time requirements were high and, ultimately, the operating frequency led to certain sampling problems. Issues surrounding the use of these instruments in river channels are discussed.

Table of Contents

List of Tables

List of Figures

Acknowledgements

I am indebted to many people who have helped me over the course of this thesis. During my fieldwork, I was fortunate to have many very competent, cheerful and hard-working people helping me, without whom there would have been no data set. In this regard, I would particularly like to thank Cathy Christie and Dave Campbell.

I would like to thank my supervisor, Mike Church, for his patience, astute advice and encouragement when I faltered, not to mention numerous days in the field. Many colleagues offered time and help, particularly Laura Rempel who was an invaluable source of information and inspiration.

Finally, thank you to Bob Lee who uncomplainingly volunteered his free time and offered unstinting support and encouragement when needed.

This work was financially supported by Natural Sciences and Engineering Research Council of Canada and by the British Columbia Habitat Conservation Trust Fund.

1 Introduction

1.1 Hydraulic geometry and alluvial channels

1.1.1 What is hydraulic geometry?

Hydraulic geometry is an attempt to describe the adjustment of the cross-sectional form of stream channels by scaling with discharge (Q). The general relations are assumed to be power functions of the independent variable, Q, as follows:

$w_s = aQ^b$, where w_s is water surface width (1)

$d^* = cQ^f$, where d^* is the mean hydraulic depth (2)

$v = kQ^m$, where v is mean velocity (3)

$S = gQ^z$, where S is channel slope (4)

(Leopold and Maddock, 1953).

Other channel parameters have been used as dependent variables, including flow resistance and suspended sediment load. The exponents describe the rate of change of the given channel parameter with discharge whereas the coefficients define a value of the dependent variable for unit discharge.

The width, mean depth and mean velocity are related by continuity:

$Q = w \times d \times v$, (5)

which implies:

$b + f + m \equiv 1.0$, and (6)

$a \times c \times k \equiv 1.0$ (7)

Thus there are only two independent relations that together determine the third relation

The concept of hydraulic geometry was first developed and applied in the mid 20th century in a seminal paper by Leopold and Maddock (1953). Data from a variety of gauging stations in the Great Plains and Southwest of the United States were used to show that water surface width, mean depth and mean velocity plotted as simple power functions (and hence, scaling functions) of discharge. This outcome was interpreted as indicating an equilibrium relation between the channel form and the flow conveyed.

Leopold and Maddock envisioned channel adjustment occurring in two different ways:

1) a channel cross-section or reach might be adjusted to accommodate the range of flows experienced at that location (termed "at-a-station" or "at-a-point" hydraulic geometry);
2) the river channel might be adjusted along its length to increasing flows resulting from increasing downstream drainage area (termed "downstream" hydraulic geometry).

Although at-a-station hydraulic geometry and downstream hydraulic geometry share a similar method of graphical representation, the consensus of present research is that they are essentially different (Ferguson, 1986; Clifford, 1996), both in terms of underlying mechanics and application.

1.1.2 At-a-station hydraulic geometry

As discharge increases or decreases at a given point along a river, there are characteristic corresponding changes in water surface elevation (stage), velocity, width and depth. This knowledge has long been applied in the use of stage-discharge relations, or rating curves, to facilitate measurement of discharge. Extending this idea, Leopold and Maddock found approximately log-linear relations between mean width, depth and velocity and discharge for their 20 study reaches (which represent a variety of rivers) and gave average values for the exponents: $b = 0.26, f = 0.40$ and $m = 0.34$ (1953). It has been customary to use gauging section data to develop at-a-station hydraulic geometry relations because these data are readily available.

The implication of the power law relation between channel parameters and discharge is that the observed channel form is in equilibrium with the forcing function, discharge. However, it is clear that, in the case of an individual cross-section or reach, the form of the channel is dictated in large part by the most recent competent flow. Lesser flows simply occupy the predetermined space without substantially altering it. Therefore, an equilibrium relation is unlikely to exist in any meaningful sense between channel parameters and the entire range of flows experienced at that cross-section, given that the majority of those flows will not exceed the competence threshold. As proof of this, theoretical at-a-station relations have been derived for a variety of cross-section shapes (which define the rate of increase of channel width with depth), using flow resistance laws to define the rate of increase of velocity with depth (Ferguson, 1986).

The derived relations are not true power laws, although they are tolerably well described by simple power laws. Given the natural variability in channel cross-section properties as a result of factors such as meandering, pool-riffle sequences and changes in bank resistance, it is not surprising that there should be large variability in at-a-station hydraulic geometry exponents and coefficients, with no obvious pattern (Park, 1977).

However, the variability induced by site-specific characteristics means that the at-a-station relations reflect individual channel characteristics. The capability of hydraulic geometry relations to offer a concise, quantitative description of channel form has many useful applications, mainly in river management (Mosley, 1982; Hogan and Church, 1989; Jowett, 1998). At-a-station relations quickly summarize the adjustment in mean channel characteristics with changing discharge. This permits the comparison of different channels or the assessment of particular channels based on the physical habitat requirements (e.g. "depth-velocity" curves, for fish species). For instance, whether channels accommodate increasing discharge primarily in increasing depth or width will greatly affect the type of habitat that exists at different discharges. However, the use of mean values of channel parameters, and gathering of data at single cross-sections (which has been the norm) means that important information about the variability within the habitat is lost by averaging. For instance, the use of mean velocity in aquatic habitat modeling is much less appropriate than the so-called "nose velocity" which expresses the velocities commonly experienced by fish (Stalnaker et al., 1989). Mean velocity can be much higher than nose velocities, since fish will preferentially avoid velocities that exceed their tolerance.

Consequently, part of the information necessary for useful habitat assessment is the distribution of velocity-depth products over a range of flows. When combined with water surface area, these data give a "disaggregated hydraulic geometry" (Hogan and Church, 1989) which can be used to make a graphic comparison of the areal or frequency distribution of velocities and depths over changing flows, and between streams. With knowledge of particular species' life cycle habitat preferences, disaggregated hydraulic geometry can be used to evaluate the potential of different streams, or different reaches within streams, to provide appropriate habitat. Alternatively, combining disaggregated hydraulic geometry relations for particular reaches with knowledge of the resident species allows conclusions to be made about habitat preference and use.

1.1.3 Downstream hydraulic geometry

Equilibrium channel form in designed channels. Although the concept of hydraulic geometry in natural channels was novel, Leopold and Maddock were explicitly influenced by research in the late 19th century on the designed channel form of stable canals. The purpose of this research was to develop a set of equations that could be used to design unlined irrigation canals, given a certain imposed discharge, slope and sediment load, which would neither silt up nor scour their beds. These stable channels were termed to be "in regime" with their governing conditions, from which derives the name "regime theory" for this body of work. One of the more well known regime relations is that derived by Gerald Lacey relating wetted channel perimeter (P) and discharge, for "silt-stable" canals (ft-sec units):

$$P = 2.67Q^{1/2} \tag{8}$$

(Lacey, 1958). Wetted channel perimeter is well approximated by water surface width, for large channels. The main criticism of Lacey's relations is that they failed to address the role of the sediment load carried in the canals, which limited their extension to channels with characteristics different from those upon which the relations were based. Blench (1952) attempted to account for the effect of bedload transport on regime form by introducing bed and side-wall factors to account for the influence of non-cohesive bed and bank materials.

Regime theory deals with equilibrium channel form in canals flowing through fine sands and silts, which were designed to carry a certain sediment and water load. The tractive force method deals with the form of designed, stable channels in coarse materials for the limiting case of no sediment transport. For a stable channel to exist in non-cohesive coarse material, the channel form must be such that the distribution of shear force never exceeds the critical shear force to induce motion. It is possible to calculate the theoretical narrowest stable channel cross-section such that everywhere sediment is on the verge of motion (the so-called threshold channel), in which the stability of the banks imposes the lower limit on stability. Lane and Carlson (1953) analyzed a series of stable canals in coarse-grained material and offered design guidelines including a factor to account for bank stability, based on side slope and natural angle of repose of the sediment.

Simons and Albertson (1963) attempted to extend the range of conditions over which the regime-type equations would apply by collecting data on canals in India (primarily fine-grained materials) and ones in the United States (coarser-grained materials). These channels would be

classified as dominantly sand-bed channels, as 22 of 24 reaches analyzed had a median bed-material grain diameter of less than 1 mm. The reaches were stratified based on bed and bank composition, and then channel parameters were graphically displayed as functions of discharge. The interesting result is that variability in the derived relations between channel parameters and discharge was dominantly expressed in the coefficients of the relations. For channels with a sand bed and cohesive banks, the relation between wetted-perimeter and discharge is (in ft-sec units):

$$P = 2.51Q^{0.512} \qquad (9)$$

Less cohesive channels plotted above this relation and more cohesive channels plotted below (Simons and Albertson, 1963). Therefore, the coefficients of the relations appear to play an important role in reflecting variation in bed and bank composition.

A substantial body of literature exists on the subject of designed equilibrium channels, from which some trends emerge such as the consistent one-half power relation of channel width to discharge. Also, results from designed channels suggest that variation in bed and bank composition may induce variability in the coefficients of the hydraulic geometry relations. However, these designed channels are a simplified representation of natural channels, and as such have fewer degrees of freedom to adjust their form. In natural channels, discharge varies, reaches are not always straight, channel pattern varies, within-channel morphology changes and bank vegetation is present, all adding extra variability to adjustments of channel form.

Equilibrium form in natural channels. As formulated by Leopold and Maddock (1953), downstream hydraulic geometry relations express the adjustment of a river channel in space to increasing flow due to tributary and groundwater inputs. Although Leopold and Maddock presented data from individual rivers in this fashion, they also added tributary cross-sections, as well as experimenting with a range of channels from different geographic locations and geologic settings. There are relatively few examples of empirical downstream hydraulic geometry relations on individual main-stem channels, due to the difficulty of gathering sufficient data on any one river. Instead, data have typically been gathered from a number of different rivers from similar physiographic settings. By stratifying natural channels by physiography, it is assumed that similar boundary conditions exist within the group. It is assumed that physiographical stratification yields regime classes within which rivers will exhibit similar channel-forming behaviour.

Data must then be gathered from the different channels at some reference discharge that occurs with a particular frequency at all stations. Although theoretically a variety of flow frequencies could be examined (cf. Leopold and Maddock, 1953), the convention is to define the reference flow to be the most regularly occurring flow which has the potential to change the cross-sectional form of the channel (through erosion and sediment transport). Once the magnitude has been determined, the frequency of its recurrence can be calculated. Leopold and Maddock (1953), using the mean annual flow as the reference discharge, found an average downstream hydraulic geometry for their study reaches yielding exponents of $b = 0.5, f = 0.4$ and $m = 0.1$. In terms of the relation of width to discharge in natural channels, this study confirmed the one-half power trend observed in the regime canals.

In effect, downstream hydraulic geometry relations can be thought of as scaling relations for channel form: w_s is a suitable choice for a scale length and the cross-sectional area of flow, A, defines a storage-discharge relation:

$$A = \mathrm{r}Q^t \tag{10}$$

The other relations of hydraulic geometry follow by continuity, since

$$A/w_s = d^* \tag{11}$$

and

$$Q/A = v \tag{12}$$

One might reasonably expect that there could be an equilibrium relation between natural channel form and some measure of a recurring, channel-shaping flow. This is borne out in the occurrence of large-scale trends such as the characteristic relation of width and depth to discharge (Figure 9 in Leopold and Maddock (1953); Figure 8 in Ferguson (1986)). Nonetheless, as with the at-a-station relations, there remains notable scatter in the downstream hydraulic relations (Park, 1977; Ferguson, 1986). Some of the scatter may be due to different reference flows used to derive the relations, each of which may have a slightly different relation to channel characteristics (Leopold and Maddock, 1953). The use of different reference flows occurs because of the operational difficulty in defining a "channel-shaping" flow. Even if the "bankfull" flow is chosen, it is not straightforward to define the frequency with which it may occur (Johnson and Heil, 1996).

The cross-sectional form of a natural channel will depend on the particular balance struck between the erosive forces of the flow and the resistive forces of the channel boundaries. In contrast to studies of at-a-station hydraulic geometry relations, some empirical evidence suggests that the exponents of the downstream hydraulic geometry relations are not strongly affected by local variation in bank materials (Knighton, 1974; Miller and Onesti, 1979). However, these results are mainly from channels with cohesive banks (e.g. banks with a substantial silt-clay content). Amongst unconstrained, non-cohesive materials the force necessary to entrain material from the channel will vary with particle diameter (Lane, 1955). Therefore we may expect that similar hydraulic geometry relations will exist for channels with similar sedimentological characteristics, *all else being equal*, with the variation between groups being expressed in the coefficients of the relations. Most empirical research has focused on variation (or lack thereof) in the exponents of hydraulic geometry while variation in the coefficients has been largely ignored (Ferguson, 1986). Given that there appears to be more variability in the coefficients than in the exponents, one assumes that the coefficients in the relations express the geological and hydrological properties unique to each drainage basin while the exponents are more strongly controlled by discharge (Parker, 1979; Griffiths, 1981; Andrews, 1984).

Bank vegetation obviously has an important role to play as far as increasing resistance to erosion. Vegetation increases bank strength through the binding effects of its root mass, reduces near-bank velocities and effective shear stress, and encourages the deposition of fine material during overbank flows. In general, it has been found that vegetated banks result in narrower and deeper channels than ones with less stable banks (Millar and Quick, 1993; Huang and Nanson, 1997; Millar, 2000). It is difficult to parameterize the effect of vegetation beyond stratification schemes by vegetation type and density. Millar and Quick (1993) use a parameter, ϕ, to indicate the extra resistance to erosion given to vegetated banks beyond what the material properties would suggest (as indicated by bank angle). However it is not straightforward to measure such a parameter in the field, where banks are commonly composed of stratified bands of material.

One additional difference between natural channels and designed channels is the ability of natural channels to adjust to changes in boundary conditions by changing their channel pattern. In an attempt to reduce potential variability induced by this consideration, most empirical research has focused on single-thread, straight channels, or, at most, straight single-channel reaches within a multi-channel river (Bray, 1973; Griffiths, 1981; Andrews, 1984). In

addition, some work has been done on braided channels. Braided rivers are defined here as having multiple channels separated by bars that are commonly submerged at high flows and bounded by floodplain banks.

1.1.4 Opportunities for new research

Obtaining the necessary field data to derive hydraulic geometry relations has typically been difficult. Field surveying with hand-held instruments is time-consuming and especially so in the case of at-a-station hydraulic geometry relations, where repeated measurements are required over a period of time to capture the variation in channel form with different discharges. Logistical considerations have imposed certain constraints on channel size that can reasonably be surveyed. More commonly, gauging data have been used. However, gauges have typically been placed in stable reaches for the purpose of obtaining long and consistent relations between water level (i.e. stage) and discharge. This raises the question whether these reaches are truly alluvial in character, and hence whether one should reasonably expect any characteristic relation between channel form and discharge. Measurement constraints have thus limited the selection of rivers for analysis and imposed a certain bias in river selection.

Although some research has investigated hydraulic geometry relations in multiple-thread channels (Mosley, 1982; Tabata and Hickin, 2003), there appear to be no studies investigating hydraulic geometry in wandering gravel-bed rivers. Wandering channels, a subcategory of so-called "anabranched" channels, are also multiple-thread channels, but the channels are separated by stable islands that are large in comparison to the channel, and these divide the flow over the entire range of discharges (Knighton, 1998). A closer examination of the data collected by Bray (1973) reveals that some of his 70 study reaches are from rivers which can be classified as wandering, although the reaches themselves are single-thread (e.g. the Oldman River at Brocket, the Red Deer River at Bindloss, the Athabasca River at Whitecourt) (Kellerhals et al., 1972; Bray, 1973).

Finally, hydraulic geometry relations have typically relied on data gathered at single cross-sections, either because of the previously mentioned logistical constraints on field data collection, or because gauging data were used. Thus, not only does using mean parameters reduce information about cross-sectional variation in channel parameters, but little longitudinal

variation in channel form is captured in these relations. Given advances in instrument technology, there is now an opportunity to collect data at the sub-reach scale, which better represents the natural variability of the channel.

1.2 Project objectives

The primary goals of this project are as follows:

1) To assess the feasibility of using mobile, digital technology to collect data for hydraulic geometry relations.

Measurements of water velocity and depth can now be taken relatively easily and quickly, in comparison with the past, by using a boat-mounted digital acoustic Doppler current profiler (aDcp). Benefits of this technology include collecting spatially distributed data within a reach, rather than relying on data gathered at a single cross-section. As well, the instrument provides measurements of water velocity profiles, rather than simply a mean velocity. The increased mobility associated with this technology will allow us to work in a previously unstudied and un-gauged system that has potentially high aquatic habitat values.

2) To compare different sub-reach morphologies of secondary channels of the Fraser River using at-a-station hydraulic geometry relations, as well as examining distributions of velocity and depth at varying discharge.

Between-channel and within-channel morphological variability will be quantified and assessed using field data collected during the 2002 freshet. At-a-station hydraulic geometry relations will be constructed for three sub-reach morphologies of four different secondary channels in the Fraser River gravel reach. Sub-reaches represent qualitatively different morphologies and at-a-station relations will be used to quantify these differences. Collection of sub-reach scale data, rather than data collection at a single cross-section, will permit analysis of spatial and frequency distributions of channel parameters.

3) To investigate the scaling behaviour of secondary channel form in the Fraser River.

Secondary channels in the Fraser River have similar boundary conditions, given their similar physiographic setting, but they exist at a range of scales. They are unconnected in the sense that they do not carry the main flow of the river, yet they are all connected to this flow. Data will be collected in a number of different secondary channels at high flow to explore the possibility of a characteristic scaling of the secondary channel system.

2 Study Site and Methods

2.1 Gravel reach, Lower Fraser River, British Columbia

The study site is located in the gravel reach of the Lower Fraser River, in southwestern British Columbia. The Fraser River drains about 25% of British Columbia (228,000 km^2, measured at Mission) and is unregulated along its length. The hydrograph is dominated by the snowmelt freshet, which normally occurs in early June. The freshet may occur earlier or later than average, depending on the meteorological conditions influencing snowmelt. The river ranks highly on a global scale as a producer of salmonine fishes (Northcote and Larkin, 1989).

The Lower Fraser River extends from Yale to the Pacific Ocean (~ 190 km) (**Figure 1**), and exhibits three distinct morphologies along this length of the river. Between Yale and Laidlaw, the river channel is single-thread, and confined. The substrate is coarse gravel and cobble. Once it emerges from the confines of the mountains, the river flows over a partially-confined cobble-gravel fan. This gives rise to a characteristic wandering channel morphology between Laidlaw and Sumas Mountain (termed the "gravel reach"). Within this reach of the river there is a clearly defined main channel as well as secondary channels which flow around and across large island-bar complexes. At Sumas Mtn., the river morphology changes back to a single-thread channel, and switches abruptly to a sand-bed channel.

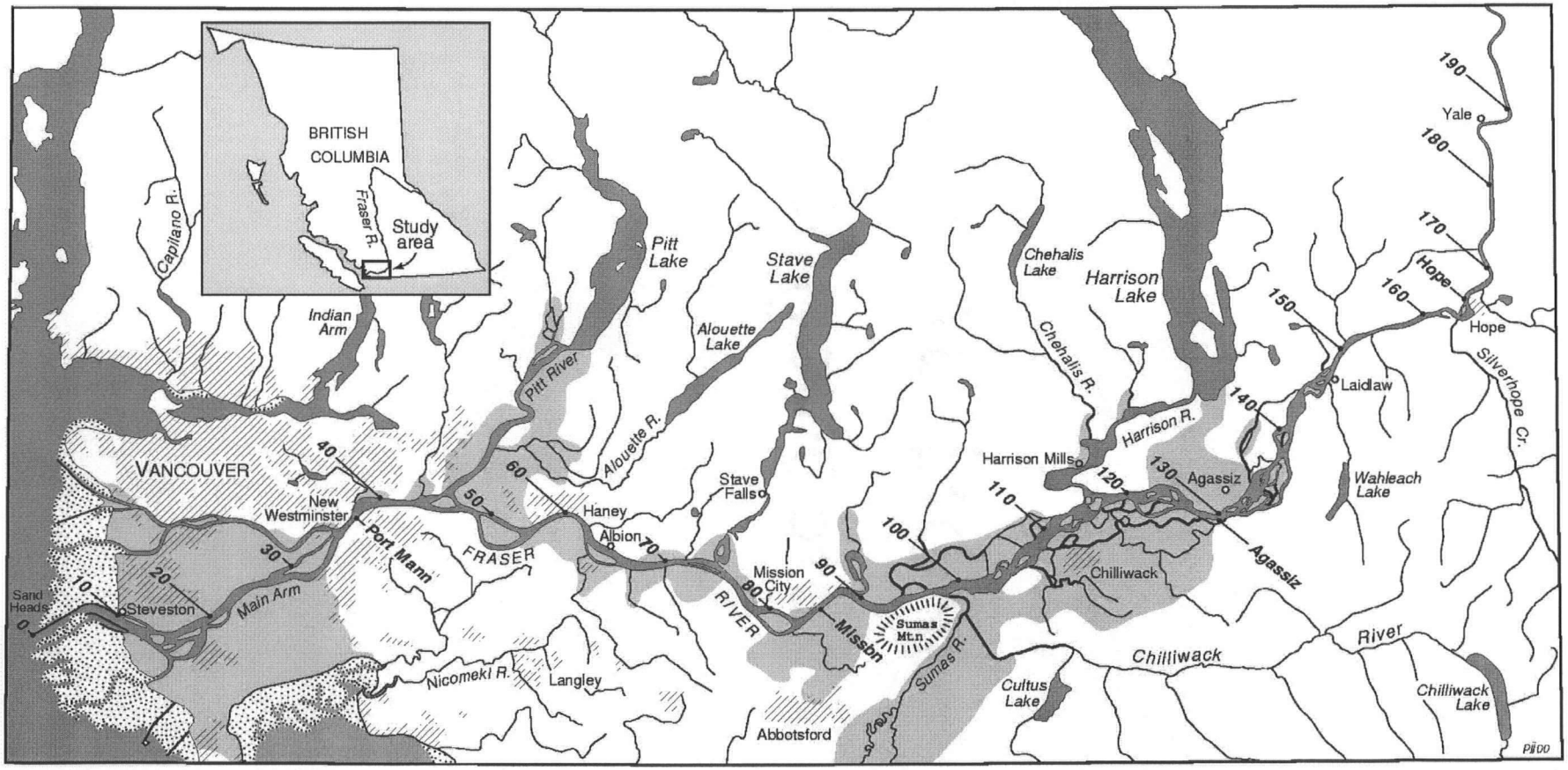

Figure 1 Location map of the Lower Fraser River, BC, showing distances from Sand Heads (km).

The at-a-station hydraulic geometry of the main channel is known at two locations: Agassiz and Mission. These locations correspond to reaches where the channel is single-thread, and where the bed composition is, respectively, gravel and sand. Gauging stations also provide a lengthy record of discharge at these two locations. The mean annual flood at Agassiz is 8,760 m^3/s and at Mission is 9,790 m^3/s (McLean et al., 1999).

A distinctive feature of wandering rivers is their seasonally persistent secondary channels. In these relatively smaller channels comparatively lower flows result in the whole channel being potentially suitable habitat for different species. In contrast, within large channels (e.g. main channels) lateral zonation creates areas of hydraulic efficiency (the thalweg of the channel) and areas of biological richness (the shore zone), the relative location and size of which are conditioned by the magnitude of the discharge (Stalnaker et al., 1989). The presence of these laterally-shifting habitat zones has been verified with reference to invertebrate habitat in the main channel of the Fraser River before, during and after the yearly freshet (Rempel et al., 1999). It is theorized that the persistent secondary channels in the Fraser River provide refuge habitat for fish during high flows and may also provide a valuable rearing habitat for juvenile fish. Ongoing research by Rempel is demonstrating the exceptionally diverse ecosystem represented in part by secondary channels of the Fraser River. Recent research indicates that these channels are also used as spawning habitat by endangered white sturgeon (*Acipenser transmontanus*) (Perrin et al., 2003).

Visual examination of secondary channels in the Fraser River suggests that there may be characteristic sub-reaches within each channel, each exhibiting distinctive hydraulic and sedimentological characteristics. Flow divergence into secondary channels at the upstream entrance produces a shallow and fast sub-reach with primarily gravel and cobble bed material. Conversely, at the downstream confluence of a secondary channel and the main channel, there is a backwater effect, which produces an "estuarine", deep and slow-flowing sub-reach with primarily fine bed sediment. A third sub-reach incorporates the transition from upstream to downstream and is intermediate in character between the upstream and downstream reach types.

2.1.1 Channel and reach selection

Channels were chosen based on the logistics of access and sampling. The channels had to be located relatively near to one another in order to keep main-channel travel time to a minimum. In addition, channels had to be free from obstructions that would prevent access to sub-reaches in low-flow conditions. Four secondary channels were chosen within the gravel reach to study the at-a-station hydraulic geometry relations: Calamity, Carey, Hamilton and Jesperson. Of the four study channels, Calamity channel flows behind the smallest and most recently formed gravel bar. It is constrained on the right bank by bedrock outcrops at the u/s and d/s ends of the channel. It is also downstream of the confluence of Fraser River and Harrison River (the only major tributary in the gravel reach). Jesperson channel (also known as Greyell Slough) is the oldest and longest of the study channels, and flows behind a large island-bar complex. Flow is controlled at the upstream end of the channel by a weir established approximately thirty years ago. Carey channel and Hamilton channel are intermediate in age and length between Calamity and Jesperson. Hamilton channel is controlled along the right bank by rip-rap. It is the site of the former main channel from approximately 1930 to 1950 (see Figure 6 in McLean and Church, 1999). A railroad runs along the upstream half of Carey channel and the right bank is protected by old rip-rap along the length of the tracks.

Rather than collecting data at a single cross-section, sampling areas were established within each channel to represent the upstream (u/s), mid (m/r) and downstream (d/s) sub-reach morphology, based on visual assessment in the field. Sub-reach length varied between 75 m and 200 m depending on the scale of the channel. The four channels used for at-a-station hydraulic geometry data collection yielded 13 sub-reaches (Carey channel was sufficiently long to have two "mid" reaches of different character). Five additional channels were chosen to study the scaling relations, and one sampling area was established in each of these channels to represent the mid-channel sub-reach morphology. **Figure 2** shows the location of all channels and sub-reaches where data collection occurred.

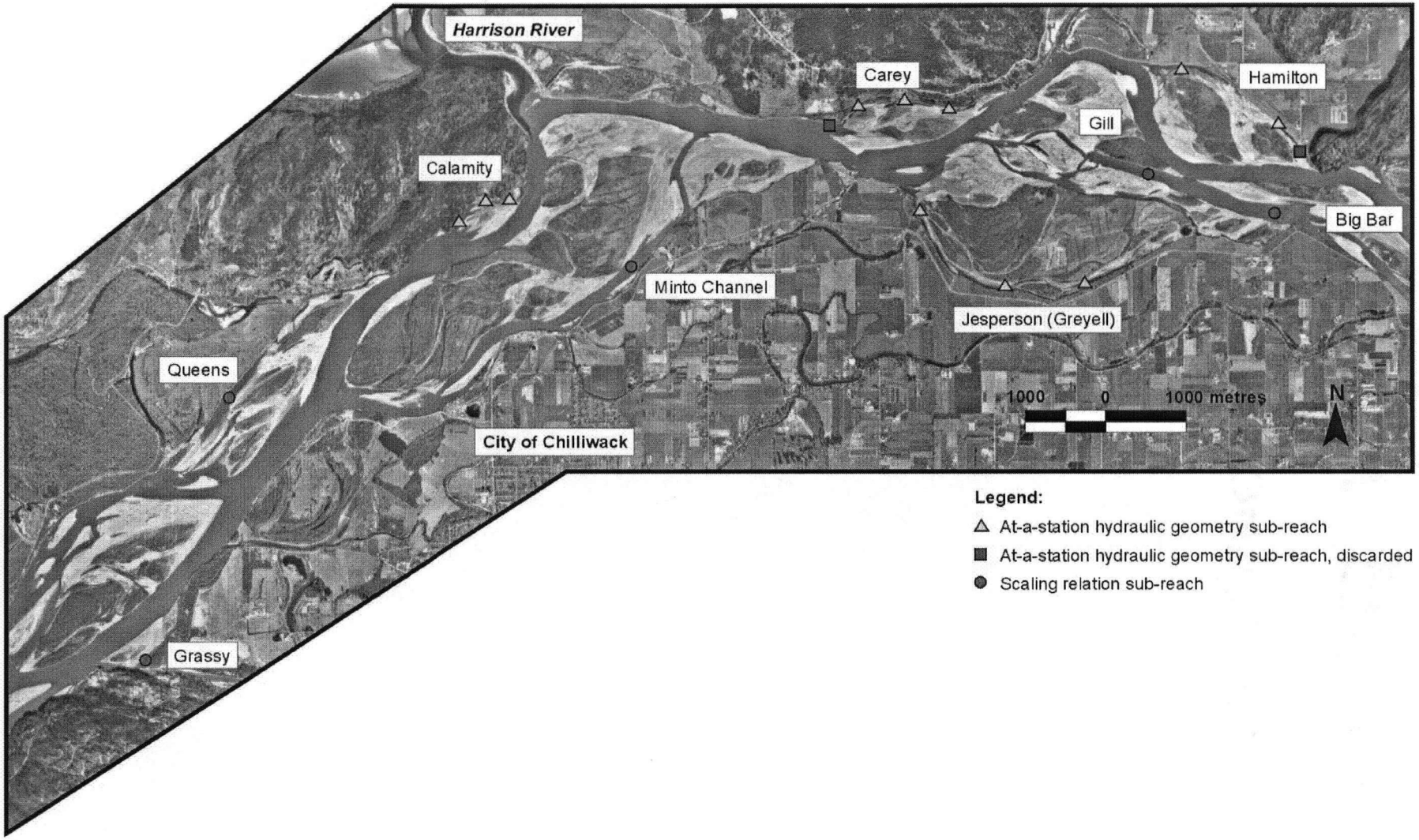

Figure 2 Location of all channels and sub-reaches where data was collected, either for at-a-station hydraulic geometry relations or for scaling relations (photos taken March 27, 1999).

2.2 Data collection

To develop at-a-station hydraulic geometry relations, a wide range of discharges is desirable because of the power-form of the relation. For the purposes of the scaling relations, data collection at a scaling flow close to bankfull is most appropriate. Although the actual magnitude of the freshet is not fully predictable, both of the previous concerns suggested that data collection for this project should begin slightly before the estimated peak of the hydrograph, and should continue on the declining limb of the flood (which is often less-steeply inclined than the rising limb, although this was not the case in 2002). Therefore, sub-reaches were established and reference surveys of permanent and semi-permanent markers were conducted in the spring preceding the 2002 freshet, between March 2002 and May 2002. These markers were used to measure water surface width, water surface slope, and stage.

The 2002 freshet had a peak daily average discharge of 10,681 m^3/s (at Hope, Water Survey of Canada station 08MF005) on June 21 (**Figure 3**), that corresponds approximately to the 5-year flood. After the snowmelt peak, there were very few inputs of precipitation and therefore the flow declined steadily and rapidly through July and August. Data collection in the secondary channels began in May 2002 and continued through the summer and fall, as long as the channels were flowing. All sedimentological data were collected in the winter following the freshet, between February and March 2003. In addition, all reference surveys of sub-reach markers were repeated during the winter period to include the high-water markers added during the freshet.

2.2.1 At-a-station hydraulic geometry relations

Starting in late May 2002, at-a-station sub-reaches were surveyed on a continuous rotation through the freshet. Out of a total of 13 sub-reaches, two sub-reaches (from two different channels) had to be discarded during data collection because of logistics. One sub-reach simply ceased to exist when the bar which defined the left bank was eroded away (Carey Channel, d/s), and the other became impossible to navigate because of the volume of gravel moved into the middle of the channel (Hamilton Channel, u/s).

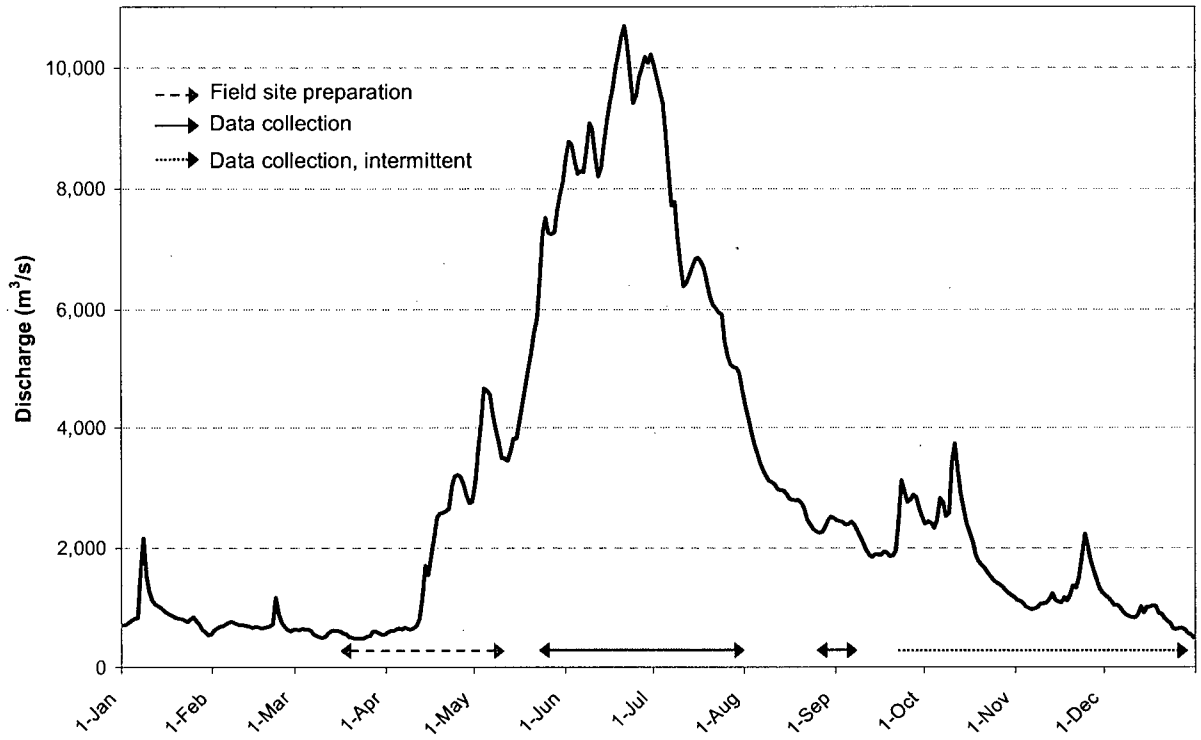

Figure 3 2002 hydrograph for the Fraser River at Hope, with approximate duration of project fieldwork indicated.

Sub-reaches were accessed via the main channel using a 16-ft aluminum boat with a 30-HP motor. Once gained, sub-reaches were quickly assessed to determine the approximate safe boundaries of sampling, and a 1.5 MHz Acoustic Doppler Profiler (ADP®, SonTek Inc.) was deployed from the boat. Velocities and depths were measured using the ADP, with a sampling rate of 1 Hz (in practice, a resolution of 0.3-0.5 Hz was achieved). Boat position was tracked and recorded using a Trimble differential global positioning system (GPS), and a continuous analogue recording of channel depth was also created using an Apelco XCD600 chart-recording depth-sounder. ADP and GPS data were recorded directly onto a laptop computer in the boat. Bank markers were used to orient and guide the in-channel measurements so that an approximate grid pattern could be maintained and replicated from round to round. Data were collected on cross-channel lines, spaced approximately equally through the reach, as well as on lines along channel, spaced less densely.

After the in-channel data had been collected, the boat was brought to each bank so that measurements of water surface width, water surface slope and stage could be made. For facility of measurement, water surface width was measured by subtraction from the total width between

pairs of left-bank and right-bank markers. Distances from the water's edge to the markers were measured with a 50-m tape. Water surface slope was measured by referencing a level survey of the water surface at the upstream and downstream ends of the reach to permanent benchmarks. This survey also served to reference the stage at each measurement round (relative to the upstream benchmark).

Bank markers were originally placed along the bankfull channel edge (defined as the beginning of permanent, woody vegetation). However, in most reaches the flow was above bankfull at and around the peak of the freshet, and submerged many bank markers. New markers were established to reference width, slope and stage measurements, where possible. Original markers were relocated after the freshet receded, although in some cases the markers were irretrievable. A second reference survey was conducted following the freshet to tie all remaining markers together. Although an attempt was always made during overbank flows to measure the true extent of the water surface (including standing water in the overbank vegetation), the presence of thick vegetation and bank levees often made this impossible. In most cases, flow through the vegetation was minimal compared with in-channel flow.

In some sub-reaches, near-shore access became impossible with the ADP as the freshet declined. Near-shore velocity and depth measurements were then collected with a hand-held electromagnetic velocity meter (Flo-Mate™ Model 2000, Marsh-McBirney Inc.) and top-set wading rod. These measurements were taken at each width marker, and paced at approximately 1 or 2-m intervals into the channel from the waterline, until the depth at which wading became impractical (and boating was possible): slightly over 1 m. Mean velocity and total depth were recorded at each measurement position.

2.2.2 Secondary channel scaling relations

Additional data collection for the channel scaling relations was conducted in five different channels, covering a range of channel sizes (**Figure 2**). Sub-reaches were established to represent the intermediate "mid" reach morphology. In-channel ADP data were collected once only, while flow was close to bankfull. The primary concern was to be able to collect data as quickly as possible, so that the flow would not have changed substantially during the time required to sample all the channels. For that purpose it was decided that a water surface width

measurement could be obtained at a later date either through photogrammetry (since the bankfull flow extended to the edge of vegetation on both banks) or from the GPS data collected at the time. A subsequent round of visits to these reaches was used to establish markers at the upstream and downstream ends of the reaches that were used for the water surface slope survey. A level survey was conducted at a later date to tie the markers together.

2.2.3 Surface and sub-surface sedimentology

Sedimentological data were collected at low flow in the winter following the 2002 freshet. In each of the at-a-station and scaling relation sub-reaches, 400-stone grid counts were conducted to derive an estimate of surface roughness (Church et al., 1987). Material was sized in half-phi increments down to 8 mm, and the number of counts of sand was also recorded. If the bed was wholly comprised of sand or finer sediment, a sample was taken for sieve analysis.

In addition, bulk samples were taken in the upstream reaches of each at-a-station channel to characterize the sub-surface sedimentology, following the sample size protocol in Church et al. (1987). Material was hand-sized or sieved and weighed in the field down to 16 mm or 22 mm and the remaining sediment was randomly split until a sub-sample of the appropriate weight was achieved. This sample was returned to the lab for processing. An effort was made to sample sediment that had been moved into reaches during the preceding freshet, to estimate the size distribution of sediment in transport.

3 Data Analysis

All data processing and analyses were performed using MATLAB® version 6.5.1.

3.1 Characteristics of ADP data

The ADP is a monostatic current meter (i.e. the same transducer functions as a transmitter and a receiver), which operates using the principle of the Doppler effect. Rather than measure the water velocity per se, the ADP measures the Doppler shift of sound reflected from particles in the water column. Particles in the water column are assumed to be moving with the flow, and therefore one must assume that their motion is equivalent to the water motion. The ADP used in this study has three beams; each oriented at 25° off the vertical axis, and at 120° relative azimuth to each other. By measuring the Doppler shift in each beam, the three-dimensional water velocity can be calculated using geometry. Although these velocity data are originally calculated with respect to a Cartesian coordinate system relative to the ADP, they can be converted to a geographically referenced system (East-North-Up, or ENU) by using data from the internal compass. Data are collected in user-specified depth bins that start after a blanking region immediately in front of the transducers.

There is inherent spatial averaging in ADP current measurements. The ADP signal processing algorithms are constructed on the assumption that the flow field is uniform across the area covered by the three beams. Although the beams are relatively narrow themselves, "area" here indicates the total area within a line circumscribed around the exterior of the three beams. Because of the geometry of the beams, the area that is covered by the beams increases with depth in an almost 1:1 relation (area $\approx$ 0.93 depth). Velocity data are averaged within depth bins, and adjacent bins have 25% overlapping information because of the convolution of the acoustic pulse length and the receive window over which it is averaged (SonTek, 1998). According to SonTek (1998), for most purposes the depth bins can be assumed to be distinct measurements without applying the true spatial definition of the bin.

With every ADP profile, the following data were collected:

- date, time
- water velocities in each of the ENU components, for each depth bin
- signal strength by beam, for each depth bin

- water temperature
- compass and tilt sensor data
- bottom-track data (where possible)
- GPS data (where possible)

Before data collection commences, the user specifies a depth bin size and a total number of bins. It is important to note that the ADP returns a value for every specified depth bin, in every profile. Given that the number of bins does not vary during data collection but that the channel depth clearly will vary, there are almost always bins which contain invalid data at the bottom of collected profiles (i.e. data from bins which extend beneath the channel bottom). The user must filter out these data.

3.1.1 Boat-velocity reference

When collecting data from a moving platform, the water velocity that the ADP measures is a combination of the motion of the water (or particles in the water) and the motion of the platform. Therefore, to know the water velocity we need a method to derive the platform velocity. There are currently two options available: (1) GPS data or (2) the ADP bottom-tracking (BT) function.

To use GPS data as a boat-velocity reference, the GPS is normally integrated into the ADP data-collection apparatus and a position fix is taken at the beginning and end of each profile. The boat velocity is then calculated as the change in position over the time interval. When the bottom-tracking option is used, the ADP uses a separate pulse to locate the channel bottom. The Doppler shift from this pulse is used to infer the motion of the platform relative to the channel bottom. GPS and bottom-tracking can be enabled simultaneously during data collection, allowing two independent boat-velocity estimates to be compared.

The accuracy of boat-velocity estimates referenced to the GPS is determined by the differential accuracy of the GPS unit. The differential signal for the unit we used was received by antenna from a beacon located approximately 120 km distant. This may have been close to the limit for reliable signal reception, as we had problems consistently receiving the beacon signal. Topography and proximity to heavily vegetated banks also may have influenced our

signal reception. When signal reception was poor, the GPS was incapable of resolving the relatively small motion of the boat between profiles and was therefore not an acceptable boat-velocity reference.

According to the manufacturer of the ADP, it is preferable to reference boat-velocity to the bottom-tracking algorithm, as they consider it to be more accurate (B.Macone, pers.comm. 2003, T.Mudge, pers.comm. 2004). However, given that bottom-tracking returns the motion of the platform relative to the bottom, if the bottom is mobile than the boat-velocity estimate will be biased (i.e. sediment moving downstream will cause an apparent boat motion in the upstream direction). Significant sediment transport would typically not be an issue in smaller channels with coarse beds, except at very high flows. However, in channels with sandy beds, bottom-tracking bias may become a factor. In those cases, it is preferable to reference the boat-velocity to the GPS if possible.

Comparison of stationary boat-velocity estimates. In a preliminary investigation of moving-boat ADP data, we found that the choice of velocity reference noticeably affected the water velocity estimates from the ADP. It became clear that the two methods of boat-velocity reference were not always returning equivalent, or nearly equivalent, values. Without a third, independent and true estimate of the boat velocity, it was impossible to select the most accurate reference. Bottom motion could be inferred for cases in which the substrate was known to be fine but, given the problems with GPS signal reception, we could not be certain that this reference was accurate either.

Additional data were collected using the same ADP and boat configuration, but with the boat stationary (either anchored or held approximately constant in the flow by motoring). Using this data set, it was possible to compare boat-velocity estimates with the expectation that they should be very close to zero. Significant and regular deviations from zero velocity would suggest a problem with the reference.

A subset of ADP profiles was extracted from each file where the boat was known to be approximately stationary and BT coverage was good. This process normally yielded at least 20 ADP profiles for analysis, and usually more than 30, with a total of 36 files. Average North and

East components of boat velocity were calculated based on GPS and BT data. Outliers were discarded (data more than three standard deviations from the mean, BT data only). The average velocity components for both references are presented in **Table 1**. As expected, velocities are generally low, on the order of a few centimeters per second. The overall mean E and N components of GPS boat velocity are an order of magnitude smaller than the BT boat velocity vectors, although the BT vectors are still less than 0.015 m/s. The data also show that the mean ± 2 SE (an approximate 95% confidence interval for the mean) contains zero, in all cases. When *weighted* overall means were calculated (weighting by sample size), the effect was to generally increase the overall mean GPS and BT boat velocity vectors.

It is clear that the GPS generally returned lower boat speeds than bottom-tracking, as is demonstrated in **Figure 4**. The GPS boat speeds are consistently very low (< 5 cm/s) and the few instances where they are higher are most likely a result of loss of beacon reception. There is much more scatter in the BT data and relatively higher speeds, although most of the data points have speeds less than 10 cm/s. Some of the higher speeds may be a result of collecting data in very shallow locations (depth < 1.5 m) where the instrument was not able to function properly. As well, some higher speeds may be attributable to bottom motion. For instance, compare the direction of the BT boat-motion vectors in the right-hand plot of **Figure 5**. These data were collected in a reach with an approximate downstream orientation of 272° (Jesperson m/r). A mobile bottom would result in apparent boat-motion upstream, as measured by bottom-tracking, and the BT data do appear to cluster around 90°.

The contrast in data patterns between the two references is also evident in **Figure 5**. Although the average GPS boat speed for this file is exceedingly small (0.0033 m/s), the pattern in the GPS boat motion vectors revealed in the left-hand plot shows motion with a consistent orientation and speed. This is unlikely to be real motion, as the direction does not correspond well to the d/s direction (272°). Rather it appears to be some sort of drift in the GPS signal. The right-hand plot shows that the direction of BT boat-motion vectors is more scattered, which is probably realistic considering the small movements possible while the boat was anchored.

Although the BT signal is noisy, for the most part the boat velocity vectors that it returns are reasonable, particularly if the effect of a moving substrate is considered. The GPS on the other hand, although it returned very low boat speeds, seems unable to resolve the small boat

movements that were likely occurring. In addition, it is clear that it may return an apparent motion due to signal drift.

Table 1 Comparison of average boat velocity vectors based on data collected while stationary.

File	Sample	n	E, GPS (m/s)	N, GPS (m/s)	E, BT (m/s)	N, BT (m/s)
225jsd03	1	71	0.0038	0.0007	0.0016	0.0037
225jsd04	1	89	0.0007	0.0060	-0.0079	-0.0126
225jsd05	1	93	0.0013	-0.0012	-0.0244	0.0086
275jsm01	1	60	0.0008	-0.0020	-0.0001	-0.0225
	2	60	-0.0021	0.0025	0.0627	-0.0119
	3	31	-0.0036	0.0046	-0.0056	-0.0183
285jsu02	1	31	-0.0011	0.0042	-0.0025	-0.0112
	2	38	-0.0206	-0.0067	0.0007	-0.0016
	3	17	-0.0051	0.0078	-0.1273	0.1249
036had02	1	27	0.00004	-0.0007	0.1213	-0.1070
	2	48	-0.1568	-0.0536	0.0597	-0.0947
	3	51	-0.0169	0.0058	-0.0049	-0.0290
046ham02	1	40	0.0062	0.0067	0.0610	-0.0512
	2	50	0.0022	-0.0001	-0.0113	0.1062
	3	51	-0.0031	0.0038	0.0305	0.0166
056hau02	1	12	0.0007	-0.0008	0.1084	0.1689
	2	21	-0.0050	-0.0137	0.0846	-0.1408
	3	19	0.0223	-0.0086	-0.0902	-0.0811
066clm02	1	40	0.0019	0.0024	0.0690	-0.0521
	2	35	0.0036	-0.0093	0.0300	-0.0191
	3	38	-0.1582	0.0103	-0.0294	0.0099
116jsu02	1	41	-0.0001	0.0002	-0.0235	0.0086
	2	3	-0.0003	0.0047	-0.0010	0.2960
	3	25	-0.0025	0.0020	-0.0512	-0.0128
136jsd02	1	58	-0.0047	-0.0010	-0.0036	-0.0022
	2	54	-0.0164	-0.0064	0.0212	-0.0023
	3	58	-0.0111	-0.0050	-0.0142	0.0047
176had02	1	45	0.0010	0.0020	0.0116	0.0260
	2	37	0.0027	-0.0002	0.0704	-0.0479
	3	40	0.0061	-0.0017	-0.0025	0.0352
196jsm02	1	64	0.0030	0.0044	0.0209	-0.0088
	2	52	0.0090	0.0004	0.0019	-0.0084
	3	57	-0.0075	0.0084	0.0219	0.0305
206jsd02	1	37	-0.0018	-0.0027	0.0149	-0.0108
256jsd02	1	39	0.0015	-0.0009	0.0057	0.0019
	2	38	-0.0041	0.0145	-0.0028	-0.0208
	Mean (*SE*)		**-0.0098** (± *0.0062*)	**-0.0006** (± *0.0018*)	**0.0110** (± *0.0081*)	**0.0021** (± *0.0127*)

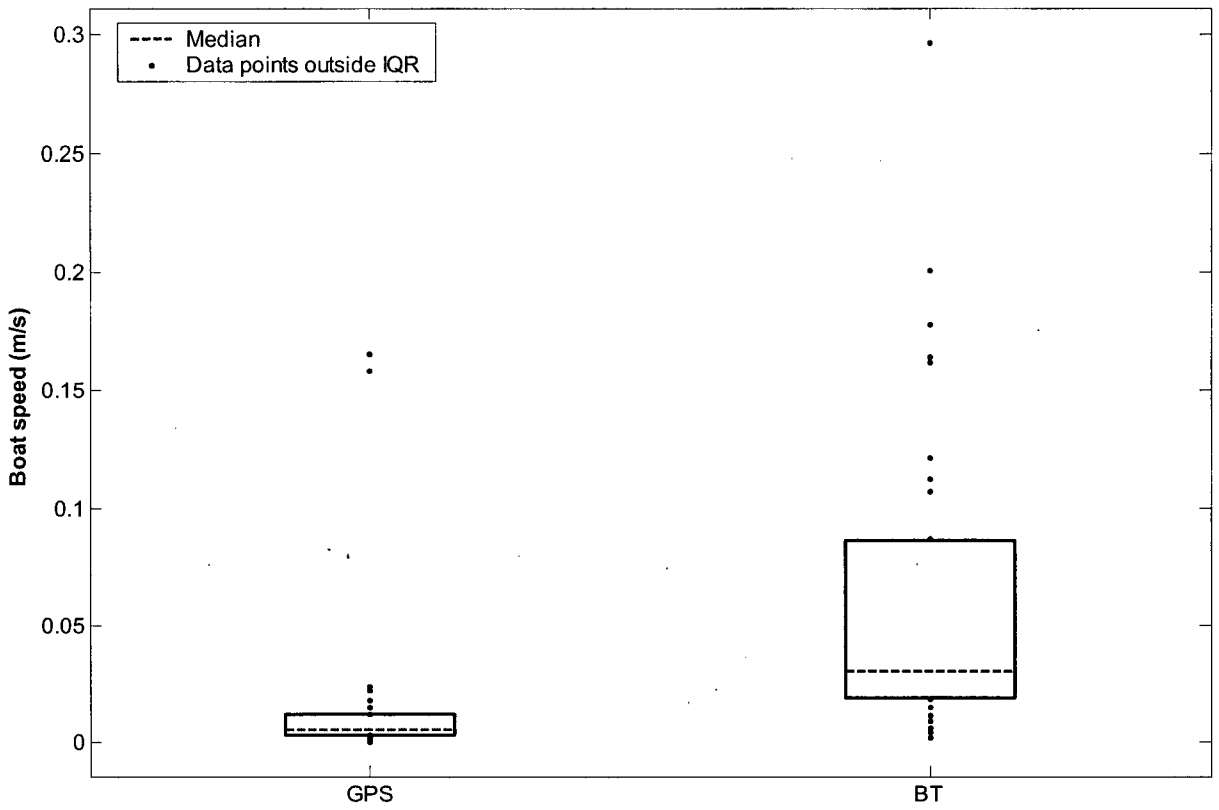

Figure 4 Box plot of average boat speeds based on data collected while stationary. The box encloses the inter-quartile range.

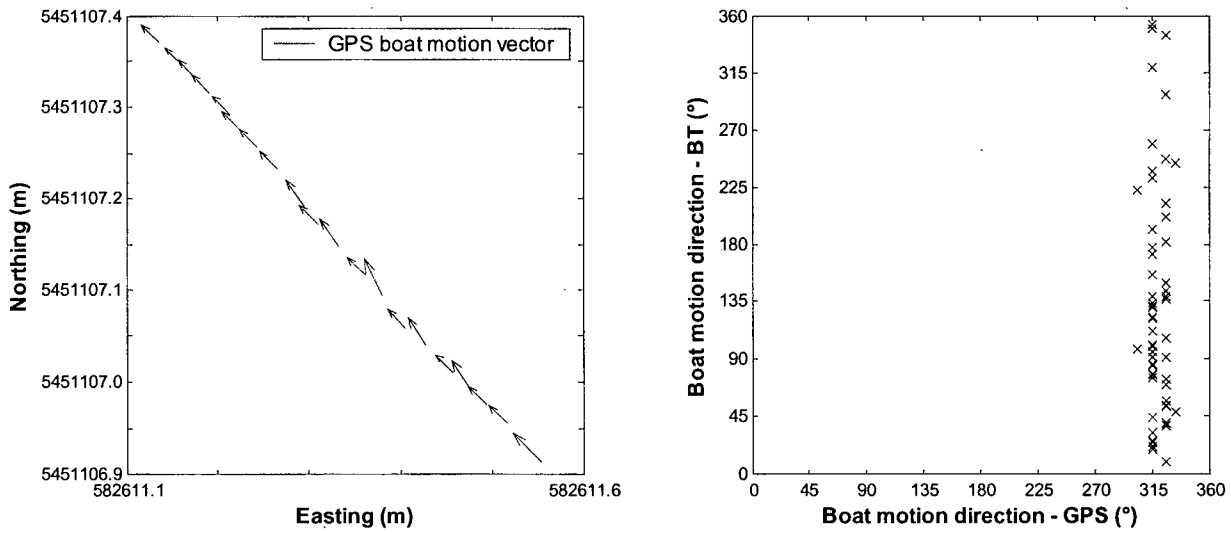

Figure 5 Contrast in data patterns between GPS and BT-derived boat motion data, for a stationary collection period (275jsm01, #2). Note the scale on the left-hand plot, in which data were collected over a 6-minute period (every third profile is shown, for clarity). The right-hand plot corresponds to the same data file, all valid points shown.

3.1.2 ADP compass bias

The ADP has an internal compass that enables velocities, which are originally referenced to the ADP's internal geometry, to be converted to a geomagnetic frame of reference. Inaccuracies in the compass will result in an inaccurate direction being assigned to velocity measurements, hence may create biased estimates of downstream and cross-stream velocity components. For this reason, before each deployment of the ADP a proper compass calibration was performed according to the manufacturer's specifications (SonTek, 1998). The ability of the compass to resolve 180° and 360° turns was checked in a controlled setting and there were no apparent problems. However, this test did not check the ability of the compass to properly resolve magnetic North (i.e. a check for a persistent bias).

One way to establish whether the compass is inaccurate or not is to compare graphically the boat-trajectories given by GPS and by bottom-tracking (properly compensated for magnetic declination). In sub-reaches where the channel bottom can be supposed to be immobile and the GPS signal reception is good, discrepancies between the two boat-velocity vectors can be attributed to compass problems. A pattern of systematic differences in velocity magnitudes depending on the cross-stream trajectory of the ADP (i.e. left-bank to right-bank or vice versa) led to an examination of data for potential problems with the compass. An apparent compass bias was discovered which appears to change magnitude depending on the cross-stream trajectory (consistently smaller in one trajectory compared with the other) and which changes sign in the longitudinal trajectories (**Figure 6**).

The boat-motion vectors in **Figure 6** clearly demonstrate the compass bias. Although this sub-reach has a dominantly coarse substrate and therefore was probably essentially immobile on 30 May ($v \approx 1.8$ m/s), a mobile bed could not in many cases explain the discrepancy between the GPS and BT. If the bed were in motion, the BT vectors would be consistently biased to the upstream direction (East) during cross-stream trajectories. Also, we would expect to see fairly good agreement between BT and GPS vector orientation from longitudinal lines, but would expect a difference in the magnitude of the vectors (with BT vectors shorter in the downstream direction and longer in the upstream direction). Neither of these patterns is discernible. This particular ADP has been known to have a sporadic and unpredictable compass bias even when calibrations have been performed (Rennie, 2002).

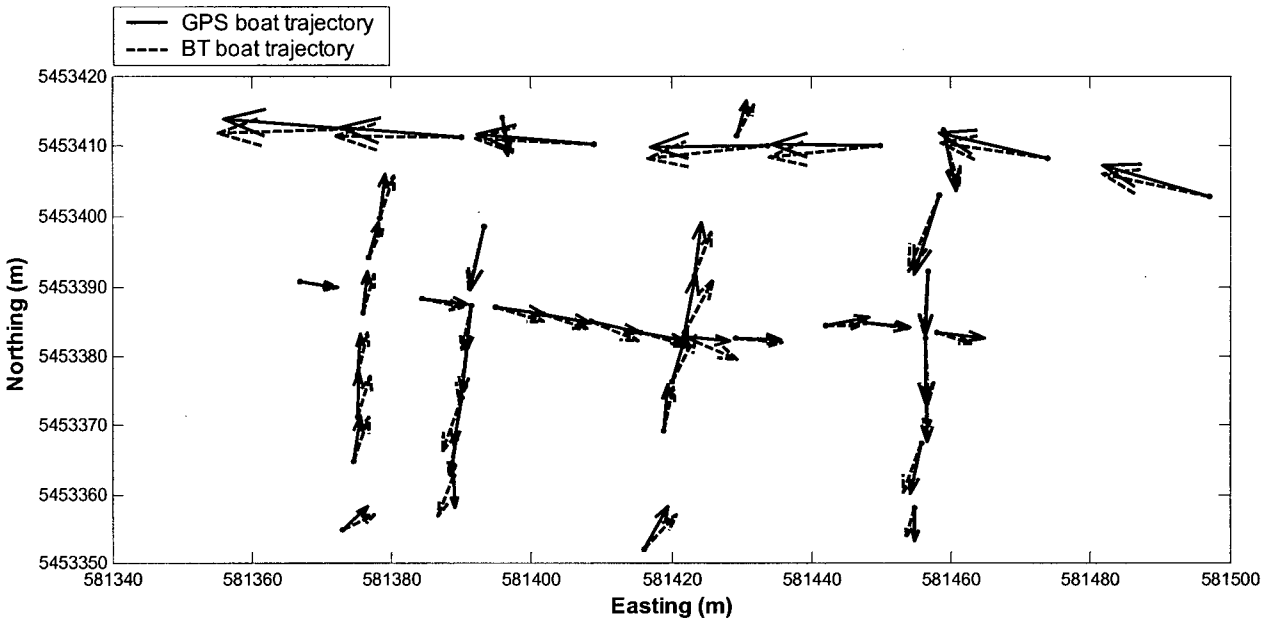

Figure 6 Discrepancy between the boat trajectory as measured by GPS and by bottom-tracking. For clarity, only a sub-set of data points is shown for the selected cross-sections.

The compass bias was discovered after all discharge calculations had been completed. Because velocities were projected into the downstream plane, a compass error translates into a change in length of the projected vector, and affects both the GPS and BT-referenced velocities. To avoid repeating all discharge calculations, a method was developed to obtain a mean bias correction for all reaches where GPS and BT boat direction could be compared (see Section 3.2.2).

3.1.3 Measurement of channel depths: ADP vs. conventional depth-sounder

Water depth was measured in two ways for all hydraulic geometry data files collected with the ADP (barring problems with instrumentation). The methods used were:

1) the ADP bottom-tracking (BT) algorithm, which returns a depth for each beam;
2) a chart-recording depth-sounder, with the transducer mounted in the boat near the stern.

While there is some redundancy in collecting water depth data twice, it is an essential procedure because of the potential for loss of BT signal. Without BT, the ADP cannot return a water depth. Therefore although the velocity can be referenced to the GPS, there needs to be an

independent estimation of water depth in order to truncate the velocity profile. Naturally, we wished to evaluate whether the depth estimates from the two instruments were equivalent, and hence could be used interchangeably. The comparison is also interesting because of the difference in measurement principle of the two instruments. The ADP returns a depth estimate for each of its beams, all oriented at 25° off-vertical, mounted near the bow of the boat, whereas the depth-sounder has a single, vertical beam and was mounted near the stern of the boat.

Charts were digitized as continuous lines and individual depths were matched to the appropriate ADP profile by assuming a constant sampling rate for the depth sounder and ADP (i.e. the width of the digitized chart was divided evenly based on the number of ADP profiles recorded). Mounting depths for each instrument were added to the raw data. The ADP mounting depth was measured with a tape and recorded with each data file. The mounting depth of the depth sounder was not as straightforward to measure and required a level survey. This was done once, with one person in the boat (plus equipment), and the offset of the transducer below the water surface was measured as 0.155 m. A subsequent simple measurement using a measuring tape, with two people in the boat, revealed a mounting offset of 0.18 m. It is assumed that the increase in offset with weight in the boat above one person plus gear is not substantial. The mounting depth of the depth-sounder transducer was assumed to be 0.155 m for all subsequent calculations. Depth-sounder data were also adjusted assuming that this instrument was calibrated for a sound speed of 1500 m/s (a marine-setting calibration). The ADP records a sound speed with every profile, based on an input salinity (set to zero) and a measurement of water temperature (to $\pm$ 0.1 °C); therefore the depth-sounder data could be adjusted based on the measured sound speed. Typically sound speeds were below 1500 m/s and therefore depths were adjusted slightly downwards.

Nine data files were chosen for the comparison because they have relatively continuous bottom-tracking coverage. In each file, chart depths were matched with ADP profiles, and the subset of data with good bottom-tracking coverage was selected. A simple linear regression was run for each file, using the ADP depths as the predictor for depth-sounder data. This allocation of variables was based on ease of access of the data: the ADP depths are readily available (when the signal is good) whereas the depth-sounder data require processing to match them to ADP profile numbers, and hence are less readily available.

Regression results are shown in **Table 2**. Overall, the adjustment of the depth-sounder data for sound speed was small given that the mean ADP sound speed for all files would yield only a 2.7% decrease in the depth-sounder depth estimates. The average regression slope is close to 1.0 (there is a slight tendency for the ADP to under-predict depth sounder depths, on average). The average regression intercept is very close to zero, which implies there is no systematic bias in the relation. However, there is fairly significant scatter between the individual regression results: slopes range from 0.924 to 1.07 and regression intercepts range from 0.284 m to –0.267 m. To highlight the significance of this scatter, if the depth sounder data from file 046ham were used to predict BT water depths, they would over-predict on average by 0.284 m. This over-prediction is greater than one depth bin (0.25 m) and therefore we run the risk of including invalid data at the bottom of profiles. It is also worth mentioning that the scatter around individual regression lines is often substantial (e.g. SEE for 810cld).

Table 2 Comparison of regression results for the ADP vs. depth-sounder water-depth regression (ADP - predictor).

file	n	mean sound speed (m/s)	b_0 [a] (m)	b_1 [b]	SEE [c] (m)
225jsd	393	1443.7	0.0372	1.02	0.244
278jsd	299	1486.4	-0.0241	1.01	0.11
127clm	585	1470.6	0.166	0.985	0.202
047qum	908	1456.9	-0.0565	1.06	0.365
046ham	402	1449.2	0.284	0.954	0.172
136crdm	209	1457.7	0.0452	1.01	0.133
047grm	437	1459.3	-0.134	1.07	0.157
097jsd	373	1462.7	-0.267	1.07	0.27
810cld	181	1452.5	0.000117	0.924	1.01
mean		**1459.9**	**0.006**	**1.011**	**0.296**

[a] regression intercept
[b] regression slope
[c] standard error of estimate of the regression

One possible source of discrepancies between water depths measured by the depth sounder and the ADP may be the combination of instrument, boat and channel geometry. In this general category, there are three potential sources of discrepancies:

1) **ADP beam geometry**: depth measurements are an average of estimates from the three beams, and therefore are spatially averaged over the channel.

2) **Spatial offset of the depth-sounder transducer from the ADP**: the depth sounder was separated from the ADP by approximately one third the length of the boat (1.6 m), and mounted toward the stern of the boat. (Although there is an additional offset of the depth-sounder transducer and the ADP transducer, in the cross-boat plane, this factor was not included in the analysis).

3) **Orientation of the boat with respect to the channel banks**: depending on local flow conditions, the orientation could be anywhere from parallel-to through perpendicular-to the bank orientation. A change in boat orientation changes the effect of the spatial offset between the depth sounder transducer and the ADP. The mounting of the ADP with respect to the boat was constant.

4) **Beam-spreading**: in addition to beam and boat geometry, we should additionally consider the shortest path 'seen' by the different beams, based on the angle of beam spreading. This factor may be quite minimal as far as the ADP is concerned, as each beam is reported to have a half-intensity beam width of approximately 1.5° (Rennie, 2002). However, it may be more noticeable in depths returned by the depth sounder, which has comparable figure of 12°.

5) **Operating frequency**: the higher the frequency of the pulse, the more likely it is that the signal returns will reflect off suspended sediment near the bottom (i.e. in soft substrates) rather than penetrating through to the harder substrate beneath. The manufacturer of the ADP claims that the bottom tracking performs well over hard channel substrates, such as gravel or sand (T.Mudge, pers.comm. 2004). The operating frequencies of the depth sounder and ADP are 200 kHz and 1500 kHz, respectively. Therefore we might expect that the ADP would return shallower depths when compared to the depth sounder, if the substrate is soft. CAL d/s would probably be considered to have a soft channel substrate, but there is no evidence of an ADP bias in this file (810cld in **Table 2**).

It would be difficult, if not impossible in some cases, to calculate and then compensate for the effects of these five factors in every file. However, to get a sense of the scale of the

discrepancy that might be induced, several generalized scenarios were conceived and the depth discrepancy calculated between the ADP and depth sounder was calculated.

Semi-artificial channel geometries were created, based on smoothed polynomials fit to depth-sounder data. Two curves were created: one based on the downstream reach of Calamity channel (~ 50 m wide, quite deep) and one based on data from Carey channel, downstream mid reach (~ 40 m wide, fairly shallow). Each channel was created with a mirror opposite, to show the effect of the two different trajectories that would be taken within a given reach (i.e. river-left to river-right, and the reverse). A flat and uniformly sloping channel configuration were also developed. The channel configurations are shown in **Figure 7**. For each channel configuration and trajectory, the geometry was calculated considering the boat to be parallel to the channel banks, as well as perpendicular to the channel banks. Beam spreading was included by considering the shortest possible path to the channel bottom representative of the depth returned by that instrument.

For each 1-m interval across the channels, the perceived depth was calculated for the ADP and for the depth sounder. The difference between the depth estimates was calculated as:

$$Depth\ discrepancy = |ADPdepth| - |depth\ sounder\ depth| \qquad (13)$$

Therefore, positive discrepancies indicate that the ADP is overestimating the channel depth compared with the depth-sounder and negative discrepancies indicate that the ADP is underestimating depth, with respect to the depth sounder. An average discrepancy was calculated for each cross-section.

As **Table 3** shows, the general trend is for the ADP to over-predict depths as compared with the depth sounder. However, due to the inclusion of beam spreading, the depth sounder is no longer a very good estimator of the true (perpendicular) depth (see **Table 4**).

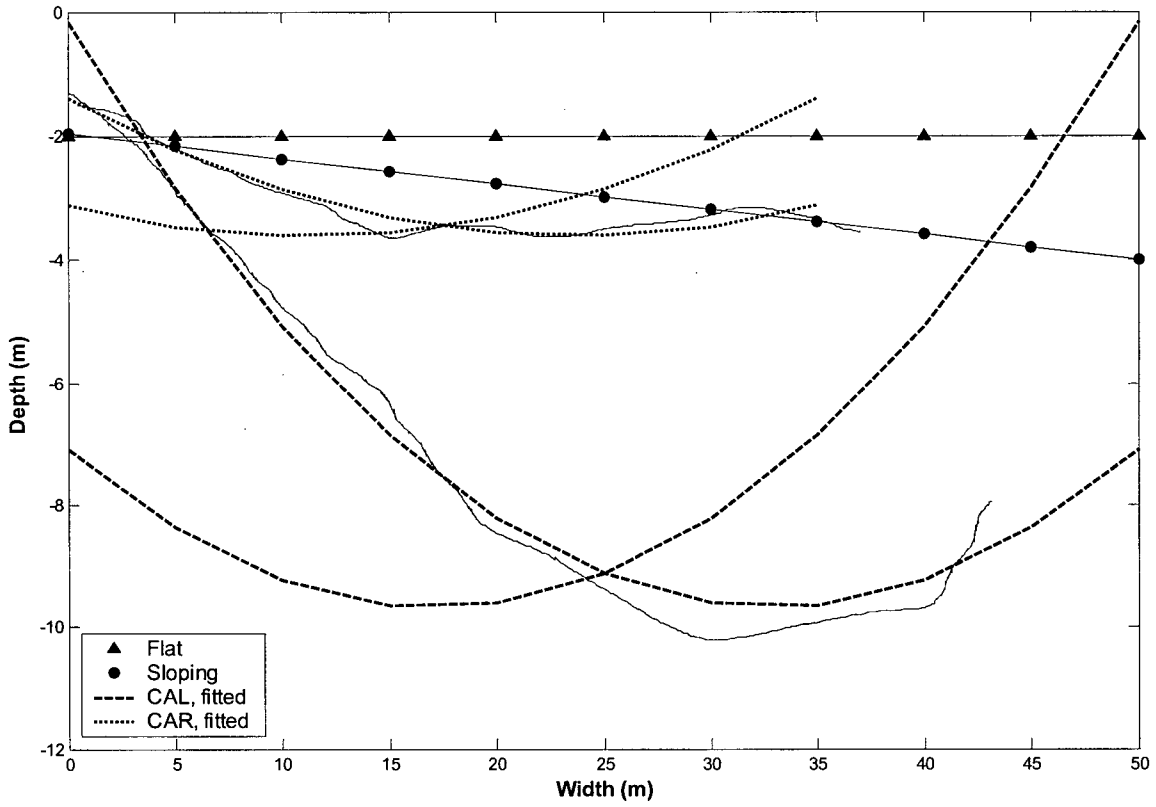

Figure 7 Channel configurations used for the comparison between the depth-sounder and ADP. Where fitted polynomials were used the raw data are shown for comparison as solid lines with no markers. The trajectory fit to the raw data is the original whereas the mirror image is specified to be the 'reverse'.

Table 3 Summary values of depth discrepancies between the ADP and depth-sounder, for different channel configurations [a] and including beam-spreading effects.

channel	orientation of boat, w.r.t. bank [b]	mean discrepancy [c] (m)	range [min – max] (m)
polyfit(CAL)	PA	0.23	[-0.06 – 0.39]
polyfit(CAL)	PE	0.47	[-0.40 – 1.29]
polyfit(CAL), reverse	PA	0.22	[-0.06 – 0.39]
polyfit(CAL), reverse	PE	-0.17	[-0.9 – 0.93]
polyfit(CAR)	PA	0.04	[0 – 0.06]
polyfit(CAR)	PE	0.11	[-0.14 – 0.38]
polyfit(CAR), reverse	PA	0.03	[-0.02 – 0.06]
polyfit(CAR), reverse	PE	0.02	[-0.14 – 0.10]

[a] see **Figure 7** for channel configurations

[b] PA = parallel, PE = perpendicular

[c] positive discrepancies indicate depths predicted by ADP are greater than those predicted by the depth-sounder

Some general observations can be made based on the data in **Table 3**:

1) Parallel orientation does not necessarily lead to the best agreement between ADP and depth-sounder depths, even though this configuration would minimize the cross-channel distance between the two instruments' transducers.
2) The ADP generally overpredicts depths compared with the depths given by the depth-sounder.
3) Predicted discrepancies are of the same order of magnitude as deviations from zero of the adjusted regression intercept. However, the discrepancies are mainly positive which would lead only to negative regression intercepts (when the ADP is the predictor variable). Thus the positive regression intercepts in **Table 2** are not well explained by geometry and beam spreading.

A close examination of the data in Table 2 reveals that the large intercept discrepancies are associated with the most extreme slopes (i.e. 127clm, 046ham, 047grm, 097jsd). Within this subset, there also appears to be a consistent association of slope steepness with intercept sign: slopes less than one are associated with positive intercepts while slopes greater than one are associated with negative intercepts. This may be simply an artifact of the regression because as correlation declines, slope declines (property of regression) and the intercept rises. Therefore correlation strength may explain the positive regression intercepts that were not explained by the analysis of beam geometry.

Given the instrument and channel geometry involved, it seems unrealistic to expect a 1:1 agreement between individual depth estimates from the ADP and the depth sounder. The disagreement between the instruments is not simply a function of a calibration error, but rather of a different way of 'seeing' the channel bottom. If we neglect beam spreading, the depth sounder may be considered to be the more accurate instrument, in the sense that it is returning a value closer to the true, perpendicular depth. The ADP, by virtue of its beam geometry, always performs a spatial average of the channel bottom depths, and the area it averages over increases with channel depth (increasing the potential for discrepancies with the depth sounder). Thus the ADP depths are less representative of the true, perpendicular water depth, when beam spreading is not a factor.

However, when beam spreading is included and predicted depths from each instrument are compared with the true perpendicular depth beneath the boat, the ADP is a better estimator in all cases (**Table 4**).

Table 4 Summary values of depth discrepancies between the instruments and the 'true', perpendicular depth beneath the boat, for different channel configurations [a].

channel configuration [b]	Δ depth: ADP – 'true' (m)	Δ depth: depth-sounder – 'true' (m)
sloping	0.00	-0.03
polyfit(CAL)	-0.09	-0.32
polyfit(CAL), reverse	-0.09	-0.31
polyfit(CAR)	-0.01	-0.05
polyfit(CAR), reverse	-0.02	-0.05

[a] the boat is parallel to the banks in all cases
[b] see **Figure 7** for channel configurations

Of concern is that the use of a depth estimate which is artificially inflated would lead to the inclusion of invalid (sub-bottom) ADP cells in calculations of flow parameters. When using only flow data which have bottom-tracking information this is not a concern as it is possible to use the ADP estimate of channel depth, which one presumes to be accurate so far as this instrument is actually 'seeing' the channel bottom. It is the cases in which bottom-tracking data are unavailable and we desire to use GPS data to reference the flow velocities that we require an independent estimate of channel depth. Although the beam geometry analysis suggests that the depth-sounder gives the more conservative estimates of channel depth, if beam spreading is neglected the results of the analysis suggest that there are also many cases in which the ADP will return the shallower depth estimate. There is also substantial between-sub-reach variability in the relation between the depth-estimates.

During discharge calculations, for files in which it was necessary to use the depth sounder to estimate depths, a regression was first performed on all profiles with bottom-tracking. On the basis of this regression, profiles with only depth-sounder coverage were used to predict the ADP-measured water depth, which was then used to truncate the velocity profiles. This method was chosen in an effort to remain consistent with the bulk of the discharge calculations which used solely bottom-tracking as the depth estimate. A potential problem with this method

is if there is an interaction between channel form and bottom-tracking coverage that would yield a particular regression in the area of the channel with bottom-tracking coverage and a markedly different one in areas without. Although there is likely to be a spatial component to the performance of the bottom tracking algorithm in that it performs less well in very shallow or very deep areas, it seems unlikely that this method would lead to very large errors in predicted profile depths.

3.2 Analysis of hydraulic data

3.2.1 Calculation of discharge

As discussed previously (Section 3.1.1), it is preferable to reference ADP velocities to a boat-velocity estimate derived from bottom-tracking rather than GPS. GPS can be used for estimates of boat position at a profile. The first method devised to calculate discharge through the at-a-station sub-reaches relies on reasonably good bottom-tracking coverage and at least partial GPS signal reception. Other methods were derived to deal with measurements in which data of this quality were not available.

Due to the deliberate spatial distribution of in-channel measurements, it was possible to derive multiple estimates of discharge for each round of measurements in a sub-reach. For example, in the case of the measurements in **Figure 8**, a discharge estimate was generated for each cross-channel line and then the distribution of estimates within the reach was examined.

Calculation of discharge through a cross-channel line followed a specific methodology. Consider the channel cross-section in **Figure 9**. Each vertical line in **Figure 9** represents a velocity and depth profile as measured by the ADP. These profiles are separated by non-standard width increments, the size of which is dictated by boat-speed and data quality. The total discharge through the cross-section (Q_{XS}) is equal to the sum of the discharges through the middle and edges of the channel:

$$Q_{XS} = Q_{LB} + Q_{ADP} + Q_{RB} \qquad (14)$$

The mid-channel (i.e. Q_{ADP}) and bank components of the total discharge were calculated using different methods, which will be described below.

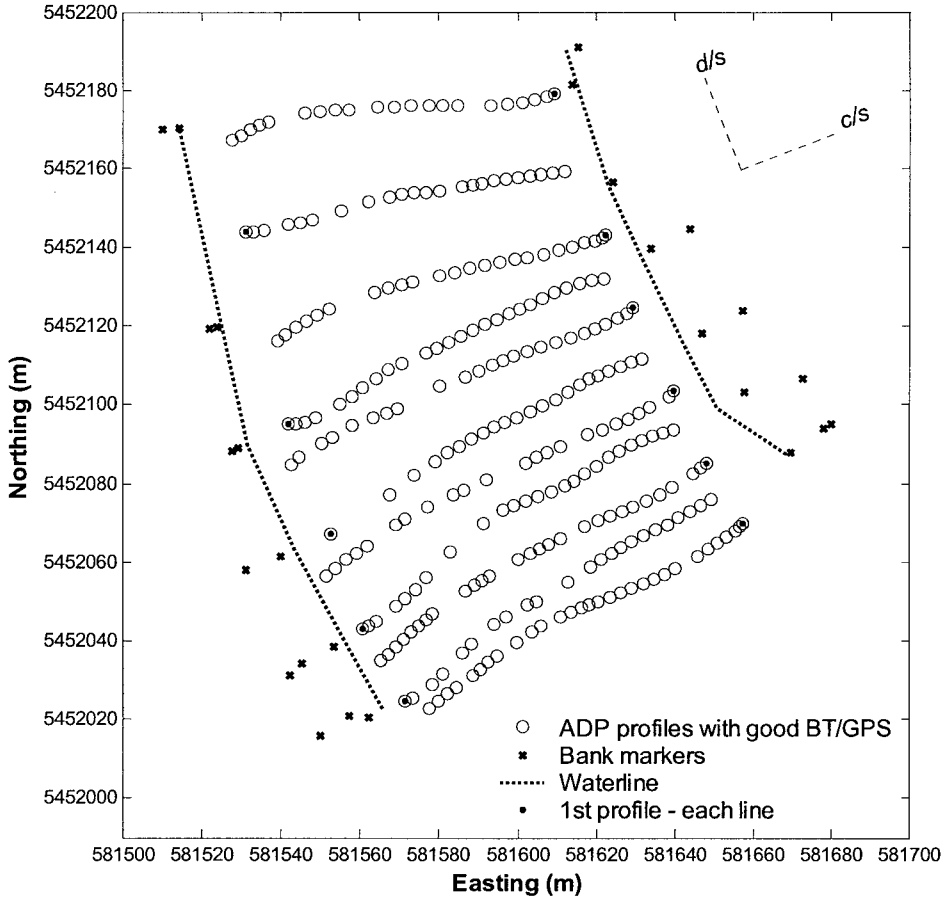

Figure 8 Plan view of in-channel data collected on July 9th, 2002, in Jesperson channel, d/s. Note the approximate grid pattern of the ADP profiles.

***Method 1**: Files with good bottom-tracking and good GPS signal reception.* The output from Method 1 yields two separate discharge estimates. The calculation is identical for each estimate but in one only BT-referenced velocities are used, and in the other only GPS-referenced velocities. This provides a test of whether there are discrepancies introduced by the boat velocity estimates.

1. Q_{ADP} (channel center)

The discharge through the middle portion of the channel, where ADP measurements were taken, is the sum of discharges, Q_v, calculated at each vertical:

$$Q_{ADP} = \sum_{v=1}^{k} Q_v \tag{15}$$

where k = number of verticals in a cross-section.

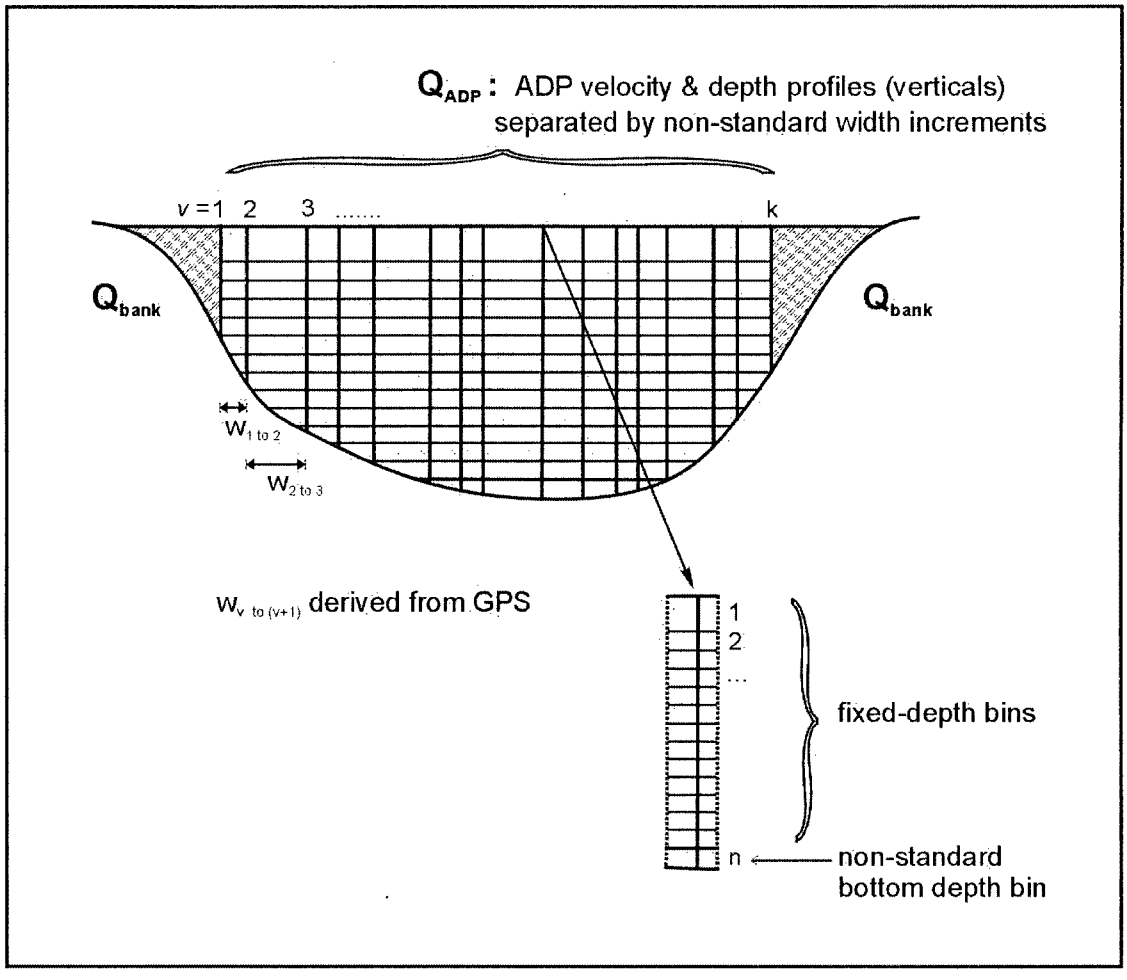

Figure 9 Diagram of a representative channel cross-section to illustrate the parameters involved in the calculation of discharge. A plan-view schematic (**Figure 10**) is required to illustrate the reduction of width data.

ADP profiles (i.e. verticals) are divided into depth bins, and in each bin the ADP returns a water velocity. Therefore, discharge at an individual vertical can be further separated into components flowing through each bin (**Figure 9**). Water *fluxes* ('*q*', m^2/s) were calculated for each bin of a given vertical, then summed and multiplied by the corresponding width interval to yield a discharge (m^3/s).

(i) q_{TOP} :

The 'top' bin is the depth bin that extends to the water surface. Its depth is equal to the sum of the blanking distance in front of the ADP transducers (constant = 0.40 m) and the mounting depth of the transducers beneath the surface (0.37 – 0.45 m). The mounting depth was constant for any given deployment in a sub-reach, although it often varied slightly between deployments. There are no measured velocities in this bin. In order to estimate the water flux

through this bin, the velocity from the next lowest bin (i.e. the shallowest measured velocity) was assumed to be constant to the surface.

(ii) q_{BOTTOM} :

The size of the 'bottom' bin is dictated by the total measured depth, the 'top' bin size and the specified bin size for data collection. The ADP will return velocities for bins that are embedded in the bottom, and therefore invalid data must be removed with knowledge of the estimated water depth, as follows:

$$b_{valid} = \left\{ \text{int} \left[(d_w - d_{md} - d_{bd}) / d_{cs} \right] \right\} - 1 \qquad (16)$$

where b_{valid} is the number of valid depth bins, 'int' is the integer part of the quotient, d_w is the total water depth, d_{md} is the mounting depth, d_{bd} is the blanking distance, and d_{cs} is the bin depth. Although the ADP user sets a bin depth for data collection, the true spatial extent of an ADP bin is twice the user-selected size (see Section 3.1). Therefore, simply calculating the integer number of possible bins of size dcs in the measured water depth would mean that the bin closest to the bottom would be incorporating at least some bottom influence. This is accounted for by subtracting one bin from the potential number of valid bins, which leaves only bins with velocities not corrupted by the bottom reflection. Thus the 'bottom' bin depth is the remainder of the total measured depth once the 'top' and valid bin depths are accounted for. A linear decrease to zero velocity at the channel boundary is assumed, therefore the velocity in the 'bottom' bin is one-half of the measured velocity in the last valid bin.

The remaining valid bins are of uniform, pre-determined size (i.e. d_{cs}) and therefore the estimated water flux at a vertical, q_v, (m^2/s) can be represented as:

$$q_v = q_{TOP} + q_{BOT} + d_{cs} \sum_{j=2}^{n-2} v_j \qquad (17)$$

where n = total number of bins in the vertical, including top and bottom.

The ADP water velocities are given in an East-North-Up coordinate system, and individual lines of data had only an approximate cross-stream orientation (**Figure 8**). To obtain a constant frame of reference, discharge for each sub-reach was defined with reference to a 'downstream' orientation derived from the sub-reach bank line orientation. Downstream

direction (with respect to true North) for each sub-reach is based on a GIS representation of the 1999 bank lines in the gravel reach (**Table 5**).

Water velocities were then projected onto the defined downstream axis to yield speeds with a uniform orientation (positive, if oriented downstream). Downstream velocities were derived as follows:

$$v_{ds} = spd \times \cos(\theta_{ds} - \theta_{ADP}) = spd \times \cos(\omega) \quad (18)$$

where spd is the ADP-derived water speed for a given bin, θ_{ds} is the downstream direction (a constant, within a sub-reach), θ_{ADP} is the ADP-derived water direction, for a given bin and ω is the difference between the two angles.

Table 5 'Downstream' direction (referenced to true North) for all sub-reaches.

channel & sub-reach	downstream (°) [a]
Calamity – u/s	260.0
Calamity – mid	269.5
Calamity – d/s	217.6
Carey – u/s	269.5
Carey – u/s mid	269.5
Carey – d/s mid	246.1
Jesperson – u/s	241.3
Jesperson – mid	272.0
Jesperson – d/s	338.3
Hamilton – mid	311.7
Hamilton – d/s	273.7
Queens – mid	225.2
Grassy – mid	227.9
Minto – mid	211.2
Gill – mid	277.4
Big – mid	282.7

[a] based on GIS map of 1999 banklines

In a similar fashion, distances between profiles were projected onto the cross-stream axis to yield a width between profiles in the cross-stream plane:

$$w_{cs} = w_{GPS} \times \cos(\theta_{cs} - \theta_{GPS}) = w_{GPS} \times \cos(\beta) \quad (19)$$

where w_{GPS} is the horizontal distance between profiles, θ_{cs} is the pre-determined cross-stream direction, θ_{GPS} is the orientation of the horizontal line connecting two profiles and β is the offset between the two angles. The width that is applied to the flux at a given vertical is the sum of one-half of the cross-stream distance to both adjacent profiles:

$$w_v = \frac{1}{2}\left(w_{cs_{v-1}} + w_{cs_v}\right) \tag{20}$$

where $1 < v < k$ (refer to **Figure 10** for clarification). If the profile is either first or last on a line, the width is simply one-half the distance to the adjacent profile, as there is no basis on which to assign a representative shoreward width. Discharge through the channel edges is handled in a separate calculation.

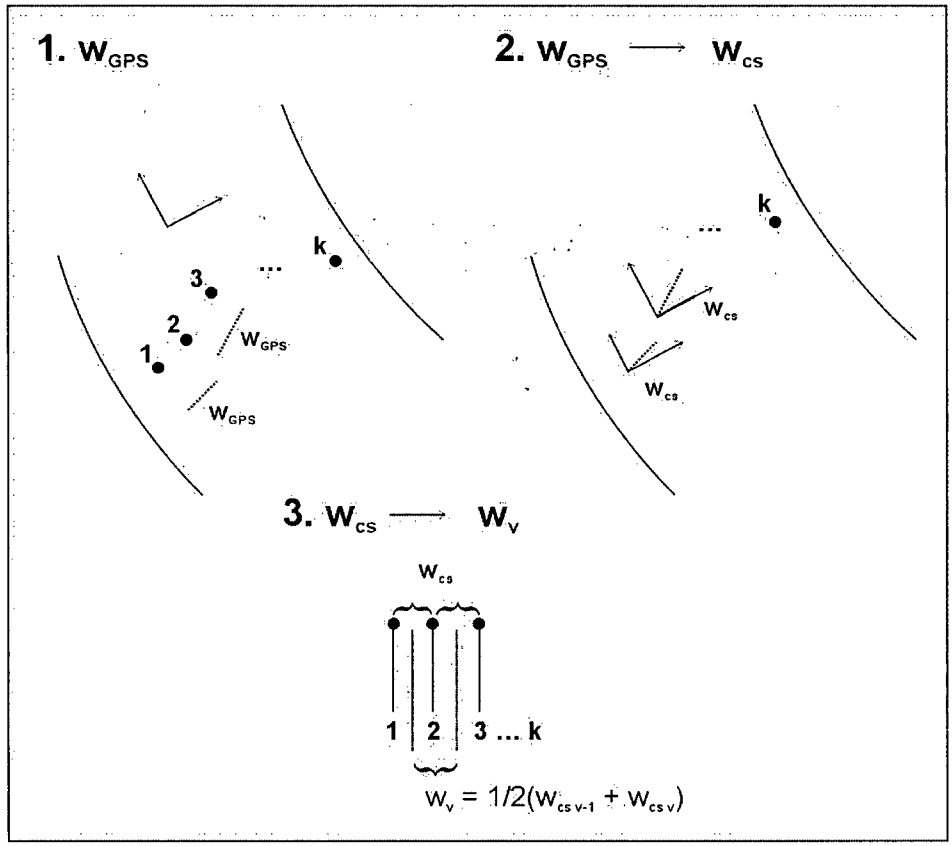

Figure 10 Schematic detailing the reduction of ADP width data. Contrast with the cross-sectional schematic in **Figure 9**.

2. Q_B (channel edges)

The discharge calculation for the near-shore areas of the channel is slightly different. Distances were measured from bank markers to the waterline for each round of measurements. Marker position was established in geographic coordinates using GPS measurements and from

those positions, the waterline could be assigned a geographic location. Thus the distance between the last ADP profile and the waterline is known. In low-flow conditions, depending on channel geometry, this distance can be a substantial part of the total water surface width. In high-flow conditions, the channel edge was defined to be at the edge of perennial, woody vegetation since water velocities overbank (as defined by this convention) were negligible in comparison with in-channel velocities. In reaches where there was minimal bank vegetation, such as in bar-head locations, the position of the on-shore markers was assumed to represent the edge of the channel. Near-shore discharge estimates were calculated independently for both banks, although equations will refer to the general term "Q_B".

(a) Extrapolation to zero

When channel geometry and flow conditions permitted boating into near-shore locations with the ADP, the bank discharge was estimated by a simple extrapolation of the last (or first) ADP flux to zero at the waterline, as follows:

$$Q_B = \frac{1}{2} \times q_v \times w_B \tag{21}$$

where v is equal to 1 or k. The width of channel (in the cross-stream plane) from the first/last profile to the waterline is determined during the analysis in MATLAB, using a plot of waterline position and ADP profile position.

(b) Near-shore velocity measurements

Where it was considered that a substantial portion of the near-shore channel was not adequately represented by the ADP measurements, hand-held velocity meter measurements were taken (see Section 2.2.1). Measurements were taken at regularly paced intervals from the waterline. An average velocity-depth product was generated from these measurements and was assumed to represent the near-shore water flux. Thus the near-shore discharge is simply a product of the distance from the last ADP profile to the waterline and the average near-shore flux:

$$Q_{BANK} = \left(\frac{1}{m} \sum_{l=1}^{m} d_l \times v_l \right) \times w_{BANK} \tag{22}$$

where m is the number of near-shore measurements taken at a given line. Values of m ranged from 3 to approximately 30, depending on the pacing interval, the channel shape and the water

level. The width is derived in the same manner as described previously for the near-shore extrapolation to zero.

***Method 2**: Files with sparse bottom-tracking and good GPS signal reception.* Where bottom-tracking coverage was poor but the GPS signal was of good quality, a different method was used to calculate discharge through the reach. Substantially, the mechanics are the same as Method 1 (see previous section). The main difference is that all profiles with good GPS are included, whether or not they have bottom-tracking. Again, similar to Method 1, two values for discharge are calculated: one value incorporates velocities referenced to bottom-tracking where the data quality permits, and GPS-referenced velocities otherwise, and the other estimate uses solely GPS-referenced velocities.

As discussed in Section 3.1.1, when using ADP data with no bottom-tracking signal, it is necessary to have an alternate measure of channel depth. Data from the chart-recording depth sounder were used for this purpose (see Section 3.1.3 for a comparison of depths from the ADP and the depth sounder). The depth estimates from these two instruments diverge and Method 1 uses only ADP bottom-tracking depths. To ensure comparability between discharge estimates derived using the different methods, in Method 2 a regression was run on profiles with both good bottom-tracking and a depth estimate from the depth-sounder. The depth sounder was used as the predictor variable for the bottom-tracking depths. Profiles without bottom-tracking were then assigned a depth by estimating a predicted bottom-tracking depth based on the regression output.

***Method 3**: Files with good bottom-tracking and no GPS signal reception.* Due to problems in GPS signal reception, there were a number of rounds of measurements in different sub-reaches that lacked reliable GPS position data. Without these data, it was not possible to run either Method 1 or Method 2 to calculate discharge. In addition, many of these reaches had sparse bottom-tracking coverage. In some cases, poor GPS reception affected every round of measurements made in a particular sub-reach (e.g. Hamilton d/s). In order to salvage these measurements, a third method was developed to attempt to estimate discharge from the available

data: depths were taken from the depth-sounder, water velocities were referenced to bottom-tracking (when available) and water surface widths were derived from on-shore measurements.

The digitized depth-sounder charts were integrated and then divided by the length of the chart to obtain an average depth for the navigable part of the channel (d_{CHART}). A mounting depth of 0.155 m was added to the average. An average was taken for all cross-sectional lines to obtain the average d_{CHART} for the sub-reach. Velocities were treated in a fashion identical to Method 1 (and Method 2) and projected into the imposed downstream plane. Profiles were truncated based on bottom-tracking (where available) and then profile averages were created for those profiles with bottom-tracking coverage. Finally, an average downstream velocity over all valid profiles was calculated. Water surface widths measured during the on-shore survey were used to calculate an average width for the sub-reach. Widths were truncated in a manner similar to that applied in Methods 1 and 2 for overbank flows. Discharge was calculated simply as the product of the average depth, width and velocity and cross-sectional area was calculated as the product of the average width and depth.

In order to test how well the results of Method 3 might agree with Method 1, Method 3 was applied to two sub-reaches with good bottom-tracking and GPS signal reception (Jesperson d/s and Carey u/s). The preliminary agreement was poor: Method 3 could predict widths very well (because the measurement was essentially identical between the two methods), but had a tendency to overestimate the average depth and hence to also overestimate the cross-sectional area and discharge. Velocities also tended to be overestimated. These overestimates were a result of not accounting for that part of the channel near the banks, where boating was not feasible. In Method 1 a near-shore extrapolation was performed on the basis of the boat position and the waterline position. However, without GPS data, it was not possible to use this method to estimate distance to shore in Method 3. Instead, distance to shore was estimated on the basis of field notes (visual estimates from the boat, to the nearest meter) or from near-shore current meter measurements (which were taken at paced intervals from the waterline). In early rounds of measurements, neither of these estimates was available and distances were estimated on the basis of information from subsequent rounds. These widths are fairly subjective and will tend to be more reliable when the distances are short (e.g. less than 5 m). However, they were used for lack of any better estimate.

The measured water surface width was divided into the mid-channel, boated width (w_{CHART}) and the left-bank and right-bank widths (on the basis of the estimates). A simple weighting scheme was applied to the depth measurements:

$$\bar{d}_{adj} = \left[\bar{d}_{chart} \times w_{chart} + \left(\frac{\left(\bar{w}_{LB} \times \bar{d}_{LB}\right) + \left(\bar{w}_{RB} \times \bar{d}_{RB}\right)}{2} \right) \right] \Big/ \bar{w}_{total} \qquad (23)$$

The weighting scheme assumes a linear extrapolation from the last measured depth to zero at the bank, and hence the left-bank and right-bank *w-d* products are divided in half. A simplified version of the correction was applied to the mean velocity: left-bank and right-bank velocities were unknown and therefore the mean velocity was used instead.

The adjusted results from Method 3 were then compared to the results from Method 1 (**Figure 11**, **Figure 12**). Some scatter is evident in the relation between the output from the two discharge calculation methods but overall the relations appear to be linear and fairly tight. However, many of the relations (particularly those based on the Carey u/s data) are biased. The magnitude of the bias is related to the ability of the nearshore correction to decrease the average depth and velocity accurately. For two rounds of measurements in Carey u/s mid, it was possible to compare nearshore width estimates derived from field notes and/or hand-held current meter measurements and those estimated from the plot of ADP profile and waterline location. Data were adjusted using both of these width estimates and then plotted on the same graphs: squares "□" were used to indicate data points where the nearshore widths had been estimated from the plot, rather than the field notes. It appears that the field note-based widths underestimated the true nearshore widths, which caused a systematic positive bias in the output from Method 3 (**Table 6**). Positive bias indicates that the output from Method 3 is greater than that from Method 1. However, when nearshore widths are more accurate the bias is fairly small (i.e. CAR b and JES, in **Table 6**). There is no way to evaluate the accuracy of the nearshore width estimates in reaches with poor GPS signal reception but we can infer from this comparison that the likely effect of a bias will be to overestimate all output parameters.

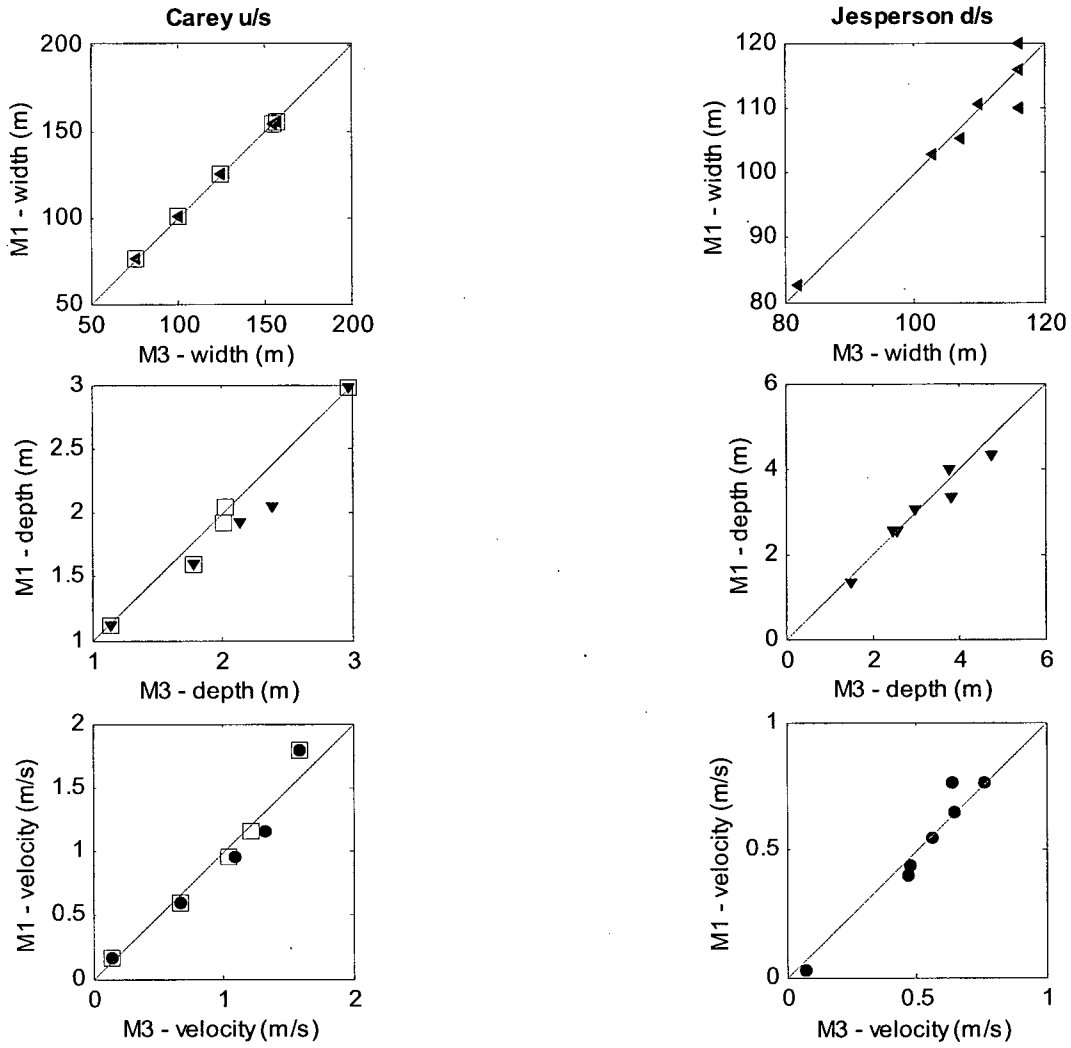

Figure 11 Results of comparison between mean velocity (m/s) and water-surface width (m) from Method 1 (M1) and Method 3 (M3) discharge calculations. Points correspond to an individual round of measurements in a given sub-reach and are averages for the sub-reach. Where two series occupy a single plot, points shown as squares "□" have alternate nearshore widths (see text for details). Points plotted with the standard symbol use nearshore widths derived from field notes. A one-to-one line is shown for comparison.

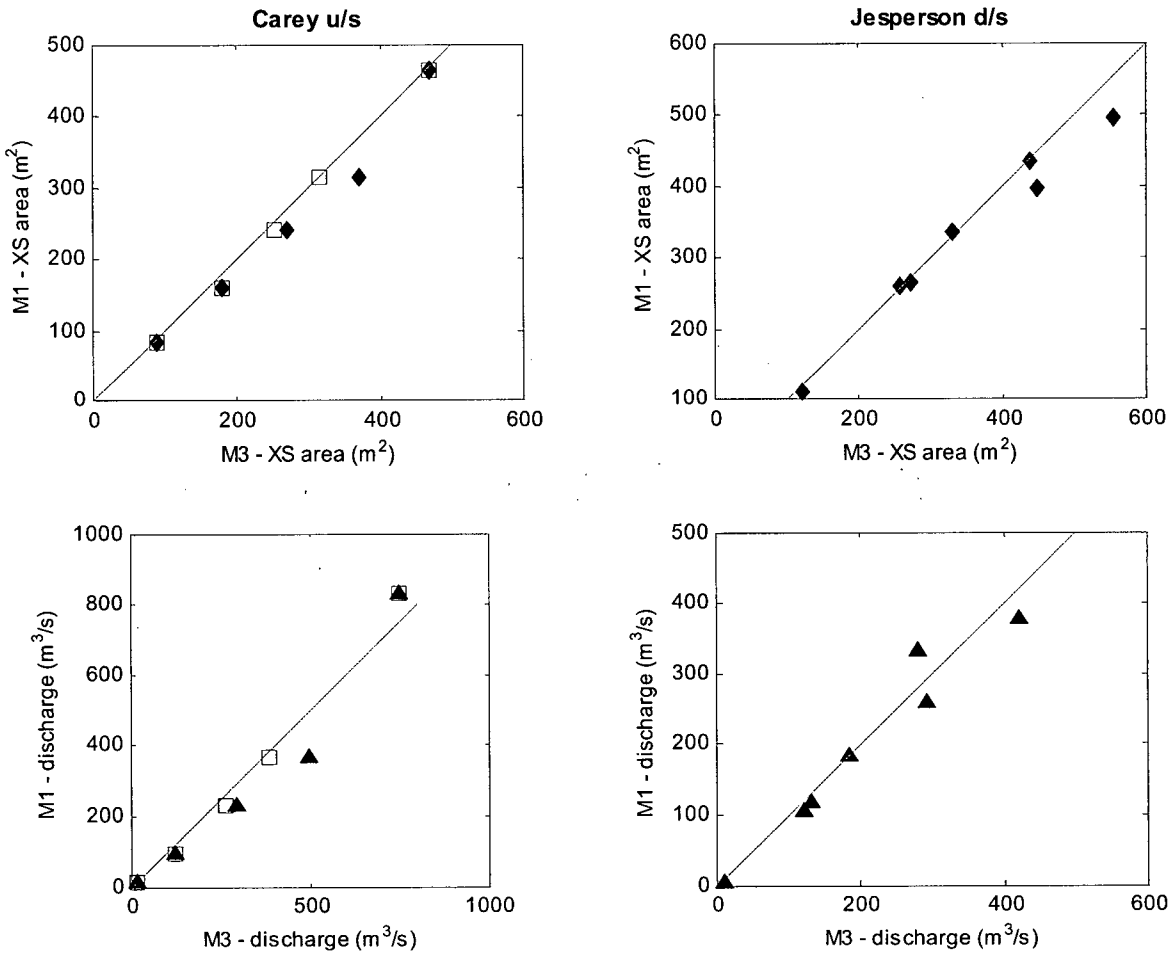

Figure 12 Results of comparison between cross-sectional area (m^2) and discharge (m^3/s) from Method 1 (M1) and Method 3 (M3) discharge calculations. See **Figure 11** caption for plot details.

Table 6 Bias[a] in relation between Method 3 and Method 1 output parameters.

	Depth		Width		Area		Velocity		Discharge	
	m	%	m	%	m^2	%	m/s	%	m^3/s	%
CAR [b]	**0.16**	*8.5*	**0.71**	*0.5*	**21.98**	*9.1*	**0.03**	*3.7*	**26.09**	*13.7*
CAR [c]	**0.06**	*3.6*	**0.71**	*0.5*	**7.35**	*4.1*	**0.001**	*0.7*	**-2.16**	*5.0*
JES	**0.14**	*4.8*	**0.49**	*0.5*	**17.87**	*5.1*	**0.003**	*18.6*	**8.29**	*25.4*

[a] absolute bias calculated as: M3 – M1, bias normalized by M1 for percentages

[b] nearshore widths estimated from field notes

[c] where possible, nearshore widths estimated from a plot of ADP profile and waterline location

***Method 4**: Low-flow measurements.* In many of the sub-reaches, boating became impossible before the channel had stopped flowing completely. Either the sub-reach was not

accessible by boat or it was impractical to deploy the ADP in the sub-reach because of shallow water depths. In these cases, an attempt was made to collect the necessary velocity data to calculate discharge by using the hand-held velocity meter. Data were collected in a manner similar to near-shore velocity measurements and simply carried on to the opposite bank, if possible. Due to variations in channel depth within individual sub-reaches, it was not always possible to collect velocity data at more than one cross-section, although this was always attempted.

Water surface widths and slope were measured in the same way as previously described for Methods 1, 2 and 3. Because the interval between velocity measurements was not measured but can be assumed to be more or less regular, discharge was calculated by assuming that each velocity measurement represented a certain increment of the channel width. The increment was defined as the water surface width divided by the number of measurements (including both waterlines, where the velocity and depth were assumed to be zero). The calculation of discharge was then a straightforward sum of all incremental discharges across the channel.

It is important to note that these rounds of data collection (often providing the lowest-flow point for the hydraulic geometry relations) represent a significant shift in methodology. The measurements were not reach-averaged when discharge was measured only at a single cross-section: although water surface widths could still be measured at all cross-sections, depths could not. Therefore, it seemed most straightforward to use only the average depth from the measured cross-section and the width estimate from that same cross-section to present the channel parameters. This suggests that depth will be underestimated, since the other cross-sections were not feasible to wade. Widths were commonly more uniform within the sub-reaches, although not always. In some sub-reaches, changes in bottom topography (e.g. riffles, point bars) became prominent at low flow and caused a major variation in water surface width (e.g. Carey m/r/d, Hamilton m/r). When data were collected at more than one cross-section, the data were averaged over the measured cross-sections.

3.2.2 Correction for compass bias

As discussed previously, the ADP's internal compass was discovered to have a bias. The magnitude of the bias was variable during any given round of data collection and seemed to be

affected by the orientation of the boat. We decided that, given the magnitude of the error induced in the downstream velocities (relatively small because it is a cosine error), a simple correction for the mean bias in cross-sectional lines would be applied in sub-reaches where the BT and GPS boat trajectories could be assessed. Mean bias was determined by comparing the direction of boat travel for the two references over all profiles in cross-sections that were determined to have valid data (**Figure 13**). The bias, ϕ, was calculated for each profile as:

$$\phi = \alpha_{BT} - \alpha_{GPS} \tag{24}$$

where α_{BT} and α_{GPS} are the direction (degrees from true North) of the boat-trajectory given by bottom-tracking and GPS, respectively. An average and median were taken over all valid profiles (in the case where the distribution of differences was highly skewed). **Figure 14** shows the distribution of compass bias measurements for cross-sectional lines in one sub-reach.

Although ADP velocities were projected onto the downstream axis on a bin by bin basis, we wished to calculate a mean correction factor that could be applied to the summary results of the discharge calculation. Considering an individual bin, recall the original projection in equation (18). The offset, ω, between the imposed downstream direction and the measured ADP velocity direction actually includes the compass bias. We would like to adjust v_{ds} for the effect of this bias by applying a correction factor, x_c:

$$v_{ds}' = spd \times \cos(\omega - \phi), \quad x_c = \frac{v_{ds}'}{v_{ds}} = \frac{\cos(\omega - \phi)}{\cos(\omega)} \tag{25}$$

The measured offset between the direction of water velocity and the imposed downstream direction, ω, varies as the velocity direction varies. In order to calculate a correction factor which is applicable to the average d/s velocity (and by extension, to the average discharge), we must estimate an average ω for the sub-reach. This was achieved by averaging the measured velocity direction for valid profiles. Given that the measured velocity direction also depends on the boat-motion reference, the average was performed separately for each boat-velocity reference. For the most part, the mean corrections were quite small: ± 0 - 3%.

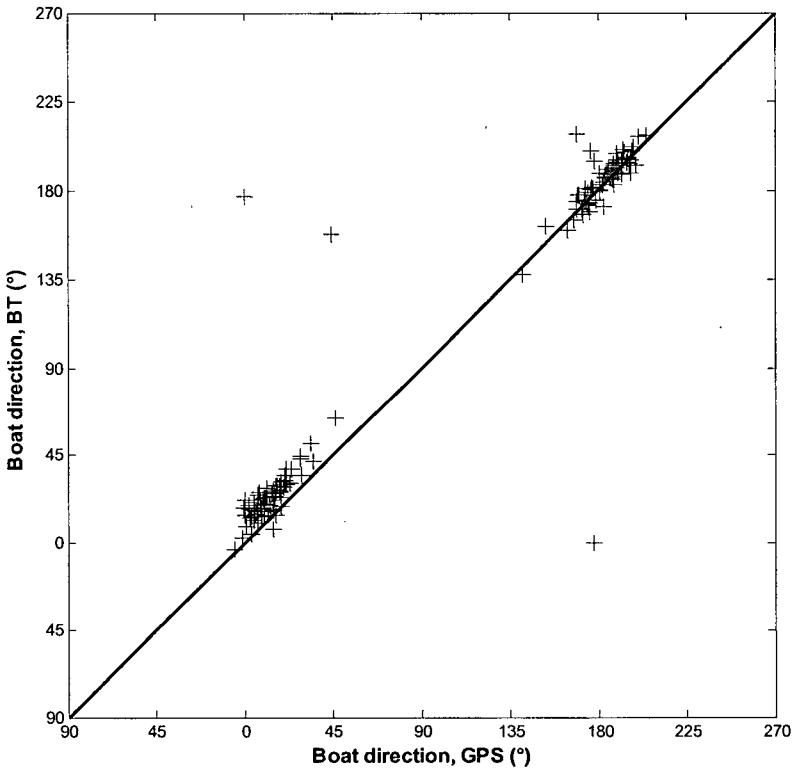

Figure 13 Scatter-plot of boat direction using different references (GPS and BT) corresponding to the data in **Figure 6**, for cross-sectional lines only. The two clusters of points represent the two cross-channel trajectories (i.e. LB to RB and vice versa). Note the change in bias magnitude between the two cross-channel trajectories.

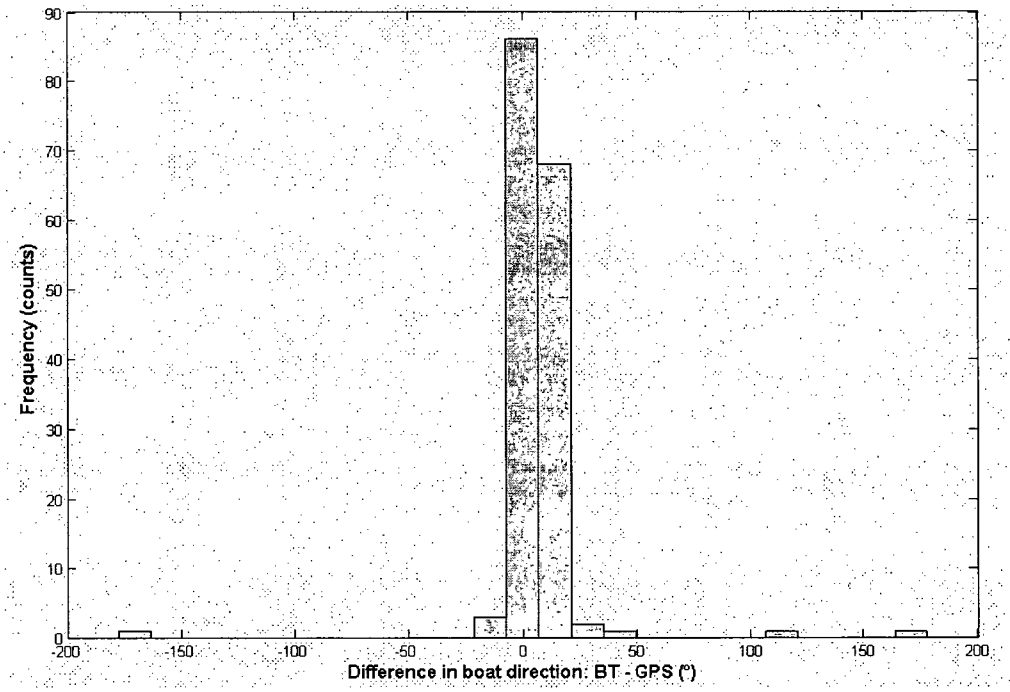

Figure 14 Histogram of the bias measurements shown in **Figure 13**.

This correction could be applied in all cases where it was possible to derive two independent boat-velocity estimates for some portion of the data. However, the files processed using Method 3 had, by definition, only one estimate of the boat velocity, by bottom-tracking. In some sub-reaches Method 3 was applied in only one or two rounds out of the total number of rounds of data collected. For these instances, the correction factor was averaged over all rounds where it could be determined, and applied to the output from Method 3. Some sub-reaches such as Hamilton m/r and d/s had no rounds in which a correction factor could be calculated. The output from these sub-reaches remains uncorrected for potential compass bias. This should not present too great a problem since the magnitude of the correction was generally small.

3.2.3 Error analysis of the discharge calculations

An error analysis was performed to determine the precision of the discharge estimates as a function of the uncertainties in the data used. Standard error propagation principles for functions of multiple variables were applied (see Beers, 1957; Taylor, 1982; Barford, 1985). The precision of certain measurements was unknown and had to be estimated. In many cases, the error estimate due to precision was smaller than the scatter in the data due to random variation.

Error analysis: ***Method 1***

1. Error in Q_{ADP} (channel center)

The error in Q_{ADP} arises from errors in the calculation of profile fluxes (q_v) and widths between profiles (w_v). The error in the calculated water flux at a vertical, q_v, is the root sum square of all the bin errors. The relative error in the flux through a bin, q_j, is calculated as:

$$\frac{\delta q_j}{q_j} = \left[\left(\frac{\delta v_j}{v_j} \right)^2 + \left(\frac{\delta d_j}{d_j} \right)^2 \right]^{\frac{1}{2}} \tag{26}$$

where j ranges from 1 to n bins, and where 'δ' indicates estimated error in a given parameter. Therefore, as the flux at a vertical is simply the sum of the bin fluxes, the error in the flux at a vertical is:

$$\delta q_v = \left[\sum_{j=1}^{n} (\delta q_j)^2 \right]^{\frac{1}{2}} \tag{27}$$

The derivation of the estimated error in the velocities and depths by bin is given below.

(a) Uncertainty in ADP velocities

The error in the velocity for any given bin is partially a function of instrument precision (i.e. Doppler noise) and partially a function of the precision of the compass. SonTek (1998) cites a formula for calculating the standard deviation of ADP horizontal water velocity measurements (in m/s), which will be assumed to represent the error in the measured water speed (δv_{spd}) :

$$\sigma_w = \pm \frac{235}{F \times \Delta z \times \sqrt{N}} \tag{28}$$

where F is the operating frequency (1500 kHz), Δz is the depth cell size (0.25 m) and N is the number of pings. The number of pings is equal to the averaging interval (1s) multiplied by the pinging rate (9 pings per second for a 1500 kHz ADP). For the configuration used during data collection, $\sigma_w = \pm 0.209$ m/s.

The second term in the downstream velocity error deals with the error introduced by compass precision. The stated accuracy of the compass is ± 2° (SonTek, 1998), which may or may not be indicative of the compass precision as well. However, in a stationary test of this ADP unit, Rennie et al. (2002) found that the range of the compass data was only ± 0.6° and the standard error was 0.01° (n = 67, 5 second ensemble averages). Given that the data used in the discharge calculation were collected using a shorter averaging interval, it seems more reasonable to assign a conservative value of ± 0.6°. The fractional error in this term is calculated as follows:

$$\delta \cos\omega = |\sin\omega| \times \delta\omega \quad \therefore \quad \frac{\delta \cos\omega}{|\cos\omega|} = |\tan\omega| \times \delta\omega \tag{29}$$

where $\delta\omega$ is in radians. Therefore the fractional error in the calculated downstream velocity is:

$$\frac{\delta v_{d/s}}{v_{d/s}} = \left[\left(\frac{\delta v_{spd}}{v_{spd}} \right)^2 + (\tan\omega \times \delta\omega)^2 \right]^{\frac{1}{2}} \tag{30}$$

The 'tan' function is undefined for θ = ± 90° and it is conceivable that, in low flows, an individual ADP depth bin might return a velocity direction equal to the defined cross-stream direction. This would yield θ = ± 90° and would cause the error-analysis code to return an error many order of magnitudes greater than it should be (due to rounding error associated with binary floating-point arithmetic). As a workaround to this problem, bins in which the velocity direction

was exactly equal to the cross-stream direction had 0.6° added to the measured direction (assuming that this represents an adequate measure of the compass precision).

(b) Uncertainty in water depth

The water depth was measured using the ADP bottom-tracking algorithm. There is no stated precision for ADP depth estimates from bottom-tracking. For one beam, over a hard surface, the error is reported to be ± 1 to 2 cm (B. Macone, SonTek Inc., pers.comm. 2003). Averaging over multiple beams and measuring over a soft or moving bottom both contribute error. For the purposes of assigning some value to the uncertainty in the depth measurement, a nominal value of ± 5 cm has been suggested (B. Macone, SonTek Inc., pers.comm. 2003). It is assumed that the bin depths are known without error between the top and bottom bins (i.e. where $d_j = d_{cs}$). Although the 'top' bin depth is fixed, there is uncertainty in the measurement of the mounting depth, estimated to be ± 1 cm. Therefore δd_{TOP} will be set to 0.01 m and δd_{BOTTOM} will be set to 0.05 m.

Once the error in the flux calculation is known, the error in the discharge calculation at an individual vertical is:

$$\frac{\delta Q_v}{Q_v} = \left[\left(\frac{\delta q_v}{q_v} \right)^2 + \left(\frac{\delta w_v}{w_v} \right)^2 \right]^{\frac{1}{2}} \tag{31}$$

The error in the width parameter is calculated slightly differently depending on whether the vertical in question is at the end of a line of ADP measurements, or surrounded by adjacent ADP measurements. In general, the error in the calculation of cross-stream width is:

$$\frac{\delta w_{cs}}{w_{cs}} = \left[\left(\frac{\delta w_{GPS}}{w_{GPS}} \right)^2 + \left(\frac{\delta \cos\beta}{\cos\beta} \right)^2 \right]^{\frac{1}{2}} \tag{32}$$

where β is the difference between the orientation of the horizontal line between two profiles and the imposed, cross-stream direction. Using the same GPS unit as was used for this project, Rennie et al. (2002) cite an average position drift of 0.7 cm/s, and a maximum of 2 cm/s based on a 15 minute stationary test, sampling at 0.2 Hz. The ADP sampling rate employed for this project was nominally 1 Hz, but in practice was between 0.5 Hz and 0.33 Hz. Assuming that there is no effect of sampling rate on the relative accuracy, average precision should range from

1.4 cm to 2.1 cm, and maximum errors should range from 4 cm to 6 cm. If we assume that the maximum error represents approximately two standard deviations, then δw_{GPS} can be set to 3 cm (using the more conservative value). The compass precision is the same as was derived for the velocity error calculation. For verticals which are either first or last (i.e. for $v = 1$ or k),

$$\frac{\delta w_v}{w_v} = \frac{\delta w_{cs}}{w_{cs}} \tag{33}$$

If the vertical is not at the end of a line (i.e. for $1 < v < k$), the error in width is:

$$\delta w_v = \left[\left(\delta w_{cs_{v-1}}\right)^2 + \left(\delta w_{cs_v}\right)^2\right]^{\frac{1}{2}} \tag{34}$$

Finally, the error for the ADP component of the total cross section discharge is simply the root-sum-square of the absolute errors at each vertical:

$$\delta Q_{ADP} = \left[\left(\delta Q_1\right)^2 + \left(\delta Q_k\right)^2 + \sum_{v=2}^{k-1}\left(\delta Q_v\right)^2\right]^{\frac{1}{2}} \tag{35}$$

2. Error in Q_B (channel edges)

(a) Extrapolation to zero

Due to the form of equation (21), the error in the bank discharge can be calculated in a manner similar to equation (31). However, unlike equation (21) the error in the width measurement for this discharge calculation is a function of multiple factors:

i. the uncertainty in a distance measurement based on data collected on different GPS units at different times
ii. the precision of the width measurement in the field from the bank marker to the waterline
iii. the precision of the width derived from the location figure.

The error in (iii) arises as a result of that part of the discharge calculation where the user is required to define a 'dummy' ADP profile at the intersection of the waterline, the cross-stream plane and the first or last profile in each cross-sectional line. Variation in the user's ability to define this intersection consistently will cause a slight variation in the resulting near-shore width. Repeating the discharge calculation for a single set of data and looking at the distribution of near-shore width estimates permitted an assessment of the possible error associated with (iii). Since no ADP or actual waterline position data were changed between runs, the variation in near-

shore widths was solely due to user input at the stage where the dummy waterline profiles are defined. When the near-shore widths from n = 15 repeats were grouped by cross-sectional line, the mean standard deviation for the left-bank widths was 0.20 m and for right-bank widths was 0.24 m.

However, it is very likely that the error in (i) will dominate over errors in the other two contributing factors. The bank marker positions were obtained by collecting GPS data during the winter following the 2002 freshet. For this application, hand-held March II GPS units were employed (Anon., 1996). Using one unit as a local base station, we were able to make a positional differential correction but there was no absolute ground control available (i.e. the position of the base station was based on the average calculated position). The other GPS unit involved in the w_B calculation is the Trimble unit attached to the ADP. Although this unit has low differential error (the error from one position fix to another) when receiving the differential beacon signal, the absolute error is probably higher (i.e. the difference between the reported position and the real position in geographic space). Absolute error depends on many factors, including the receiver type, availability of differential correction, satellite coverage, atmospheric interference and satellite-to-unit geometry. I consulted with Public Works and Government Services Canada (PWGSC) because of their experience surveying the Fraser River using differential GPS. In general, they find that their differentially corrected data have an *absolute* accuracy of ± 2 m (D. Couture, PWGSC, pers.comm. 2003). Additionally, they have performed some limited testing of non-differentially corrected units and found that the absolute accuracy is approximately ± 10 m.

The calculation of w_B is a simple difference between the position of the first or last ADP profile and the waterline. The position of the waterline is based on the measured distance from bank markers to the water's edge, in the field. It seems safe to assume, based on an order of magnitude assessment, that the error in the waterline position can be approximated by the error in the absolute position of the bank markers. Therefore, the error in w_{BANK} can be calculated as:

$$\delta w_{BANK} = \left[(\delta ap_T)^2 + (\delta ap_M)^2 \right]^{\frac{1}{2}} \qquad (36)$$

where ap_T is the absolute position of the Trimble (ADP) unit, and ap_M is the absolute position of the March unit. Using the suggested values for the errors in these terms yields a δw_{BANK} of 10.198 m. This is likely a very conservative estimate, since errors of that magnitude would be

noticeable when ADP position and bank marker position are plotted together (e.g. apparent boating on top of bank surfaces). However, a more subtle error (i.e. ± 5 m) would be difficult to pick out and would be more representative of the probable error in w_B. Therefore I have set δw_{BANK} to 5 m.

(b) Near-shore velocity measurements

When the bank discharge is derived from separately collected near-shore measurements, the error in the discharge calculation is slightly different. The error in the depth measurement is a function of the precision of measurements taken with a top-set wading rod, estimated to be ± 2 cm. Again, assuming that this figure represents approximately two standard deviations, the value of δd_l will be set at 1 cm. The velocity accuracy is given as ± 2 % of the reading + (± 0.05 ft/sec), based on the specifications for the instrument (Marsh-McBirney, 1990). Based on the previous rationale, the velocity precision, δv_l, is assumed to be 1 % of the reading + 0.01 m/s (after rounding). The precision of the width measurement is given in the previous section. If we let each velocity and depth product be represented by x_l, then the error in the mean product is:

$$\delta\bar{x} = \frac{1}{m} \times \left[\sum_{l=1}^{m} (\delta x_l)^2 \right]^{\frac{1}{2}} \tag{37}$$

and the error in the bank discharge can be calculated in a straightforward manner.

Error analysis: ***Method 2***. The error analysis for discharge calculations using Method 2 is predominantly the same as that used for Method 1. It differs only in the way that uncertainties in the depth measurement are dealt with, as that is where the discharge calculations differ. Profiles that use bottom-tracking to estimate depth are subject to the same error analysis as in Method 1. However, profiles for which the regression of depth-sounder depths against bottom-tracking depths is used are treated slightly differently. I assume that the uncertainty of interest is related to the capability of the depth sounder to accurately predict bottom-tracking depths. A measure of this uncertainty is the standard error of the estimated depth, which takes into account the standard error of the regression and the distance of the predictor from the mean:

$$s_{\hat{Y}_i} = \sqrt{s^2_{Y \cdot X} \left[\frac{1}{n} + \frac{(X_i - \bar{X})^2}{\sum x^2} \right]} \tag{38}$$

where s_{YX} is the standard error of estimate of the regression, and Σx^2 is the sum of squares of the depth-sounder depths (Zar, 1999). The standard error of the estimated depth is the value assigned to δd_{BOTTOM}, whereas δd_{TOP} is the same as in Method 1 (0.01 m).

Error analysis: ***Method 3.*** Discharge calculated using Method 3 is a straightforward product of mean width, mean depth (adjusted for nearshore effects) and velocity (adjusted for nearshore effects):

$$Q_{adj} = \overline{w} \times \overline{d}_{adj} \times \overline{v}_{adj} \tag{39}$$

Therefore the error in Q derives from the error in the product terms:

$$\frac{\delta Q_{adj}}{Q_{adj}} = \left[\left(\frac{\delta \overline{w}}{\overline{w}} \right)^2 + \left(\frac{\delta \overline{d}_{adj}}{\overline{d}_{adj}} \right)^2 + \left(\frac{\delta \overline{v}_{adj}}{\overline{v}_{adj}} \right)^2 \right] \tag{40}$$

Derivations of the formulae for the component errors were determined according to standard rules governing error propagation.

(a) Uncertainty in total width and nearshore width

The water surface width measurements, from which the mean width derives, are based on the distances measured from on-shore markers and the total distance between the markers (given by the survey). The survey had high accuracy and the majority of the uncertainty in the width is likely to be a result of the tape measurements in the field. The error in each individual measurement of total water surface width is not likely to be greater than ± 0.25 m and therefore the error in the mean is simply:

$$\delta \overline{w}_{total} = \frac{1}{n} \times \sqrt{\sum_{i=1}^{n} (\delta w_i)^2} \tag{41}$$

where $\delta w_i = 0.25$ and n is the number of cross-sections measured.

To perform the nearshore adjustment, estimates of left-bank and right-bank distance to shore are necessary. These estimates are based on either visual assessment of the distance or on pacing from shore at estimated 1 m or 2 m intervals (while taking hand-held current-meter measurements). Given the subjectivity of these estimates, it seems likely that the error in the nearshore width estimates will increase with the width being estimated. Therefore the estimated

uncertainty was set at 20% of the estimated width (e.g. when the estimated width is equal to five meters, the error is unlikely to be greater than ± 1 m). Again, these are mean quantities, so the error is pooled in a similar manner to equation (41).

(b) Uncertainty in depth

Although no error specifications are available for the depth sounder used in this project, a commonly specified uncertainty is ±10% of the measured depth. This will likely dominate over other potential sources of error such as errors induced in digitizing the charts or variability in the mounting depth.

(c) Uncertainty in velocity

Estimated uncertainty in individual water velocity measurements was calculated in the same manner as for Methods 1 and 2, following equation (30). The error in the mean velocity is proportional to the inverse of the sample size.

Error analysis: ***Method 4.*** The error analysis for discharge estimates based on hand-held velocity meter measurements taken at a single cross-section was, for the most part, consistent with the error analysis applied to near-shore flow estimates. Estimated precision values for the velocity and depth measurements were identical to those discussed in the Method 1 error analysis (i.e. error in Q_B, when based on hand-held velocity measurements). The water surface width measurement was assigned the same precision as that used in Method 3 (0.25 m). Using these values, standard error-propagation principles were applied to derive an absolute error in the calculated discharge, average depth, average velocity and width estimate.

When more than one cross-section was measured, there was often considerable variation between cross-section estimates (similar to the results of Methods 1 and 2). In these cases, it was decided that the natural variability was more representative than the estimated error (which, by definition, would decrease with the number of cross-sections measured). For these rounds of measurements, errors in average discharge and average depth were calculated as the standard error of the mean for those quantities. The error in mean width was calculated assuming the standard precision value for each width estimate. The average velocity was calculated from the

average discharge and calculated cross-sectional area (from the product of the mean depth and mean width), and thus was assigned an error estimate based on the errors in those terms.

3.2.4 Derivation of "reach-averaged" channel parameters

The intent of this project was to collect data in a distributed fashion over an area of channel, rather than relying on a single cross-section. Spatial averaging could then be performed by estimating the volume of water sampled within the sub-reach, and dividing by the sub-reach length to determine a reach-averaged cross-sectional area of flow. A regular pattern of cross-sectional and longitudinal data-collection lines was maintained to facilitate the calculation of discharge. However, the density of longitudinal lines was much less than that of the cross-sectional lines, due to time constraints during data-collection.

Given the irregular spacing between depth and velocity measurements, averaging over the reach had to incorporate a weighting scheme to emphasize those data in lightly-sampled areas of the channel. We decided to use Voronoi regions (also called Thiessen polygons) to calculate what portion of the total sub-reach area was closest to each point, and to use that area as a weight. Points representing zero depth (i.e. the waterline) were included at the end of each cross-sectional line. A boundary representing the left-bank and right-bank waterline and upstream-most and downstream-most markers was then imposed on the Voronoi regions to truncate them. The volume of water in the sub-reach was then calculated as the sum of the products of all truncated Voronoi region areas multiplied by their corresponding depth measurement. The average cross-sectional area was determined by dividing the volume by the average of the left-bank and right-bank sub-reach lengths (to account for any bank curvature).

There were difficulties in implementing this methodology to calculate volume. In particular, the density of data points in the sub-reach often overwhelmed the MATLAB "Voronoi" algorithm. The problem appeared to be two-fold: the large number of points in general was problematic, and also the tendency for the points to be closely spaced or even co-located, either along lines or because lines overlapped accidentally. In order to allow the algorithm to run successfully, first the cross-sectional data were thinned by including every other point (usually this was a sufficient thinning but in a few cases only every third point could be included). Once a stable configuration had been achieved, the longitudinal points and waterline

points were added and Voronoi regions were calculated again. If the algorithm failed at this point, the longitudinal data were thinned on the basis of proximity to the nearest cross-sectional or waterline point until a second, stable configuration was reached. If the longitudinal data points were too closely spaced (e.g. when collecting data and attempting to make headway against the current), the data were manually thinned until the algorithm ran successfully.

Figure 15 shows one example of Voronoi regions calculated for the d/s mid sub-reach of Carey channel, at moderately high flow. The regions are relatively homogeneous in size, except near the right (North) bank where they are slightly larger. Heavy overhanging bank vegetation prevented the boat from accessing the near-shore area on this bank.

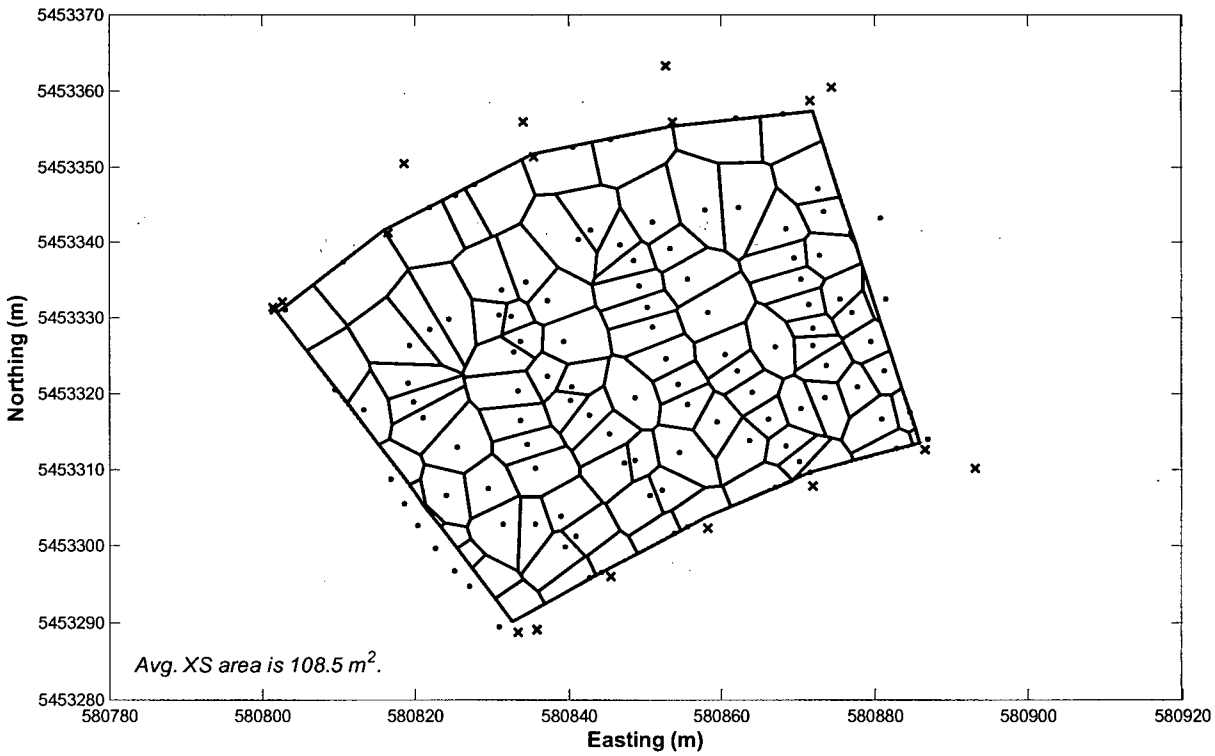

Figure 15 Example of Voronoi regions used to calculate the volume of water in a given sub-reach (9-July-02, Carey m/r/d). Depths corresponding to each region are shown as small points, bank markers are shown as solid 'x's.

Error analysis of volume calculation. The total volume of water sampled in a sub-reach is simply the sum of products of a number of depths and areas. If one assumes that the algorithms used to calculate the Voronoi regions operate without error, then the uncertainty in

each volume is a linear function of the uncertainty in the depth measurement. The errors in the depth measurements, which were considered on a bin-by-bin basis in the error analysis for Methods 1 and 2, were summed for each profile in this error analysis. In each profile, the error for the profile is the root-sum-square of the top-bin and bottom-bin error.

The volume of water sampled divided by the sub-reach length yields an average cross-sectional area. Therefore the uncertainty in the average cross-sectional area must also consider the uncertainty in the measurement of sub-reach length. The average sub-reach length is determined during the volume-calculation algorithm by having the user specify the four corners of the sub-reach boundary. This method was used rather than a pre-specified boundary because of cases in which only a sub-set of the data collected had good GPS coverage. The uncertainty in the length is some function of the accuracy with which the user can specify on-screen a point with a pre-determined coordinate. A simple test of repeatedly specifying the same point on a similar plot in MATLAB yielded an average deviation from the true coordinates of 0.182 m (SD = 0.114 m, n = 20). On this basis, a value of 0.2 m was assigned to the estimated reach length uncertainty.

3.2.5 Analysis of water-surface slope data

Data were collected during each round of measurements in both the at-a-station sub-reaches and the sub-reaches used solely for the scaling relations. In order to facilitate data collection in the field, a simple level survey relating water surface elevation to a local benchmark elevation was conducted separately at both the u/s and d/s ends of each sub-reach. Due to the high water levels, benchmarks in many sub-reaches were submerged at high flow. In some sub-reaches it was possible to place high-water markers on higher ground, but not in some sub-reaches such as CAL d/s, which is bounded by rock on the right-bank and relatively low in elevation on the opposite bank. Because many markers were replaced, a second survey was conducted at low flow (winter 2003) in order to relate the position of the original and high-water markers. Only at this point was it possible to reduce the water-surface slope data.

In general, the water-surface slope data quality was unreliable and the data will not be presented. It proved to be exceedingly difficult to measure the change in water surface elevation over the relatively short channel distances that the sub-reaches represented. Simply ensuring an

accurate placement of the rod on the water surface was often challenging, either due to local fluctuations in the flow, or the logistics of holding the rod on steep or heavily vegetated banks. We avoided areas of slow or stagnant water where possible, but often the logistics of placing markers required a measurement to be conducted in a less than optimal location. Heavy bank vegetation interfered with water movement in nearshore areas, and also made surveying difficult. In sub-reaches where replacement markers could not be implemented, many high-flow measurement rounds lacked data.

3.2.6 Analysis of sedimentological data

(a) Surface sedimentology

Samples were collected, sized in half-phi intervals and tabulated in the field. Grain-size distribution curves were created for each sample and size parameters such as the median grain-size (D_{50}) were interpolated from each curve.

In the case of fine material (both bank sand samples and pipe dredge samples), the field samples were dried at 200°C for 24 hours and then sieved into half-phi categories down to 0.063 mm (phi = 4). Dredge samples were further sized using a sedigraph analysis. Sedigraph samples were comprised of material < 0.125 mm and were first burned in a muffle-furnace at 450°C for 4 hours to remove organic material (which can cause problems for the sedigraph). The sedigraph record was used to separate the material in half-phi increments down to 0.5 micrometers. A composite grain-size distribution was then developed for the original sample.

(b) Sub-surface sedimentology

Field samples were dried at 200°C for 24 hours and then sieved into half-phi categories down to 0.063 mm (phi = 4). A composite grain-size distribution was developed based on the field weights and the laboratory weights. Size parameters were interpolated from the grain-size distribution curves.

4 Results

4.1 Characterisation of sub-reach morphology

Using the data collected in this study, it is possible to create characterisations of sub-reach morphology that encompass flow hydraulics, channel shape and substrate texture. The most compact summary of the channel shape and hydraulics data is in the form of at-a-station hydraulic geometry relations, which will be presented in the following section. Because the data were collected over an area of channel, it is also possible to generate maps showing the spatial distribution of velocities and depths within a given sub-reach. These data can be represented as bivariate histograms of joint velocity and depth distribution. Finally, surface and (in some cases) sub-surface grain-size distribution curves can be presented for each sub-reach.

4.1.1 Hydraulic geometry relations

Once all data files had been analyzed using one of Methods 1-4, and the output had been corrected for compass bias (where possible), the adjusted output was used to create at-a-station hydraulic geometry relations. Given the nature of the classical at-a-station relations, we require only an estimate of discharge as well as two of the three available parameters (i.e. surface width, hydraulic mean depth and mean velocity). The third relation should then be estimated by continuity from the other two. It seems logical that we should use the two parameters which are known with the least error, or which are known most directly. In the case of this study, the water surface width was the parameter which was measured most directly and which was known with low error. The remaining two parameters were derived by less direct means. Based on the collected water depth data, a volume of water was calculated for each round of measurements in a sub-reach. The volume divided by the shore length that it represented provided an average cross-sectional area for the sub-reach. From the average cross-sectional area, the water surface width and the discharge both the hydraulic mean depth and the mean velocity were derived. However, it seemed that the depths had less associated error than the velocity measurements, and therefore the at-a-station relations for average velocity were derived from continuity from the water surface width and hydraulic mean depth relations, using equations (6) and (7).

The at-a-station relations were derived using functional analysis, rather than simple least-squares regression. The functional analysis should be used in situations such as this where we

desire to estimate the parameters of a curve either for descriptive or comparative purposes (Mark and Church, 1977). Regression would have been inappropriate since the 'predictor' datum is not known without error. The functional analysis will fall somewhere between the conventional regression line and the inverse regression (i.e. a regression where 'Y' is used to predict 'X'). The factor used to convert a regression to a functional relation is the ratio of error variances:

$$\lambda = \frac{E_y^{\,2}}{E_x^{\,2}} \tag{42}$$

As the error in the 'X' variable goes to zero, λ approaches infinity and the functional relation approaches the conventional regression. If the relations are strong and R^2 is high (e.g. > 0.9), the difference between the regression and the functional analysis is not great.

Estimates of error in the hydraulic geometry parameters are therefore necessary for the functional analysis. In the case of the calculated discharges, error estimates resulting from the error analyses were most often smaller than the actual scatter in the data about the best fit line (represented by the standard error of the mean over all cross-section estimates). This suggests that the error estimates may have been too optimistic or that there may be additional sources of error not accounted for in the error analysis. Another possibility is the presence of real, unreduced random or systematic variance in the data. The standard error of the mean of the discharge estimate was used to represent the error in this parameter. For all other parameters, errors were assigned on the basis of the error analyses that were performed.

For the relation of width to discharge and the relation of depth to discharge, λ was calculated by averaging the fractional error of both parameters over all rounds and calculating the appropriate ratio of errors. These values are given in the tables of results (see **Table 7 – 10**). Although λ could be calculated for the relation of velocity to discharge, it was not meaningful because the relation was derived by continuity. Therefore λ was not provided.

The results of the functional analyses are presented for each sub-reach, in a tabulated form. A complete record of the figures corresponding to each relation can be found in **Appendix A**, which includes plots of residuals. The power form is the conventional form chosen to represent the at-a-station hydraulic geometry relations, but there is no *a priori* reason why it must be used (Ferguson, 1986). Each relation was developed using the power form but if there was

significant lack of fit in the residuals, a linear fit was also attempted. If the linear fit improved the goodness of fit (as assessed by the R^2, SEE and residuals plot), it was also presented in the table of results.

In some sub-reaches (JES, CAR and HAM), low-flow data showed a lack of agreement with the trend of the high-flow data, indicating the potential effect of non-zero residuals when Q = 0. These residuals appear as a result of the presence of stagnant water in the sub-reaches, once the channels have ceased to flow. The presence of non-zero residuals cannot be incorporated into a power-law fit, and therefore where these effects were in evidence, high-flow data were analyzed separately. The fit based on the high-flow data was then extended for comparison with the low-flow data (see plots in **Appendix A**). If the goodness of the fit was reduced substantially by analyzing the high-flow data separately, the original relation was also presented, for contrast. No high-flow analyses were performed on the CAL data because of generally poor data quality: it was not possible to discern a plausible non-zero residual effect.

Table 7 At-a-station hydraulic geometry relations for Jesperson channel.

Sub-reach & parameter	Equation [a]	R^2 or I^2 [b]	SEE or SEE* [b]	95% C.I. for slope	n	λ [c]
u/s, w	$w = 51.08Q^{0.141}$	0.996	0.49 m	[0.132 - 0.150]	6 [d]	0.02
u/s, d	$d = 0.097Q^{0.577}$	0.999	0.012 m	[0.568 - 0.587]	6 [d]	0.34
u/s, v [e]	$v = 0.20Q^{0.282}$	n/a	n/a	n/a	6 [d]	n/a
m/r, w	$w = 63.45Q^{0.084}$	0.84	1.95 m	[0.048 - 0.127]	6 [d]	0.03
m/r, w	$w = 53.88Q^{0.114}$	0.99	2.25 m	[0.107 - 0.121]	8	0.06
m/r, d	$d = 0.18Q^{0.531}$	0.95	0.21 m	[0.410 - 0.672]	6 [d]	0.65
m/r, v [e]	$v = 0.088Q^{0.385}$	n/a	n/a	n/a	6 [d]	n/a
d/s, w	$w = 62.08Q^{0.106}$	0.85	2.49 m	[0.062 - 0.163]	6 [d]	0.03
d/s, w	$w = 67.51Q^{0.091}$	0.97	2.27 m	[0.079 - 0.105]	7	0.01
d/s, d	$d = 0.26Q^{0.459}$	0.997	0.04 m	[0.226 - 0.344]	6 [d]	0.12
d/s, v [e]	$v = 0.063Q^{0.435}$	n/a	n/a	n/a	6 [d]	n/a

[a] relations are functional, rather than least-squares regressions

[b] relations which were log-linear were back-transformed in order to calculate comparable goodness-of-fit measures

[c] ratio of errors in the dependent variate to errors in the independent variate (Mark and Church, 1977)

[d] high-flow data only

[e] relation derived from continuity

Table 8 At-a-station hydraulic geometry relations for Carey channel.

Sub-reach & parameter	Equation [a]	R^2 or I^2 [b]	SEE or SEE* [b]	95% C.I. for slope	n	λ [c]
u/s, w	$w = 36.26Q^{0.226}$	0.84	11.92 m	[0.139 - 0.399]	5 [d]	0.03
u/s, w	$w = 43.43Q^{0.197}$	0.94	9.70 m	[0.158 - 0.250]	6	0.02
u/s, d	$d = 0.41Q^{0.288}$	0.95	0.15 m	[0.199 - 0.390]	5 [d]	0.36
u/s, v [e]	$v = 0.068Q^{0.486}$	n/a	n/a	n/a	5 [d]	n/a
m/r/u, w	$w = 48.14Q^{0.098}$	0.96	0.94 m	[0.071 - 0.127]	5 [d]	0.05
m/r/u, d	$d = 0.17Q^{0.476}$	0.94	0.16 m	[0.341 - 0.650]	5 [d]	0.34
m/r/u, v [e]	$v = 0.12Q^{0.426}$	n/a	n/a	n/a	5 [d]	n/a
m/r/d, w	$w = 38.01Q^{0.066}$	0.73	0.999 m	[0.014 - 0.127]	5 [d]	0.05
m/r/d, w	$w = 29.84Q^{0.120}$	0.96	1.50 m	[0.010 - 0.145]	6	0.01
m/r/d, d	$d = 0.36Q^{0.421}$	0.94	0.12	[0.315 - 0.579]	5 [d]	0.10
m/r/d, v [e]	$v = 0.073Q^{0.513}$	n/a	n/a	n/a	5 [d]	n/a

[a] relations are functional, rather than least-squares regressions

[b] relations which were log-linear were back-transformed in order to calculate comparable goodness-of-fit measures

[c] ratio of errors in the dependent variate to errors in the independent variate (Mark and Church, 1977)

[d] high-flow data only

[e] relation derived from continuity

Table 9 At-a-station hydraulic geometry relations for Hamilton channel.

Sub-reach & parameter	Equation [a]	R^2 or I^2 [b]	SEE or SEE* [b]	95% C.I. for slope	n	λ [c]
m/r, w	$w = 46.12Q^{0.104}$	0.98	0.47 m	[0.072 - 0.140]	4 [d]	0.04
m/r, d	$d = 0.098Q^{0.554}$	0.985	0.06 m	[0.431 - 0.693]	4 [d]	0.93
m/r, v [e]	$v = 0.22Q^{0.342}$	n/a	n/a	n/a	4 [d]	n/a
d/s, w	$w = 76.25Q^{0.123}$	0.86	4.57 m	[0.068 - 0.214]	5 [d]	0.02
d/s, w	$w = 58.29Q^{0.167}$	0.96	6.06 m	[0.140 - 0.204]	6	0.01
d/s, d	$d = 0.97Q^{0.246}$	0.98	0.09 m	[0.196 - 0.296]	5 [d]	0.78
d/s, v [e]	$v = 0.0094Q^{0.690}$	n/a	n/a	n/a	5 [d]	n/a

[a] relations are functional, rather than least-squares regressions

[b] relations which were log-linear were back-transformed in order to calculate comparable goodness-of-fit measures

[c] ratio of errors in the dependent variate to errors in the independent variate (Mark and Church, 1977)

[d] high-flow data only

[e] relation derived from continuity

Table 10 At-a-station hydraulic geometry relations for Calamity channel.

Sub-reach & parameter	Form of relation [a]	Equation	R^2 or I^2 [b]	SEE or SEE* [b]	95% C.I. for slope	n	λ [c]
u/s, w	log	$w = 27.21Q^{0.199}$	0.98	3.75 m	[0.174 - 0.226]	5	0.09
u/s, d	log	$d = 0.55Q^{0.273}$	0.89	0.33 m	[0.200 - 0.352]	5	0.47
u/s, d	linear	$d = 0.71 + 0.00767Q$	0.95	0.23 m	[0.005 - 0.010]	5	0.47
u/s, v [d]	log	$v = 0.066Q^{0.528}$	n/a	n/a	n/a	5	n/a
m/r, w	log	$w = 126.34Q^{0.016}$	0.98	0.12 m	[0.012 - 0.020]	4	0.01
m/r, d	log	$d = 0.0031Q^{1.255}$	0.79	0.65	[0.670 - 5.169]	4	0.15
m/r, v [d]	log	$v = 2.52Q^{-0.271}$	n/a	n/a	n/a	4	n/a
d/s, w	log	$w = 51.19Q^{0.078}$	0.595	6.54	[0.0003 - 0.3957]	5	0.01
d/s, d	log	$d = 6.08Q^{0.019}$ [e]	0.17	0.48	[-0.047 - 0.090] [e]	5	0.04
d/s, v [d]	log	$v = 0.0032Q^{0.903}$	n/a	n/a	n/a	5	n/a

[a] relations are functional, rather than least-squares regressions

[b] relations which were log-linear were back-transformed in order to calculate comparable goodness-of-fit measures

[c] ratio of errors in the dependent variate to errors in the independent variate (Mark and Church, 1977)

[d] relation derived from continuity

[e] slope not significantly different from zero ($\alpha = 0.05$)

When the power form was used for curve fitting, the derived functional relation was back-transformed into original units before the goodness of fit was assessed. This enabled a direct comparison to be made between the linear and log-transformed fits. A 95% confidence interval was also calculated for each slope estimate (Church and Mark, 1980) and used to assess whether the slope was statistically different from zero. All slopes shown are statistically different from zero unless otherwise stated.

For the most part, the individual at-a-station relations show good agreement and have relatively low scatter. The notable exception is Calamity m/r and d/s. The range of discharge captured in the m/r did not include a particularly low flow. In addition, the negative slope in the CAL m/r v-Q relation suggests that there may have been a backwater effect in this sub-reach. This theory is further supported by the relation of CAL m/r discharge to main channel discharge, which shows a clearly non-linear trend (**Figure C-15**, p.179). In addition to a backwater effect, this sub-reach was rather heterogeneous in character, with a mid-channel longitudinal bar separating a wide and quiet LB from a narrower, faster-flowing RB. The bar was apparently enlarged during the 2002 freshet by the deposition of new sediment, and thus the 'ponding' effect on the LB was exacerbated. Because of these complications, data from Calamity m/r were excluded from subsequent analyses. In the d/s sub-reach, both width and depth showed little change with discharge and had nearly non-significant or non-significant slopes ($\alpha = 0.05$).

The effect of analyzing high-flow data separately was to generally improve the fit of the d-Q relations. The plots of sub-reach d-Q relations in **Appendix A** clearly show the tendency for lower flow points to plot on a separate trend from higher-flow points (e.g. **Figure A-3**, p.129). The trend almost always indicates the presence of a positive residual (i.e. the lower-flow data plot higher than the high-flow trend would indicate they should). The exception is CAR m/r/d (**Figure A-28**, p.144) where the low-flow datum plots on a lower trend than the high-flow data. This datum point indicates the difficulties of collecting data at low flow, when the presence of cross-section irregularities is most apparent. At this flow, there was an extreme contrast in cross-section parameters (i.e. narrow/shallow/fast-flowing vs. wide/deep/slow-flowing). Although the data were averaged, the presence of the shallow cross-section seems to be still indicated.

In contrast, the fit of the w-Q relations was often poorer when only the high-flow data were considered. By definition, a non-zero depth residual requires the existence of a non-zero

width residual and therefore if the effect of the non-zero behaviour was detected in the d-Q relation, the same analysis was applied to the w-Q relation, and because of continuity, to the v-Q relation. In all cases where the 'high flow' w-Q and 'all-data' w-Q relations are presented, the 95% confidence intervals overlap. The decrease in I^2 in the high-flow analyses is likely more a result of decreasing the range of the 'X' variate, than a true indication of lack of fit. However, the high-flow w-Q data may be less amenable to the power-law fit than the d-Q data because of the imposed maximum width.

Exponents for the at-a-station width and depth relations are plotted in **Figure 16** for comparison. The mean slope for all width-discharge (w-Q) relations is 0.123 (SD = ±0.052), and the mean of all depth-discharge (d-Q) relations is 0.425 (SD = ±0.127). Simply based on the mean exponents, the change in Q is expressed dominantly in a change in mean depth and velocity (slope = 0.452, by continuity), rather than width.

There appears to be a clear stratification of slopes in the w-Q and d-Q relations, which corresponds to sub-reach morphology. Relative to other sub-reach types, u/s sub-reaches tend to have higher slopes for the w-Q relation and lower for the d-Q relation, although JES u/s deviates from this trend by having a relatively high d-Q slope. This deviation may result from the fact that the u/s sub-reach in JES is not really an entrance vicinity sub-reach (like the CAL and CAR u/s sub-reaches). Due to the presence of the flow-control structure, the 'u/s' sub-reach in JES was placed further downstream in the channel, and therefore may bear a stronger resemblance to a m/r morphology. D/s and m/r sub-reaches tend to show the opposite pattern: relatively low w-Q slopes and relatively high d-Q slopes (except for HAM d/s, which has a low d-Q slope). In general, the m/r and d/s morphologies show more resemblance to a straight-sided 'box' cross-section, where there is little change in width with discharge and more change in depth and velocity. The u/s sub-reaches tend more toward a shallow parabolic configuration with greater change in width. These patterns are most likely a result of the proximity of bank vegetation to the channel, which would explain why individual sub-reaches show deviations from the pattern (i.e. HAM d/s, JES u/s). U/s sub-reaches tend to be in bar-head environments where vegetation is newly established and sparse. Jesperson channel does not fit that classification, though; being a very old channel with fully established vegetation. Similarly, slower velocities in the d/s sub-reaches often permit vegetation to establish earlier in comparison to the u/s reaches thus constraining channel width somewhat. However, HAM d/s is the exception, having quite a large

unvegetated sandy expanse on the left-bank. In general, the patterns and the deviations from the pattern simply reinforce the fact that at-a-station hydraulic geometry relations are truly descriptive and will be as variable as the sub-reaches themselves.

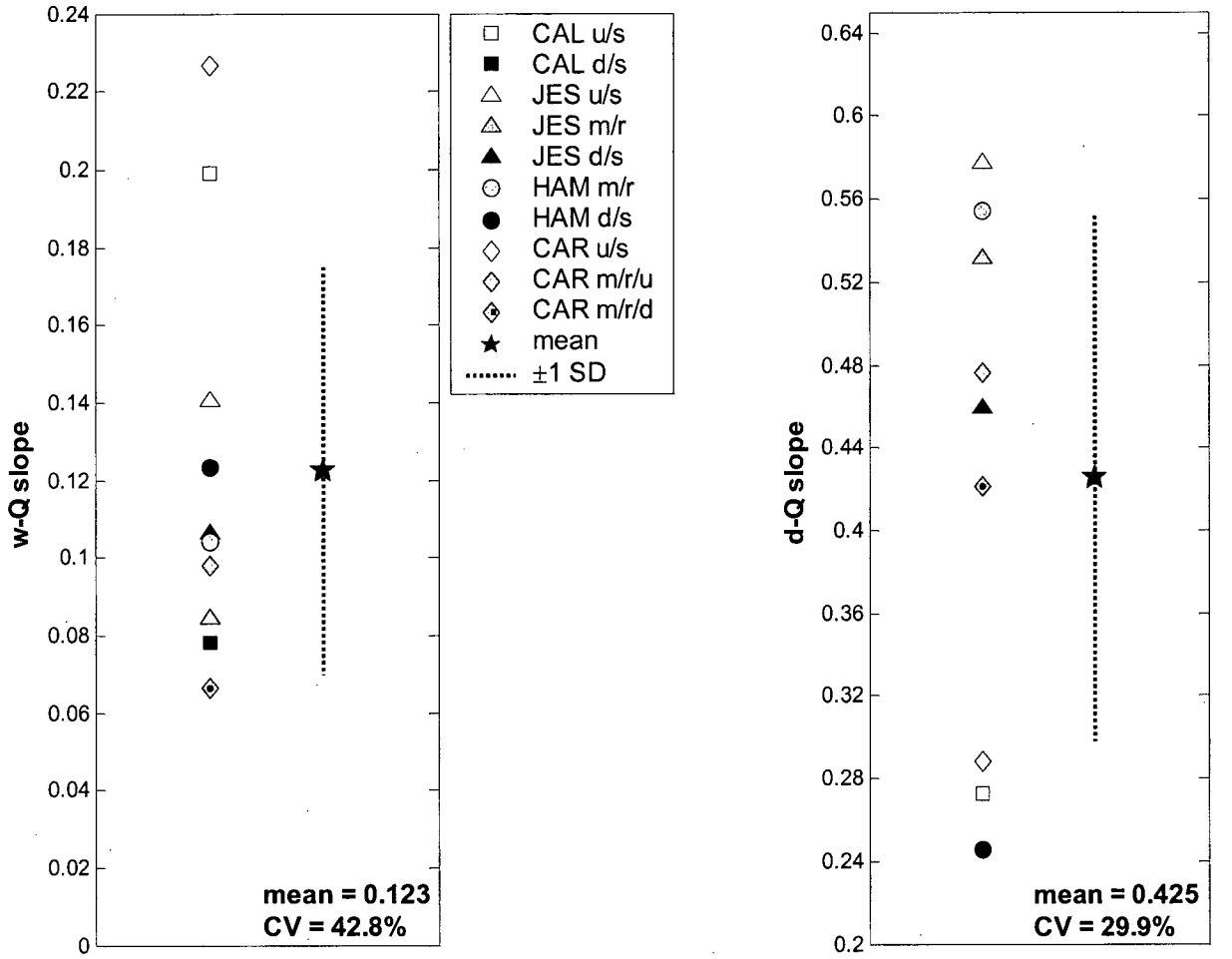

Figure 16 Slopes for at-a-station functional relations (power fit only), for the width-to discharge and depth-to-discharge relations. Note the change in scale between axes. Where separate analyses of high-flow data were performed, the slope presented is that corresponding to the high-flow data only. Non-significant slopes were not plotted and data from CAL m/r were excluded because of their irregularity.

4.1.2 Distributions of depth and velocity

Although hydrologic data are summarized in at-a-station hydraulic geometry relations, a common criticism of these relations is that one loses a great deal of useful information in the process. Mean channel parameters yield little information about variance, which is often of paramount interest when assessing channels for habitat potential. By collecting spatially distributed data in each channel sub-reach, we were able to assess the variance in hydrologic parameters of interest such as velocity and depth. In the case of velocity, we were able to assess not simply the depth-averaged velocity but rather the near-bottom velocity, a quantity that is far more applicable to assessments of fish habitat (Stalnaker et al., 1989).

In order to assess the distribution of near-bottom velocity and depth within the at-a-station sub-reaches, a sub-set of data was chosen corresponding to the highest-flow measurements in each sub-reach (i.e. $Q_{MC} > 8000$ m^3/s). During peak flows, it is hypothesized that fish seek refuge in the secondary channels and therefore it is interesting to assess what sorts of environments are available as refuge. In addition, high flow data points are generally evenly spatially distributed within each sub-reach, since high water levels permitted boating from bank to bank. Even distributions of data points permit better quality spatial mapping and also make interpretation of frequency distributions more transparent. Lower-flow data from certain sub-reaches were also assessed for comparison with the high-flow results, where the channel shape permitted fairly good data coverage (JES m/r, JES d/s and CAR u/s), and/or GPS data permit us to assess which part of the channel did not get surveyed.

Bivariate frequency distributions. For each data file, the subset of ADP profiles with good bottom-tracking coverage was selected, both in the cross-sectional and longitudinal data collection lines. In each ADP water velocity profile, the deepest bin that was uncorrupted by the channel bottom was located. The distance of this bin above the channel bottom varied from profile to profile but ranged from 0.25 to just under 0.5 m (distance from the bottom of the bin to the channel bottom) and the bin size is 0.25 m. Channel depth was measured by bottom-tracking. Water speed data (referenced to BT) were selected from the appropriate profiles and bins. It was assumed that the water speed, independent of direction, would be the most relevant variable to examine for habitat assessment purposes, rather than the projected d/s velocity used

in the calculations of discharge. A correction for compass bias was not required because the correction was applied to direction only. A bivariate histogram of depth and near-bottom d/s velocity was then produced, with bin sizes of one-half m/s for velocity and one-half m for depth. When maximum depths were greater than eight meters, the depth bin size was increased to one meter to maintain the clarity of the graphical presentation. The bivariate histogram output was transformed to percentages and plotted as a contour map. Plots for each sub-reach (grouped by channel) are presented in **Figure 17**, **Figure 18**, **Figure 19** and **Figure 20**.

High-flow data did not always have good GPS coverage, and in one instance (CAL d/s), did not have good BT coverage either. Poor GPS data coverage meant that the evenness of the spatial distribution of data points within the sub-reach could not be assessed. Sub-reaches where this was the case are: JES m/r, CAR u/s, CAL u/s, CAL m/r, HAM m/r and HAM d/s. In the case of CAL d/s, the reverse was true and GPS coverage was good while BT coverage was generally poor. Unlike all other sub-reaches, the GPS was used for a boat velocity reference. In addition, the maximum number of depth bins was set slightly too low for this round of data collection in CAL d/s. Therefore in 37 of 326 profiles the true depth exceeded the maximum number of bins implying that in the deepest parts of the channel, the "near-bottom" velocities may be further from the bottom than expected and therefore have potentially higher speeds than expected.

The frequency plots are shaded, with darker colours corresponding to higher frequencies. The contour interval was generally set to show the 0%, 1% and maximum percent boundaries, with an interval of 2% between these limits. However, the contour interval was sometimes altered to improve the legibility of the plot. All contours except the 0% contour (which forms the inner box around the plot) have been labeled for reference. The bin boundaries are indicated on each plot, although they vary slightly from plot to plot. Data in each bin are greater than the lower boundary and less than or equal to the upper boundary.

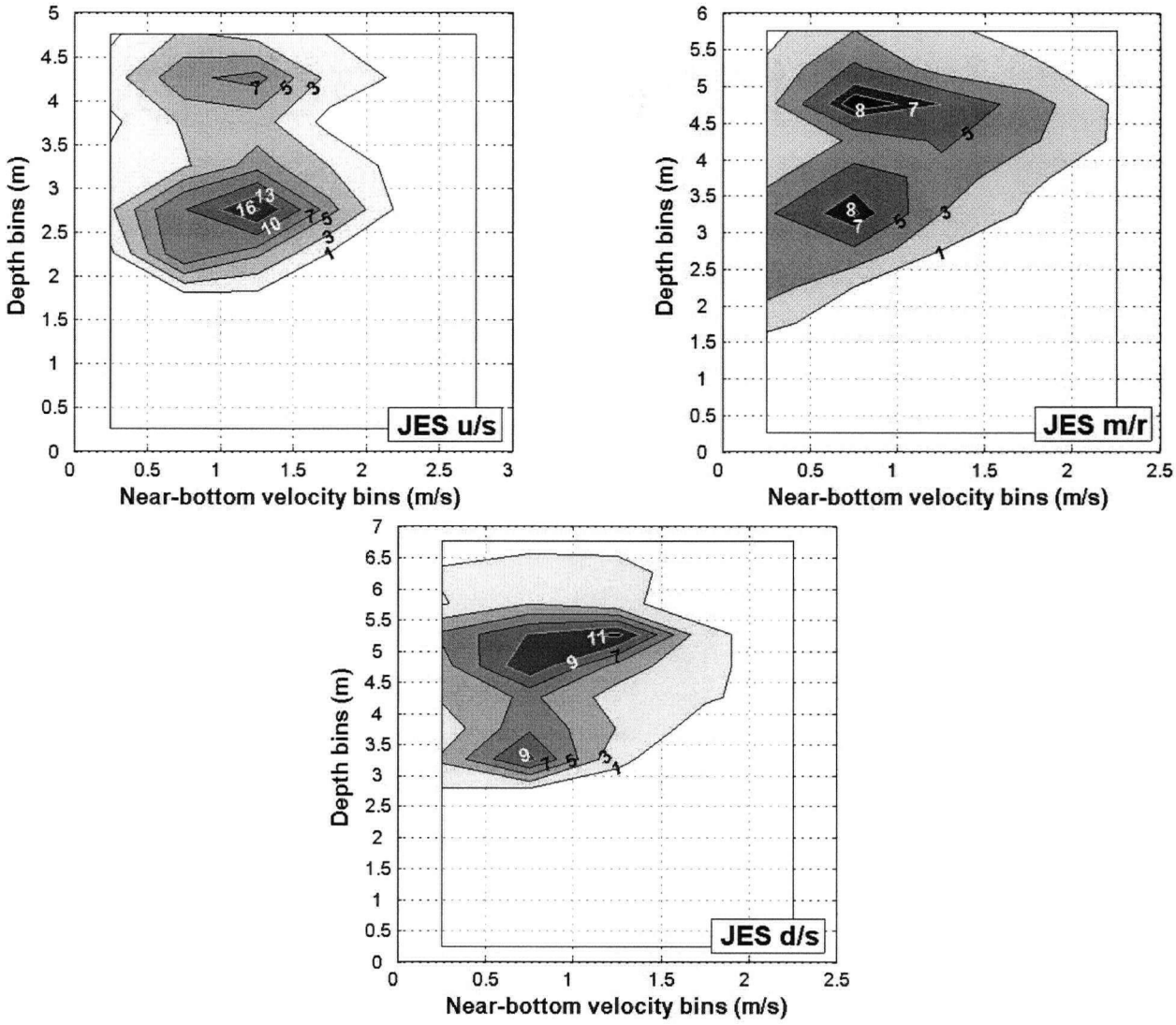

Figure 17 Bivariate frequency distributions of near-bottom d/s velocity (m/s) and depth (m) for all sub-reaches in Jesperson channel at high flow (**JES u/s**: Q_{MC} = 10,015 m^3/s, Q_{SR} = 394 m^3/s; **JES m/r**: Q_{MC} = 10,225 m^3/s, Q_{SR} = 384 m^3/s; **JES d/s**: Q_{MC} = 10,521 m^3/s, Q_{SR} = 447 m^3/s). Histogram output has been converted to percent and mapped as contours of equal percent. Contour interval is variable but contours are labeled, see text for explanation.

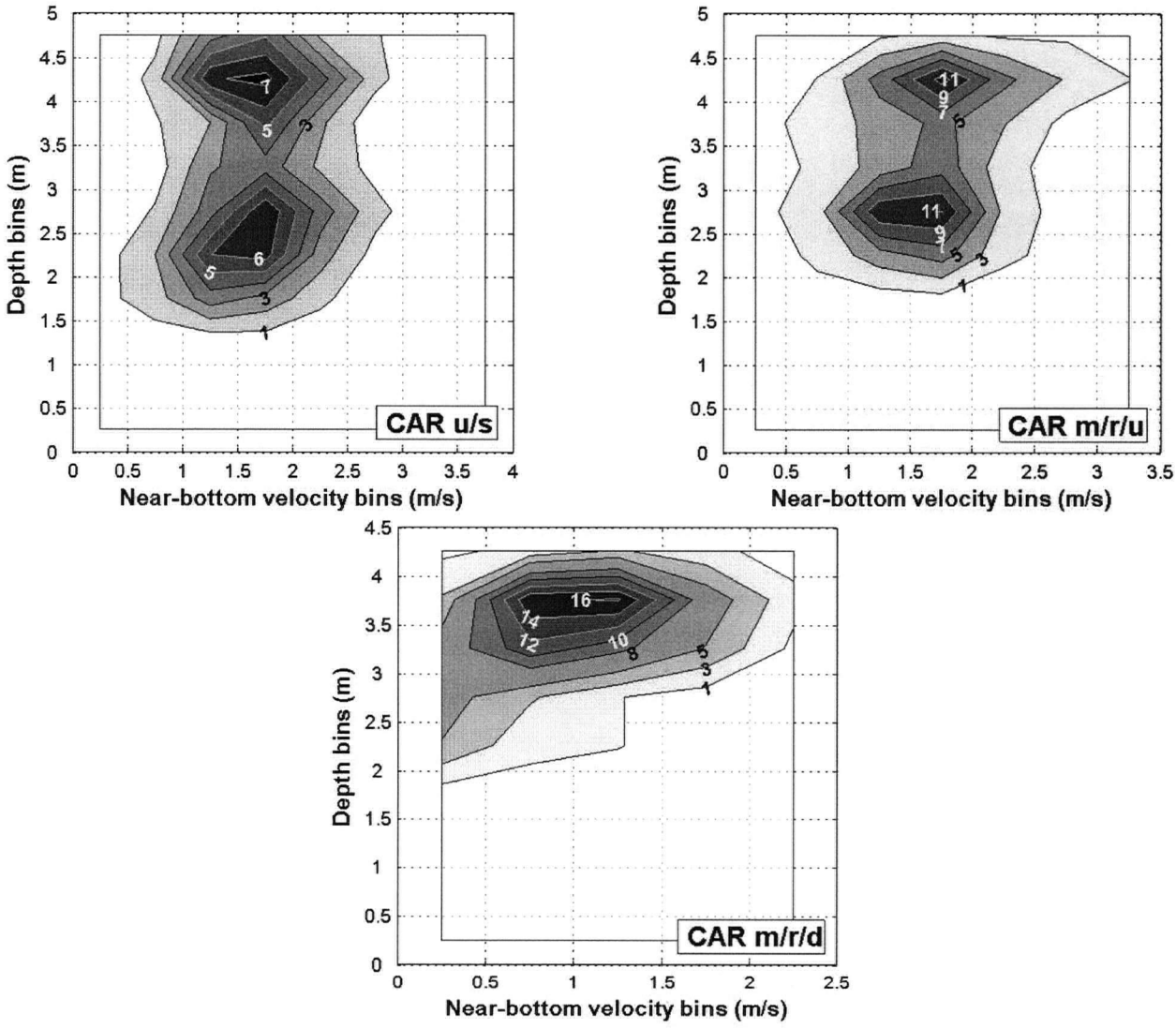

Figure 18 Bivariate frequency distributions of near-bottom d/s velocity (m/s) and depth (m) for all sub-reaches in Carey channel at high flow (**CAR u/s**: Q_{MC} = 9841 m^3/s, Q_{SR} = 853 m^3/s; **CAR m/r/u**: Q_{MC} = 9841 m^3/s, Q_{SR} = 452 m^3/s; **CAR m/r/d**: Q_{MC} = 9556 m^3/s, Q_{SR} = 129 m^3/s). Histogram output has been converted to percent and mapped as contours of equal percent. Contour interval is variable but contours are labeled, see text for explanation.

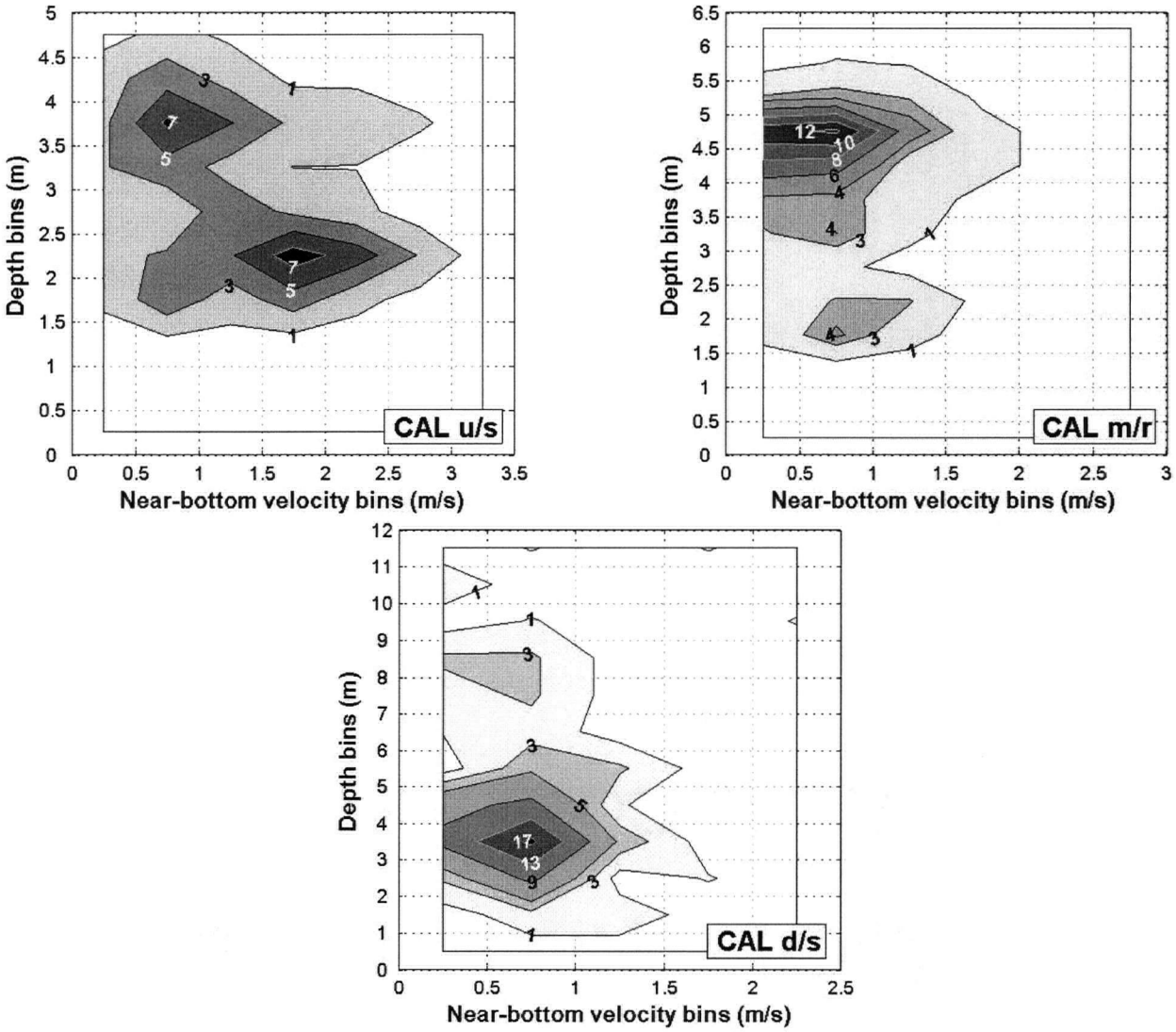

Figure 19 Bivariate frequency distributions of near-bottom d/s velocity (m/s) and depth (m) for all sub-reaches in Calamity channel at high flow (**CAL u/s**: Q_{MC} = 10,681 m^3/s, Q_{SR} = 316 m^3/s; **CAL m/r**: Q_{MC} = 10,681 m^3/s, Q_{SR} = 274 m^3/s; **CAL d/s**: Q_{MC} = 8295 m^3/s, Q_{SR} = 205 m^3/s). Histogram output has been converted to percent and mapped as contours of equal percent. Contour interval is variable but contours are labeled, see text for explanation.

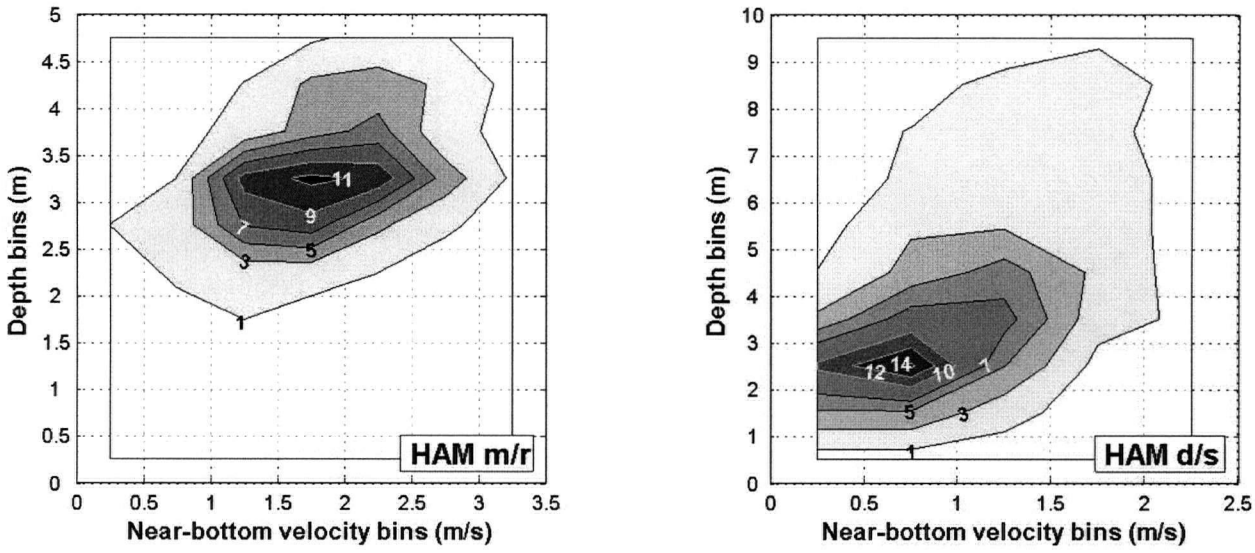

Figure 20 Bivariate frequency distributions of near-bottom d/s velocity (m/s) and depth (m) for both sub-reaches in Hamilton channel, at high flow (**HAM m/r**: Q_{MC} = 10,017 m^3/s, Q_{SR} = 574 m^3/s; **HAM d/s**: Q_{MC} = 10,017 m^3/s, Q_{SR} = 667 m^3/s). Histogram output has been converted to percent and mapped as contours of equal percent. Contour interval is variable but contours are labeled, see text for explanation.

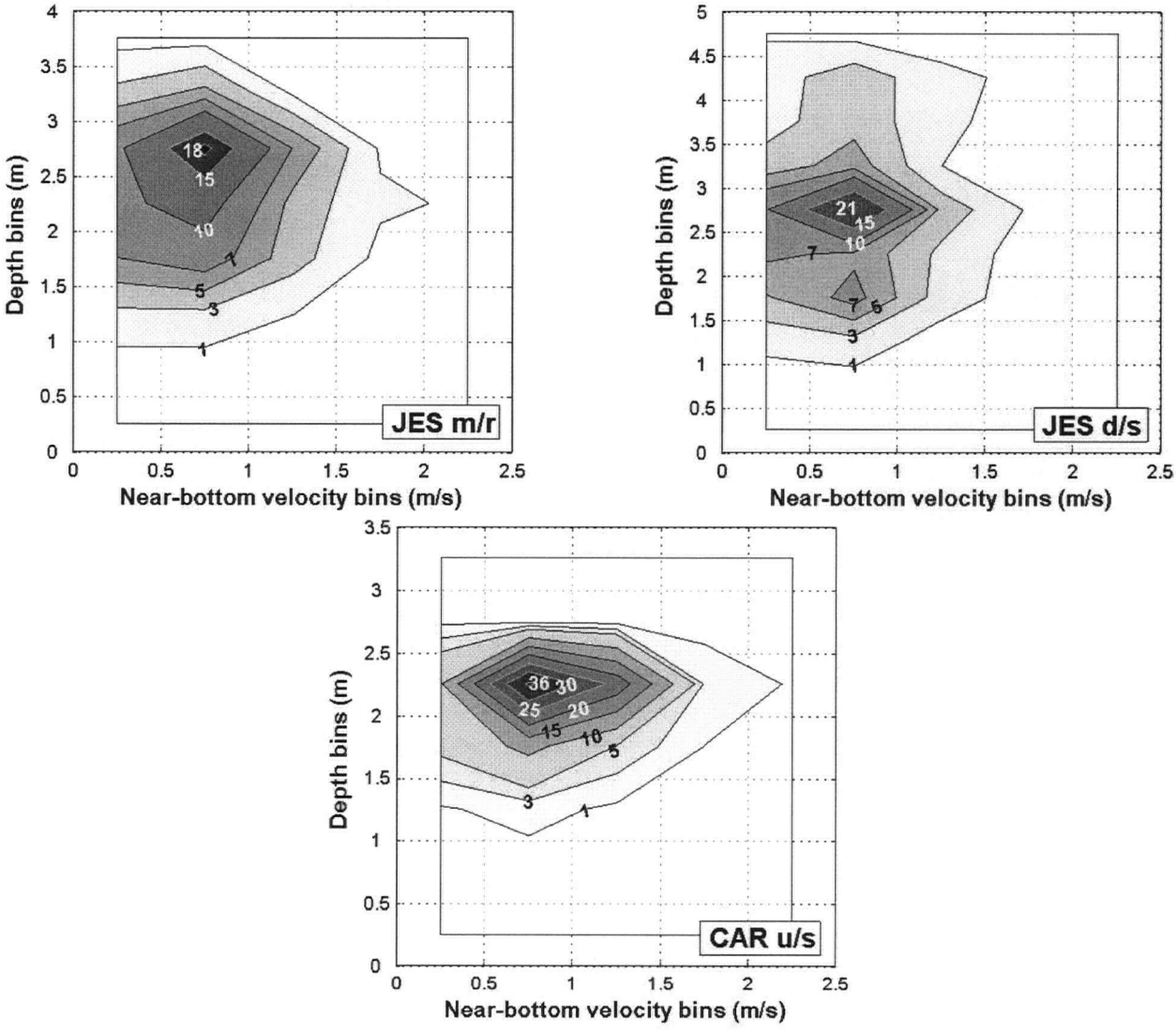

Figure 21 Bivariate frequency distributions of near-bottom d/s velocity (m/s) and depth (m) for selected channels and sub-reaches, at moderate flow (**JES m/r**: $Q_{MC} = 4615$ m^3/s, $Q_{SR} = 94$ m^3/s; **JES d/s**: $Q_{MC} = 4938$ m^3/s, $Q_{SR} = 147$ m^3/s; **CAR u/s**: $Q_{MC} = 3741$ m^3/s, $Q_{SR} = 96$ m^3/s). Histogram output has been converted to percent and mapped as contours of equal percent. Contour interval is variable but contours are labeled, see text for explanation.

Clear patterns in the variation of high-flow bivariate distributions between sub-reach types and between channels are difficult to discern. Many of the high-flow distributions are strongly or weakly bimodal, with a secondary peak frequency of observations at the same or similar velocity but greater or lesser depth. D/s sub-reaches do not demonstrate the high near-bottom velocities (i.e. v > 2.5 m/s) that are present at high flow in the u/s and m/r sub-reaches. However, there is considerable overlap both in the range of velocities and in the range of depths between all sub-reach types. Comparing only u/s and m/r sub-reaches between channels shows that JES is a generally slower-flowing channel, although CAL has a relatively slow-flowing m/r (i.e. the wide, quiet LB). By comparison, CAR u/s, m/r/u and HAM m/r have dominantly fast-flowing water (i.e. the majority of observations have a near-bottom velocity > 0.5 m/s), which suggests that there is little refuge for fish in these sub-reaches at high flow. Comparison of selected high-flow frequency distributions with their accompanying spatial maps of depth and velocity reveals that the distribution of velocity is largely uniform across the sub-reach, while the depth distribution varies. This leads to the observed bimodality of the frequency distributions (see following section on spatial distributions). It is interesting to note that HAM d/s does not show a bimodal distribution. Without good GPS data for this sub-reach, it is not possible to examine the spatial distribution of the data points but, given the generally poor performance of BT in deep channels (> 6 m), it would not be surprising if the data points were not evenly distributed over the channel. This sub-reach should have a bimodal depth distribution since it has a wide, shallow LB and a very deep RB, but this is only vaguely suggested by the frequency distribution.

The frequency distributions of the more moderate flow data show expected shifts in depth and velocity. In each case, the distribution as a whole has shifted to shallower depths and generally slower velocities. The lower-flow distributions are simplified as well in that they are no longer bimodal. In each distribution, the peak frequency of observations shows a dramatic decrease in depth (2 – 2.5 m shallower). The shift in velocity is less consistently strong: in two of the sub-reaches, the peak frequency falls in the same category as at high flow (JES m/r, JES d/s), and in the other sub-reach (CAR u/s) there is a decrease of two bins (i.e. 1 m/s). However, in this case the plot of the ADP water profiles juxtaposed against the waterline shows that a part of the channel was not sampled (see **Figure 27**). On the left bank, the depths were too shallow to permit boating to the waterline and therefore the frequency distribution is truncated in the

region of shallow depths and slow velocities (depth ~ 0-1 m, d/s velocity ~ < 0.5 m/s, from hand-held current meter observations of mean velocity and total depth).

Spatial distributions of near-bottom velocity and depth. In a few of the high-flow and moderate-flow data sets, GPS data quality permitted the creation of contour maps which show the spatial distribution of depth and near-bottom d/s velocity (see **Figure 22** to **Figure 27**). For the purposes of the spatial mapping, the velocity data were projected into the d/s plane and corrected for compass bias. Therefore, the contours indicate the strength of the near-bottom velocity in the imposed d/s direction. The depth data are identical to those used to generate the frequency distributions. Maps were generated in SURFER v.6.04, using the 'kriging' option to interpolate a regular grid from irregularly distributed data. A map that shows the distribution of data points within each sub-reach accompanies the contour maps of depth and near-bottom d/s velocity.

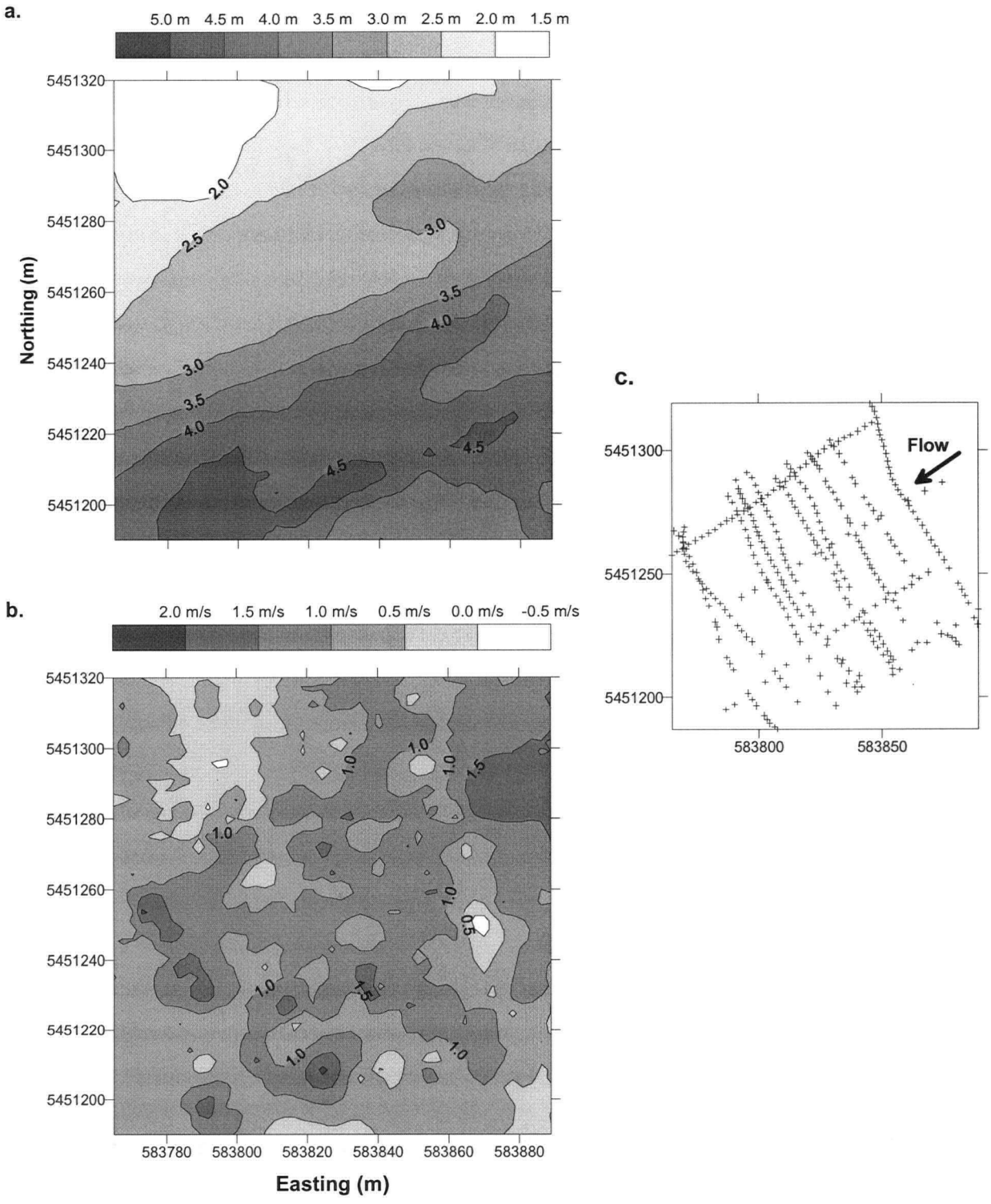

Figure 22 Spatial distribution of (**a**) depth (m), (**b**) near-bottom d/s velocity (m/s), and (**c**) data points for JES u/s at high flow (Q_{MC} = 10,015 m^3/s, Q_{SR} = 394 m^3/s). Approximate d/s direction is indicated on (**c**).

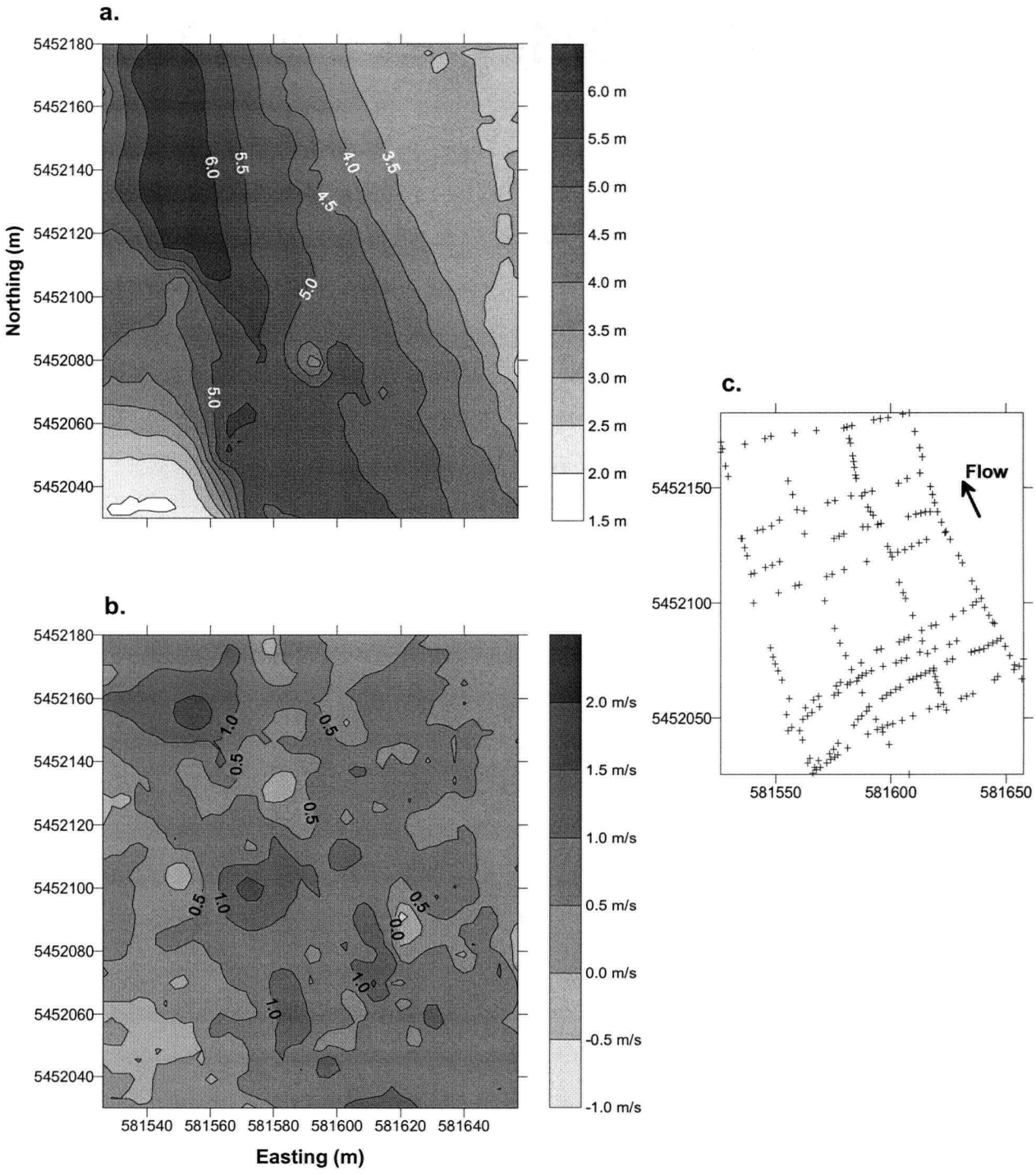

Figure 23 Spatial distribution of (**a**) depth (m), (**b**) near-bottom d/s velocity (m/s), and (**c**) data points for JES d/s at high flow (Q_{MC} = 10,521 m^3/s, Q_{SR} = 447 m^3/s). Approximate d/s direction is indicated on (**c**).

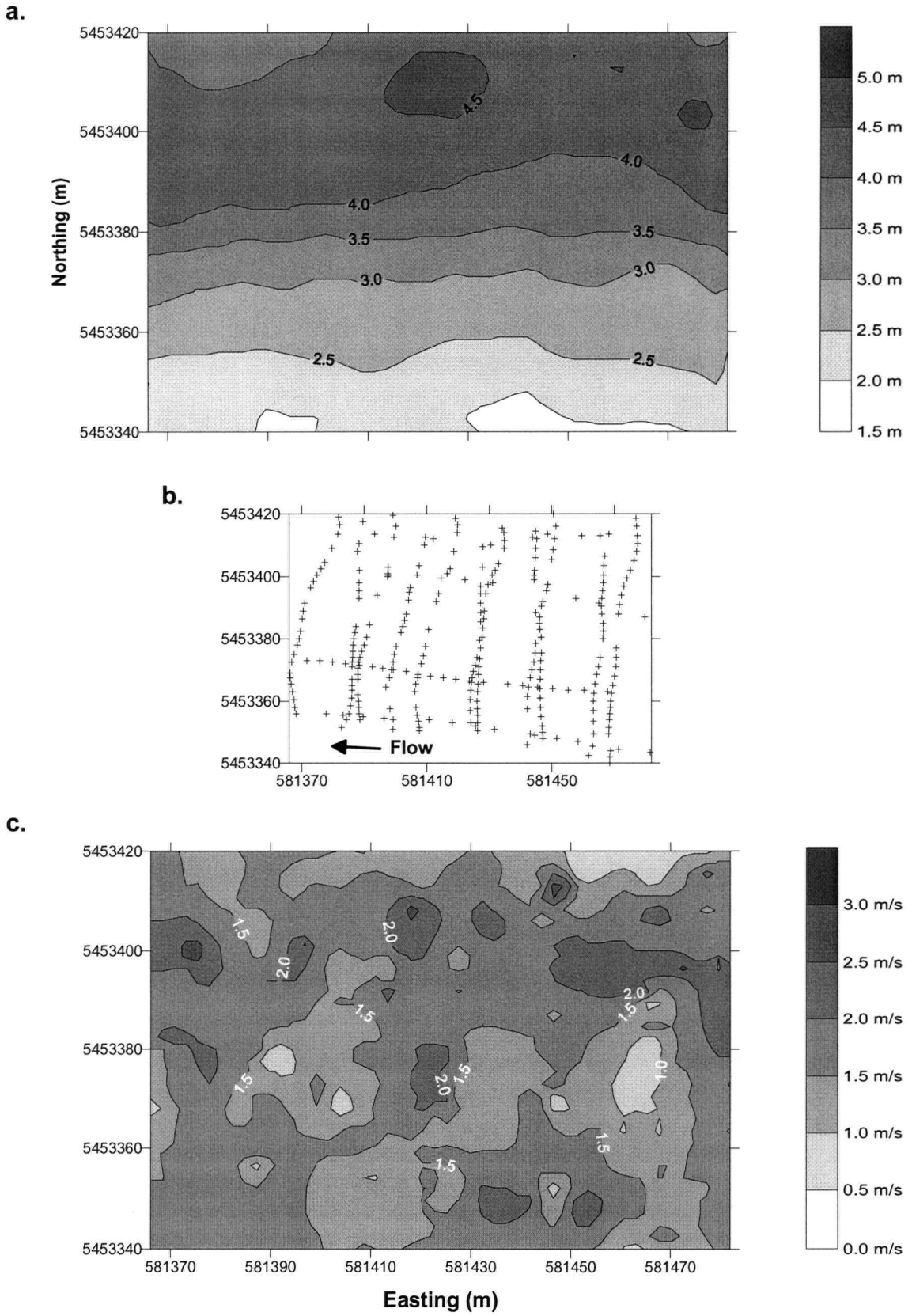

Figure 24 Spatial distribution of (**a**) depth (m), (**b**) data points, and (**c**) near-bottom d/s velocity (m/s) for CAR m/r/u at high flow (Q_{MC} = 9841 m^3/s, Q_{SR} = 452 m^3/s). Approximate d/s direction is indicated on (**b**).

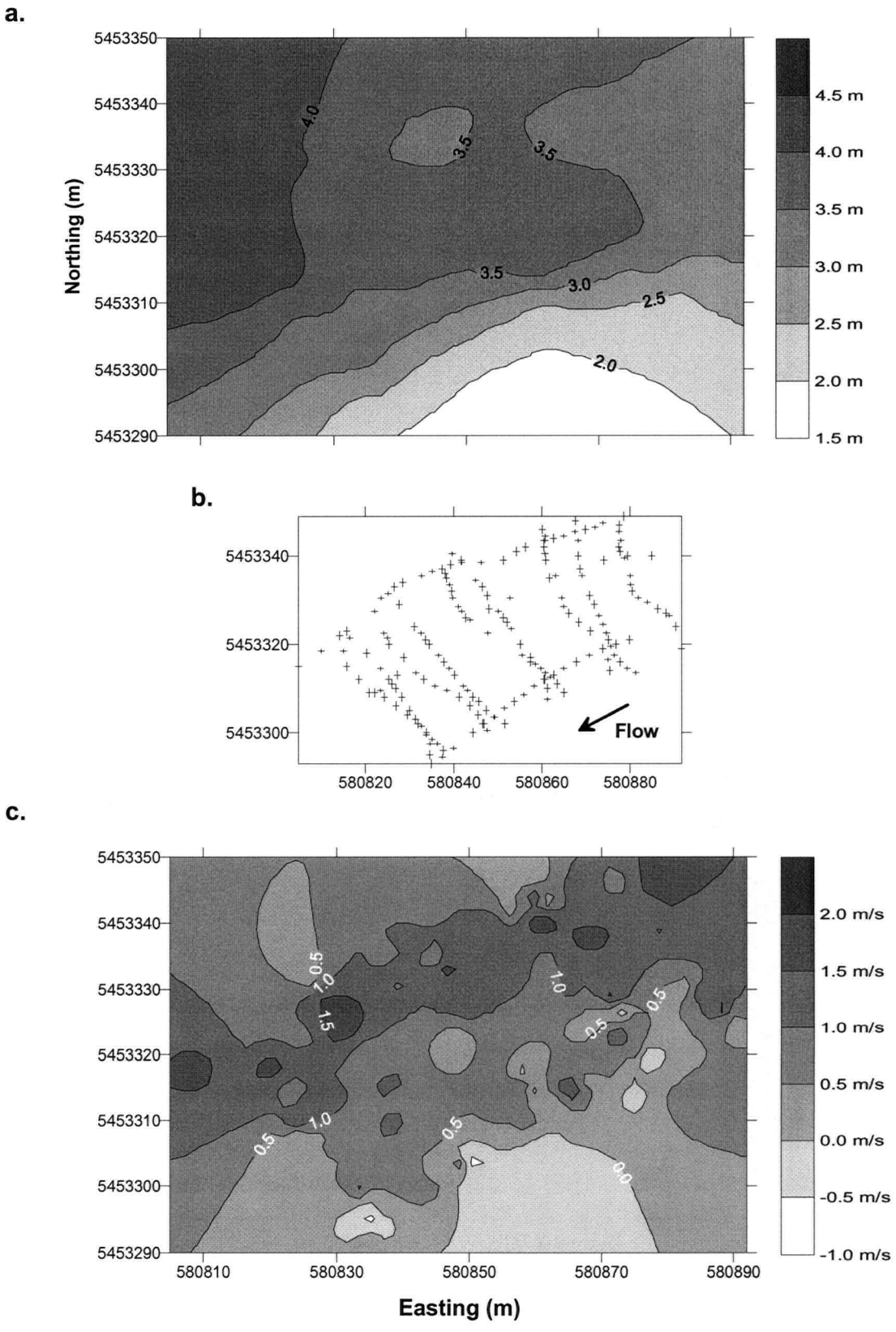

Figure 25 Spatial distribution of (**a**) depth (m), (**b**) data points, and (**c**) near-bottom d/s velocity (m/s) for CAR m/r/d at high flow (Q_{MC} = 9556 m^3/s, Q_{SR} = 129 m^3/s). Approximate d/s direction is indicated on (**b**).

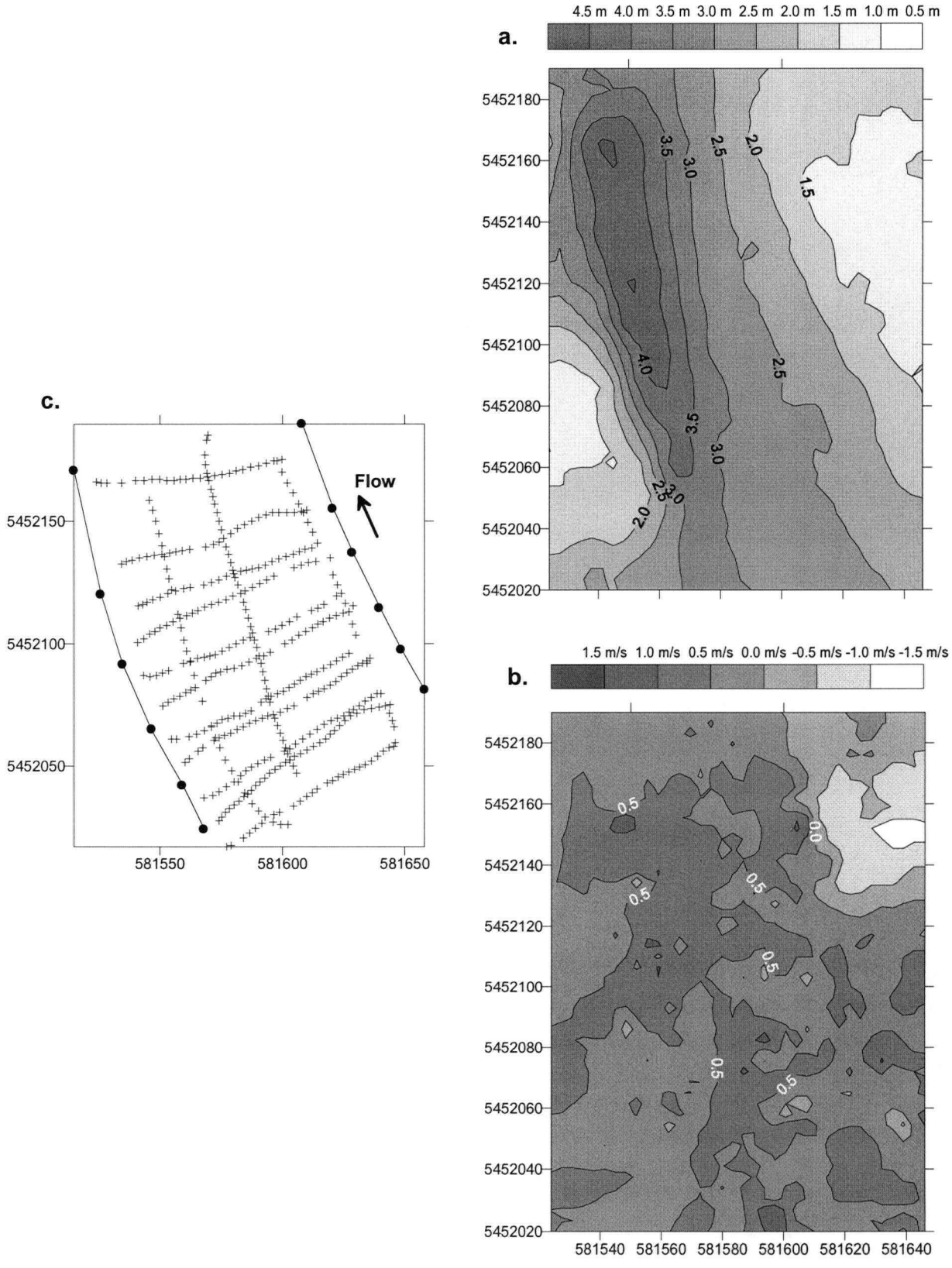

Figure 26 Spatial distribution of (**a**) depth (m), (**b**) near-bottom d/s velocity (m/s), and (**c**) data points for JES d/s at moderate flow (Q_{MC} = 4938 m^3/s, Q_{SR} = 147 m^3/s). The additional points in (**c**) indicate the position of the waterline during data collection. The approximate d/s direction is indicated as well.

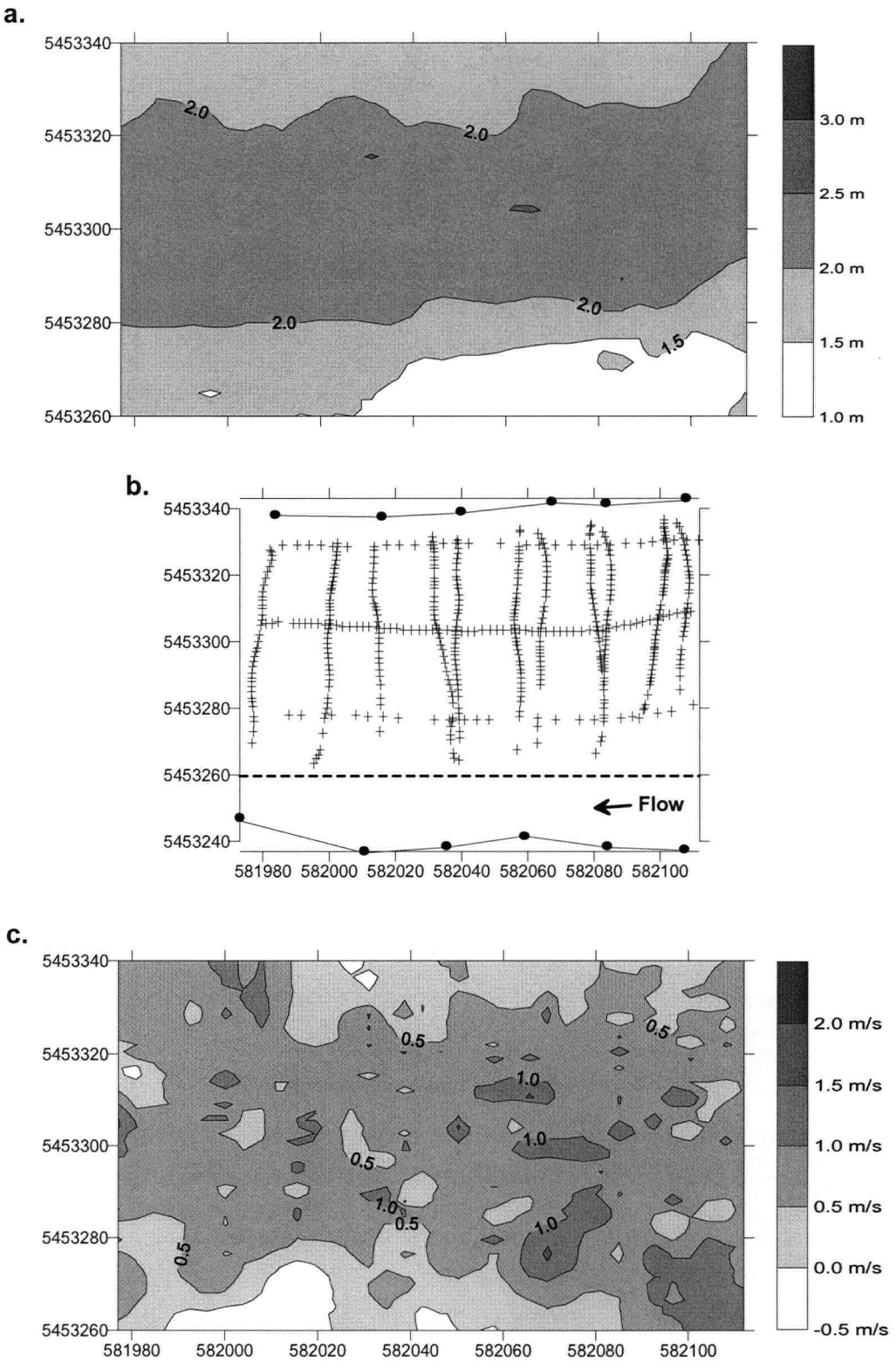

Figure 27 Spatial distribution of (**a**) depth (m), (**b**) data points, and (**c**) near-bottom d/s velocity (m/s), for CAR u/s at moderate flow (Q_{MC} = 3741 m^3/s, Q_{SR} = 96 m^3/s). The filled circles in (**b**) indicate the position of the waterline during data collection and the dashed line indicates the axis limit of (**a**) and (**c**). Approximate d/s direction is indicates as well.

It is interesting to compare the spatial distributions with the frequency distributions. JES u/s (**Figure 22**) has a fairly abrupt gradient in depth from the shallow RB (the NW corner of the maps) to the deeper LB (SE corner of the maps). However, the distribution of near-bottom d/s velocity is relatively uniform across the channel and is dominated by flows between 1 and 1.5 m/s. Therefore the bimodal frequency distribution is simply a result of the channel bed configuration (i.e. there is proportionately less area with a depth between 3 and 4 m, and therefore proportionately fewer observations in this range of depths). JES d/s, high-flow (**Figure 23**), has a similar distribution of depths and also shows a rather uniform distribution of the dominant velocity category (flows between 0.5 and 1 m/s). However, there seems also to be a tendency for faster flows in the deeper part of the channel, a trend that is borne out in the frequency distribution. This pattern is repeated again in CAR m/r/u (**Figure 24**), in which the frequency distribution is a combination of a uniform distribution of a dominant flow class (between 1 and 1.5 m/s) over a bimodal depth distribution, with an additional tendency for faster velocities at higher depths. CAR m/r/d is slightly different. First of all, it has a unimodal frequency distribution, unlike many of the sub-reaches. An examination of the map of channel depths (**Figure 25**) reveals that the majority of the channel area has a depth of between 3 and 4 m. Within this area the pattern of velocities is similar to the other sub-reaches already described: the dominant velocity category is the 0.5 to 1 m/s category (although the 1-1.5 m/s category is also quite prevalent) and there is the tendency for faster velocities where depth is greater. However, in that part of the channel where depths are less than 3 m, velocities are relatively slower reflected in the corresponding 'bulge' in the frequency distribution.

Plots of JES d/s at high flow (**Figure 23**) and moderate flow (**Figure 26**) can be compared to examine the changes in spatial distribution of near-bottom d/s velocity and depth, as flow declines. Colour scales have been standardized to facilitate comparison between these two plots. One can see how the configuration of the channel (steep banks, relatively deep channel) permitted boating from bank to bank until quite low flow. Due to the steep-sided banks, the shape of the depth distribution at moderate flow is more or less identical to that at high flow, but simply shifted. The near-bottom d/s velocity plots are both relatively uniform, with a dominant category of 0.5 – 1 m/s at both flow levels (although at moderate flow there is far more of the 0 – 0.5 m/s category evident, and much less of the > 1 m/s). It is interesting to speculate why there would not be a more dramatic shift, as in the other moderate-flow bivariate distributions. One possibility is that a backwater effect at high flow caused by the confluence with the main channel

eliminated the possibility of higher sub-reach velocities. The spatial plots of CAR u/s at moderate flow (**Figure 27**) are a useful accompaniment to the frequency distribution, as previously mentioned.

4.1.3 Sedimentological data

Summary parameters from surface grain-size distributions (GSD) are presented in **Table 11** (this includes samples of fine material from bank sands or substrate dredge samples). The tendency for the d/s sub-reaches of the at-a-station channels to have a fine, sandy substrate is clearly demonstrated. In the case of the dredge samples from the sub-reach channel bottoms, there is also a fairly strong silt component (see also the grain-size distribution plots in **Appendix B**). The m/r and u/s substrates are dominantly gravel, and there are only a few instances in which the D_{84} falls in the cobble category. The sub-reaches in which the D_{84} is of cobble size are most likely heavily armoured since there was no observed sediment transport in the reaches where it would have been possible (CAR u/s, HAM m/r), and no significant transport possible in Jesperson because of the flow-control structure. There is a general trend of increasingly fine sediment as one progresses downstream in any of the study channels, although both JES and HAM have the coarsest deposits in the m/r sub-reach. These are likely to be very old deposits, since there is no evidence of recent sediment movement that far downstream in those channels. In sub-reaches where surface samples were taken in contrasting 'new' and 'old' deposits (CAL m/r, HAM u/s), the two distributions are quite similar (see also plots in **Appendix B**). The new deposit in CAL m/r is slightly finer than the underlying older deposit, as indicated by the summary GSD parameters. The new deposit in HAM u/s is well sorted, slightly more so than the older deposit. However, the two distributions are otherwise very similar. The lack of difference between the new and old sediment suggests that the bed in this sub-reach is potentially mobile at high flow.

The corresponding information for all sub-surface grain-size distributions can be found in **Table 12**. These data are primarily from u/s sub-reaches only since they are likely to be the most sedimentologically active, at least in longer channels. In u/s sub-reaches where new sediment had been deposited, we sampled the new rather than the old sediment (e.g. HAM u/s, CAL m/r, CAL u/s). The new sediment had clearly been deposited during the 2002 freshet and therefore gives an indication of the grain-size distribution that was in transport during the measured flows.

Based on the data from CAL u/s and HAM u/s, sediment that was moved by the 2002 freshet had an approximate D_{50} of 26 mm and a D_{84} of 45 mm. In contrast to the u/s sub-reaches, the mobile sediment in CAL m/r was smaller.

One can also visually compare the coarse fraction of the sub-surface GSD plots with the surface GSD plots in the corresponding sub-reaches to evaluate their agreement. In the case of CAL u/s, the coarse sub-surface GSD is very similar to the surface sample, except at the finer end of the GSD (i.e. 8-11 mm, Ψ = 3-3.5). In this region of the GSD there is, not surprisingly, relatively more material in the sub-surface than the surface GSD. In CAL m/r (new), the sub-surface coarse and surface GSD are very similar in shape and share the same mode (16 mm, Ψ = 4), but there is disproportionately more material in this size category in the sub-surface than the surface. Also, there is again more fine material in the sub-surface than the surface GSD. Finally, the comparison of the HAM u/s sub-surface coarse fraction to both of the surface samples shows that the sub-surface fraction very closely resembles the old surface, although there is slightly more of the largest size category present in the surface sample. The new surface, being better sorted, has less material in the fine end of the GSD, although the modes and general shapes of the distributions are similar. Agreement between the sub-surface coarse fraction and the surface GSD simply indicates that the sediment has not been reworked. This is not surprising in the case of the new deposits, because the hydrograph was quite steep-sided in 2002, both on the rising and the declining limbs. There would perhaps have been sufficient time for the smaller material on the surface to be mobilized. However, it is interesting to note that the older surface in HAM u/s still shows good agreement with the sub-surface GSD of the new deposit. We do not know when the 'old' surface was deposited because, although the two preceding freshets were not as large as 2002, they were both of a magnitude that would allow for significant sediment transport, at least in the main channel.

Table 11 Surface grain-size parameters, all sub-reaches.

Channel & sub-reach	D_{50} (mm)	D_{84} (mm)	Notes
JES u/s	24.4	64.4	
JES m/r	44.3	77.6	
JES d/s	0.21	0.30	sandy substrate, dune features apparent
CAL u/s	33.4	54.6	
CAL m/r (old)	21.5	34.1	
CAL m/r (new)	18.1	29.4	
CAL d/s (bank)	0.19	0.20	sand
CAL d/s (dredge)	0.031	0.15	silty sand
CAR u/s	50.0	79.3	
CAR m/r/u	33.5	57.5	
CAR m/r/d	30.2	49.4	
HAM u/s (old)	32.3	55.0	
HAM u/s (new)	36.9	55.7	
HAM m/r	48.5	75.5	
HAM d/s (bank)	0.19	0.21	
HAM d/s (dredge)	0.047	0.14	silty sand, dune features apparent
Minto	36.9	61.7	
Big Bar	29.8	49.5	
Gill	29.2	54.3	
Queens	42.4	64.9	
Grassy	12.0	22.2	

Table 12 Sub-surface grain-size parameters.

Channel & sub-reach	D_{50} (mm)	D_{84} (mm)	Notes
JES u/s	15.5	51.4	
CAL u/s	25.7	45.4	new sediment (post-2002 freshet)
CAL m/r	16.0	27.9	new sediment (post-2002 freshet)
CAR u/s	23.8	49.4	
HAM u/s	26.4	45.1	new sediment (post-2002 freshet)

4.2 Scaling behaviour of secondary channels

4.2.1 Relation of main-channel discharge to sub-reach discharge

Once a 'bankfull' flow can be specified for a given sub-reach, the appropriate parameters can be calculated from the at-a-station relation for entry into scaling relation analysis (classical downstream hydraulic geometry). In studies using gauging data, it has been common to specify the bankfull flow by a return period and by this mechanism ensure that comparable flows from each gauge were used. When using field data, surveying the channels in question while flow is not changing appreciably ensures the comparability of the data. One must then choose the flow at which to sample in the field, and that requires defining what flow is considered to be 'bankfull'.

Deriving 'bankfull' sub-reach discharges for this study required multiple steps and assumptions, which will be listed:

1) We interpreted 'bankfull' flow the sense of the "channel-shaping" flow. Therefore we assumed that bankfull main-channel flows would be represented adequately by flows greater than 5000 m^3/s, at which discharge significant sediment transport is initiated (McLean et al., 1999).
2) We also assumed that main channel gauging data at Hope would reasonably represent main channel discharges in the study area. There is only one major tributary in the study reach (Harrison River), which is estimated to add less than 10-15% to main-channel flood flows (McLean et al., 1999). Five sub-reaches are downstream of the entrance of Harrison River, from a total of sixteen sub-reaches (**Figure 2**).
3) We made the further assumption that the main channel and secondary channels would experience bankfull conditions simultaneously. Therefore, by relating individual sub-reach discharges to main channel discharge, sub-reach bankfull discharge could be *predicted* based on a main channel bankfull discharge.

Based on these assumptions, a methodology for deriving sub-reach bankfull flows was developed and implemented.

A high main channel flow (i.e. $Q > 5000\ m^3/s$) was selected to acquire data for the scaling relations. Data collection in the additional sub-reaches occurred approximately one week

after the 2002 peak flow. The average main-channel discharge during data collection in the additional sub-reaches was 8873 m^3/s (measured at Hope). This average flow was then defined as the main channel 'bankfull' flow for the scaling relations. It is slightly greater than the mean annual flood measured at Hope (8766 m^3/s, (McLean et al., 1999)). Main channel discharge at Hope was obtained from the Water Survey of Canada, as hourly data, which were then converted to daily averages and represent the main-channel flow for sub-reach data collected on that date. In order to derive the corresponding sub-reach parameters at the defined main-channel bankfull flow it was necessary to relate each measured sub-reach flow to the main-channel flow by regression.

Results of the main-channel Q (Q_{MC}) to sub-reach Q (Q_{SR}) regressions are presented in **Table 13**. Corresponding scatter-plots and plots of residuals can be found in **Appendix C**. Of the four study channels, three were clearly (Carey, Hamilton) or potentially (Calamity) affected by flow across the bar and therefore the discharges from these sub-reaches were not grouped by channel for the regression. Only Jesperson was not affected in this way and therefore all sub-reach flows were grouped together for the regression with main-channel discharge. There is the possibility of sub-surface flow through the channel substrate, but this seems unlikely to be a major component of the discharge, given the configuration of this channel.

There is a clear non-linear trend in the JES data (see **Figure C-1**, p.172), with the suggestion of either a quadratic polynomial trend, or perhaps a threshold near $Q_{MC} = 8000\ m^3/s$ separating two different trends. Different models were explored to fit this data including a quadratic polynomial and robust Lowess smoothing (resistant to outliers, domain = 50% of the data set). The resulting fits are shown in **Figure 28**. Clearly, for the purposes of predicting Q_{SR} there is almost no difference between the different models. For a description of the underlying trend(s) in the data, although the linear equation suffers from lack of fit, the quadratic polynomial also displays lack of fit in the range $Q_{MC} < 7000\ m^3/s$. The line produced by the Lowess smoothing appears to fit the data well but is inconvenient in the sense that it cannot be described by a simple mathematical function and is therefore difficult to present except in graphical format. For the purposes of this study, Q_{SR} bankfull predictions were made using the linear model since the models are nearly coincident at $Q_{MC} = 8873\ m^3/s$. The results from the polynomial fit on the JES data are also presented in **Table 13**.

The R^2 value for CAL m/r in **Table 13** is poor in comparison to the results from other sub-reaches. Both CAL m/r and d/s show evidence for a backwater effect once the main channel discharge exceeds approximately 6500 m^3/s (at Hope) (see **Figure C-15**, p.180 and **Figure C-17**, p.181). The strong non-linear trend in the CAL m/r plot explains the poor performance of the linear model. This non-linearity makes the assumption of a linear relation between sub-reach discharge and main channel discharge unlikely, and also complicates the issue of determining a channel-shaping flow for these sub-reaches. In the remaining sub-reaches there were no clear non-linear trends and insufficient data points to make a judgement as to whether a subtle non-linear trend was present, and therefore the linear fit was applied.

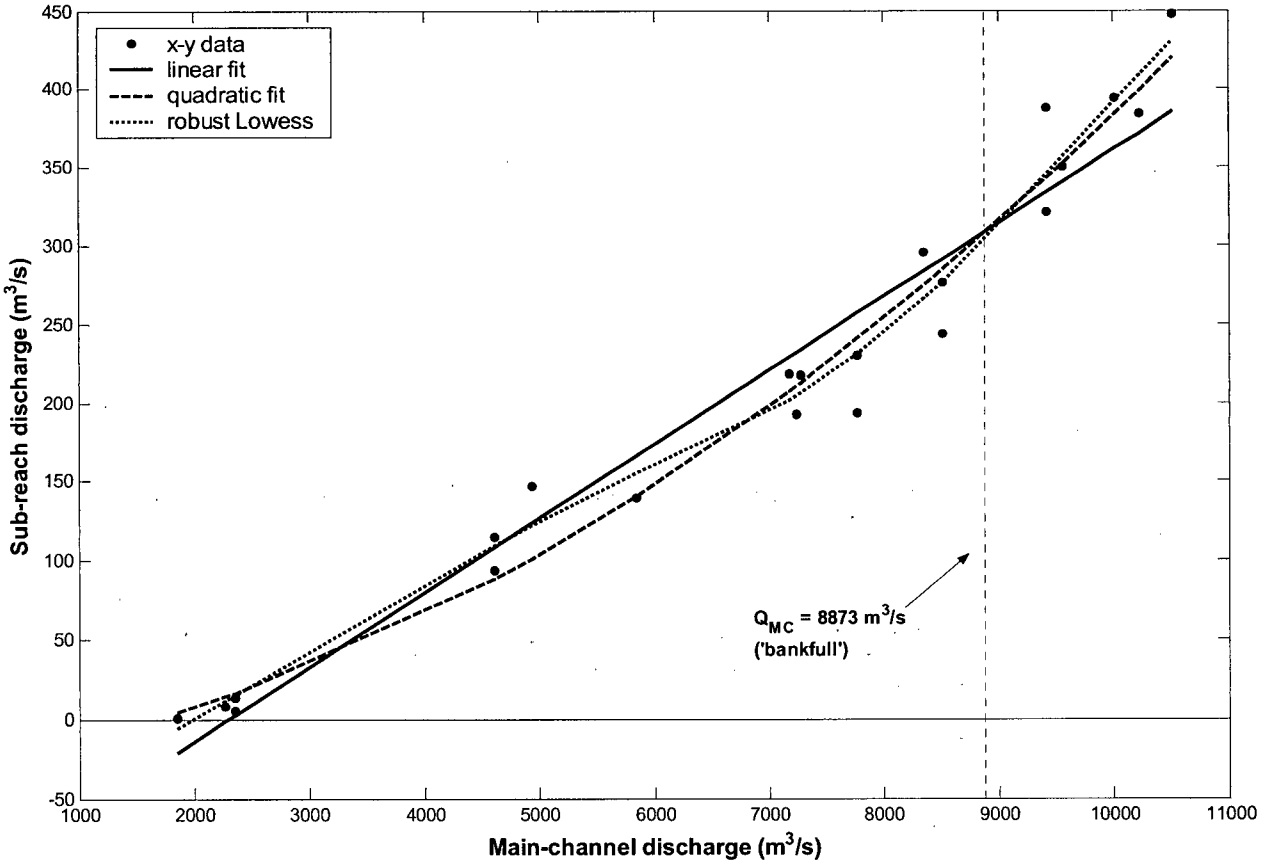

Figure 28 Comparison of different statistical models fit to JES Q_{MC} and Q_{SR} data (all sub-reaches). Main-channel 'bankfull' flow at which Q_{SR} will be evaluated is indicated.

Table 13 Relation of sub-reach discharges to main-channel discharge (at Hope).

Sub-reach	Least-squares regression	R^2	SEE (m^3/s)
JES (all sub-reaches)	$Q_{SR} = -107.49 + 0.0468\ Q_{MC}$	0.95	± 30.97
JES (all sub-reaches)	$Q_{SR} = 2.95\times10^{-6}\ Q_{MC}^2 + 0.0115\ Q_{MC} - 27.26$	0.97	± 24.00
CAR, u/s	$Q_{SR} = -317.61 + 0.117\ Q_{MC}$	0.97	± 70.93
CAR, u/s mid	$Q_{SR} = -157.57 + 0.0658\ Q_{MC}$	0.94	± 51.71
CAR, d/s mid	$Q_{SR} = -43.10 + 0.0180\ Q_{MC}$	0.92	± 15.17
HAM, mid	$Q_{SR} = -153.69 + 0.0744\ Q_{MC}$	0.99	± 14.17
HAM, d/s	$Q_{SR} = -214.93 + 0.0873\ Q_{MC}$	0.98	± 35.66
CAL, u/s	$Q_{SR} = -46.74 + 0.0335\ Q_{MC}$	0.92	± 35.74
CAL, mid [a]	$Q_{SR} = 24.29 + 0.0262\ Q_{MC}$	0.60	± 56.03
CAL, d/s [a]	$Q_{SR} = -65.74 + 0.0368\ Q_{MC}$	0.92	± 32.19

[a] data show evidence of a backwater effect

4.2.2 Secondary channel scaling relations

On the basis of the regressions presented in Section 4.2.1, sub-reach flows for at-a-station reaches were estimated for the defined main-channel 'bankfull' flow (i.e. $Q_{MC} = 8873\ m^3/s$) (**Table 14**). In most cases, this involved an interpolation rather than an extrapolation of the regression, since the range of main channel discharge was high. The SEE of the regression was assumed to represent the estimated uncertainty in each sub-reach bankfull discharge estimate. In the case of CAL m/r and d/s, the linear regression does not describe the relation of sub-reach to main channel discharge adequately. In CAL d/s, sub-reach flows never exceeded approximately 200 m^3/s, although the very highest range of main channel discharge ($Q_{MC} > 9000\ m^3/s$) was not sampled. Therefore it seems more appropriate to set the bankfull Q_{SR} in this sub-reach to 200 m^3/s. Although CAL m/r presents a similar difficulty, this sub-each was excluded from the scaling relation analysis on the basis that the narrow (and high) range of discharge that was sampled in this sub-reach had resulted in anomalous relations.

Using these estimated sub-reach flows as inputs for at-a-station functional relations, bankfull flow parameters for each sub-reach were generated. In cases where a linear fit had produced a better fit, this form of the relation was used to make the estimate, and in sub-reaches where a high-flow analysis was performed, the high-flow at-a-station relation was used. Again, the SEE of the relation was assumed to represent the error in the predicted channel parameter of interest. In addition to excluding all data points from CAL m/r, the at-a-station d-Q relation in

CAL d/s was not used because of its non-significant slope. All other at-a-station sub-reaches were included.

Data collected in the reaches specifically designated for the scaling relations were analyzed in a manner similar to that described in Section 3.2.1. Four out of the five scaling relation sub-reaches had good GPS signal reception and reasonable bottom-tracking, and hence could be analyzed using Method 1. The 'Big Bar' sub-reach was the exception: the GPS signal reception was poor and Method 3 had to be applied. The only way in which these analyses differed from the at-a-station analyses is that no near-shore estimation was applied, since it was assumed that, at this high flow, the ADP was able to capture essentially all in-channel discharge. This assumption was also in part necessitated by the requirement that the sub-reaches investigated solely for scaling relations be surveyed in rapid succession.

Table 14 Computed sub-reach bankfull discharge estimates (m^3/s) with associated uncertainty.

Channel & sub-reach	Q_{SR}, bankfull (m^3/s)	SEE (m^3/s)
JES (all sub-reaches)	308	31.0
CAR u/s	718	70.9
CAR m/r/u	426	51.7
CAR m/r/d	117	15.2
HAM m/r	507	14.2
HAM d/s	560	35.7
CAL u/s	250	35.7
CAL m/r	256	56.0
CAL d/s [a]	261 (*200*)	32.2

[a] Q_{SR} estimate in italics is suggested based on the potential backwater effect

An on-shore survey to measure the location of the waterline with respect to some known markers would have greatly increased the length of time necessary for data collection at each sub-reach. The net result of this assumption is that water-surface width is estimated by summing all cross-stream width increments in each cross-section, and averaging the estimates for the sub-reach. The only other difference in the analysis is that the volume calculation algorithm, which requires an estimate of the waterline location to function properly, was given a 'dummy' waterline corresponding to a point just slightly beyond the end of each cross-section. The intent was simply to provide bounds to the volume calculation without inflating the channel area.

The scaling relation sub-reaches comprise the largest surveyed secondary channels in this study excluding Grassy, which plots with the at-a-station sub-reaches. In fact, it could be argued that the Gill channel, at least after the 2003 freshet, appears to be the new main channel in this part of the river. We made a deliberate attempt to choose scaling sub-reaches that would extend the range of discharge past the range covered by the at-a-station relations. In terms of character, the sub-reaches were situated in an intermediate position in their respective channels, to represent the m/r sub-reach morphology.

The results of the functional analysis on the bankfull w-Q data and the bankfull d-Q data are presented in **Table 15**, and are shown with residual plots in **Appendix D**. In general, the results are quite good, although there is more scatter around the line of best fit than in many of the at-a-station relations. As the functional analysis is still the appropriate analysis to employ, it was necessary to arrive at a value for λ. The bulk of the data (10 of 15 points, and 9 of 14 points, for the width and depth relations, respectively) were derived from the at-a-station hydraulic geometry relations and the main-channel to secondary-channel discharge regressions. It was assumed that the SEE values of these relations are reasonable error estimates, in contrast to derivation of λ for the at-a-station relations (i.e. using standard error of the mean, or error estimates from error analyses). Using SEE data to calculate an average error ratio yielded the values of λ for the functional analysis of scaling relation data.

Table 15 Functional scaling relations for secondary channel bankfull parameters.

Parameter	Equation	I^2 [a]	SEE*[a]	95% C.I. for slope	n	λ [b]
w	$w = 4.57Q^{0.526}$	0.83	± 33.68 m	[0.431 - 0.641]	15	0.31
d	$d = 0.72Q^{0.254}$	0.69	± 0.62 m	[0.161 - 0.358]	14	0.36
v [c]	$v = 0.31Q^{0.220}$	n/a	n/a	n/a	n/a	n/a
w [d]	$w = 4.03Q^{0.539}$	0.84	± 35.19 m	[0.439 - 0.665]	12	0.25
d [d]	$d = 0.68Q^{0.258}$	0.77	± 0.57 m	[0.169 - 0.356]	12	0.45
v [c]	$v = 0.37Q^{0.203}$	n/a	n/a	n/a	n/a	n/a

[a] log-linear were back-transformed in order to calculate goodness-of-fit measures
[b] ratio of errors in the dependent variate to errors in the independent variate (Mark and Church, 1977)
[c] relation derived from continuity
[d] all d/s sub-reaches excluded

λ used for the w-Q scaling relation is higher than was typically used in the at-a-station analyses. According to Mark and Church (1977), the ratio of the functional analysis slope to the

conventional regression slope is not a rapidly changing function of λ, particularly for higher values of R^2 (cf. Figure 2, (Mark and Church, 1977)). This would suggest that the change in the slope of the bankfull w-Q scaling relation would not be substantial if λ were reduced. The trend would be to increase the slope of the functional relation slightly.

The scaling relations are presented again in **Figure 29**, **Figure 30** and **Figure 31** with the data points formatted to distinguish each point by its sub-reach of origin. Mean-annual flood main-channel parameters at Hope, Agassiz and Mission have been added to each plot for comparison (from Table 1 in McLean et al., 1999). Stratification by sub-reach morphology or by channel does not appear to explain the scatter in the w-Q scaling relation. Both the Agassiz and Mission points agree very well with the w-Q relation, suggesting that bankfull water surface width exhibits true scaling behaviour. In the case of Mission, this agreement is surprising, first because it falls in a different regime class (sand bed) and therefore the results of Simons and Albertson (1963) suggest that it should plot above points from gravel-bed channels. Second, the river is constrained by dykes at Mission and therefore we might expect a deviation from the other data points from (relatively) unconstrained sub-reaches. Possibly the dykes are constraining the channel width from what it might naturally achieve, and this might explain the agreement with the other data points. The point for Hope plots well below the w-Q relation, but the river is confined by rock at this location and therefore may be considered to be non-alluvial in character.

There is more evidence of morphological stratification in the d-Q relation, since the u/s sub-reaches plot below the best-fit line (i.e. shallower), while d/s sub-reaches plot above the best-fit line (i.e. deeper). The m/r points appear truly intermediate in character since they straddle the best-fit line fairly evenly (recall that the sub-reaches used solely in the scaling relations can also be considered to fall into the m/r category). Again, the Agassiz point falls very close to the best-fit line suggesting that the bankfull mean hydraulic depth also exhibits true scaling behaviour. Both Hope and Mission plot well above the best-fit line for the reasons previously mentioned. The bankfull v-Q relation shows the most scatter about the best-fit line (derived by continuity from the w-Q and d-Q relations). There is a weak tendency for u/s sub-reaches to plot above the best-fit line (i.e. faster) and d/s sub-reaches to plot below the best-fit line (i.e. slower). Once more, Agassiz plots on the best-fit line, while Hope and Mission do not. CAL d/s also plots quite far from the best-fit line but the point itself is questionable since it was derived by continuity using the d-Q relation with a non-significant slope.

There appears to be some evidence in the d-Q and v-Q plots that the d/s sub-reaches are different in character from the other sub-reaches. These differences may arise from the markedly finer substrate and potential backwater effects. For this reason, a separate analysis was run which explicitly excluded all d/s sub-reaches, the results of which are presented in the lower part of **Table 15**. The effect of removing the d/s sub-reaches is to slightly increase the exponents of both the w-Q and d-Q relations by 2.5 % and 1.6 %, respectively (with the necessary decrease in the slope of the v-Q relation). The slopes of the relations excluding d/s sub-reaches are not statistically different from the slopes calculated based on all sub-reach types. The coefficients of the w-Q and d-Q relations both decrease as a result of excluding the d/s sub-reaches (–11 % and –5.6 %, respectively), a result which may partially be explained by the steepening of the slopes of the relations.

In summary, bankfull scaling relations based on a range of secondary channels in lower Fraser River gravel reach appear to indicate that alluvial channels in this reach (up to and including the main channel) obey true scaling laws. Deviations from the best-fit line in the case of mean hydraulic depth and mean velocity may be plausibly explained by sub-reach morphology (i.e. different regime classes). The distinctiveness of the different sub-reach positions could be explored using an analysis of covariance, however there are insufficient reliable data to implement it successfully.

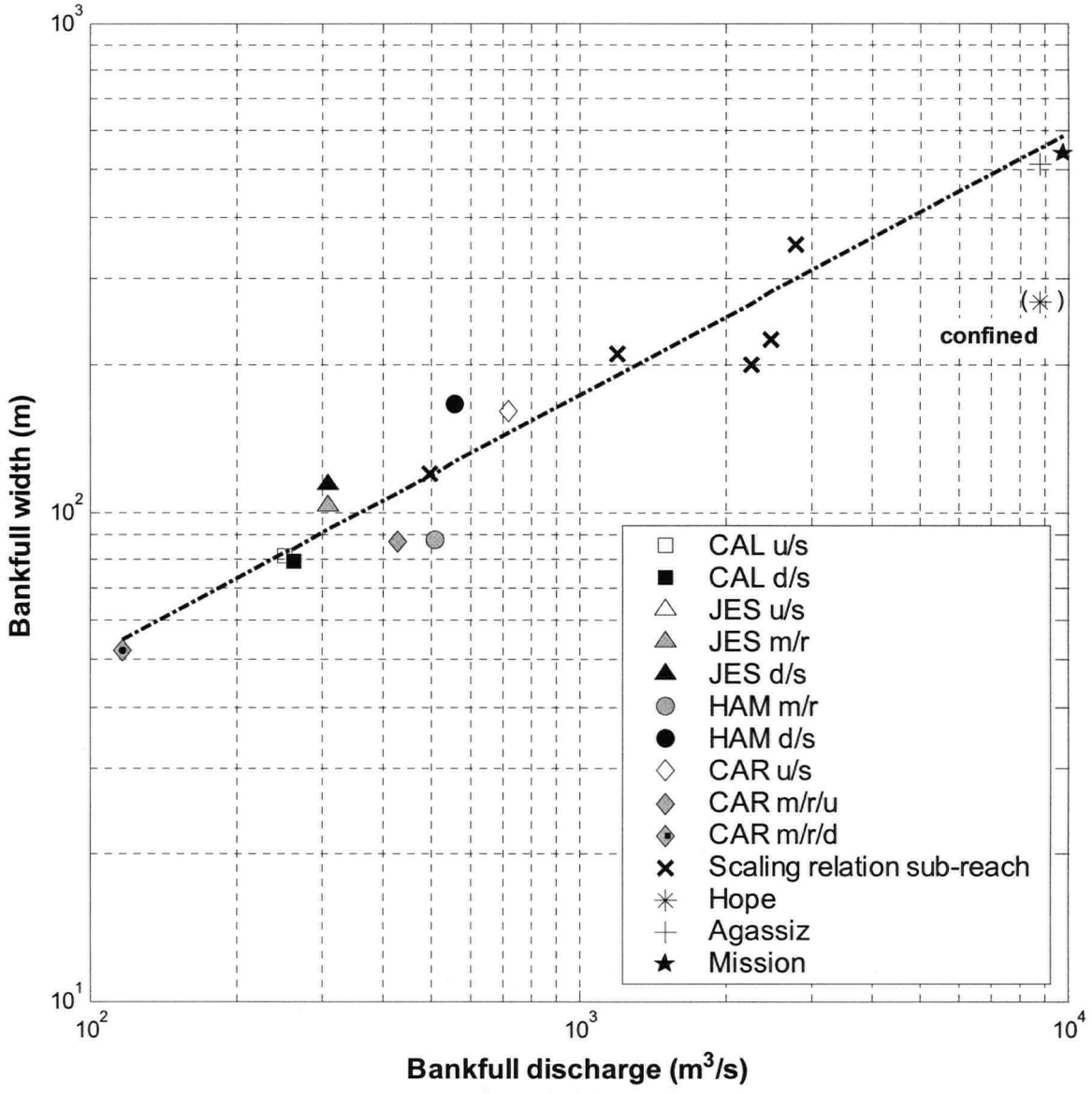

Figure 29 Functional scaling relations for bankfull width and discharge, stratified by channel and sub-reach morphology. Bankfull at-a-station parameters are based on the high-flow analyses, where performed (JES, HAM, CAR). The JES u/s data point is obscured by the JES d/s data point.

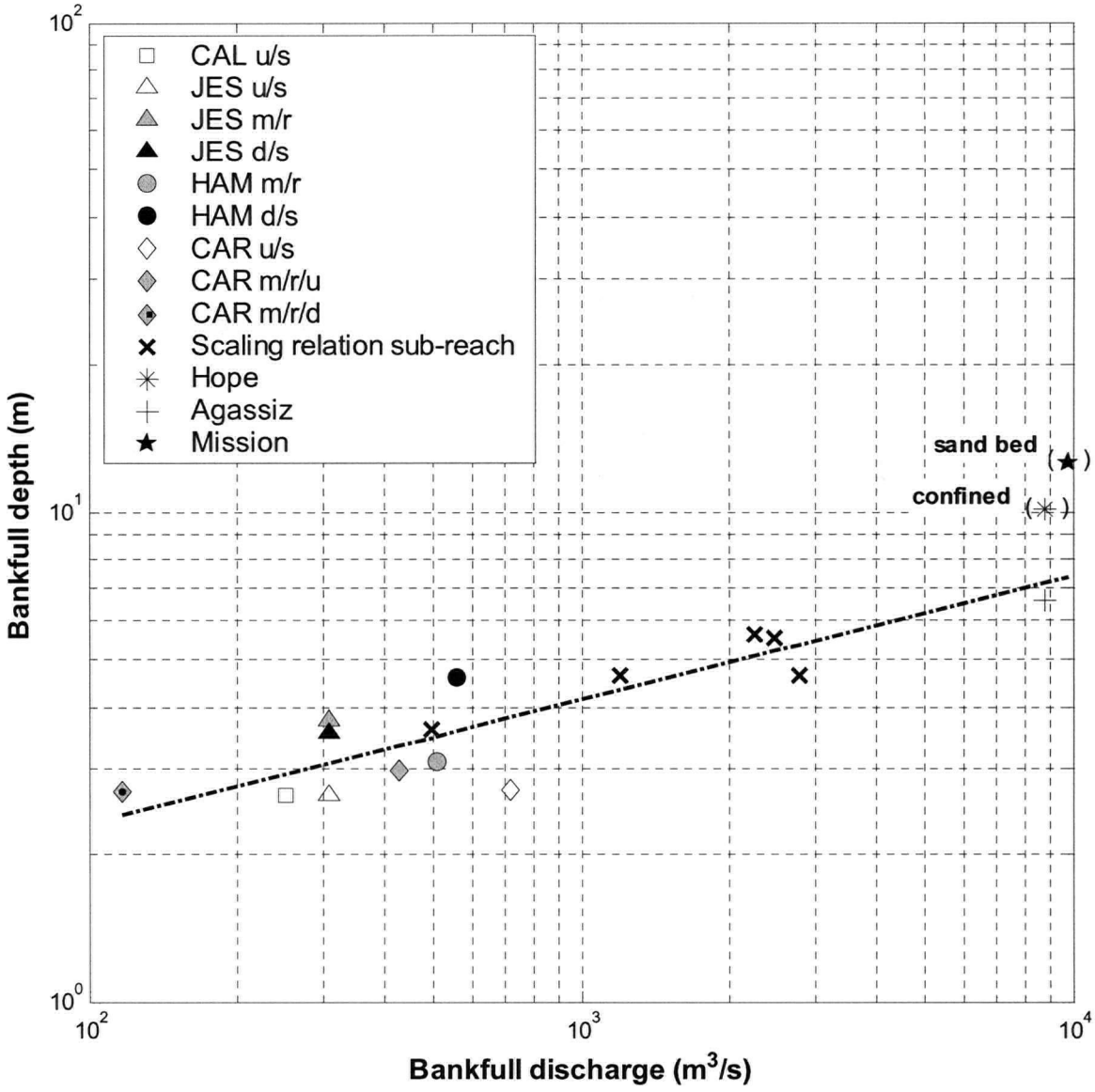

Figure 30 Functional scaling relations for bankfull depth and discharge, stratified by channel and sub-reach morphology. Bankfull at-a-station parameters are based on the high-flow analyses, where performed (JES, HAM, CAR).

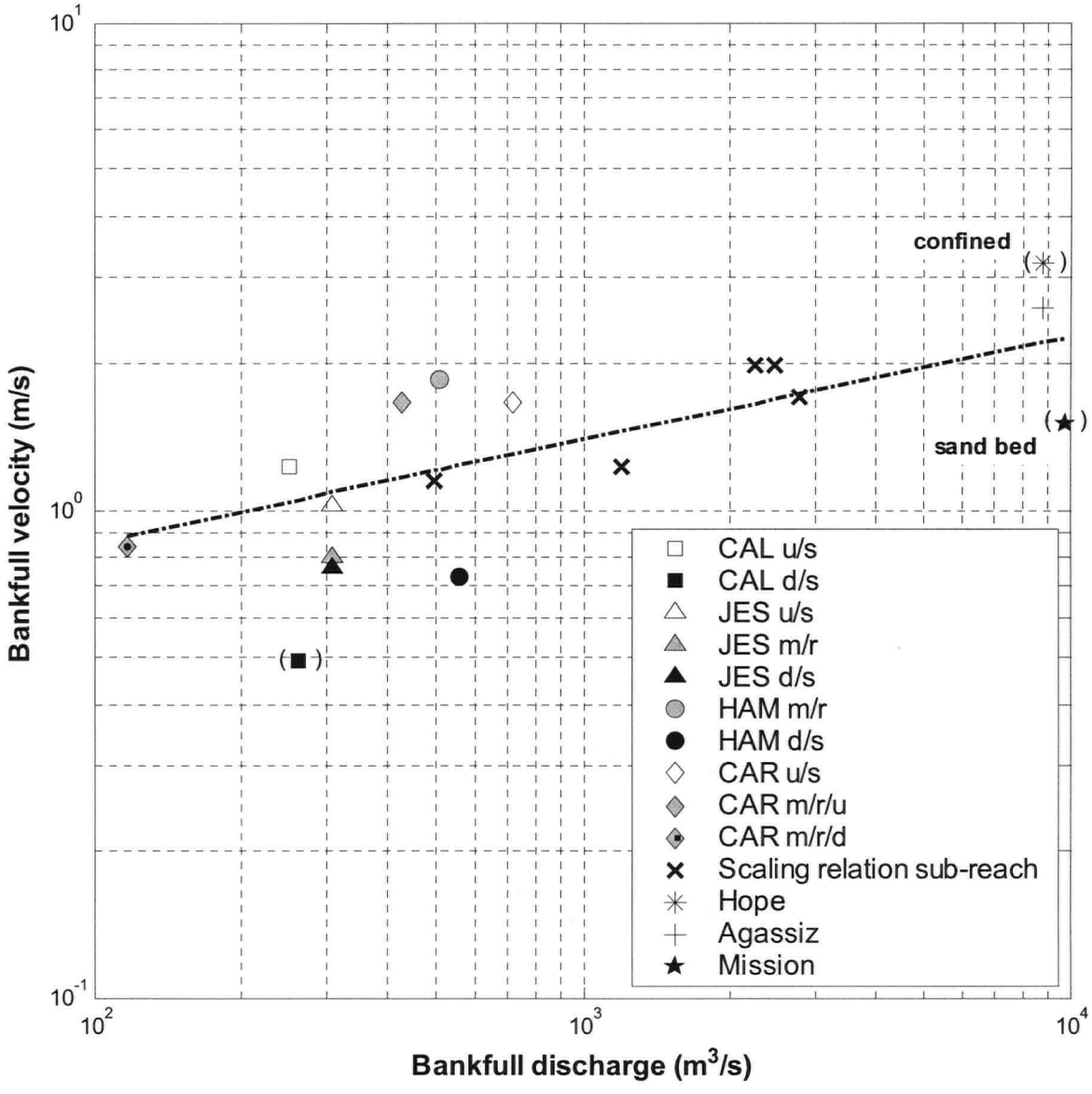

Figure 31 Functional scaling relations for bankfull velocity and discharge, stratified by channel and sub-reach morphology. Relation was derived by continuity from the w-Q and d-Q scaling relations. Bankfull at-a-station parameters are based on the high-flow analyses, where performed (JES, HAM, CAR). CAL d/s parentheses indicate that the data quality is questionable because of a non-significant ($\alpha = 0.05$) d-Q relation.

5 Discussion

5.1 Secondary channel morphology and hydraulics

5.1.1 Patterns in sub-reach morphology

One of the goals of this study is to compare apparently different sub-reach morphologies, to see if any systematic morphological or hydrological trends can be discerned. Trends in at-a-station hydraulic geometry relation exponents, surface and sub-surface sedimentological characteristics, and distributions of near-bottom d/s velocity and depth have been discussed separately in the preceding sections.

Within each sub-reach, the data collected for at-a-station hydraulic geometry relations conformed well to the classical power-form equations, although there were clearly non-power-law departures at low flow. In the mean, the at-a-station hydraulic geometry results suggest that increasing discharge is primarily taken up by increases in mean velocity ($m_{mean} = 0.452$, by continuity) and then by increases in depth ($f_{mean} = 0.425$). However, the relatively wide scatter in the w-Q and d-Q exponents can at least partially be explained by sub-reach morphology. Within the average trend, u/s sub-reaches tend to accommodate more incremental discharge through expansion in water surface width with than do the m/r or d/s sub-reaches. The u/s sub-reaches correspondingly accommodate less incremental discharge through depth than do m/r or d/s sub-reaches. This suggests that u/s sub-reaches will tend to be wider and shallower than m/r and d/s sub-reaches. However, there are exceptions to this trend (e.g. JES u/s, HAM d/s) which suggest that local factors such as the geomorphic history of the channel and bank vegetation must also be considered.

Sedimentological data suggest that surface grain-size distributions tend to be progressively finer with increasing distance down-channel, in an individual secondary channel. D/s sub-reaches are composed of fine sand and silty sand, and show evidence of dune features, whereas the u/s and m/r sub-reaches tend to be composed of gravel and cobbles. Sediment influx from the main channel is likely to terminate in the u/s sub-reaches, except in channels such as CAL, which are quite short. Thus sediment in the m/r of many secondary channels is likely to be relatively immobile. In some reaches, the large calibre of the sediment suggests that it is a lag deposit (e.g. HAM m/r, JES m/r). New deposits in some of the u/s sub-reaches at disparate

points in the river show good agreement in the sub-surface grain-size distribution ($D_{50} \sim 25$ mm, $D_{84} \sim 45$ mm). However, not all secondary channels are likely to receive sediment inputs from the main channel, even if the flow strength were sufficient to mobilize sediment. The angle at which a secondary channel diverges from the main channel, and the main channel planform upstream of the divergence will strongly influence whether sediment is directed away from or into the secondary channel entrance.

Trends in sedimentology of the at-a-station sub-reaches can be linked to the observed trends in hydraulic geometry. U/s sub-reach channel surfaces are composed of cobble or coarse gravel, which suggests that scour is likely to be quite limited. Thus, increases in flow are taken up primarily in changes in width, as demonstrated in the relatively higher at-a-station width exponents of the u/s sub-reaches. In contrast, m/r and d/s sub-reaches have progressively finer sediment and therefore a greater propensity to adjust their depth.

An examination of bivariate frequency distributions of depth and near-bottom velocity suggests that u/s and m/r reaches have generally faster velocities than d/s reaches. Near-bottom velocities in the u/s and m/r sub-reaches can be quite fast, with peak frequencies in the 1-1.5 m/s and 1.5-2 m/s categories. However, sub-reaches in JES tend to be somewhat slower than their counterparts in other channels. The frequency distributions reveal that many of the sub-reaches have a bimodal depth distribution at high flow because of cross-channel depth variation. However, the distribution of near-bottom velocities is relatively uniform across the channel, both at high flow and at more moderate flows. There is considerable overlap in the ranges of the velocity and depth distributions at high flow, although their far greater depth range and tendency to have slower velocities (< 0.5 m/s) often distinguishes the d/s sub-reaches. At more moderate flow levels, the frequency distributions are simplified, generally because the depth distribution tends to be more unimodal. There is a more obvious change in depth with decreasing flow, than in velocity, although this is perhaps a function of the larger total range of depths.

5.1.2 Scaling behaviour of secondary channels

The scaling relations presented in Section 4.2.2 suggest that channels within the Lower Fraser River gravel-reach tend to scale with bankfull discharge. This scaling behaviour is consistent over the large size range of channels surveyed: two orders of magnitude in discharge,

one order of magnitude in water surface width and approximately one-half an order of magnitude in depth. The results of work by Simons and Albertson (1963) suggest that we might expect to see that points from channels in different boundary materials would plot differently (i.e. different coefficients, although the exponent would remain the same). Sample sizes are small for the u/s and d/s sub-reach types (i.e. $n \leq 3$). However according to the results of Simons and Albertson we would expect to see that in the w-Q and d-Q relations points from the d/s sub-reaches (in which the boundary materials are sand and silty-sand) would plot above the other data points (in which boundary materials are coarser). This does appear to be the case, although there are exceptions (e.g. CAL d/s in the w-Q relation, JES d/s in the d-Q relation). A comparison of the points from Mission (sand) and Agassiz (gravel) does not show the expected offset because of the reasons previously discussed. The v-Q scaling relation shows more scatter than either of the other two scaling relations, although some of the points are either questionable (CAL d/s) or have valid reasons why they do not conform (Hope, Mission).

There does not appear to be a comparable set of results from secondary channels in a large, gravel-bed river with which we could compare these results. Tabata and Hickin (2003) explore the idea of scaling behaviour in the anastomosing reach of the Columbia River but, given that these channels are uniformly sand-bed channels, their results are likely to represent a different regime class. Although this study appears to represent the first attempt to explicitly characterize secondary channels in a wandering gravel bed river, a comparison with the data collected in gravel bed rivers of Alberta by Bray (1973) may be informative. Even though his 70 reaches are single-thread, some are from rivers which can be classified as wandering, (e.g. the Oldman River at Brocket, the Red Deer River at Bindloss, the Athabasca River at Whitecourt) (Kellerhals et al., 1972; Bray, 1973). The downstream hydraulic geometry relations that he presents are based on the channel parameters at the 2-year flow (Q_2), which is at or above the threshold for gravel movement in those channels. For further comparison, the results of this study are presented with results from Tabata and Hickin (2003), Andrews (1984), Griffiths (1981), Bray (1973), Simons and Albertson (1963) and the classical exponents from Leopold and Maddock Jr. (1953) in **Table 16**. Bray's results and the results of Simons and Albertson have been converted to SI units from the original presentation in Imperial units. Possible sources of discrepancies are noted for each set of results, such as the choice of scaling flow, channel substrate (if unspecified, the substrate is gravel), and the use of gauging data (if unspecified, field data were used).

Table 16 Comparison of selected downstream hydraulic geometry relations (scaling relations).

Study	w-Q relation	d-Q relation	v-Q relation
Fraser R. gravel reach, 2002 [a]	$w = 4.29Q^{0.535}$	$d = 0.72Q^{0.254}$	$v = 0.32Q^{0.211}$
Tabata and Hickin, 2003 [b]	$w = 3.24Q^{0.64}$	$d = 1.04Q^{0.19}$	$v = 0.30Q^{0.17}$
Andrews, 1984 [c]	$b = 0.478$ or 0.482	$f = 0.377$ or 0.370	$m = 0.145$ or 0.144
Griffiths, 1981 [d]	$w = 7.09Q^{0.48}$	$d = 0.21Q^{0.43}$	$v = 0.61Q^{0.11}$
Bray, 1973 [e]	$w = 4.75Q^{0.527}$	$d = 0.266Q^{0.333}$	$v = 0.79Q^{0.140}$
Simons and Albertson, 1963 [f]	$w = 3.4Q^{0.512}$	$d = 0.273Q^{0.361}$	$v = 1.08Q^{0.127}$
Leopold and Maddock, 1953 [g]	$b = 0.5$	$f = 0.4$	$m = 0.1$

[a] Q = 'bankfull', see Section 4.2.2 for explanation
[b] Q = 'bankfull', sand-bed channels
[c] Q = 'bankfull', relations are dimensionless therefore only exponents are given, results stratified by presence of vegetation: thin and thick vegetation, respectively
[d] Q = mean annual discharge, gauging data used
[e] Q = 2-year flood flow
[f] canals in coarse, non-cohesive materials
[g] Q = mean annual flow, gauging data used

The agreement among the w-Q relations is good, especially when one considers that the 95% confidence interval for the exponent in this study ranges from 0.438 to 0.654, which easily encompasses the range of variation present in **Table 16**. However, the results of Tabata and Hickin clearly diverge from the other w-Q relations in terms of the exponent. The w-Q coefficients show some variation. Theoretically, four of the five w-Q relations belong to the same regime class (gravel-bed rivers), and hence should have similar coefficients. However, only the coefficients from Fraser River and from Bray's Alberta gravel bed rivers show good agreement. When the canal-derived relation of Simons and Albertson for coarse, non-cohesive materials is superimposed on the Fraser River w-Q scaling relation, all data points fall above the line except for Hope. The relation based on canals having sand beds and cohesive banks is actually a far better fit to the data ($w = 4.75Q^{0.512}$). It would appear that the canals do not in this instance serve as perfect physical models of natural river channels, although they may suggest typical patterns of behaviour. The New Zealand gravel-bed river w-Q results presented by Griffiths (1981) have a noticeably higher coefficient than the other gravel-bed relations. Two potential sources of discrepancies are noted. In particular the use of gauging data may mean that non-alluvial reaches were selected. Although the exponents from the Leopold and Maddock Jr.

study are also presented for reference, they represent data gathered from gauging stations and relatively few if any gravel-bed rivers were included.

The agreement between exponents diverges somewhat when one considers the d-Q results. The value of f in this study is noticeably lower than all presented gravel-bed river results. However, there is scatter in the Fraser River results and the 95% confidence interval overlaps with Bray's result ($0.160 \geq f \geq 0.358$), although at the very high end of the interval. Even though Bray does not appear to have used a functional analysis, the trend in the exponent induced by functional analysis would in fact decrease the agreement between the two studies. The coefficients are relatively consistent (all < 0.75), although the Fraser River coefficient is on the high end of the range. The other gravel-bed river d-Q coefficients cluster between 0.2 and 0.3. As the v-Q relations were derived by continuity, the lack of agreement between this study and Bray's results follow from the discussion of the d-Q relations.

All results in **Table 16** except for Fraser River and Columbia River (Tabata and Hickin, 2003) are based on data sets from multiple rivers. Leopold and Maddock Jr. deliberately included rivers from a wide range of physiographic and geologic settings, whereas Bray, Griffiths, and Andrews attempted to sample from within one physiographic setting. The results from this study are from an even more homogeneous physiographic setting since they represent a single morphological reach within one river. In the sense that the Fraser River results are from channels in one river, they represent a genuine regime group, although sediment deposition and backwater effects make the d/s sub-reaches distinct. However, the scaling flow for these relations was chosen in a different way than potentially all preceding studies. We have assumed that the scaling flow in all channels is set by the main channel magnitude-frequency series. However, the side channels flow only part of the year and therefore their magnitude-frequency distributions could differ from the main channel. If one assumes that the zero flows should be included in the distribution, then the side-channel magnitude-frequency distributions should be sensibly the same as the main channel distribution. Another issue complicating the definition of a coherent regime group is the age of the channels. The channel heads are wide and shallow because the sediments are coarse and they are aggradation zones, but they are also young and therefore vegetation is generally sparse. Farther downstream where sediment deposition is less frequent and finer in calibre, vegetation has been established which will thus alter bank strength properties.

Similar secondary channel scaling relations (called "interchannel hydraulic geometry") presented by Tabata and Hickin (2003) for sand-bed channels in the anastomosing reach of Columbia River also diverge from the classical exponents, as well as from other studies. The value of b for the anastomosing reach (0.64) is markedly higher than conventional mean of 0.5, whereas their value for f (0.19) is lower than would be expected (~0.33). They propose that the lack of variation in water surface slope and boundary materials in the anastomosing reach gives rise to a different set of relations than in classical downstream hydraulic geometry, where both of these factors vary in the downstream direction. This would be true if preceding studies had actually implemented downstream hydraulic geometry in the way that it was presented (i.e. as the change along one river channel, measured at many different locations). However, many if not most studies have substituted multiple rivers of different sizes, measured at some common frequency of flow for multiple measurements on one river, simply because the data are easier to obtain. When this substitution has been applied, generally researchers have selected rivers with similar boundary materials and physiographic setting (i.e. a particular regime class). Therefore, it seems less likely that boundary materials would vary in any significant way, although water surface slope might be more variable.

In the case of the present results, the w-Q secondary channel scaling relation shows relatively good agreement with results from other similar regime groups. However, the variation in secondary channel depth with bankfull flow is less variable than would be expected based on preceding results.

5.2 *Issues arising from technological advances in instrumentation*

One of the goals of this study was to evaluate the use of mobile, digital technology in collecting hydraulic data in the field. Acoustic Doppler profiling technology offers the possibility of gathering data much more quickly and easily than has been possible in the past. This technology has been widely used in oceanographic and estuarine applications, for many years. Although when first developed these instruments were suitable for use only in deep channels or in ocean environments, the technology has been refined now to allow their deployment in shallower environments, such as river channels. The use of these instruments in large-scale stream gauging programs is becoming very common (Yorke and Oberg, 2002).

The main advantage that these instruments offer is the possibility of collecting water velocity profile measurements while deploying only a single instrument. In addition, the boat-mounted instrument can potentially account for platform motion, allowing very flexible deployment. And finally, because the data are in a digital format, they can be saved directly onto a computer, saving the effort of entering data by hand. Gathering the same type of data using conventional instrumentation would be far more time-consuming, involving either concurrently deploying a number of current meters on a cable (which would have to be adjusted manually as the channel depth varied), or deploying one current meter at a number of different depths. The boat would normally need to remain stationary during these deployments. It is not surprising that much field research has concentrated on small and medium-size rivers (where hydrologic measurements can be taken either by hand, or from a bridging structure), or that field research has been avoided completely in favour of using gauging data. Given the potential advantages offered by the acoustic Doppler technology, it seems likely that they will become more commonly used and may gradually replace more 'old-fashioned' current-meters.

After having collected and analyzed acoustic Doppler current profiler (aDcp) data, certain issues about the data and the instrument seem worthwhile raising (or emphasizing), for the benefit of those who have not had experience with these instruments. Although some issues may be specific to this study (i.e. as a result of the study location or configuration of the instrument), some are rather more general. Where I refer to acoustic Doppler current meters in general, I will use the term 'aDcp', as opposed to the particular instrument used in this project (ADP).

5.2.1 What is being measured exactly, and with what accuracy and precision?

A major assumption is made when collecting water velocity data with an acoustic Doppler current profiler. That assumption is that the signal returns from which the velocity is calculated are reflected off particles suspended in the water column (often called "scatterers"). Therefore, the instrument does not directly measure the water velocity but rather assumes that particles in the water column are moving at the same speed as the water. Because scatterers of different sizes and shapes are likely to be moving at disparate speeds in the water column, a certain amount of noise is induced into the velocity signal. In an early lake test comparing an acoustic Doppler profiler with conventional current meters (Price AA current meter and a Neil Brown current meter), the investigator concluded that the instrument provided a good measure of velocity during low and medium flow conditions (i.e. $v \sim 0.15 - 1$ m/s), although a 20 second averaging interval was required (Simpson, 1986). However, Simpson noted the tendency of the aDcp velocity measurements to diverge from the conventional measurements as depth increased, although the total profile error due to the divergence was not large (+0.3 % and –2.74% for the Price AA current meter, on two separate tests). It is also interesting to note that, in a concurrent test of the aDcp bottom-track software, the instrument overestimated the course distance in 13 of 14 runs, although the magnitude of the overestimates was relatively small (course length = 1405 m, distance error range: -0.2 - +2.6 %). Although this technology has progressed quite markedly since the early 1990s, there has been relatively little independent work related to the calibration of aDcps. This is attributable to many factors including the difficulties of using pre-existing calibration facilities for aDcp calibration, rapid changes in aDcp technology (Oberg, 2002) and the relative difficulty of comparing traditional current meters (point measurements) with aDcp measurements (spatially-averaged depth bins).

We conducted one test in this project in which the ADP was simultaneously deployed with another current meter. In order to determine whether a constant extrapolation to the surface of the shallowest ADP-measured velocity was reasonable, we deployed a hand-held electromagnetic current meter concurrently with the ADP, while stationary. This was not a true calibration exercise because of the spatial offset of the two instruments. The ADP was deployed as per normal, while the current meter was deployed at a depth which was centered in the upper part of the water profile that was not sampled by the ADP (usually ~ 0.45 m depth). A data file was composed of a number of simultaneous velocity measurements, which were averaged for

each data file. The results of a regression using the average ADP top-bin velocity (v_{ADP}) to predict the average current-meter velocity (v_{em}) deviated significantly from a 1:1 fit:

$$v_{em} = 1.21 v_{ADP} - 0.41 \qquad (42)$$

(n = 34, R^2 = 0.90, SEE = ±0.17 m/s). From the form of the regression, it is clear that the slope deviates from a 1:1 relation, and that a large zero bias is also present (i.e. at slower velocities, the ADP returns faster speeds than the current meter). It was logistically more difficult to perform these measurements at higher velocities, and therefore the bulk of the data points fall between 0 m/s and 1.25 m/s (i.e. n = 28, based on v_{em}), meaning that we can be less confident of the upper part of the curve. However, the data suggest a convergence to a 1:1 relation above 1.25 m/s. Although this exercise was not strictly speaking a calibration, the magnitude of the difference between the two instruments at lower speeds seemed unwarranted given the relatively small distance which separated them (approximately 0.4 m, from the current meter to the center of the top-most ADP bin). Time did not permit the collection of more data and a true calibration was beyond the scope of this project.

As large organizations such as the US Geological Survey (USGS) are increasingly using aDcp instruments for the purposes of stream gauging, they have realized the importance of appropriately calibrating these instruments to conventional measurements, to ensure continuity in their data records. However, their studies have largely relied on the comparison of aDcp-derived discharge estimates with conventionally-derived discharge estimates (e.g. rating curves, Price current meter), rather than a direct comparison of velocities (Mueller, 2002a; Mueller, 2002b). Some tow-tank testing of ADCP units has been performed, with relatively good results (mean velocity differences, BT – tow cart, ranged from –6.6% to +5.9 %), although stationary tests showed an unexplained, small (< 1 cm/s) bias (Oberg, 2002).

Instrument-induced uncertainty due to Doppler noise can be calculated for the instrument used in this study, as specified by the manufacturer (SonTek, 1998) and serves as an indicator of instrument precision. This does *not* include uncertainty due to real variations in the water velocity, and uncertainty induced by platform motion. Uncertainty due to Doppler noise is inversely proportional to depth bin size and the number of samples, and therefore the user can decrease this source of uncertainty by increasing the depth bin size and lengthening the averaging interval. However, some of the advantages of this technology are thereby reduced (e.g. vertical resolution, spatial density of measurements along a cross-section). In addition,

increasing the length of the averaging interval increases the likelihood that a spatial, as well as temporal, average will be performed.

The speed with which measurements can be taken with an aDcp means that instantaneous fluctuations in the flow can be measured, leading to problems in specifying an "average" discharge. To compensate for this possibility, the USGS recommends that all discharge measurements be based on an average of four transects, and that if any one transect varies by more than 5% from the mean, that a second round of four transects be made and an average taken over all transects. This will obviously decrease the potential speed of the sampling process, although it may still be faster than using conventional methods.

There are also concerns regarding ADCP accuracy, in terms of potential sources of bias. Negatively-biased velocities result from referencing boat-motion over a mobile substrate to the bottom-tracking algorithm (Kolb, 1995; Callede et al., 2000). It appears that the higher the operating frequency of the aDcp, the more likely the instrument will be to detect a mobile bottom (Mueller, 2002a). However, determination of a mobile substrate requires both good BT signal coverage and good GPS coverage, something which can be difficult to achieve (see **(3)** as well). In this study we found that the instrument's internal compass suffered from a persistent, unpredictable bias, which affected the magnitude of the projected d/s water velocities. Relatively few studies have discussed the issue of aDcp compass bias (Callede et al., 2000; Rennie, 2002). Most reference material seems to assume that any compass bias would be related to the presence of disturbances in the magnetic field, and that the presence of such disturbances would be verified in the manufacturer-approved compass calibration process. However, we performed a compass calibration before each deployment of the ADP and did not collect data unless the calibration score was acceptable based on the manufacturer's specifications.

5.2.2 Potential vs. actual sampling range

Most manufacturers will specify a maximum sampling range for an acoustic Doppler profiler, based on the operating frequency of the instrument. Lower frequencies are suitable for deeper channels. The maximum profiling range of the instrument used in this study is 15-25 m (SonTek, 1998), which is much deeper than any of the secondary channels that were sampled. However, although the signal strength was consistently strong even in deep water, the bottom-

tracking signal became unreliable at greater depths. The signal appeared to be most reliable at depths between approximately 2 m and 6 m, which effectively set a much shallower limit on useful deployment of the instrument. It is difficult to say whether the loss of signal was simply a result of depth since the deepest sub-reaches were also sand-bed channels, rather than gravel-bed channels, and this may have affected the ability of BT to properly resolve the bottom (see Section 5.2.3 as well). Although loss of BT does not mean that the velocity data are compromised, it does mean that the user must do far more post-processing of the velocity data, even if boat velocity can be adequately measured by using a GPS. This is because the velocity profiles must be truncated at the channel bottom, the location of which would normally be specified by the BT signal. Although the location of the channel bottom is usually marked by a strong increase in signal strength, it is tedious and time consuming to locate that signal 'spike' for every beam in each profile. This could potentially be avoided by deploying a bathymeter or depth-sounder in conjunction with the ADP.

When considering the minimum sampling range, the user must consider the spatial definition of the depth bins, as well as the mounting depth and blanking distance. At a minimum, the instrument deployed in this study required approximately 1.25 m before it could return a velocity measurement, a not insignificant depth especially in channels where the maximum depth might only be four or five meters. In this upper portion of the water column, it has been customary to extrapolate to the surface based on the measurements collected in the remaining part of the profile. The mounting depth can be varied, but it is critical that the transducer head be far enough submerged that a wake not be generated under the transducer face, since the air bubbles greatly impede signal transmission. Also, in the case of this instrument, although the depth cell size was set as low as possible (0.25 m) the spatial definition of the depth cells meant that some information from the next cell was required to return a value for the first cell, setting an effective two-cell minimum limit. As improvements are made to this technology, depth cell sizes, blanking distances and even the instrument itself will no doubt shrink, which will decrease the minimum water depth necessary to sample.

The spatial definition of the depth cells affected the lower part of the water velocity profile as well, since the last 'good' cell requires that the cell beneath it not contain any of the channel bottom. Therefore, a maximum of one cell depth is missing at the bottom of each profile, and an extrapolation must be made in this portion of the profile as well.

It is clear that the potential sampling range that is dictated by a single operating frequency would not be appropriate for all channels. This is particularly the case where channels have high variability (e.g. large shallow areas, such as point bars). An instrument capable of simultaneously operating at two distinct frequencies would be more appropriate for many channels, in order to capture the full range of channel conditions.

5.2.3 Choice of boat-velocity reference

The possibility of deploying an aDcp from a moving platform while being able to measure and compensate for platform motion is one of the very attractive features of these instruments. However, as has been discussed at some length in this document, our experience suggests that the measurement of boat velocity is by no means trouble-free. Although the manufacturer of this instrument recommended the BT boat velocity reference, we had problems with BT signal reception that may have been related to channel depth or channel substrate type. The averaging interval may have played a role in poor BT signal reception, since it was set very low (1s, although in practice 2-3 s). Currently, the manufacturer-supported software will allow a minimum averaging interval of only 5 seconds. However, in a subsequent separate deployment of our instrument using the 5-s averaging interval, we still had problems with BT signal reception. Again, these problems occurred in deeper parts of the channel (depth $\geq$ 6m, approximately), and the substrate was sandy. The stationary data reveal that the BT signal is also somewhat noisy. Although it is known that the BT signal can be biased by a moving bottom (Kolb, 1995; Callede et al., 2000), it is sometimes difficult to infer bottom motion when the signal contains so much noise. To establish whether there is bedload transport before choosing an appropriate boat velocity reference requires a comparison of boat-velocity measurements that have good BT and GPS data. As previously mentioned, it appears that instruments with higher operating frequencies will be more likely to detect moving bottom effects (Mueller, 2002a). Also, in some cases noise in the BT signal appears unrelated to a potentially mobile substrate and may be related to shallow channel depths.

Theoretically, collecting GPS data and BT data allows the user to compensate for BT signal bias induced by a mobile substrate by simply substituting GPS-derived boat velocity data. However, it is worth noting that the manufacturer of this instrument did not recommend using

GPS data as a boat-velocity reference in general, saying that the GPS was not as accurate a reference. This study relied on GPS data mainly to locate aDcp water velocity profile measurements in a common frame of reference, so that inter-profile distances and distances to shore could be calculated. However, had the BT signal been constant (or more nearly so), it would have been possible to derive a relative boat position in the channel by integration of the signal, and thus have no dependence on the GPS. The user would then need to derive a strategy to deal with the near-shore extrapolation. The problems that we experienced with GPS signal reception suggest that (extensive) preliminary testing of potential study sites may be necessary before one can be assured of having a reliable GPS signal. Although some sub-reaches had consistently poor GPS signal reception, in others signal reception was variable over a period of weeks and months. Differential signal reception may thus restrict study sites, although post-hoc differential reception could be explored. An examination of GPS data gathered while stationary suggests that the signal may be affected by persistent, slow drift, even when signal reception appears to be good. Certainly in files where the GPS signal was known to be poor, it was clear that some kind of drift was occurring as large apparent 'leaps' in position were shown. The USGS recommends examining peripheral information recorded with the GPS position that may yield clues as to whether the signal is reliable or not (Mueller, 2002b). Sudden unexplained changes in elevation, loss of satellites and an increase in the horizontal dilution of precision (HDOP) are all signs that the GPS signal *may be* unreliable. We were unable to examine elevation data, number of satellites or HDOP in this study because of the software used to deploy our instrument, which only returned geographical coordinates (in the horizontal plane).

No matter which boat-velocity reference is used, there is one final issue that deserves attention and that is the boat speed while sampling. The recommendation is that the boat speed not exceed the speed of the water being sampled, and preferably be less than the water speed. This requirement may lead to two different problems: (a) choosing a motor capable of low sampling speeds but also capable of sufficient speed that transit along the river is practical, and (b) sampling of low-velocity environments. To address these issues, an additional trolling motor, capable of consistently low speeds may be required in addition to a larger motor for navigation. Alternatively, more recently aDcps are being mounted on smaller platforms that can be deployed remotely, or on a manual tether.

5.2.4 Measurement of channel depth

Although the ADP was capable of measuring channel depth by means of the bottom-tracking algorithm, our experience in this study suggests that the BT depth may not be comparable with the more traditional vertical depths returned by depth-sounders or bathymeters. The lack of agreement in this study between ADP depths and chart-sounder depths could be attributable to the spatial offset between the two instruments in the boat, and therefore it would have been interesting to have deployed a bathymeter in conjunction with the ADP, for comparison. Depth is measured along each ADP beam and therefore a spatial average over some part of the channel is performed at each depth measurement. More traditional depth measurements employ one beam and therefore represent the depth at a single vertical, although beam-spreading effects may bias these measurements. Another potential source of disagreement may be the different operating frequencies of the two instruments. Particularly over soft bottoms, operating frequency may lead to large discrepancies between an aDcp and conventional depth sounder, although some manufacturers are now offering the possibility of integrating an echo-sounder into aDcp data collection. There appear to be no studies systematically comparing ADCP depth estimates with conventional depth estimates.

5.2.5 Post-processing of ADCP data

Although an ADCP may allow the user to collect more data more rapidly, and thereby decrease the expense of fieldwork, time spent on post-processing is likely to be higher. Manufacturers supply software for data collection and data processing but, in our experience, the software is rather limited in its output (e.g. depth-averaged velocities, discharge estimates). To explore or manipulate the data in more detail will almost certainly require knowledge of a programming language, preferably one with good graphical capabilities. The sheer volume of the data that can be collected means that more time may be required to reduce the data to a more manageable and desirable format.

6 Conclusions

In this study, we have attempted to characterize the hydraulics and morphology of 11 sub-reaches of secondary channels within the lower Fraser River gravel reach, through analysis of sub-reach averaged channel characteristics (at-a-station hydraulic geometry), distributions of depth and near-bottom d/s velocity, and surface and sub-surface sedimentology. Hydraulic and morphological data were collected over a wide range of flows in all sub-reaches, using an ADP for in-channel velocity measurements. Traditional power-law formulations of the at-a-station hydraulic geometry relations provide a good fit to the majority of the higher flow data, although at low flow, deviations become apparent. It was hypothesized that different sub-reach types (u/s, m/r and d/s) would stratify along gradients of width, depth, velocity and surface grain-size. There is some evidence for this stratification, although local effects are also clear. U/s sub-reaches tend to be wider and shallower than either m/r or d/s sub-reaches. U/s and m/r sub-reaches also tend to be faster-flowing and to have coarser substrates than d/s sub-reaches. Individual sub-reaches can differ from these trends, and individual channels such as JES show differences from other secondary channels.

Additional data were collected at high flow in order to generate scaling relations for a range of secondary channels within the lower Fraser River gravel reach. These data are also well described by simple power-law formulations, and suggest that bankfull secondary channel form scales with discharge. Where expected, main channel data agree with the scaling relations, suggesting that the scaling behaviour is consistent up to and including the largest channels in this reach. The scaling relation of water surface width to discharge compares well with the corresponding downstream hydraulic geometry relation of Bray (1973), for Alberta gravel bed rivers. However, the agreement between the d-Q relations is not as good. It is not known whether scaling relations for individual river reaches may prove to be specific to each river rather than being more broadly applicable to a regime group.

This study tested the feasibility of collecting field data using an acoustic Doppler current profiler. In short, we would not have been able to collect the volume of data that we did, had we been using conventional instruments. However, data collection with an ADCP requires constant monitoring in the field to ensure quality control, a fact that became clear in the post-processing of this data. Post-processing was labour intensive and very time-consuming, which to a large extent offset the time saved during data collection. It is likely that with the benefit of knowledge

gained through this exercise, much time could have been saved in the post-processing stage: first, by ensuring good data quality in the field (through changes to the configuration and deployment of the instrument, and monitoring of real-time data); and secondly because of my familiarity with the idiosyncrasies of the data, and with the programming language that I learned in order to analyze the data. Ultimately, the profiling range of this instrument was somewhat problematic for sampling in these relatively shallow channels, except at high flows. However an instrument with a higher operating frequency would have been unusable in the d/s sub-reaches and the larger channels sampled for the scaling relations. There is a need for an instrument that has the capability to simultaneously sample shallow and deep channel environments, for use in naturally heterogeneous river environments.

References

Andrews, E.D., 1984. Bed-material entrainment and hydraulic geometry of gravel-bed rivers in Colorado. Geological Society of America Bulletin, 95: 371-378.

Anon., 1996. MARCH I/II Operator's Manual. Corvallis Microtechnology, Inc., Corvallis, OR.

Barford, N.C., 1985. Experimental Measurements: precision, error and truth. John Wiley & Sons, Chichester, 159 pp.

Beers, Y., 1957. Introduction to the Theory of Error. Addison-Wesley Publishing Company, Inc., 66 pp.

Blench, T., 1952. Regime theory for self-formed sediment-bearing channels. Transactions of the American Society of Civil Engineers, 117: 383-400, discussion 401-8.

Bray, D.I., 1973. Regime relations for Alberta gravel-bed rivers, Proceedings of Hydrology Symposium No. 9: Fluvial Processes and Sedimentation. National Research Council of Canada, pp. 440-452.

Callede, J., Kosuth, P., Guyot, J.-L. and Guimaraes, V.S., 2000. Discharge determination by Acoustic Doppler Current Profilers (ADCP): a moving bottom error correction method and its application on the River Amazon at Obidos. Hydrological Sciences Journal, 45(6): 911-924.

Church, M. and Mark, D.M., 1980. On size and scale in geomorphology. Progress in Physical Geography, 4: 342-390.

Church, M.A., McLean, D.G. and Wolcott, J.F., 1987. River bed gravels: sampling and analysis. In: C.R. Thorne, J.C. Bathurst and R.D. Hey (Editors), Sediment Transport in Gravel-bed Rivers. John Wiley & Sons Ltd., New York, pp. 43-79.

Clifford, N.J., 1996. Classics in physical geography revisited: Leopold, L.B. and Maddock, T.M. jr 1953: The hydraulic geometry of stream channels and some physiographic implications. USGS Professional Paper 252. Progress in Physical Geography, 20(1): 81-87.

Ferguson, R.I., 1986. Hydraulics and hydraulic geometry. Progress in Physical Geography, 10(1): 1-31.

Griffiths, G.A., 1981. Hydraulic geometry relationships of some New Zealand gravel bed rivers. Journal of Hydrology (New Zealand), 19(2): 106-118.

Hogan, D.L. and Church, M., 1989. Hydraulic geometry in small, coastal stream: progress toward quantification of salmonid habitat. Canadian Journal of Fisheries and Aquatic Sciences, 46: 844-852.

Huang, H.Q. and Nanson, G.C., 1997. Vegetation and channel variation: a case study of four small streams in southeastern Australia. Geomorphology, 18: 237-249.

Johnson, P.A. and Heil, T.M., 1996. Uncertainty in estimating bankfull conditions. Water Resources Bulletin, 32(6): 1283-1291.

Jowett, I.G., 1998. Hydraulic geometry of New Zealand rivers and its use as a preliminary method of habitat assessment. Regulated Rivers: Research and Management, 14(5): 451-466.

Kellerhals, R., Neill, C.R. and Bray, D.I., 1972. Hydraulic and geomorphic characteristics of rivers in Alberta, River Engineering and Surface Hydrology Report 72-1.

Knighton, A.D., 1974. Variation in width-discharge relation and some implications for hydraulic geometry. Geological Society of America Bulletin, 85: 1069-1076.

Knighton, D., 1998. Fluvial forms and processes: a new perspective. Arnold, London, 383 pp.

Kolb, M., 1995. Experiences with vessel borne ADCPs in shallow waters, Proceedings of the IEEE Fifth Working Conference on Current Measurements. IEEE, pp. 79-82.

Lacey, G., 1958. Flow in alluvial channels with sandy mobile beds. Proceedings of the Institution of Civil Engineers (London), 9: 145-251.

Lane, E.W., 1955. Design of stable channels. Transactions of the American Society of Civil Engineers, 120: 1234-1279.

Lane, E.W. and Carlson, E.J., 1953. Some factors affecting the stability of canals constructed in coarse granular materials, Proceedings of the Minnesota International Hydraulics Convention, Joint Meeting of the International Association for Hydraulics Research and Hydraulics Division. American Society of Civil Engineers, pp. 37-48.

Leopold, L.B. and Maddock Jr., T., 1953. The hydraulic geometry of stream channels and some physiographic implications. United States Geological Survey Professional Paper, 252.

Mark, D.M. and Church, M., 1977. On the misuse of regression in earth science. Mathematical Geology, 9(1): 63-75.

Marsh-McBirney, 1990. Model 2000 Installation and Operations Manual. Marsh-McBirney, Frederick, MD.

McLean, D.G. and Church, M., 1999. Sediment transport along lower Fraser River, 2, Estimates based on the long-term gravel budget. Water Resources Research, 35(8): 2549-2559.

McLean, D.G., Church, M. and Tassone, B., 1999. Sediment transport along lower Fraser River, 1, Measurements and hydraulic computations. Water Resources Research, 35(8): 2533-2548.

Millar, R.G., 2000. Influence of bank vegetation on alluvial channel pattern. Water Resources Research, 36(4): 1109-1118.

Millar, R.G. and Quick, M.C., 1993. Effect of bank stability of alluvial channel pattern. Journal of Hydraulic Engineering, 119(12): 1343-1363.

Miller, T.K. and Onesti, L.J., 1979. The relationship between channel shape and sediment characteristics in the channel perimeter. Geological Society of America Bulletin, 90: 301-304.

Mosley, M.P., 1982. Analysis of the effect of changing discharge on channel morphology and instream uses in a braided river, Ohau River, New Zealand. Water Resources Research, 18(4): 800-812.

Mueller, D.S., 2002a. Field assessment of acoustic-Doppler based discharge measurements. In: T.L. Wahl, T.B. Vermeyen, K.A. Oberg and C.A. Pugh (Editors), Hydraulic Measurements and Experimental Methods 2002. American Society of Civil Engineers, Estes Park, CO.

Mueller, D.S., 2002b. Use of acoustic Doppler instruments for measuring discharge in streams with appreciable sediment transport. In: T.L. Wahl, T.B. Vermeyen, K.A. Oberg and C.A. Pugh (Editors), Hydraulic Measurements and Experimental Methods 2002. American Society of Civil Engineers, Estes Park, CO.

Northcote, T.G. and Larkin, P.A., 1989. The Fraser River: A major salmonine production system. In: D.P. Dodge (Editor), Proceedings of the International Large River Symposium. Special Publications of the Fisheries and Aquatic Sciences 106, pp. 172-204.

Oberg, K.A., 2002. In search of easy-to-use methods for calibrating ADCP's for velocity and discharge measurements. In: T.L. Wahl, T.B. Vermeyen, K.A. Oberg and C.A. Pugh (Editors), Hydraulic Measurements and Experimental Methods 2002. American Society of Civil Engineers, Estes Park, CO.

Park, C.C., 1977. World-wide variation in hydraulic geometry exponents of stream channels: an analysis and some observations. Journal of Hydrology, 33: 133-46.

Parker, G., 1979. Hydraulic geometry of active gravel rivers. Journal of Hydraulic Engineering, 105(HY9): 800-812.

Perrin, C.J., Rempel, L.L. and Rosenau, M.L., 2003. White sturgeon spawning habitat in an unregulated river: Fraser River, Canada. Transactions of the American Fisheries Society, 132: 154-165.

Rempel, L.L., Richardson, J.S. and Healey, M.C., 1999. Flow refugia for benthic macroinvertebrates during flooding of a large river. The North American Benthological Society, 18(1): 34-48.

Rennie, C.D., 2002. Non-invasive measurement of fluvial bedload transport velocity using an acoustic Doppler current profiler. PhD Thesis, University of British Columbia, Vancouver, 233 pp.

Rennie, C.D., Millar, R.G. and Church, M.A., 2002. Measurement of bed load velocity using an acoustic Doppler current profiler. Journal of Hydraulic Engineering, 128(5): 473-483.

Simons, D.B. and Albertson, M.L., 1963. Uniform water conveyance channels in alluvial material. Transactions of the American Society of Civil Engineers, 128: 65-167.

Simpson, M.R., 1986. Evaluation of a vessel-mounted acoustic doppler current profiler for use in rivers and estuaries, Proceedings of the IEEE Third Working Conference on Current Measurement, Airlie, VA, pp. 106-121.

SonTek, 1998. SonTek ADP™ Acoustic Doppler Profiler Documentation. SonTek, San Diego, CA.

Stalnaker, C.B., Milhous, R.T. and Bovee, K.D., 1989. Hydrology and hydraulics applied to fishery management in large rivers, Proceedings of the International Large River Symposium. Canadian Special Publication of Fisheries and Aquatic Sciences 106, pp. 13-30.

Tabata, K.K. and Hickin, E.J., 2003. Interchannel hydraulic geometry and hydraulic efficiency of the anastomosing Columbia River, southeastern British Columbia, Canada. Earth Surface Processes and Landforms, 28: 837-852.

Taylor, J.R., 1982. An Introduction to Error Analysis: the study of uncertainties in physical measurements. University Science Books, Mill Valley, CA.

Yorke, T.H. and Oberg, K.A., 2002. Measuring river velocity and discharge with acoustic Doppler profilers. Flow Measurement and Instrumentation, 13: 191-195.

Zar, J.H., 1999. Biostatistical Analysis, 4th edition. Prentice-Hall, Inc., Upper Saddle River, 663 pp.

Appendix A: Plots of sub-reach at-a-station hydraulic geometry relations

Plots of all at-a-station hydraulic geometry relations are provided. The functional regression (FR) and simple linear regression (SLR) are both provided for comparison, as well as statistical measures of goodness-of-fit. The latter correspond solely to the functional form of the relation.

Table of figures: Appendix A

1. Jesperson

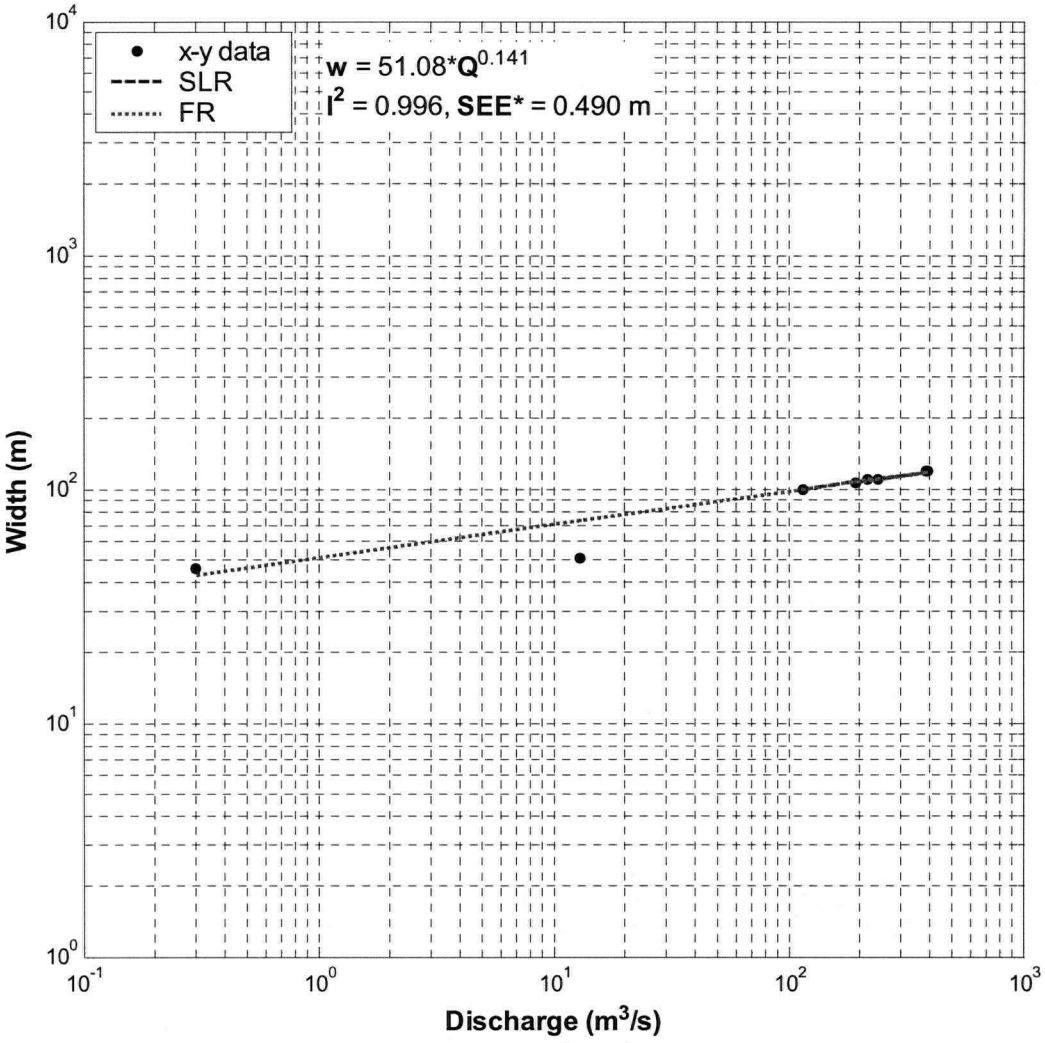

Figure A-1 Jesperson u/s sub-reach, at-a-station hydraulic geometry relation of width (m) with sub-reach discharge (m^3/s). Fit is based on high-flow data (upper six points) and has been extended for comparison with low-flow data.

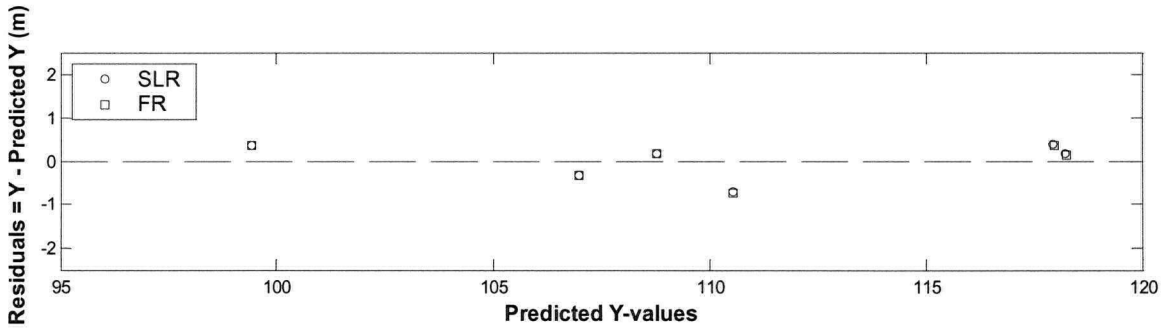

Figure A-2 Jesperson u/s sub-reach, residuals corresponding to high-flow data in **Figure A-1**.

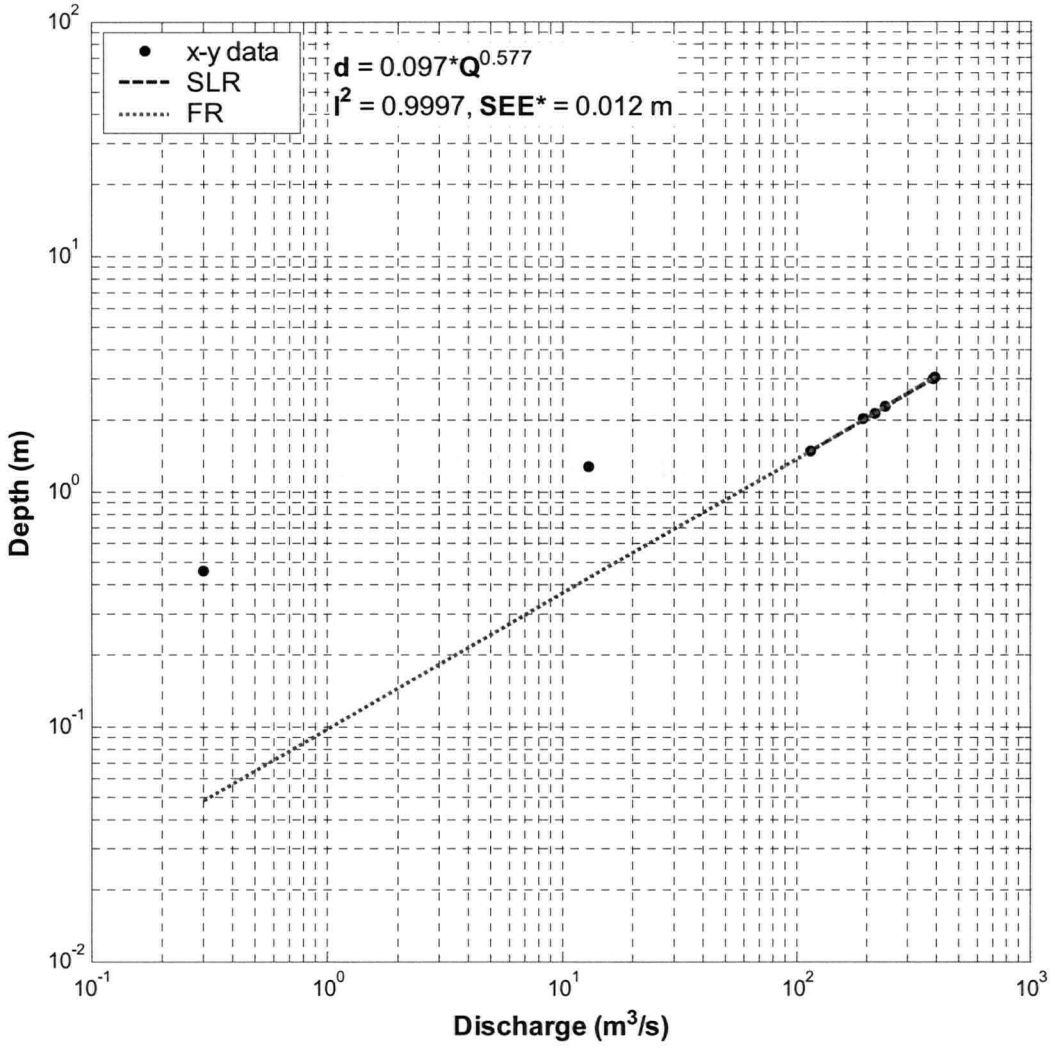

Figure A-3 Jesperson u/s sub-reach, at-a-station hydraulic geometry relation of depth (m) with sub-reach discharge (m^3/s). Fit is based on high-flow data (upper six points) and has been extended for comparison with low-flow data.

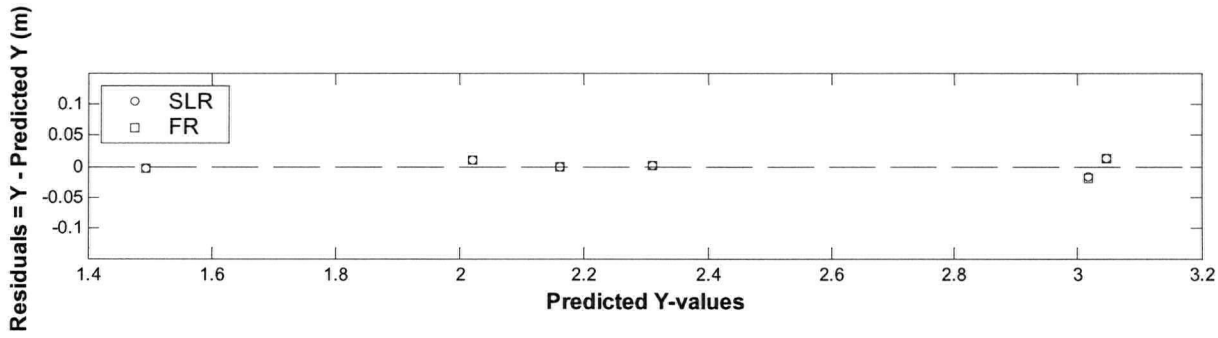

Figure A-4 Jesperson u/s sub-reach, residuals corresponding to high-flow data in **Figure A-3**.

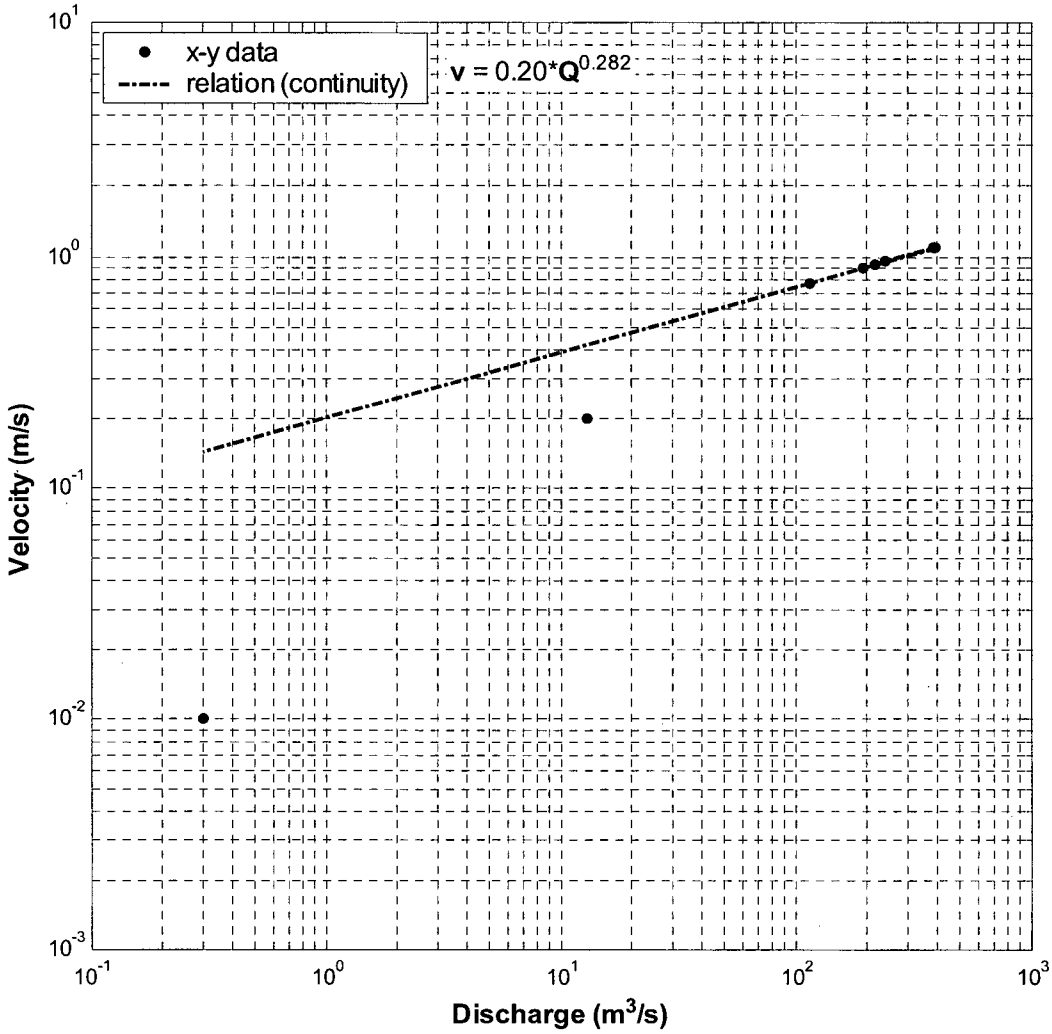

Figure A-5 Jesperson u/s sub-reach, at-a-station hydraulic geometry relation of velocity (m/s) with sub-reach discharge (m^3/s). The relation was derived by continuity (see Section 4.1.1) and super-imposed on the actual data points.

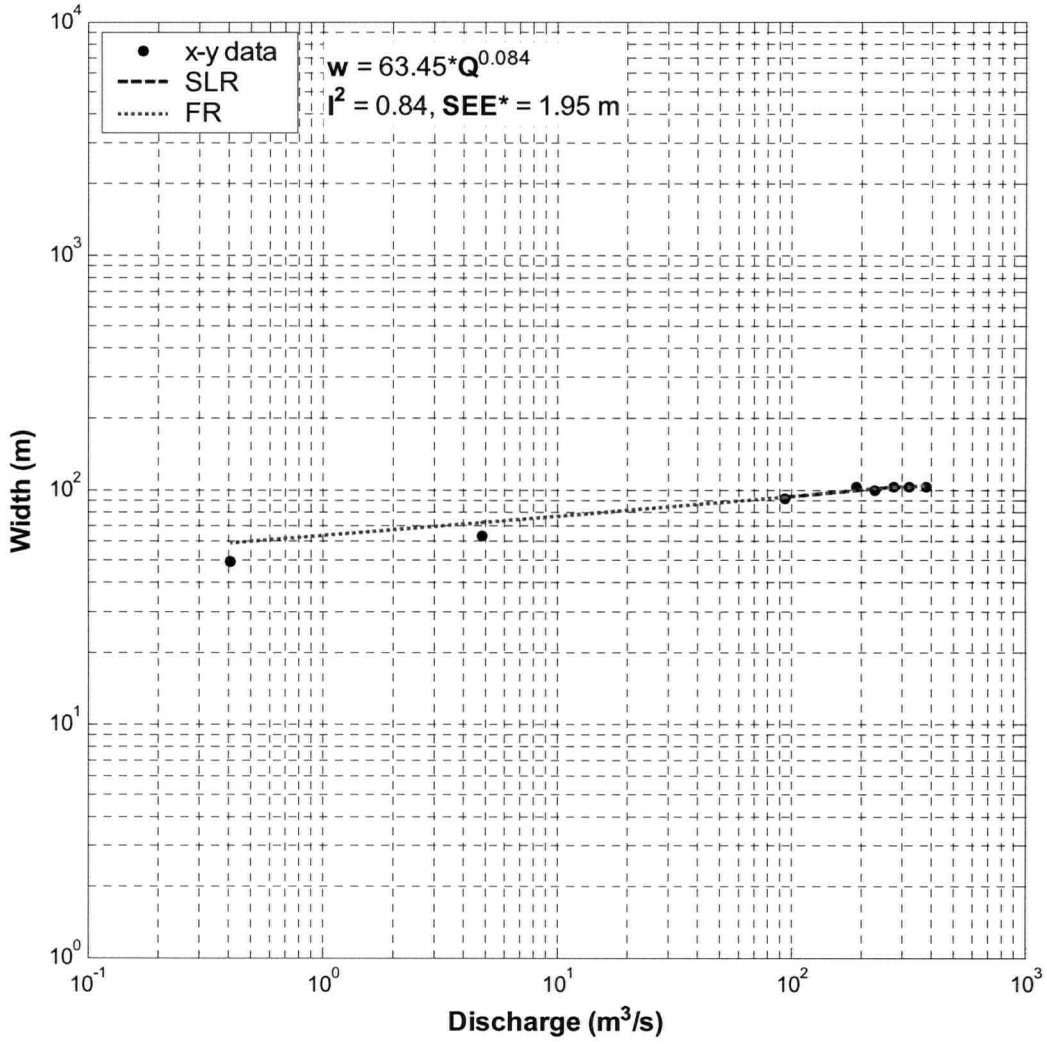

Figure A-6 Jesperson mid sub-reach, at-a-station hydraulic geometry relation of width (m) with sub-reach discharge (m^3/s). Fit is based on high-flow data (upper six points) and has been extended for comparison with low-flow data.

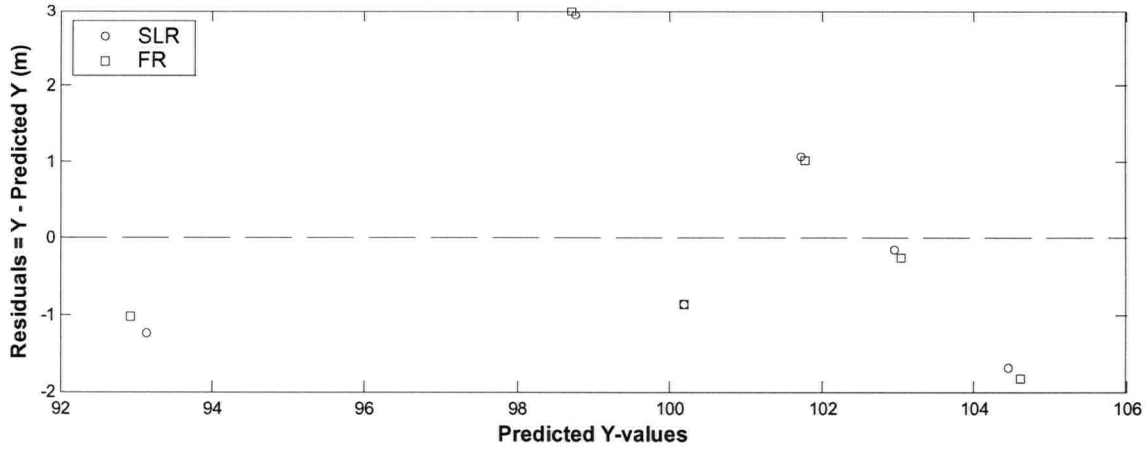

Figure A-7 Jesperson mid sub-reach, residuals corresponding to high-flow data in **Figure A-6**.

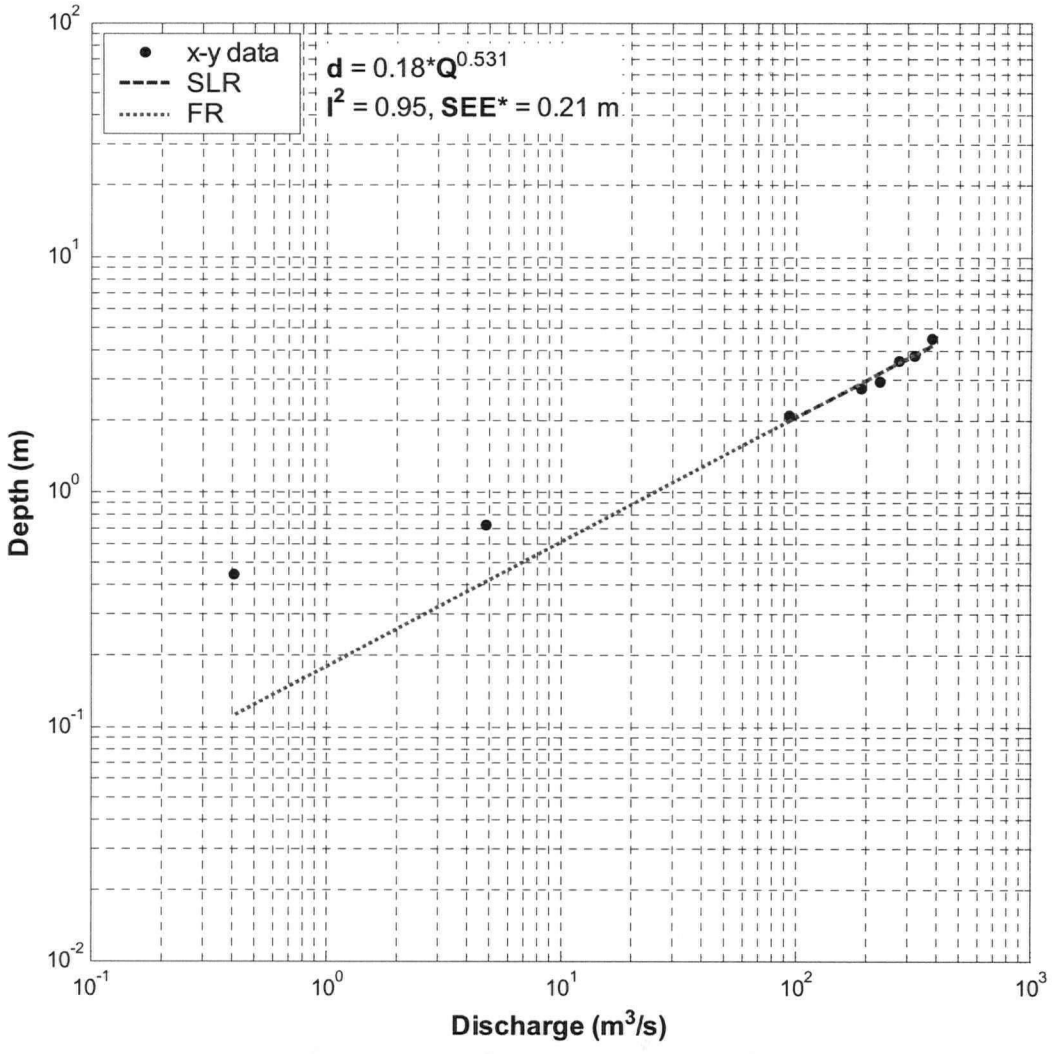

Figure A-8 Jesperson mid sub-reach, at-a-station hydraulic geometry relation of depth (m) with sub-reach discharge (m^3/s). Fit is based on high-flow data (upper six points) and has been extended for comparison with low-flow data.

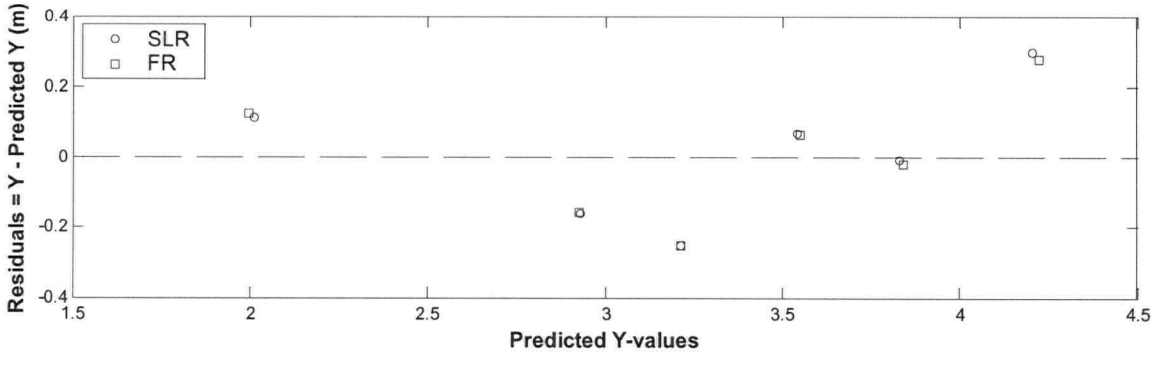

Figure A-9 Jesperson mid sub-reach, residuals corresponding to high-flow data in **Figure A-8**.

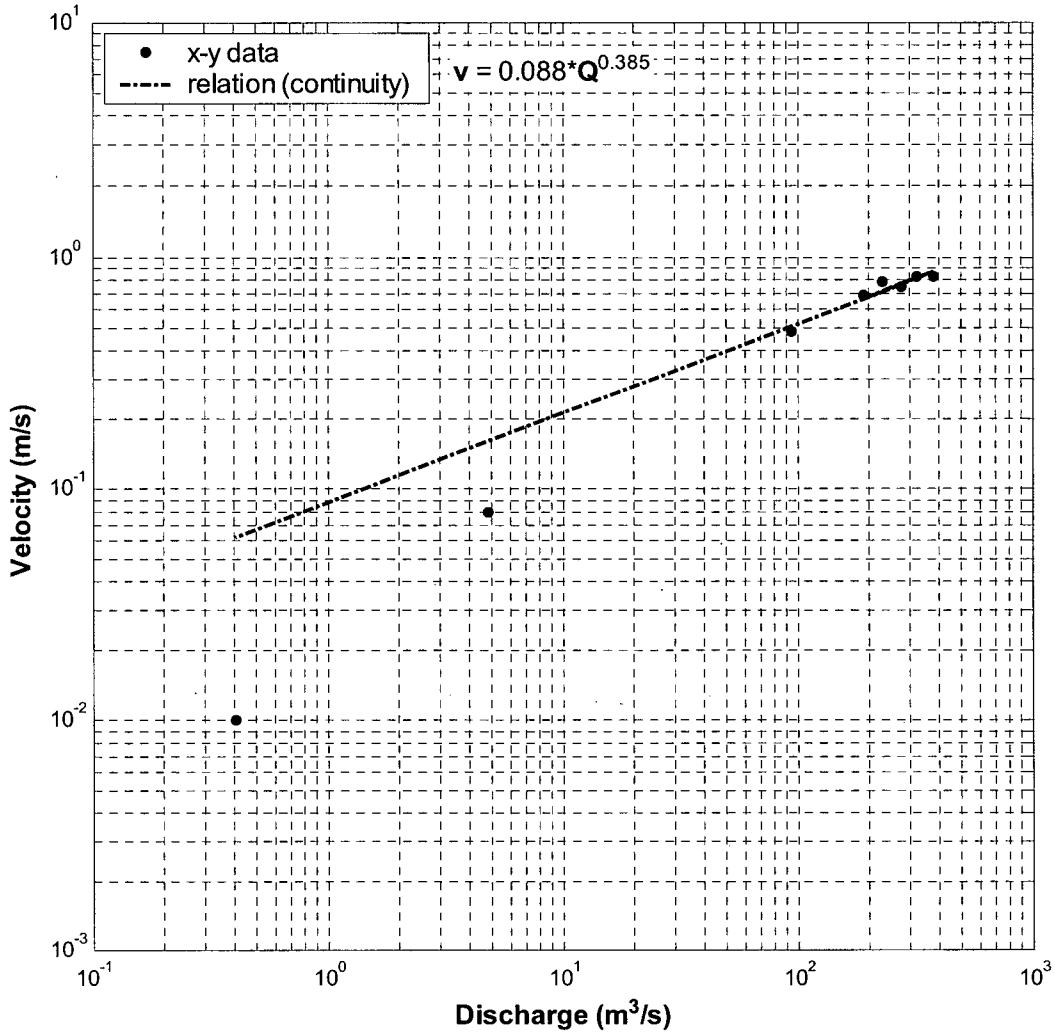

Figure A-10 Jesperson mid sub-reach, at-a-station hydraulic geometry relation of velocity (m/s) with sub-reach discharge (m^3/s). The relation was derived by continuity (see Section 4.1.1) and super-imposed on the actual data points.

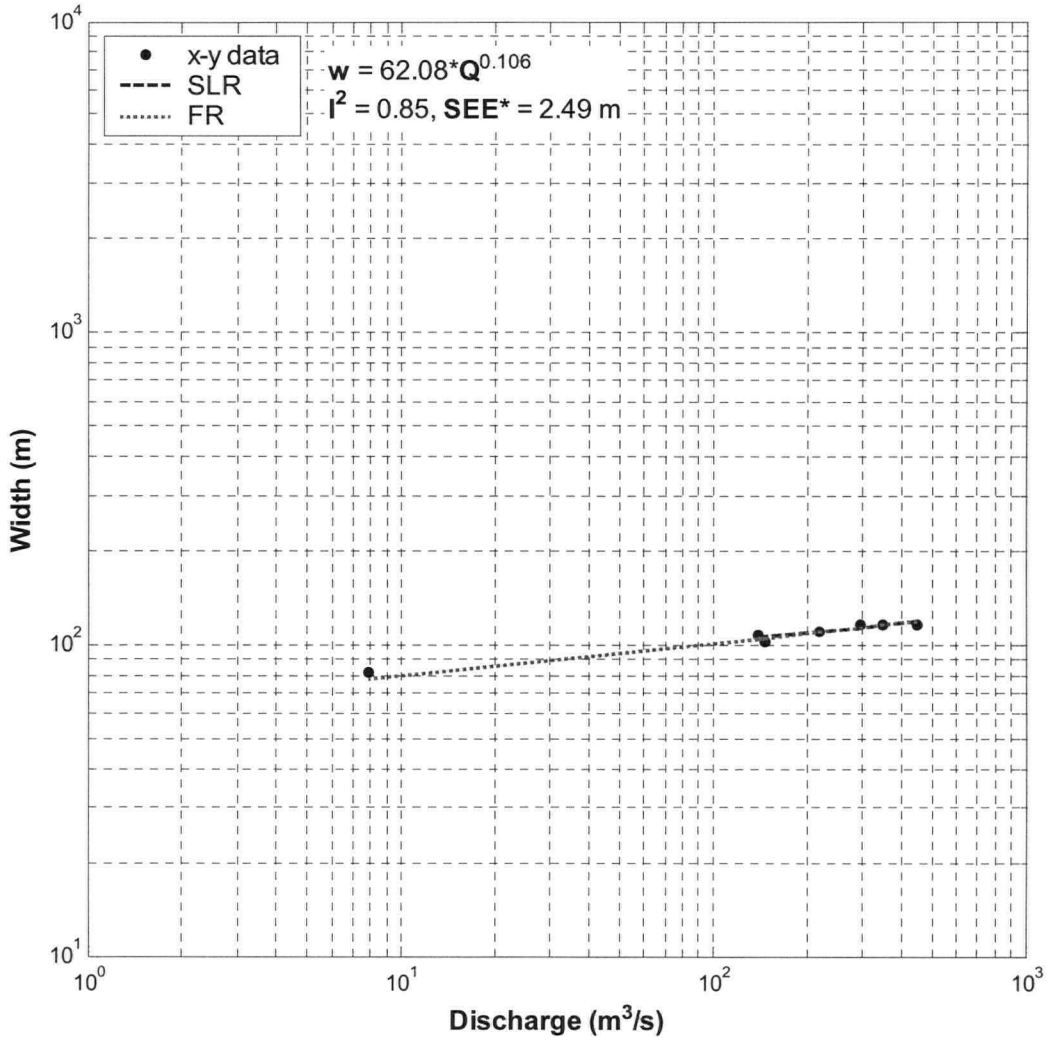

Figure A-11 Jesperson d/s sub-reach, at-a-station hydraulic geometry relation of width (m) with sub-reach discharge (m^3/s). Fit is based on high-flow data (upper six points) and has been extended for comparison with low-flow data.

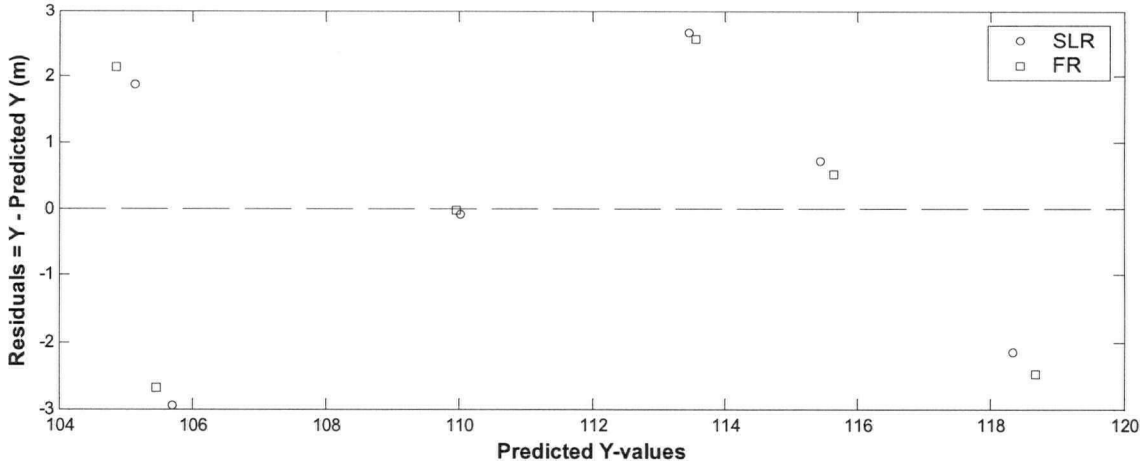

Figure A-12 Jesperson d/s sub-reach, residuals corresponding to high-flow data in **Figure A-11**.

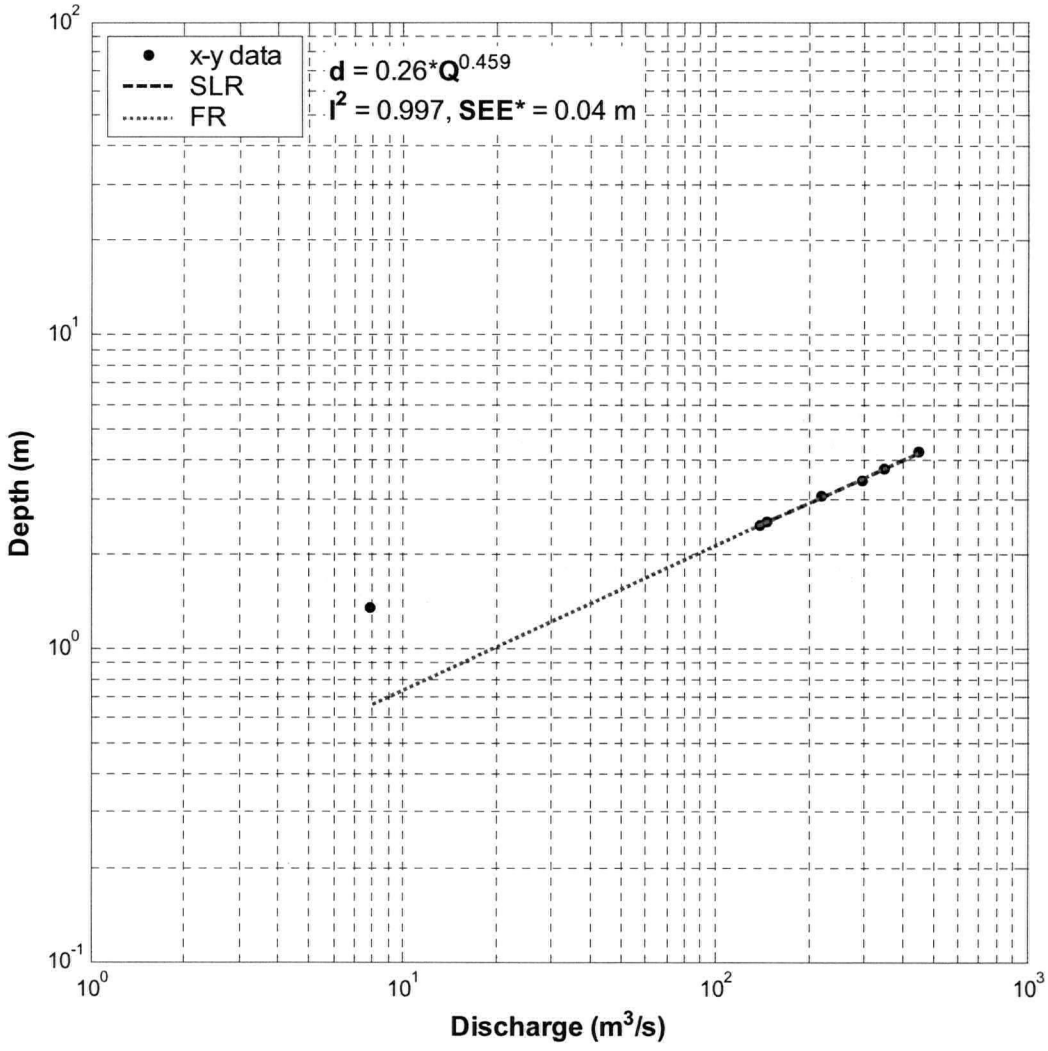

Figure A-13 Jesperson d/s sub-reach, at-a-station hydraulic geometry relation of depth (m) with sub-reach discharge (m^3/s). Fit is based on high-flow data (upper six points) and has been extended for comparison with low-flow data.

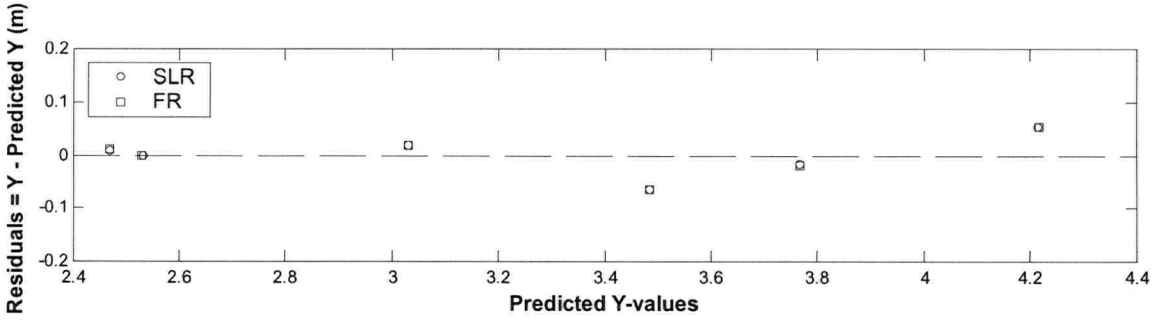

Figure A-14 Jesperson d/s reach, residuals corresponding to high-flow data in **Figure A-13**.

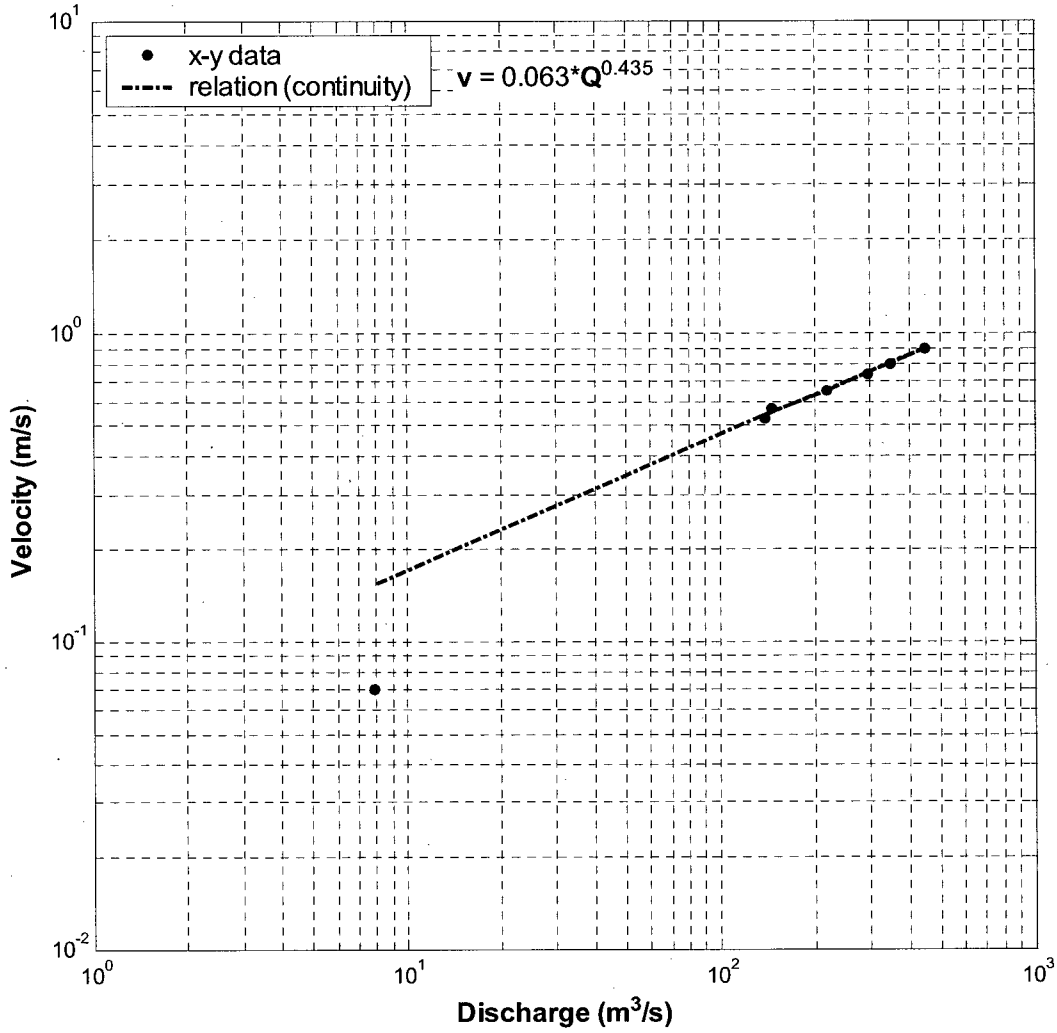

Figure A-15 Jesperson d/s sub-reach, at-a-station hydraulic geometry relation of velocity (m/s) with sub-reach discharge (m^3/s). The relation was derived by continuity (see Section 4.1.1) and super-imposed on the actual data points.

2. Carey

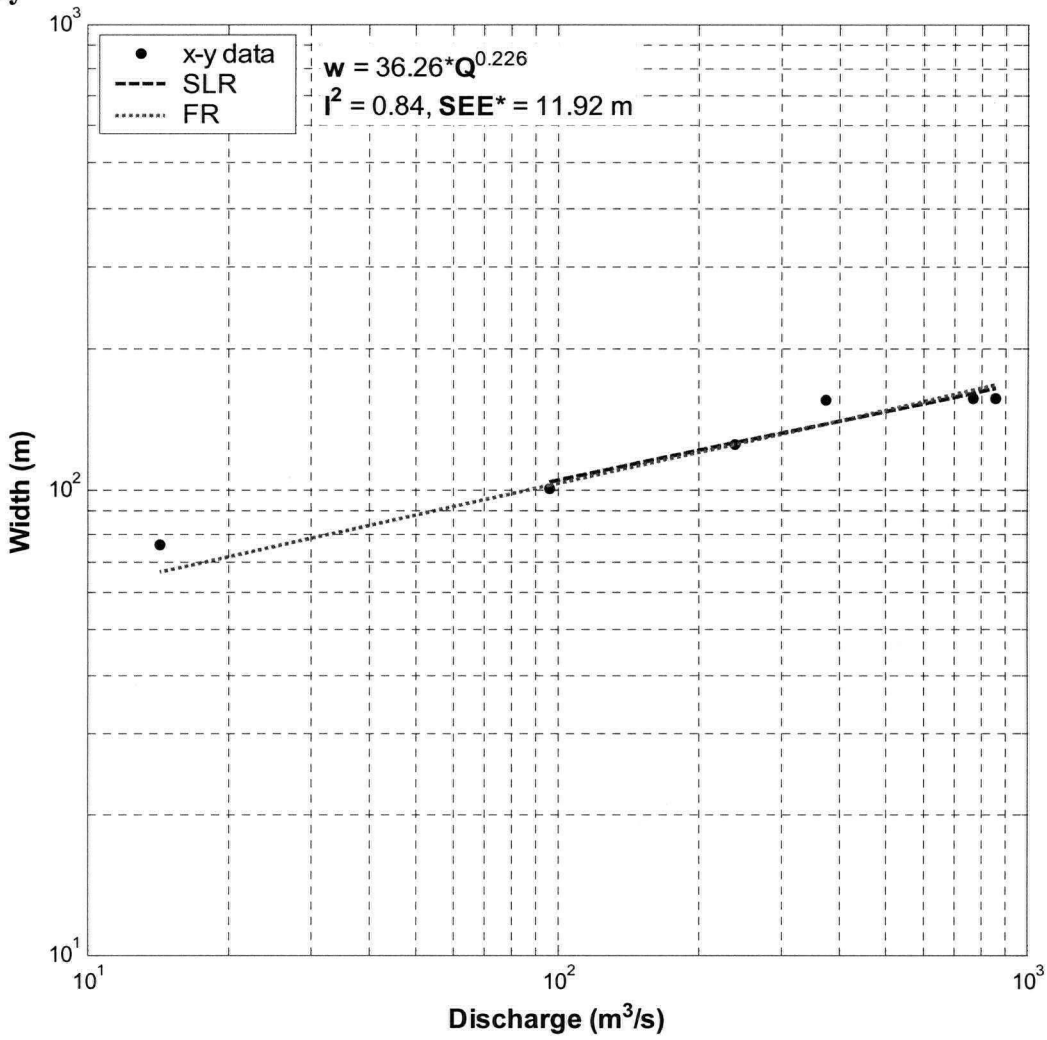

Figure A-16 Carey u/s sub-reach, at-a-station hydraulic geometry relation of width (m) with sub-reach discharge (m^3/s). Fit is based on high-flow data (upper five points) and has been extended for comparison with low-flow datum.

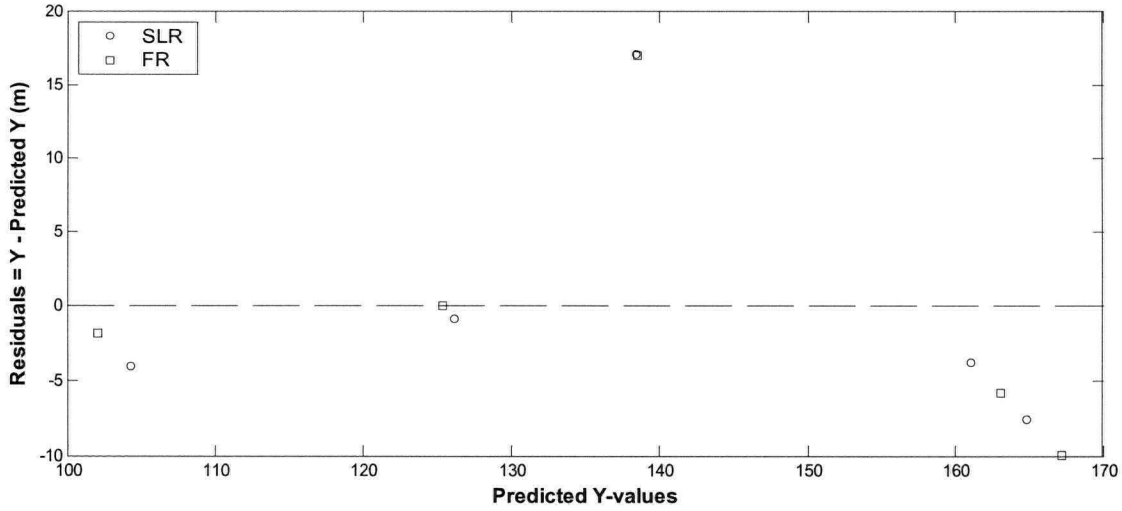

Figure A-17 Carey u/s sub-reach, residuals corresponding to high flow data in **Figure A-16**.

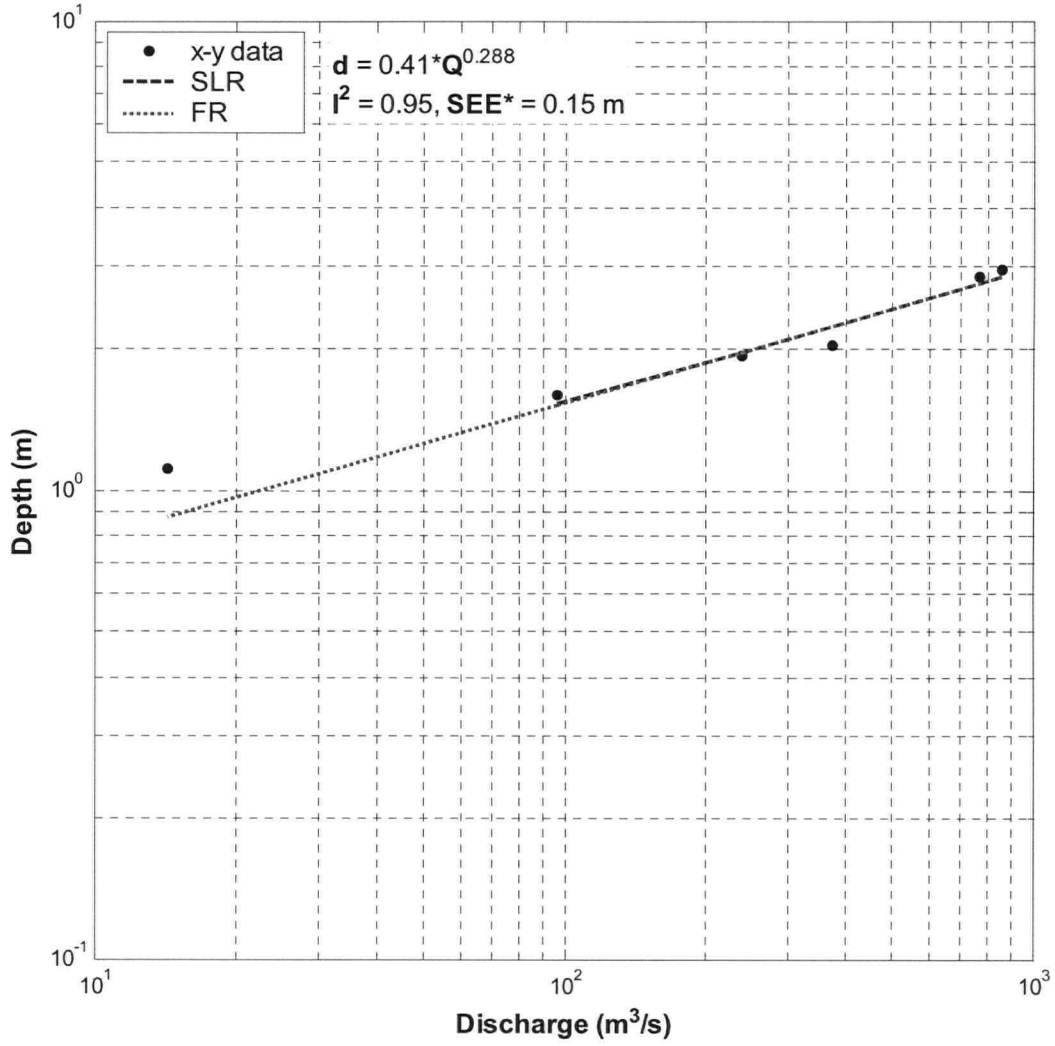

Figure A-18 Carey u/s sub-reach, at-a-station hydraulic geometry relation of depth (m) with sub-reach discharge (m^3/s). Fit is based on high-flow data (upper five points) and has been extended for comparison with low-flow datum.

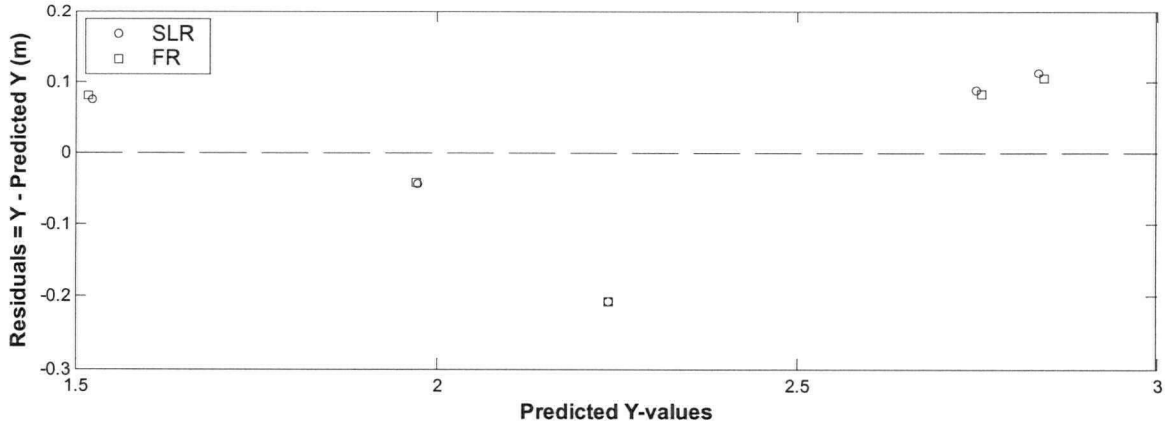

Figure A-19 Carey u/s sub-reach, residuals corresponding to high-flow data in **Figure A-18**.

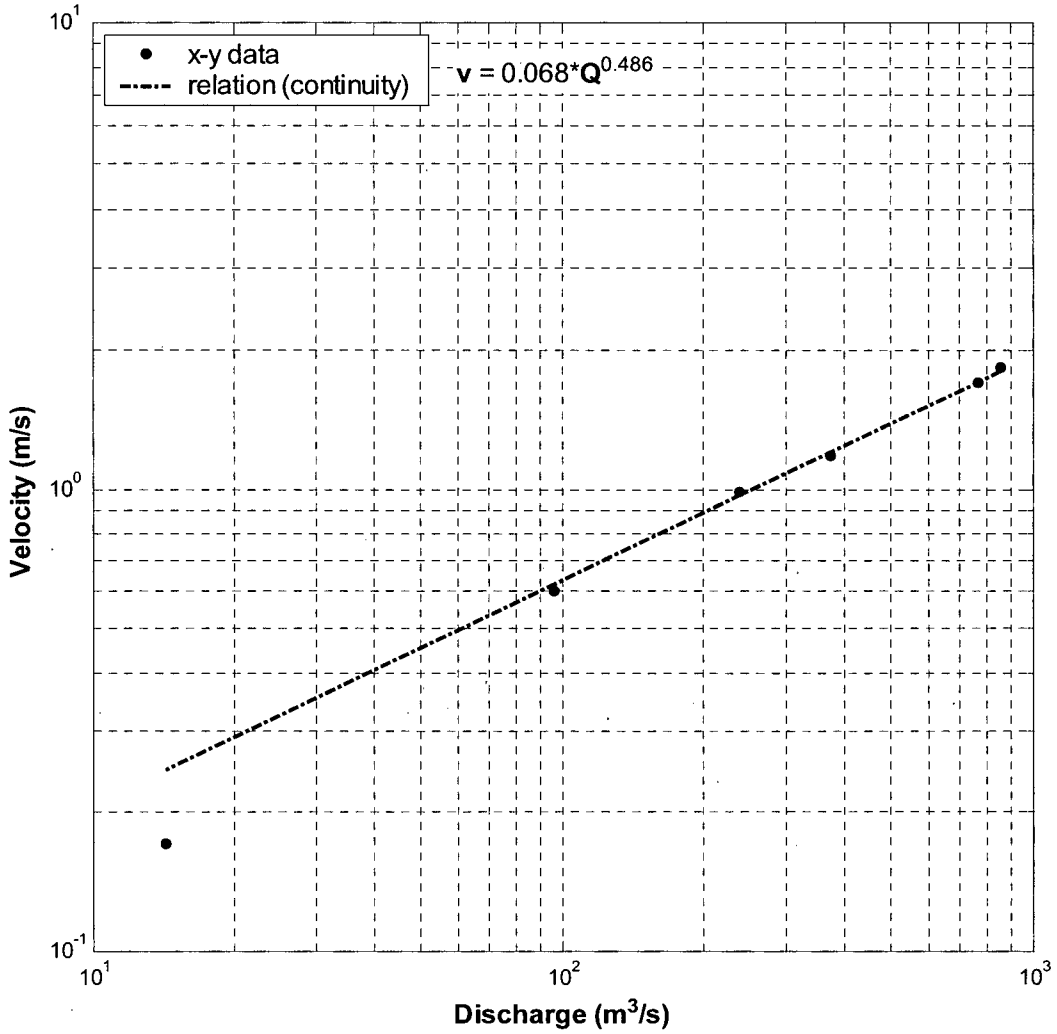

Figure A-20 Carey u/s sub-reach, at-a-station hydraulic geometry relation of velocity (m/s) with sub-reach discharge (m^3/s). The relation was derived by continuity (see Section 4.1.1) and super-imposed on the actual data points.

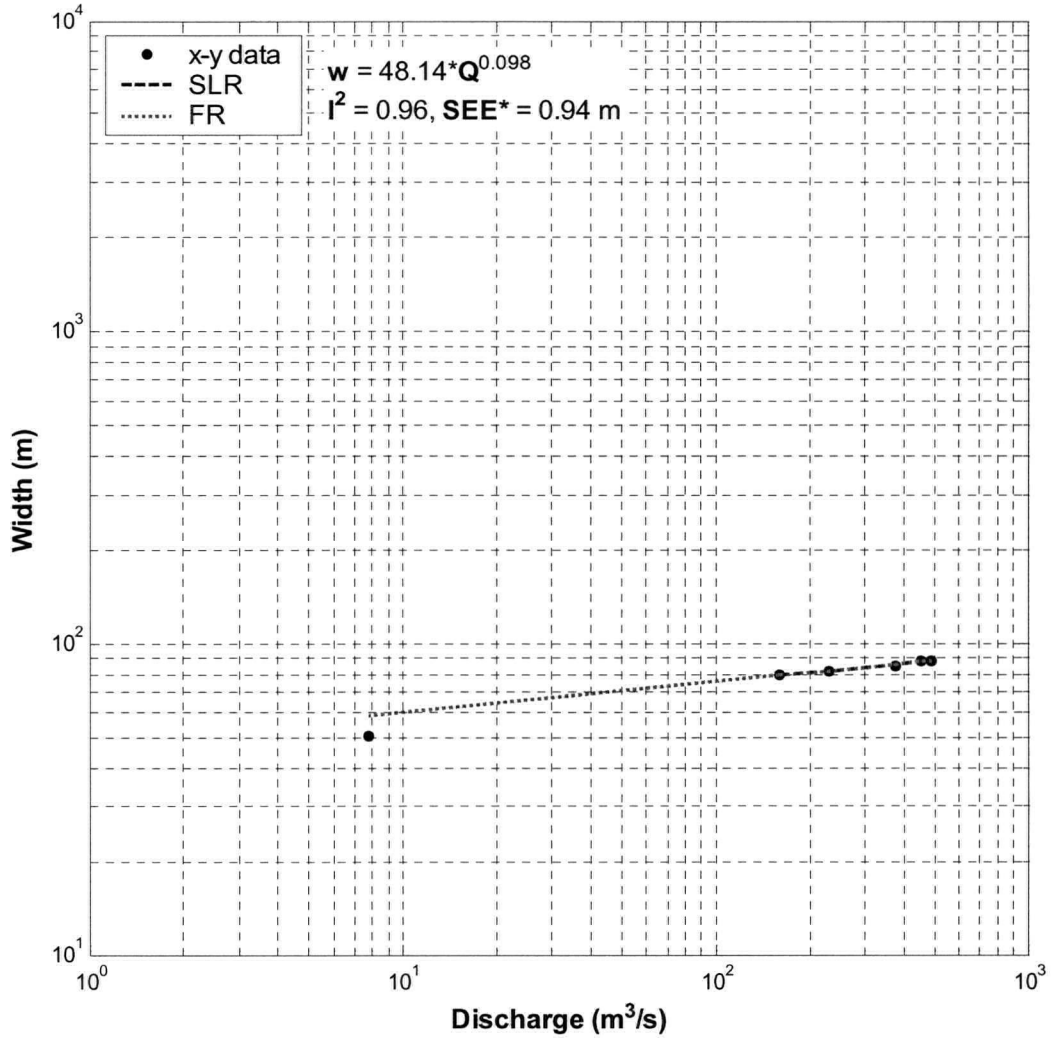

Figure A-21 Carey u/s mid sub-reach, at-a-station hydraulic geometry relation of width (m) with sub-reach discharge (m^3/s). Fit is based on high-flow data (upper five points) and has been extended for comparison with low-flow datum.

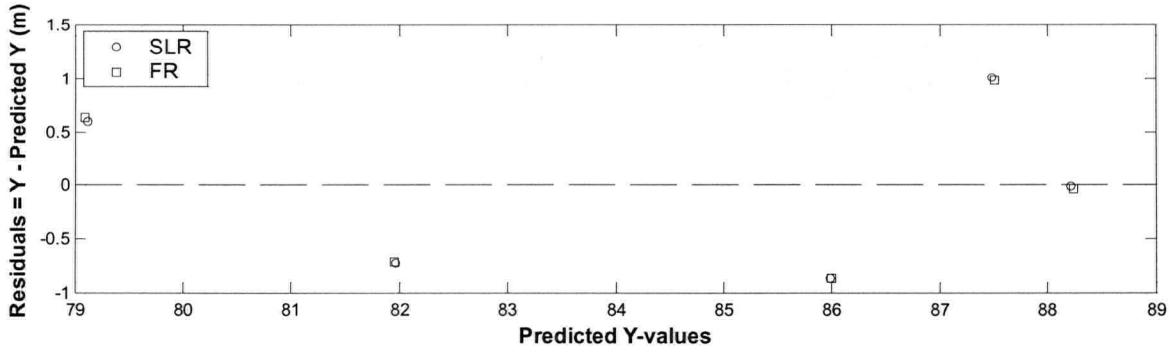

Figure A-22 Carey u/s mid sub-reach, residuals corresponding to high-flow data in **Figure A-21**.

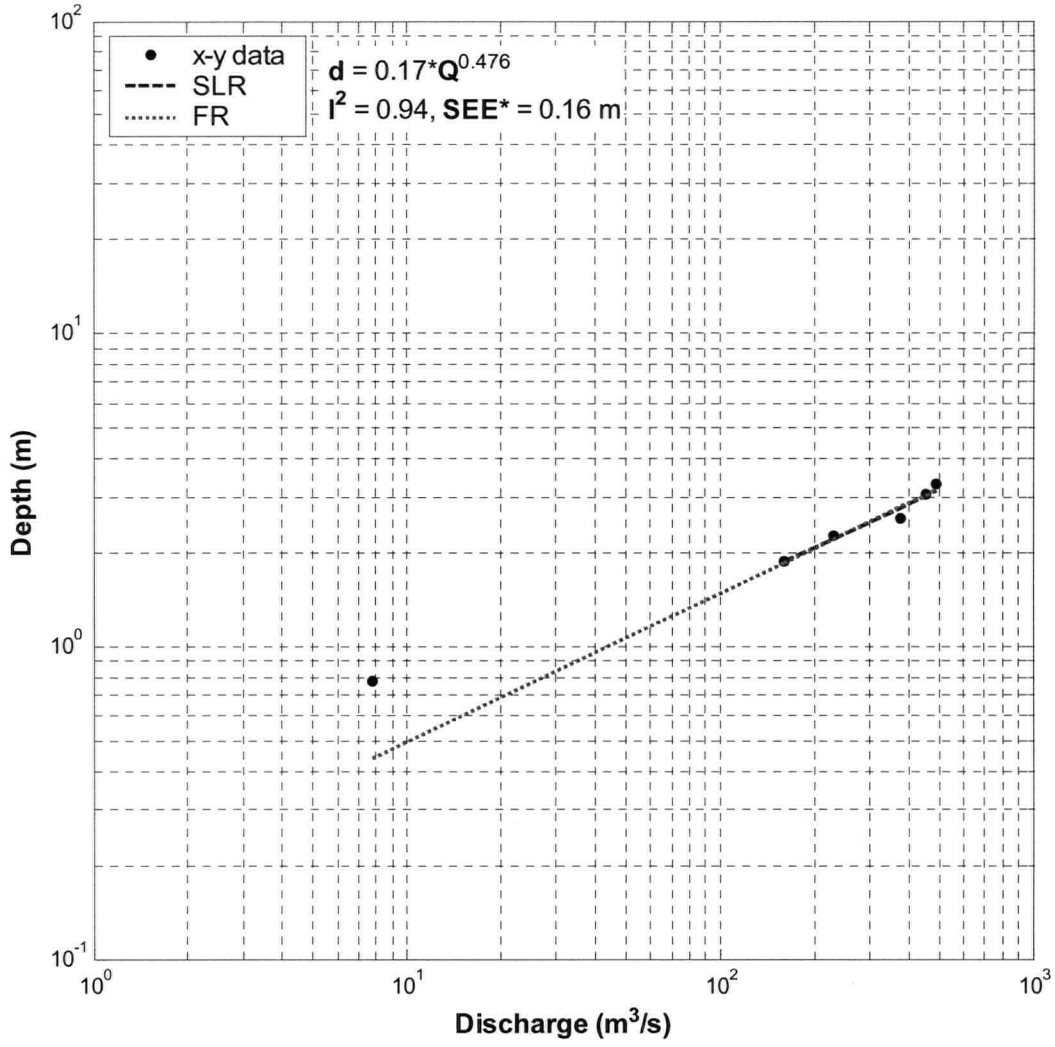

Figure A-23 Carey u/s mid sub-reach, at-a-station hydraulic geometry relation of depth (m) with sub-reach discharge (m^3/s). Fit is based on high-flow data (upper five points) and has been extended for comparison with low-flow datum.

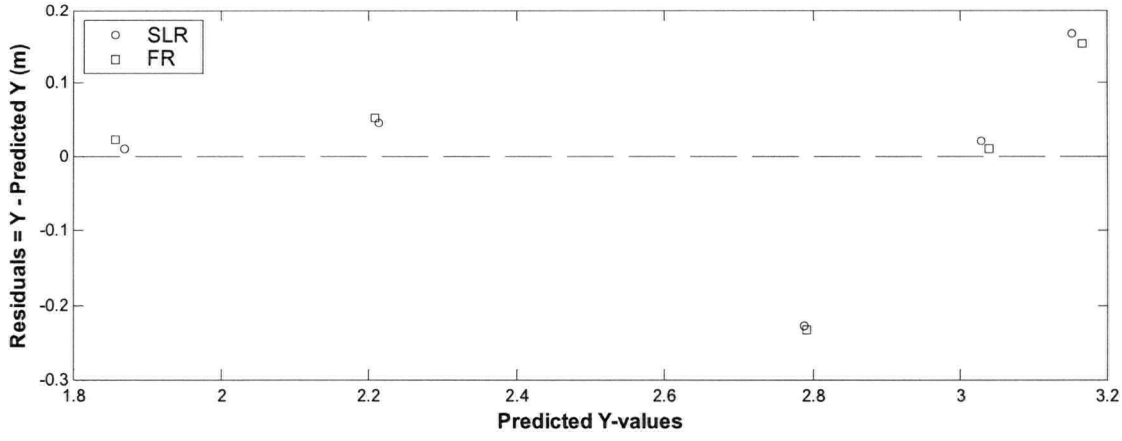

Figure A-24 Carey u/s mid sub-reach, residuals corresponding to high-flow data in **Figure A-23**.

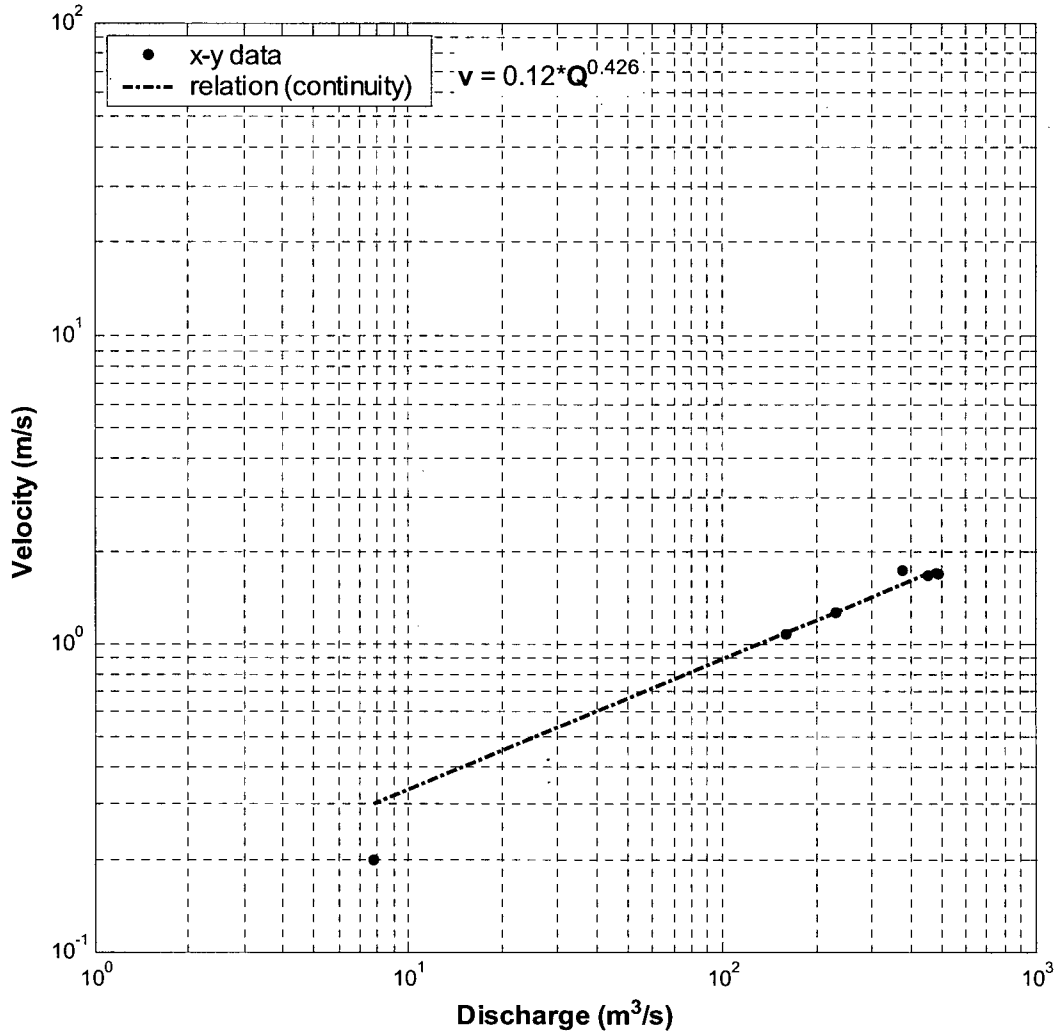

Figure A-25 Carey u/s mid sub-reach, at-a-station hydraulic geometry relation of velocity (m/s) with sub-reach discharge (m^3/s). The relation was derived by continuity (see Section 4.1.1) and super-imposed on the actual data points.

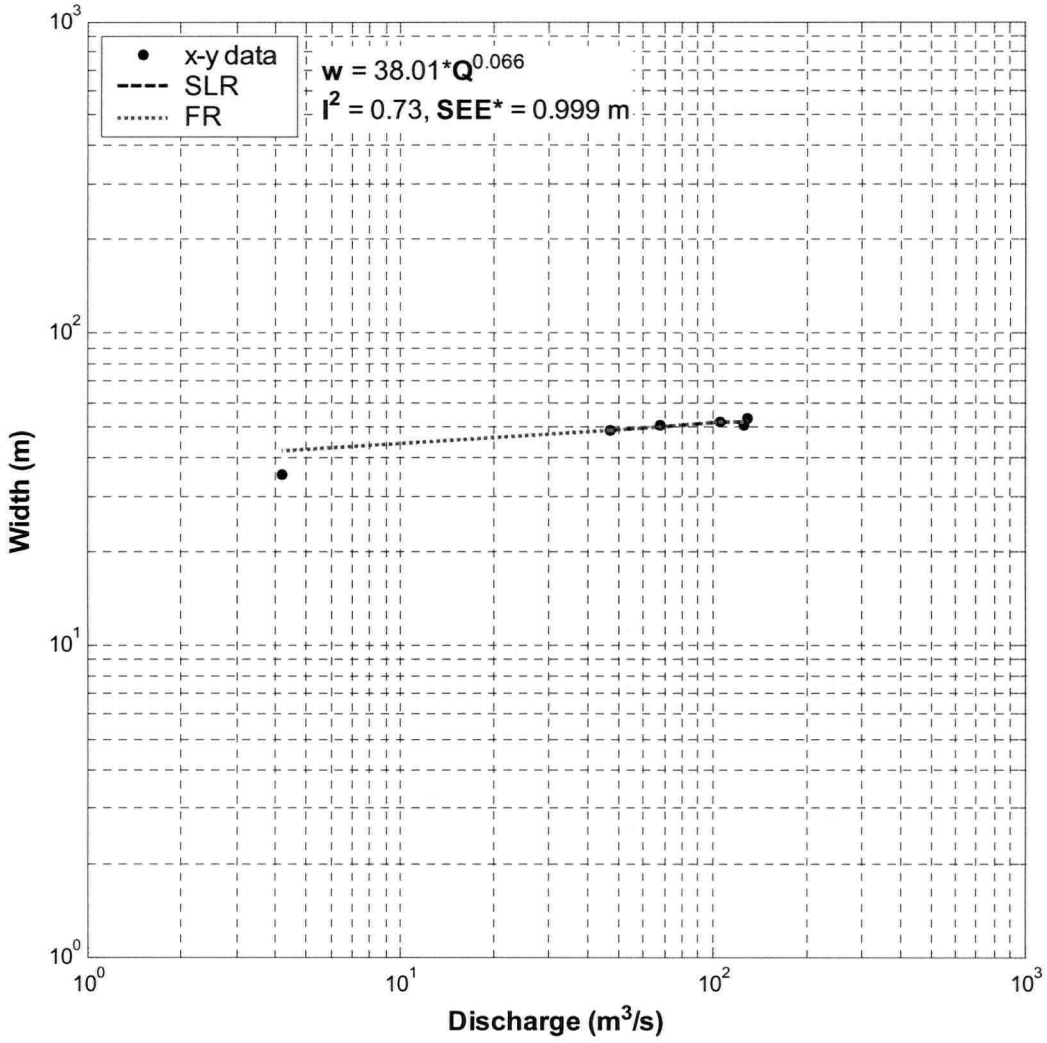

Figure A-26 Carey d/s mid sub-reach, at-a-station hydraulic geometry relation of width (m) with sub-reach discharge (m^3/s). Fit is based on high-flow data (upper five points) and has been extended for comparison with low-flow datum.

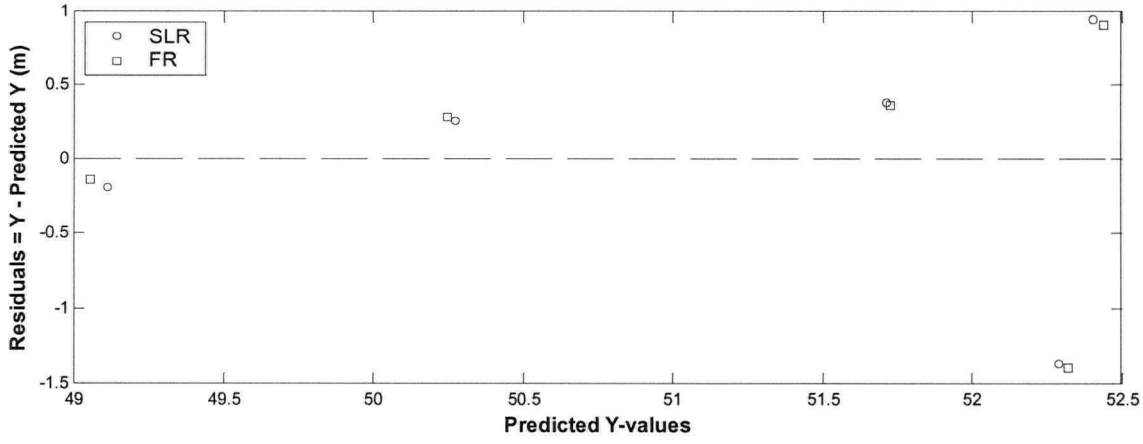

Figure A-27 Carey d/s mid sub-reach, residuals corresponding to high-flow data in **Figure A-26**.

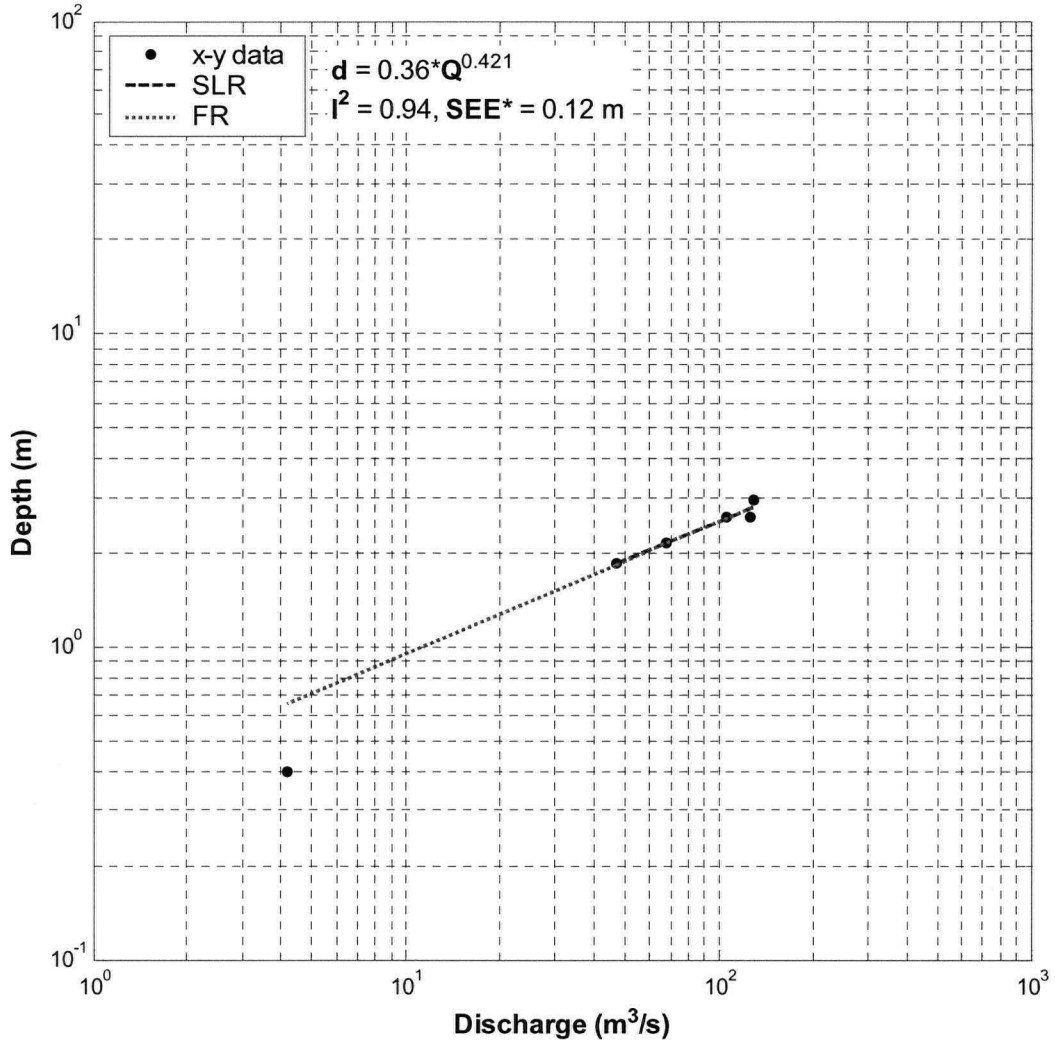

Figure A-28 Carey d/s mid sub-reach, at-a-station hydraulic geometry relation of depth (m) with sub-reach discharge (m^3/s). Fit is based on high-flow data (upper five points) and has been extended for comparison with low-flow datum.

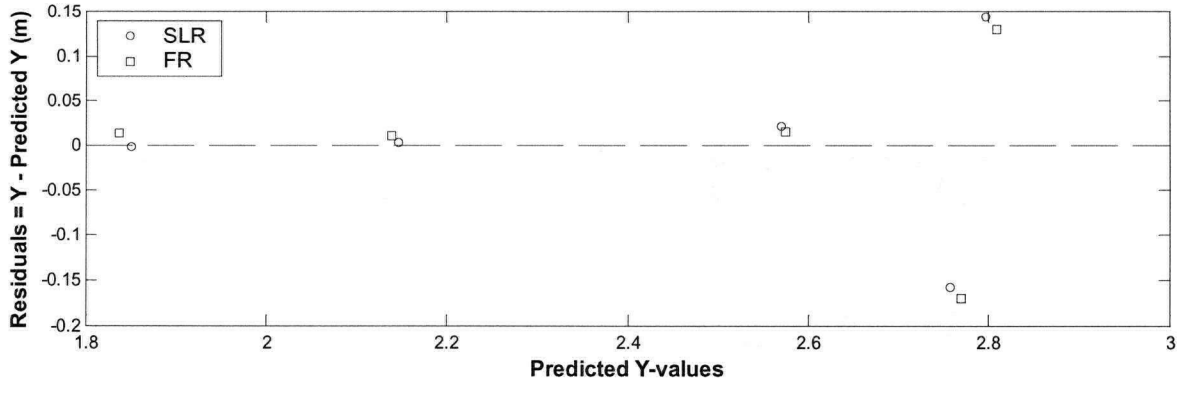

Figure A-29 Carey d/s mid sub-reach, residuals corresponding to high-flow data in **Figure A-28**.

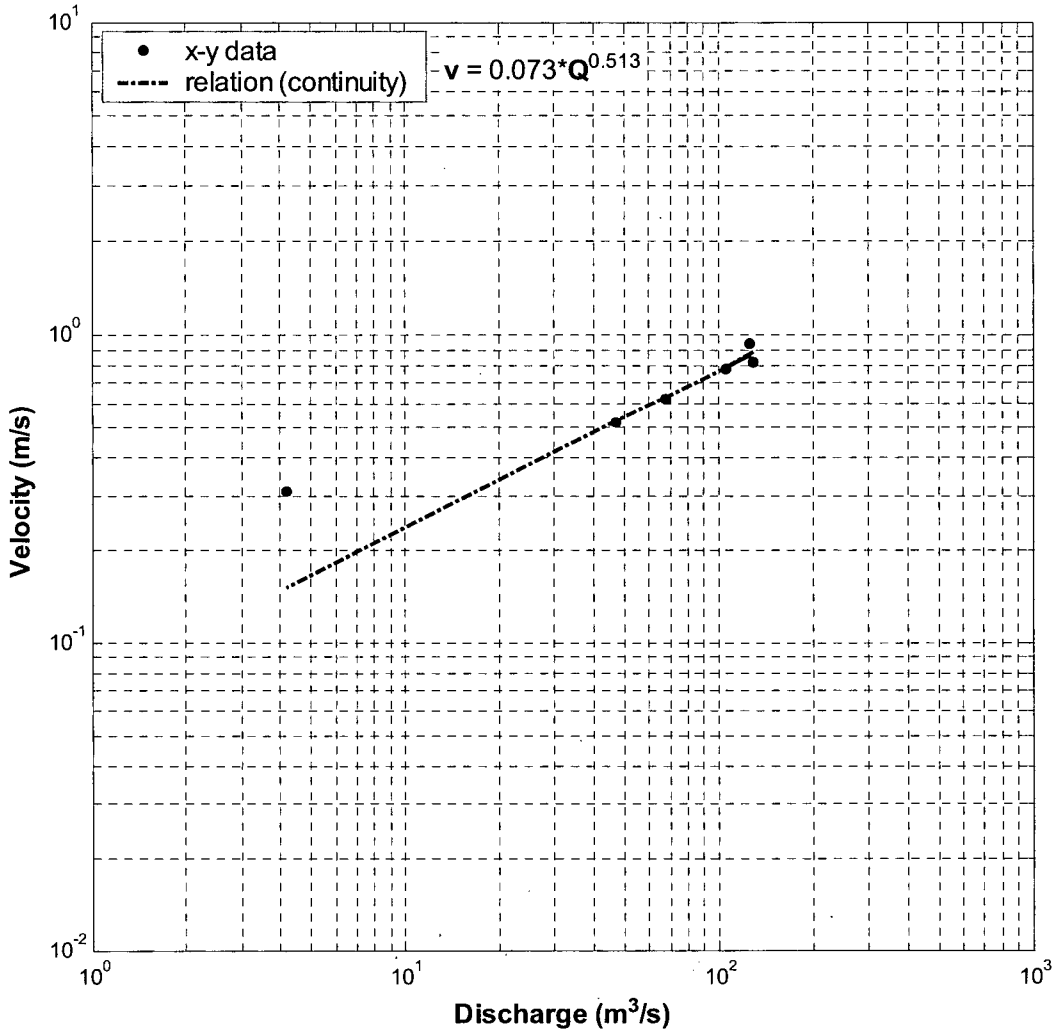

Figure A-30 Carey d/s mid sub-reach, at-a-station hydraulic geometry relation of velocity (m/s) with sub-reach discharge (m^3/s). The relation was derived by continuity (see Section 4.1.1) and super-imposed on the actual data points.

3. Hamilton

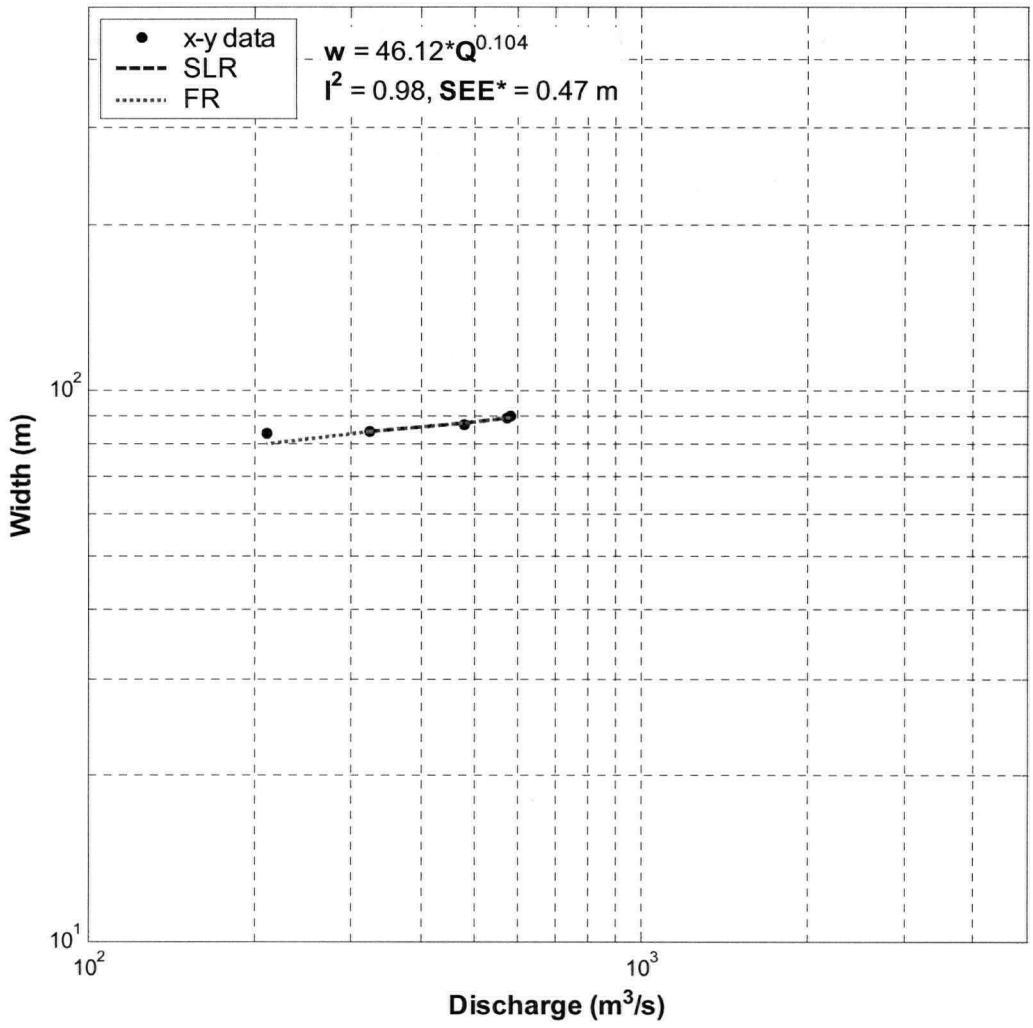

Figure A-31 Hamilton mid sub-reach, at-a-station hydraulic geometry relation of width (m) with sub-reach discharge (m^3/s). Fit is based on high-flow data (upper four points) and has been extended for comparison with low-flow datum.

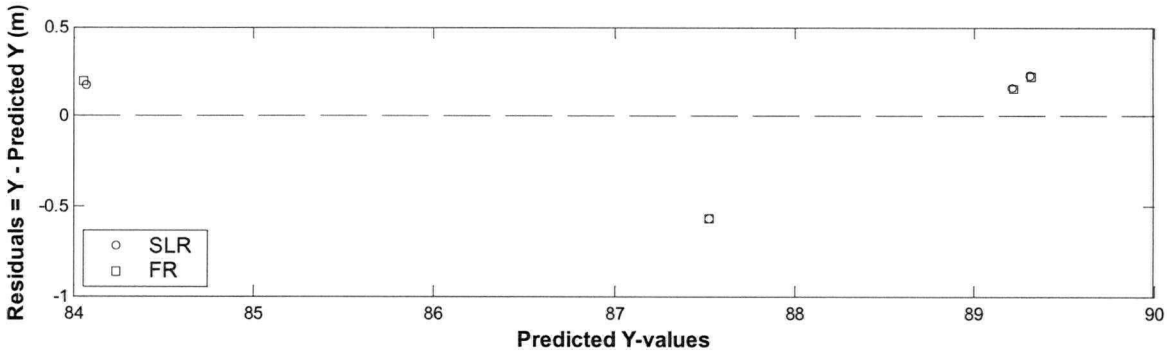

Figure A-32 Hamilton mid sub-reach, residuals corresponding to high-flow data in **Figure A-31**.

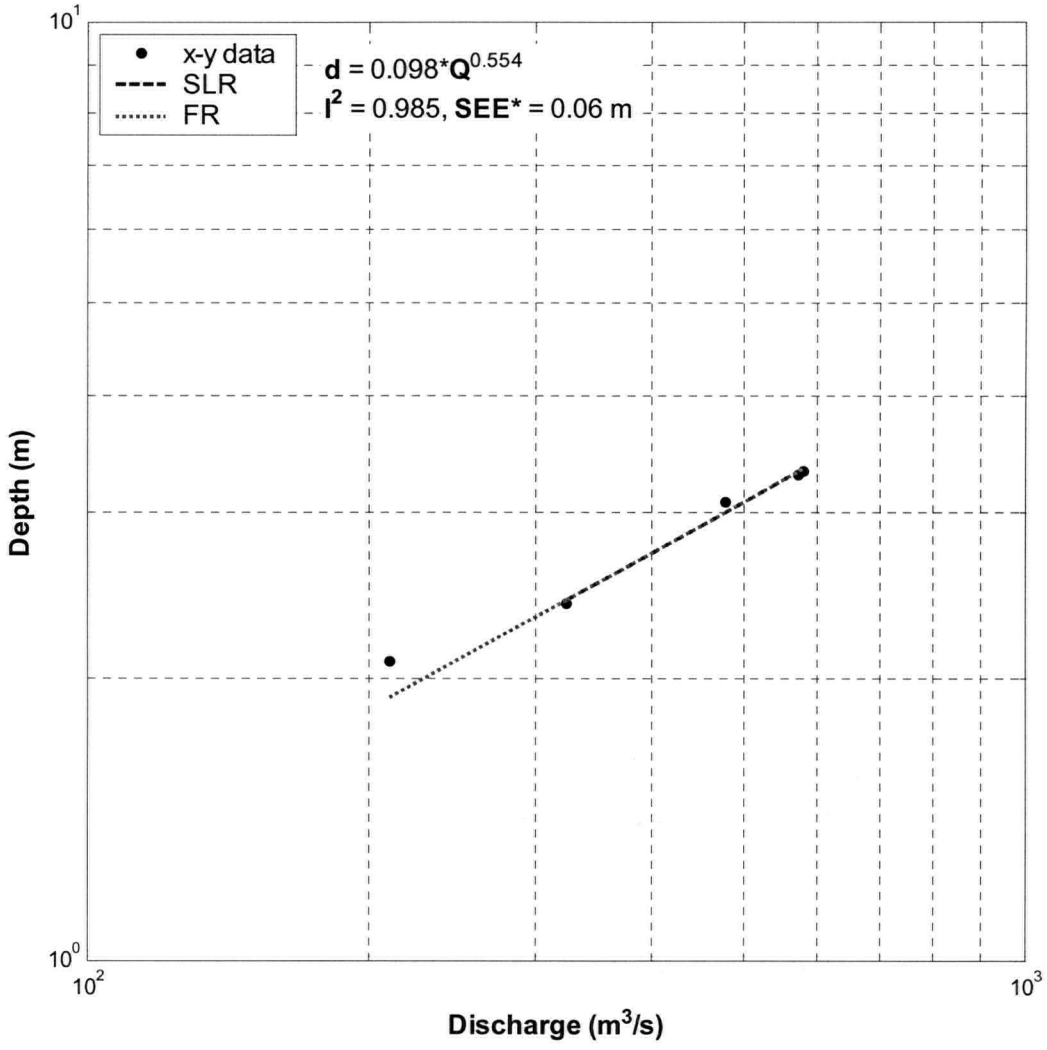

Figure A-33 Hamilton mid sub-reach, at-a-station hydraulic geometry relation of depth (m) with sub-reach discharge (m^3/s). Fit is based on high-flow data (upper four points) and has been extended for comparison with low-flow datum.

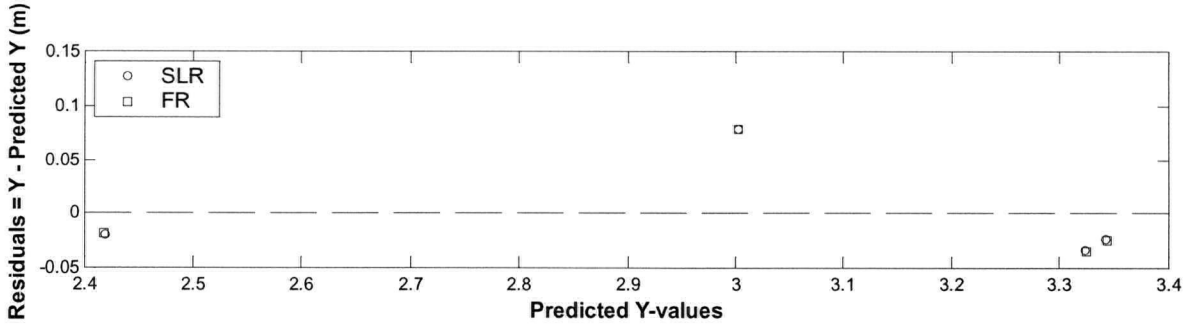

Figure A-34 Hamilton mid sub-reach, residuals corresponding to high-flow data in **Figure A-33**.

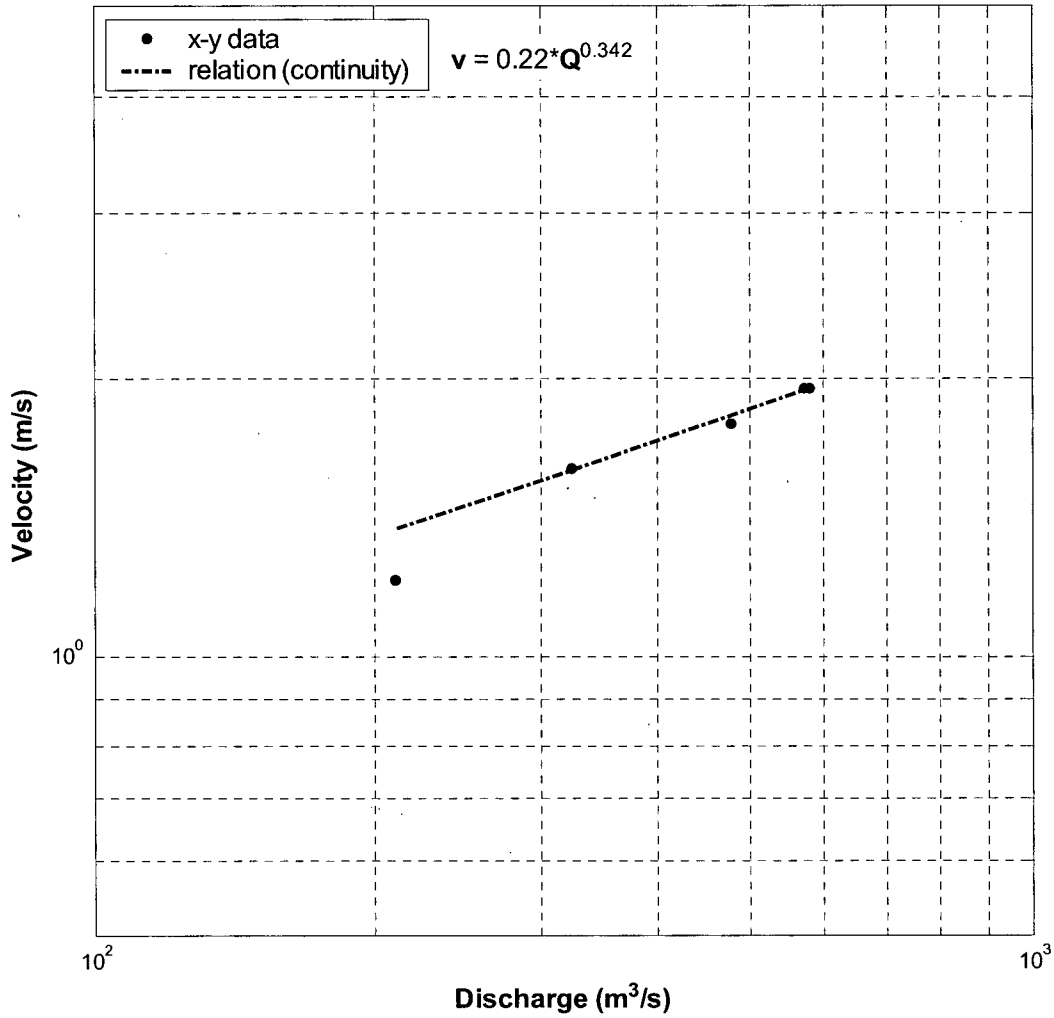

Figure A-35 Hamilton mid sub-reach, at-a-station hydraulic geometry relation of velocity (m/s) with sub-reach discharge (m^3/s). The relation was derived by continuity (see Section 4.1.1) and super-imposed on the actual data points.

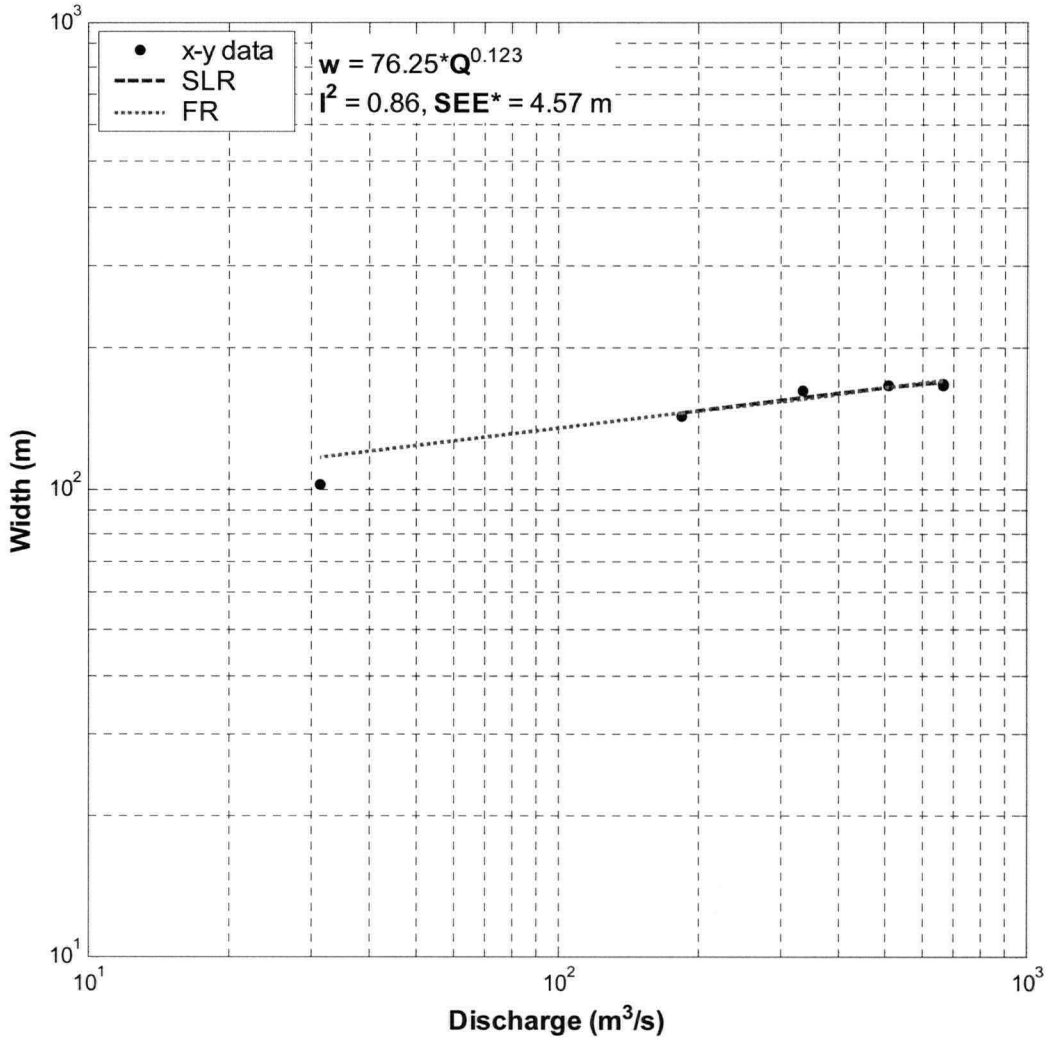

Figure A-36 Hamilton d/s sub-reach, at-a-station hydraulic geometry relation of width (m) with sub-reach discharge (m^3/s). Fit is based on high-flow data (upper five points) and has been extended for comparison with low-flow datum.

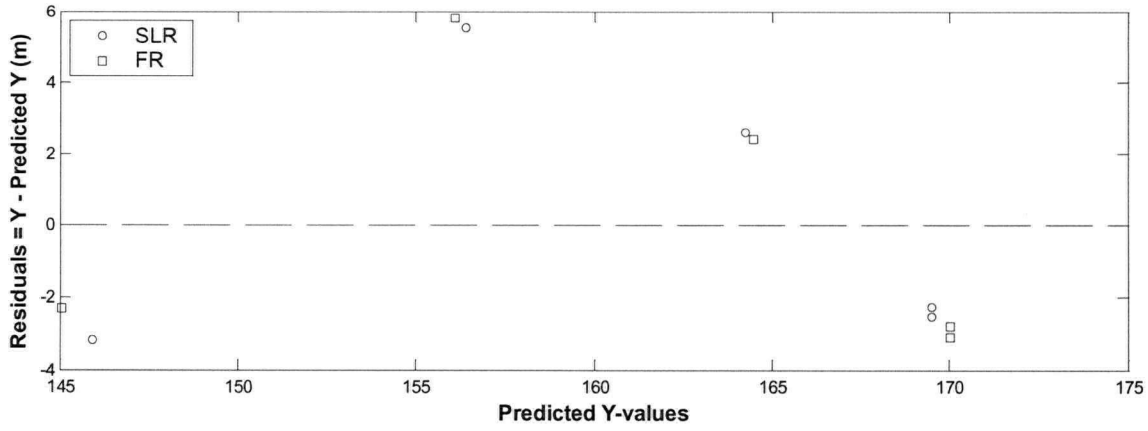

Figure A-37 Hamilton d/s sub-reach, residuals corresponding to high-flow data in **Figure A-36**.

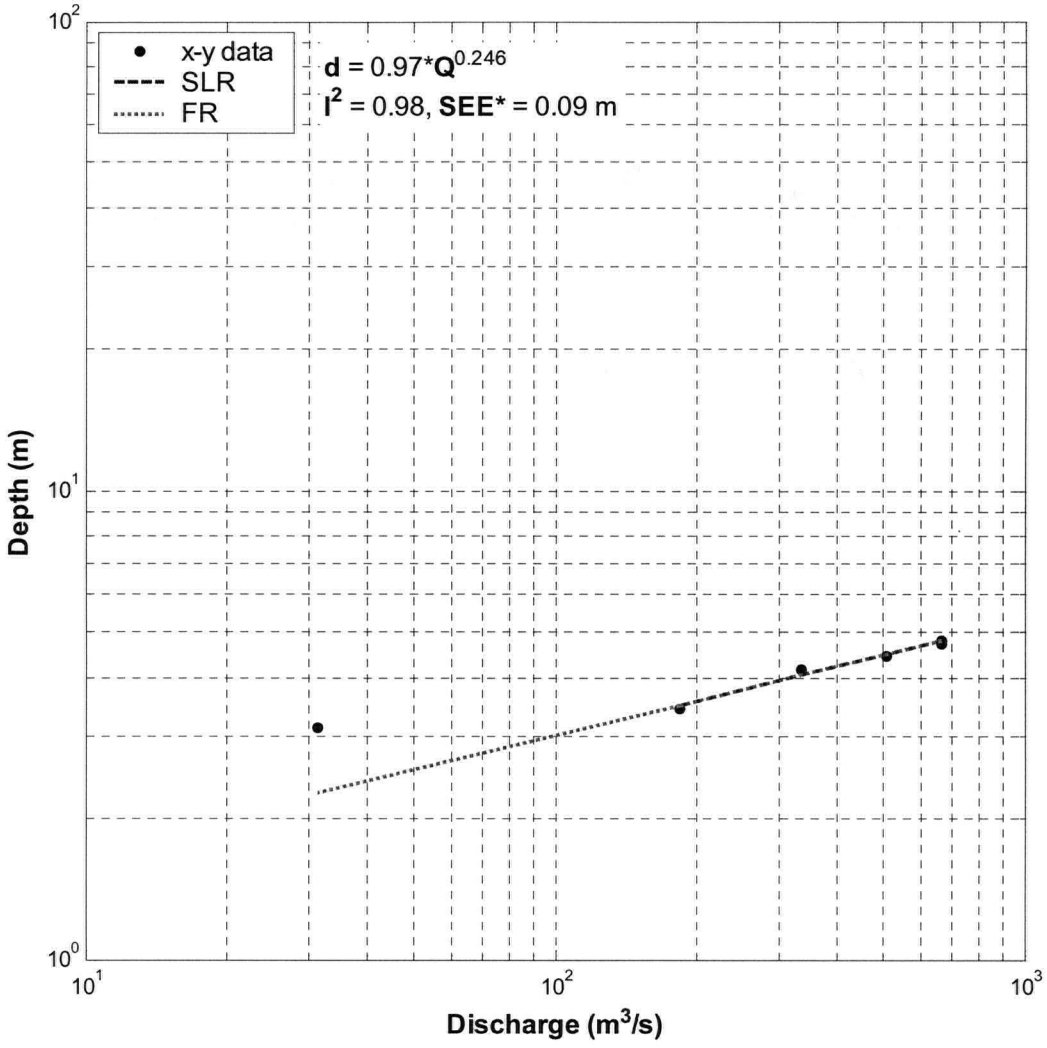

Figure A-38 Hamilton d/s sub-reach, at-a-station hydraulic geometry relation of depth (m) with sub-reach discharge (m^3/s). Fit is based on high-flow data (upper five points) and has been extended for comparison with low-flow datum.

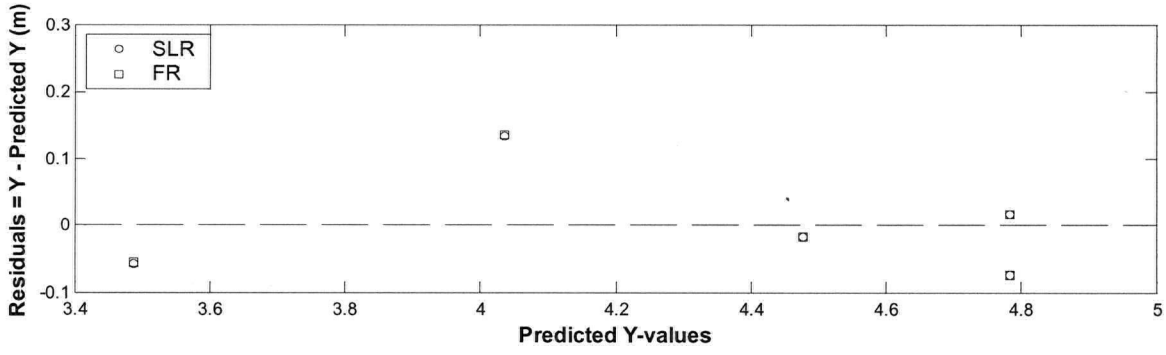

Figure A-39 Hamilton d/s sub-reach, residuals corresponding to high-flow data in **Figure A-38**.

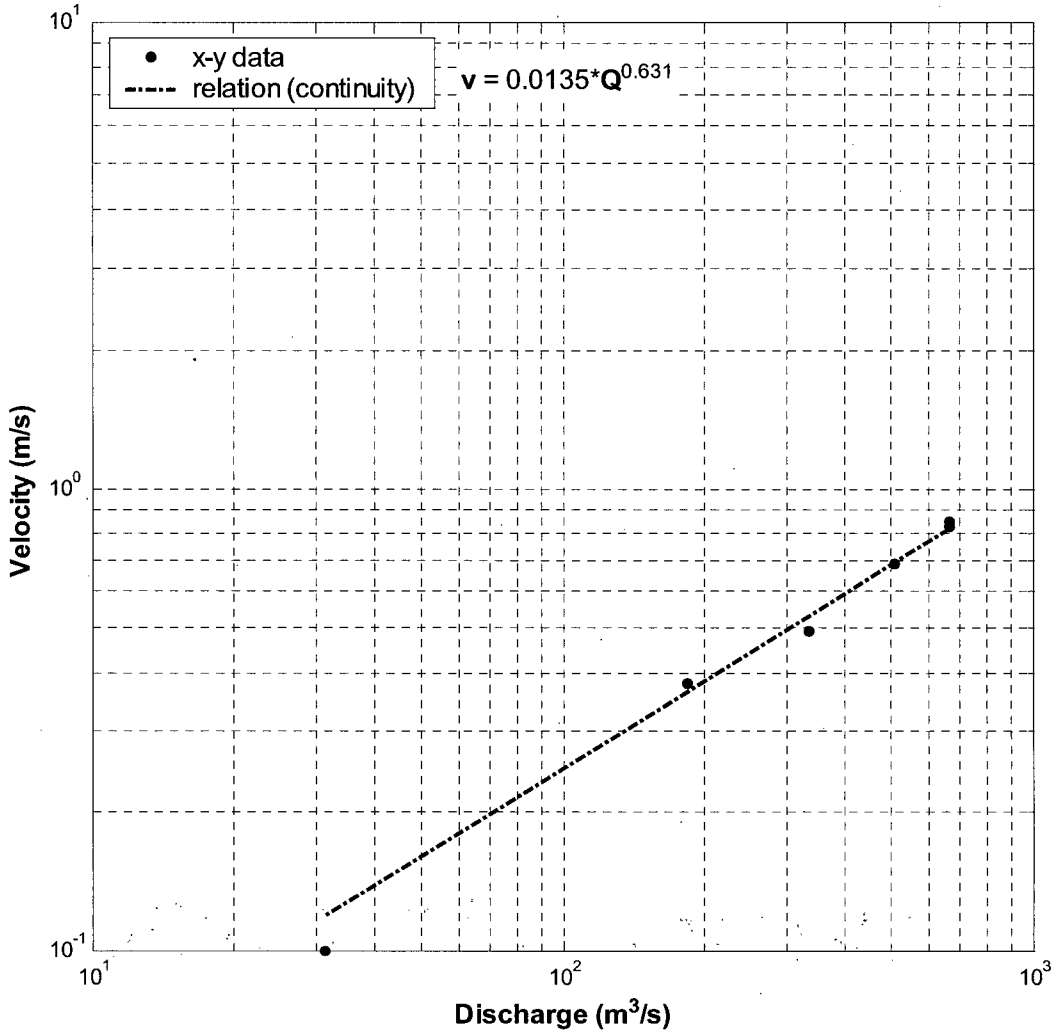

Figure A-40 Hamilton d/s sub-reach, at-a-station hydraulic geometry relation of velocity (m/s) with sub-reach discharge (m^3/s). The relation was derived by continuity (see Section 4.1.1) and super-imposed on the actual data points.

4. Calamity

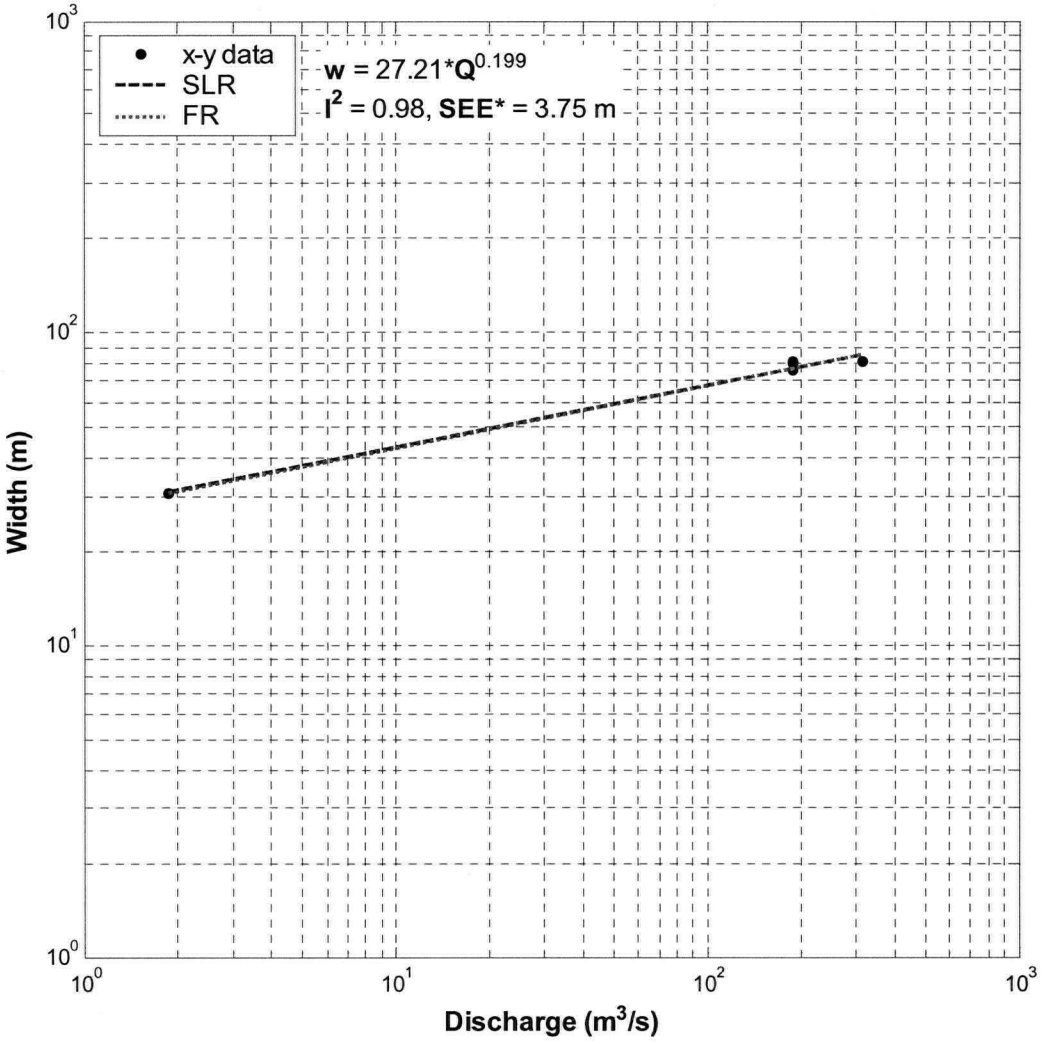

Figure A-41 Calamity u/s sub-reach, at-a-station hydraulic geometry relation of width (m) with sub-reach discharge (m^3/s).

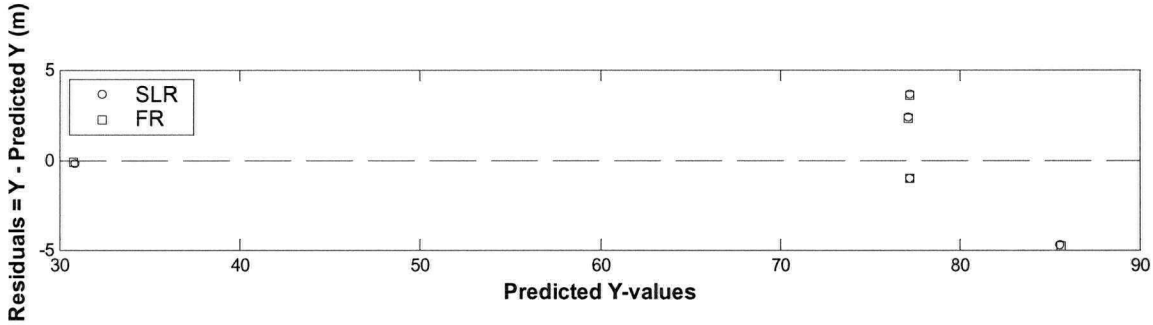

Figure A-42 Calamity u/s sub-reach, residuals corresponding to **Figure A-41**.

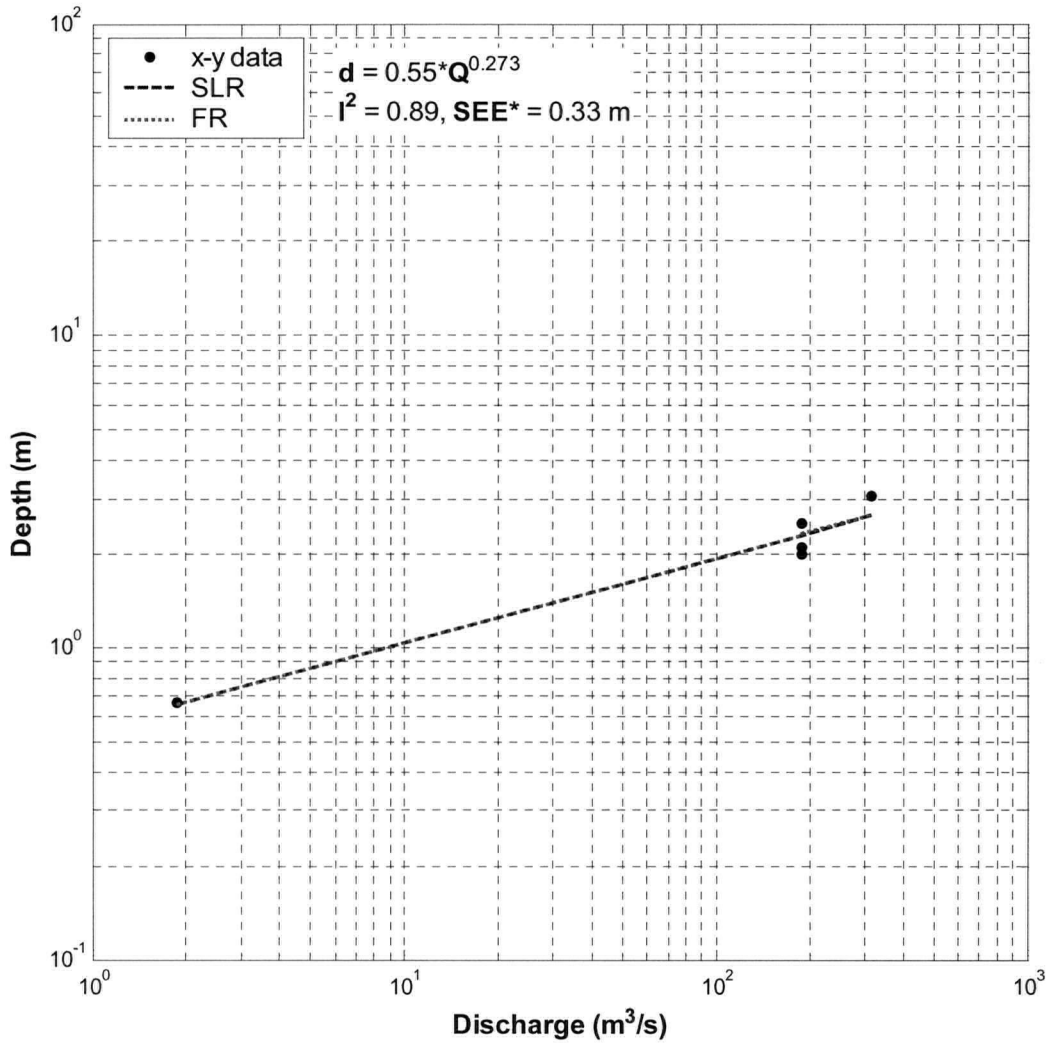

Figure A-43 Calamity u/s sub-reach, at-a-station hydraulic geometry relation of depth (m) with sub-reach discharge (m^3/s). Conventional power-law form is shown although a better fit is achieved using a linear model (**Figure A-45**).

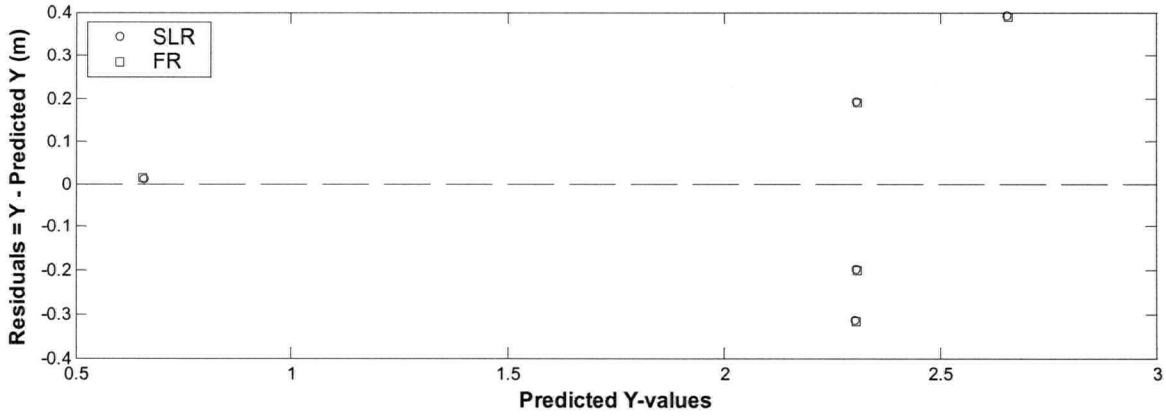

Figure A-44 Calamity u/s sub-reach, residuals corresponding to **Figure A-43**.

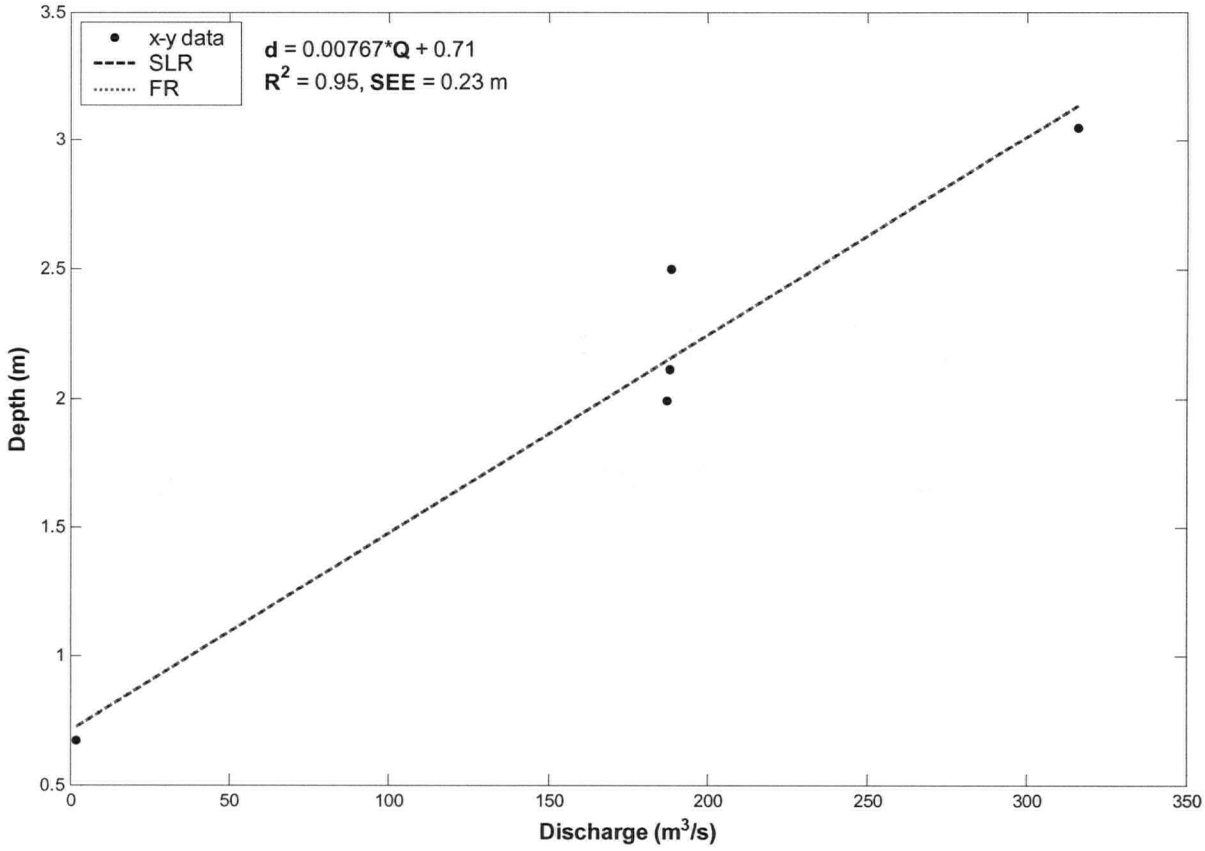

Figure A-45 Calamity u/s sub-reach, at-a-station hydraulic geometry relation of depth (m) with sub-reach discharge (m^3/s).

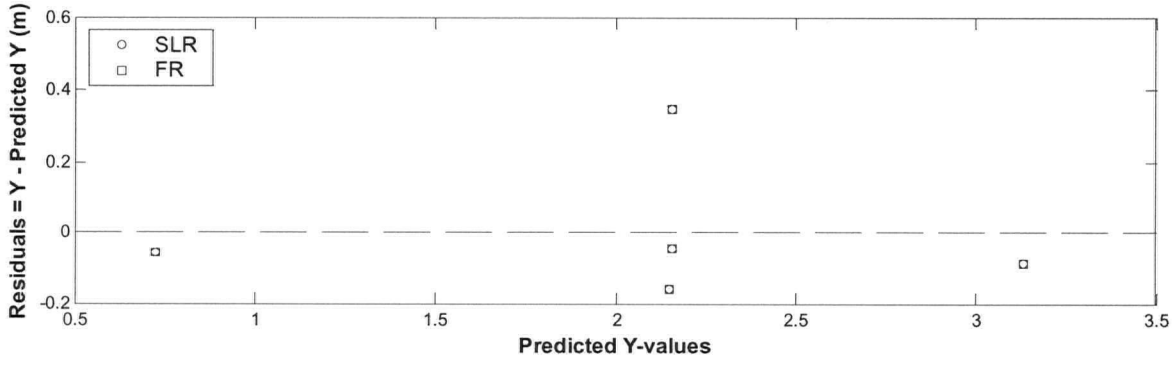

Figure A-46 Calamity u/s sub-reach, residuals corresponding to **Figure A-45**.

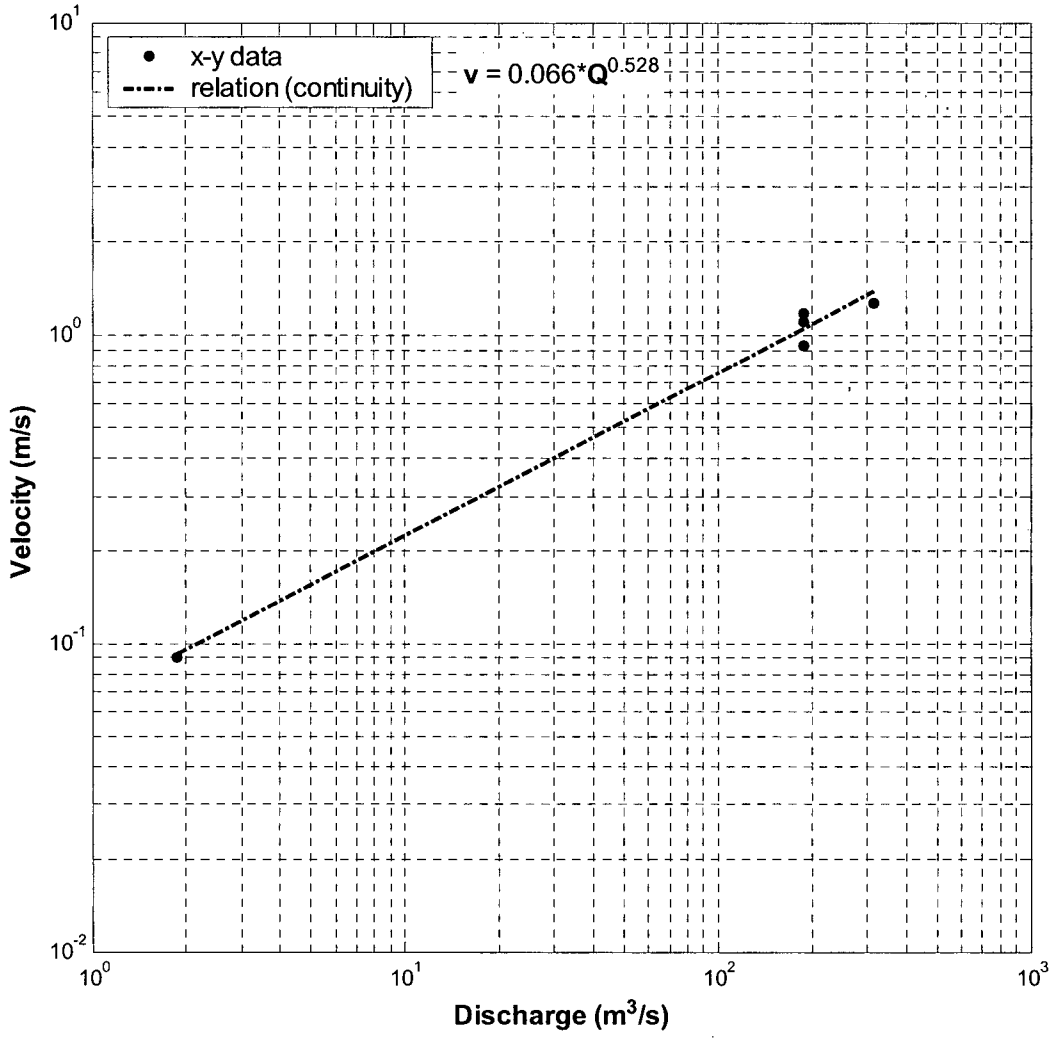

Figure A-47 Calamity u/s sub-reach, at-a-station hydraulic geometry relation of velocity (m/s) with sub-reach discharge (m^3/s). The relation was derived by continuity (see Section 4.1.1) and super-imposed on the actual data points.

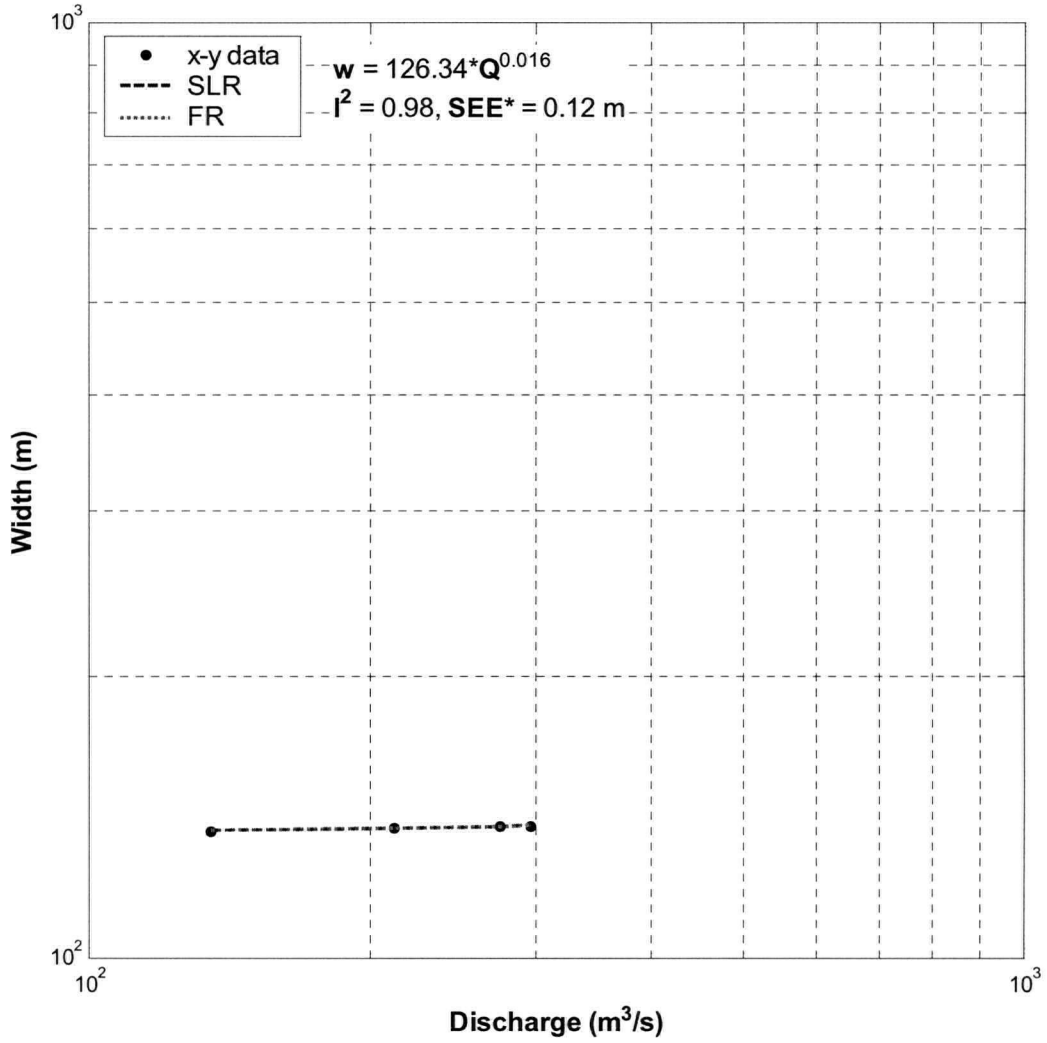

Figure A-48 Calamity mid sub-reach, at-a-station hydraulic geometry relation of width (m) with sub-reach discharge (m^3/s). Note the limited range of discharges.

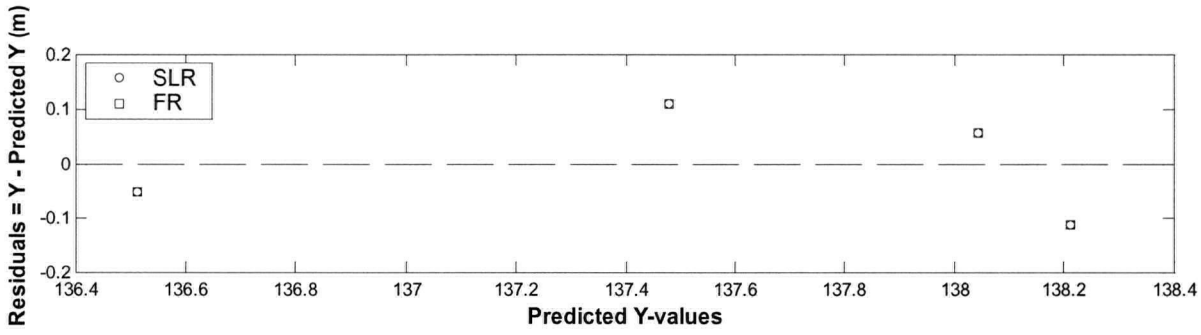

Figure A-49 Calamity mid sub-reach, residuals corresponding to **Figure A-48**.

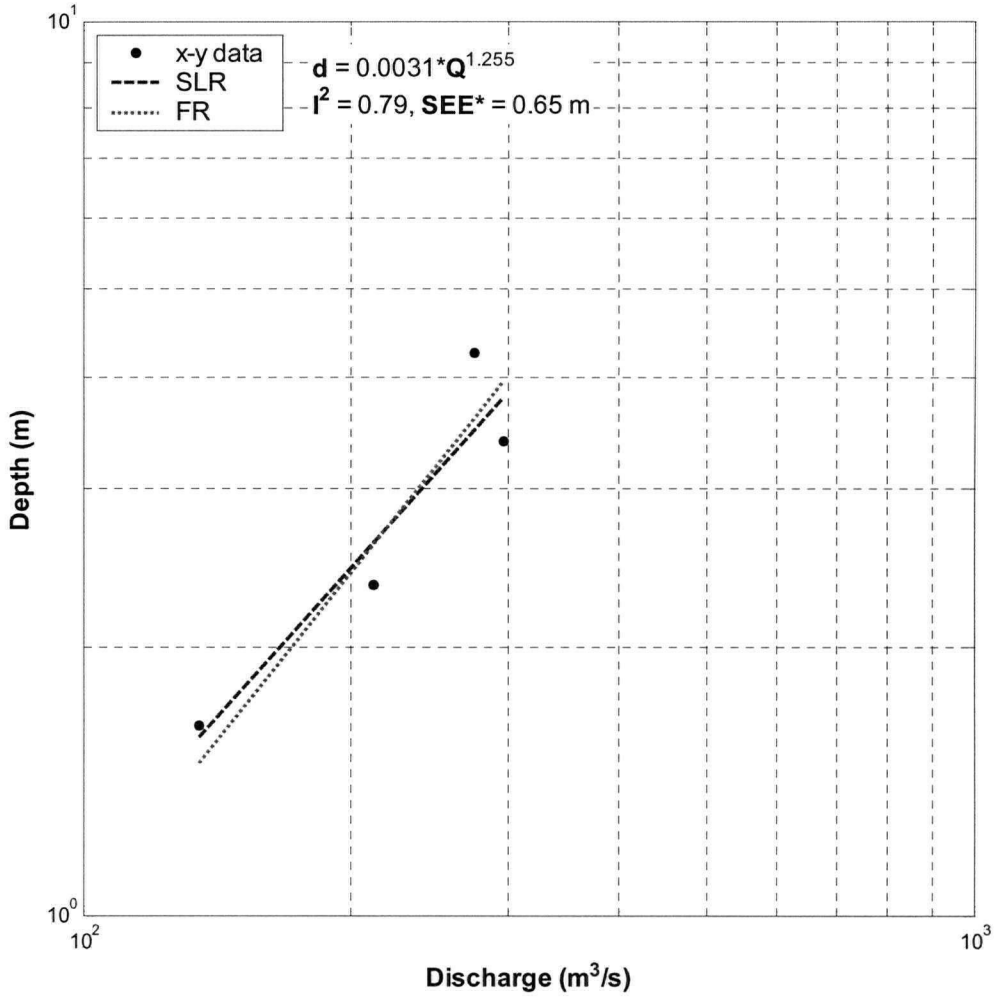

Figure A-50 Calamity mid sub-reach, at-a-station hydraulic geometry relation of depth (m) with sub-reach discharge (m^3/s). Note the limited range of discharges.

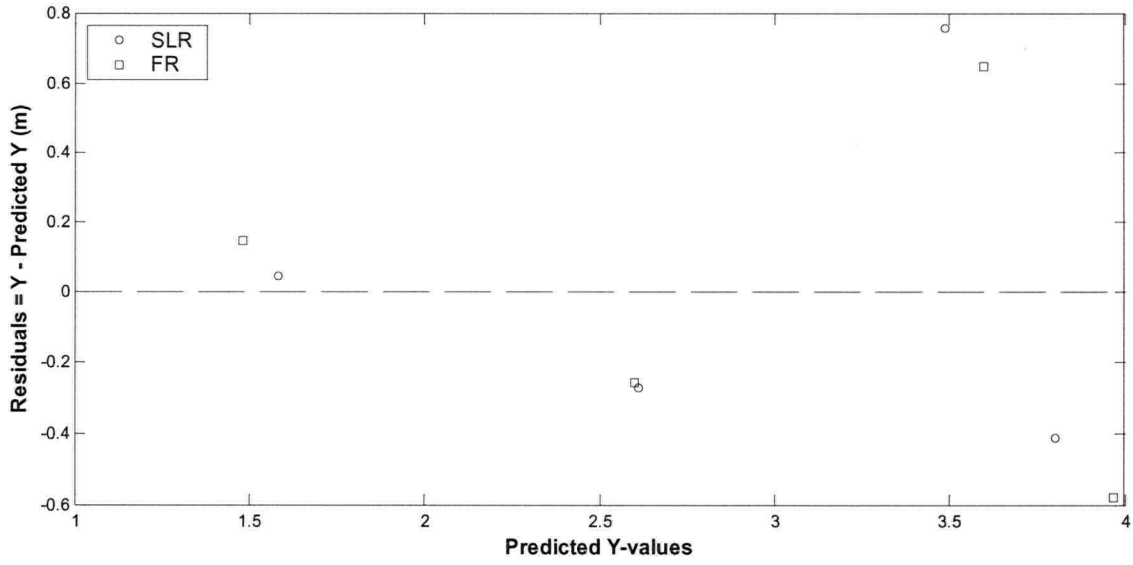

Figure A-51 Calamity mid sub-reach, residuals corresponding to **Figure A-50**.

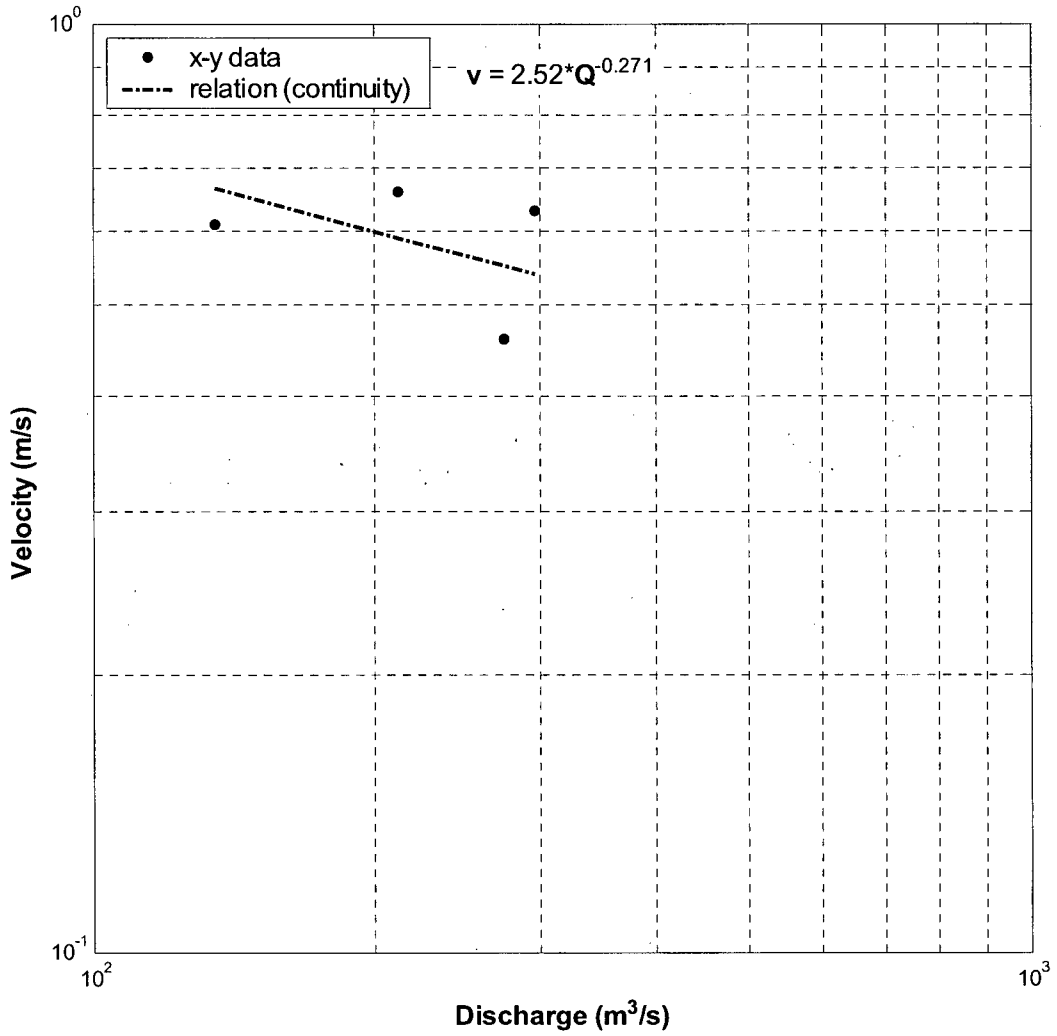

Figure A-52 Calamity mid sub-reach, at-a-station hydraulic geometry relation of velocity (m/s) with sub-reach discharge (m^3/s). The relation was derived by continuity (see Section 4.1.1) and super-imposed on the actual data points.

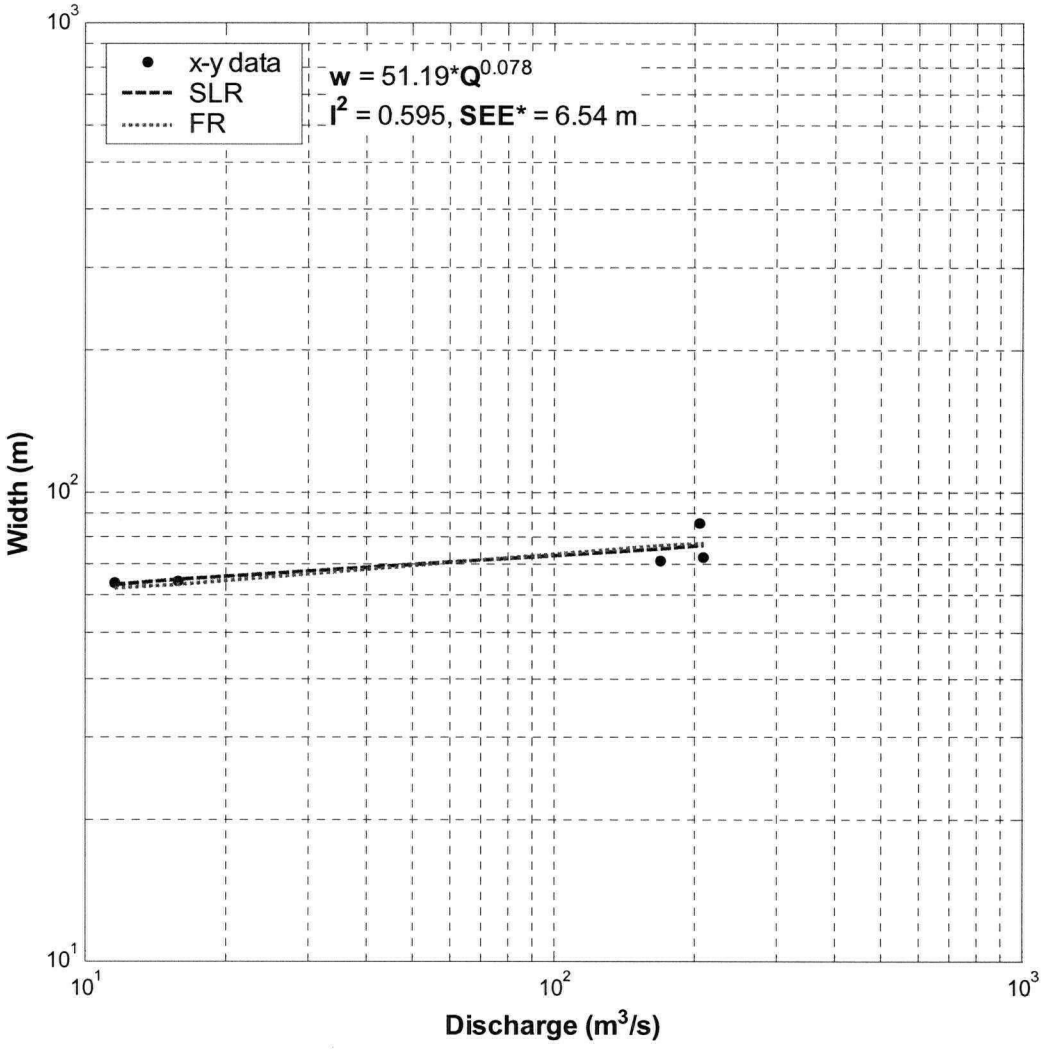

Figure A-53 Calamity d/s sub-reach, at-a-station hydraulic geometry relation of width (m) with sub-reach discharge (m^3/s).

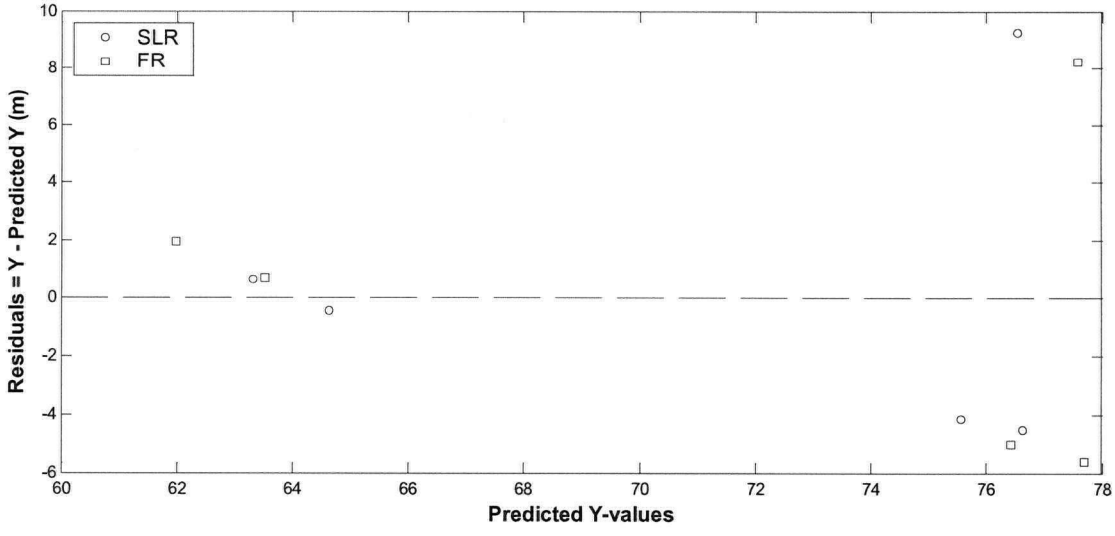

Figure A-54 Calamity d/s sub-reach, residuals corresponding to **Figure A-53**.

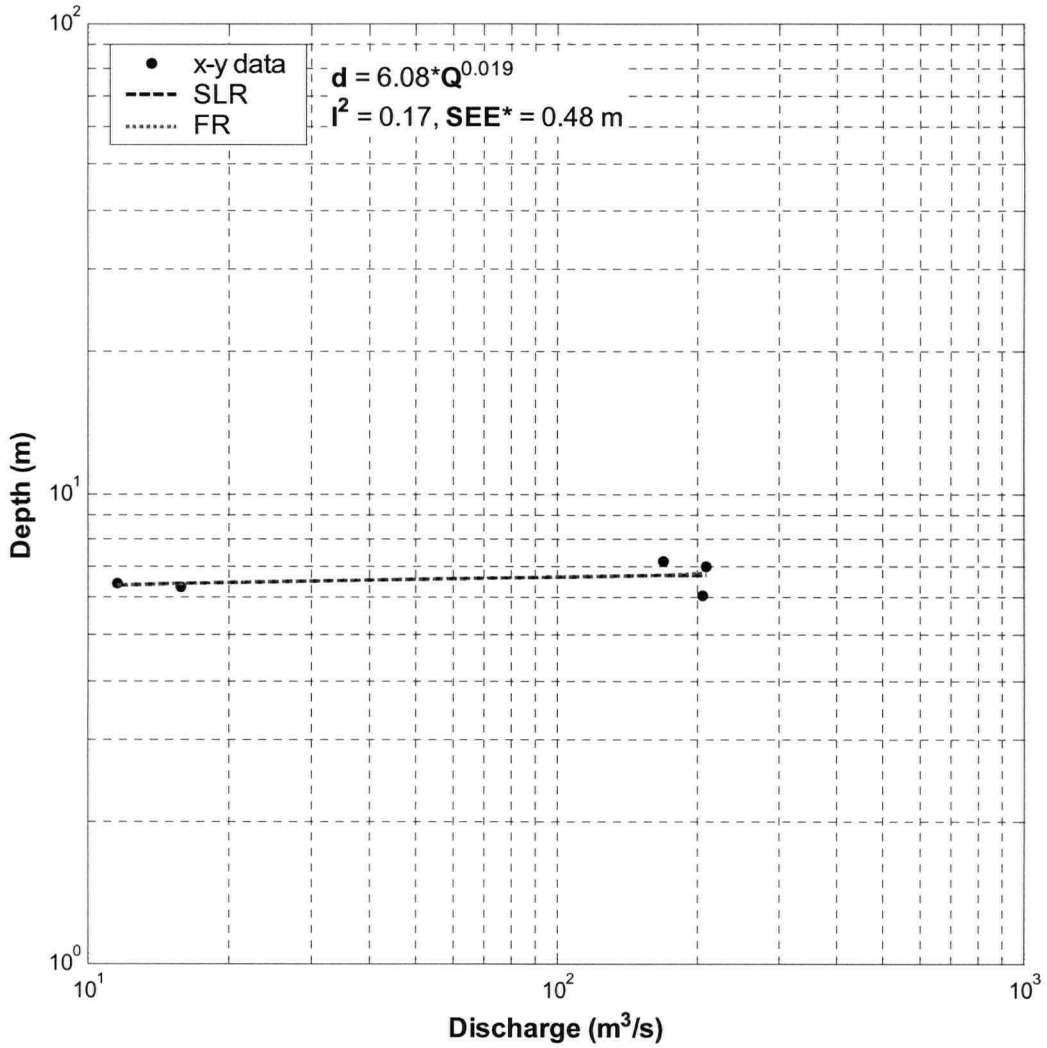

Figure A-55 Calamity d/s sub-reach, at-a-station hydraulic geometry relation of depth (m) with sub-reach discharge (m^3/s). The slope is not significantly different from zero (α = 0.05).

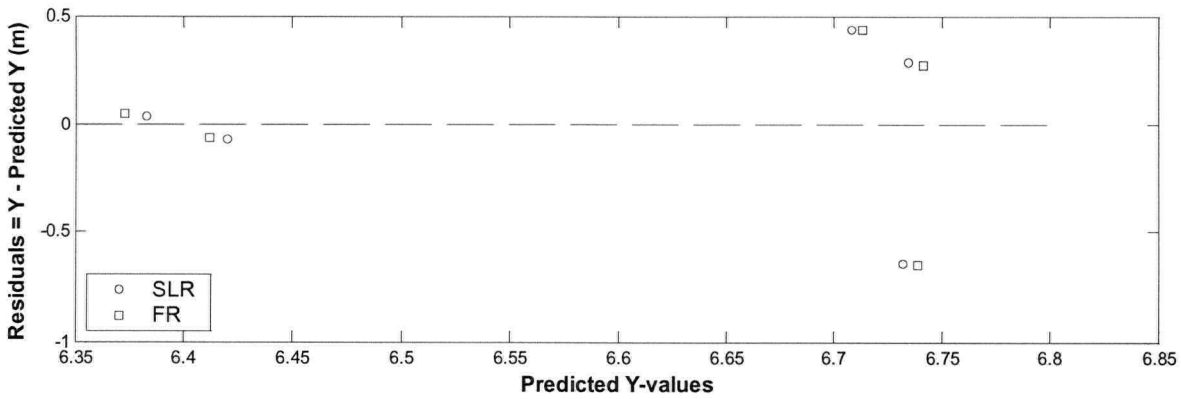

Figure A-56 Calamity d/s sub-reach, residuals corresponding to **Figure A-55**.

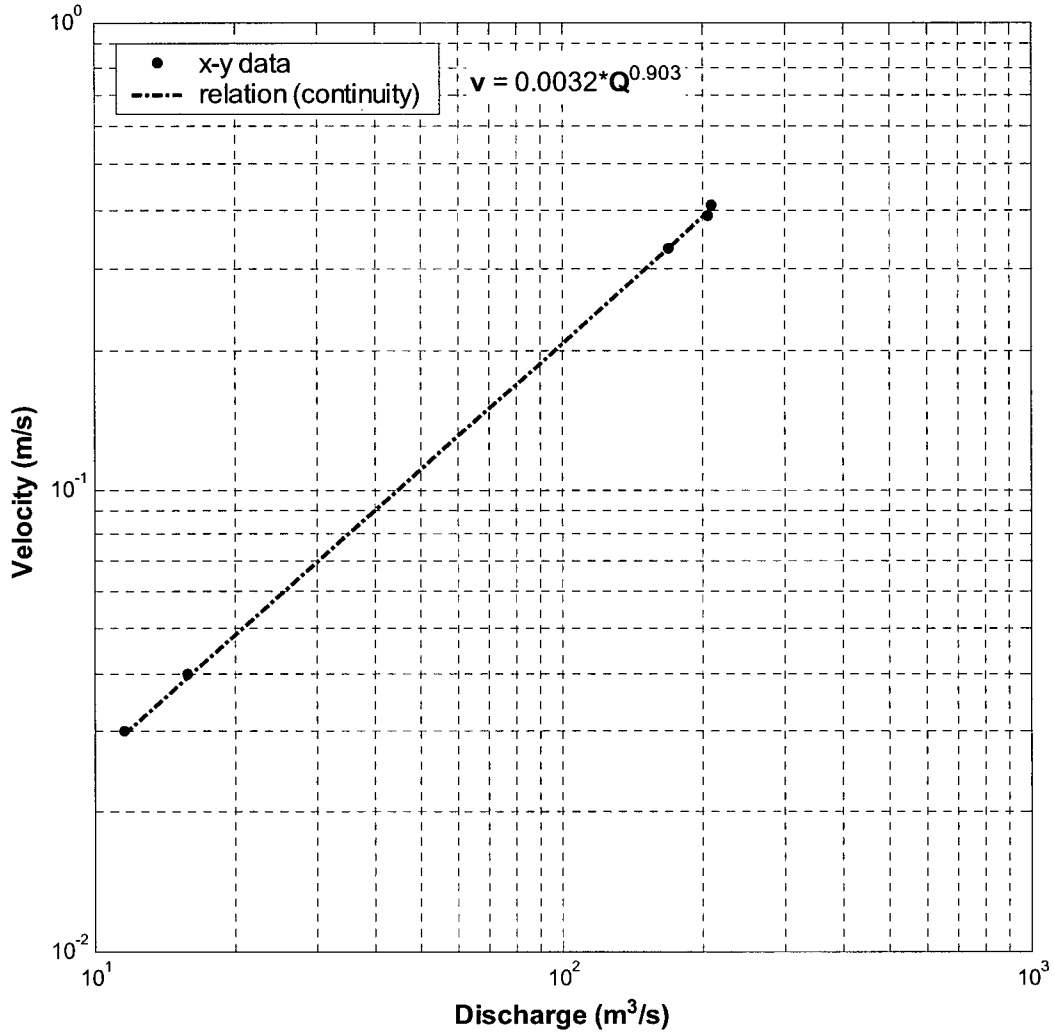

Figure A-57 Calamity d/s sub-reach, at-a-station hydraulic geometry relation of velocity (m/s) with sub-reach discharge (m^3/s). The relation was derived by continuity (see Section 4.1.1) and super-imposed on the actual data points.

Appendix B: Plots of grain-size distributions

Plots of grain-size distributions for all surface and sub-surface samples are shown. Both the percent retained by size category and the cumulative percent finer are shown in each plot. Percent retained in a given size category is the fraction coarser than the particle size boundary associated with the histogram bar, except where noted.

Table of figures: Appendix B

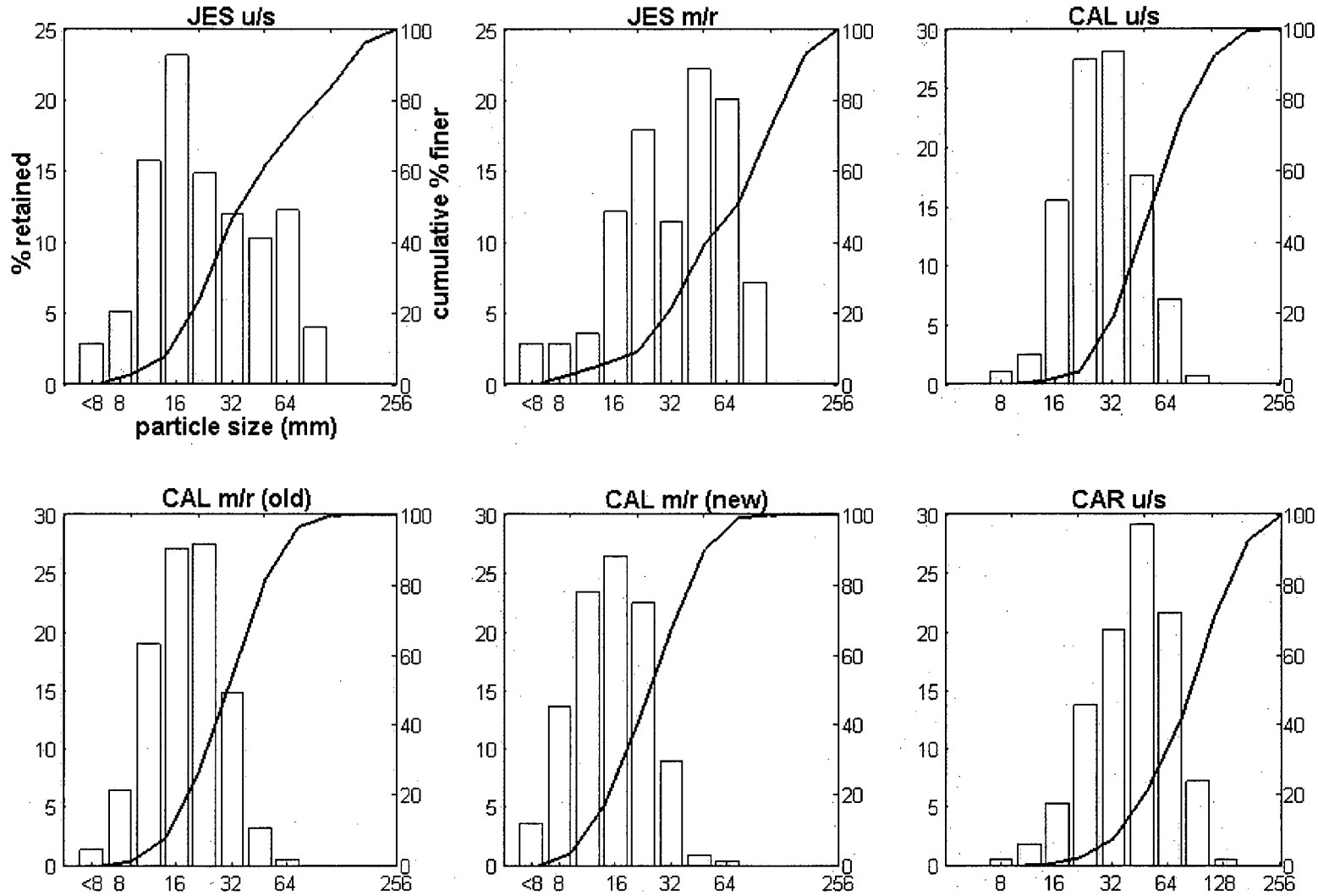

Figure B-1 Surface grain-size distributions for coarse (i.e. gravel and larger) substrates in JES u/s and m/r, CAL u/s, m/r (old) and m/r (new) and CAR u/s. Note that the analyses have been truncated at 8 mm.

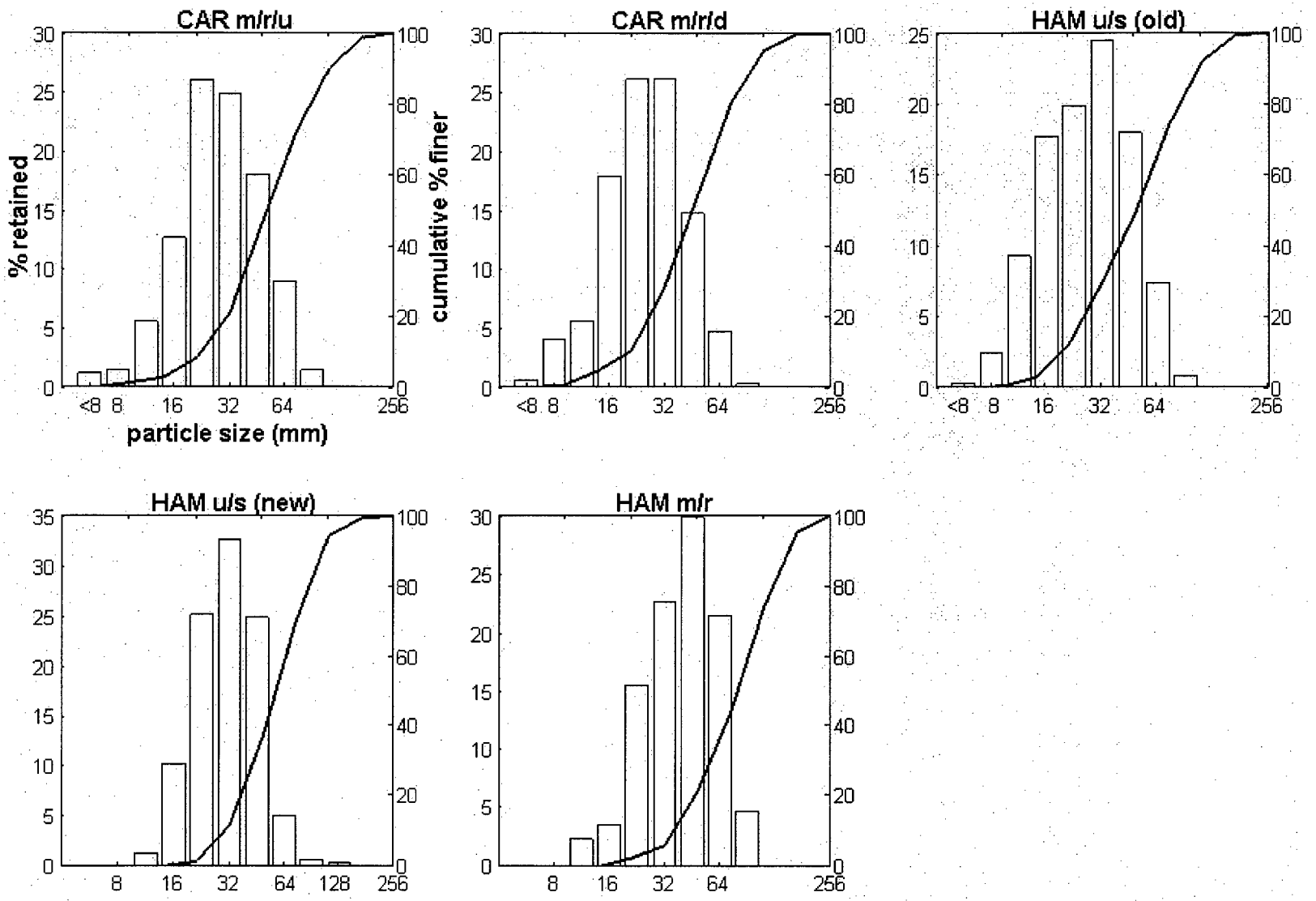

Figure B-2 Surface grain-size distributions for coarse (i.e. gravel and larger) substrates in CAR m/r/u and m/r/d, HAM u/s (old), u/s (new) and m/r. Note that the analyses have been truncated at 8 mm.

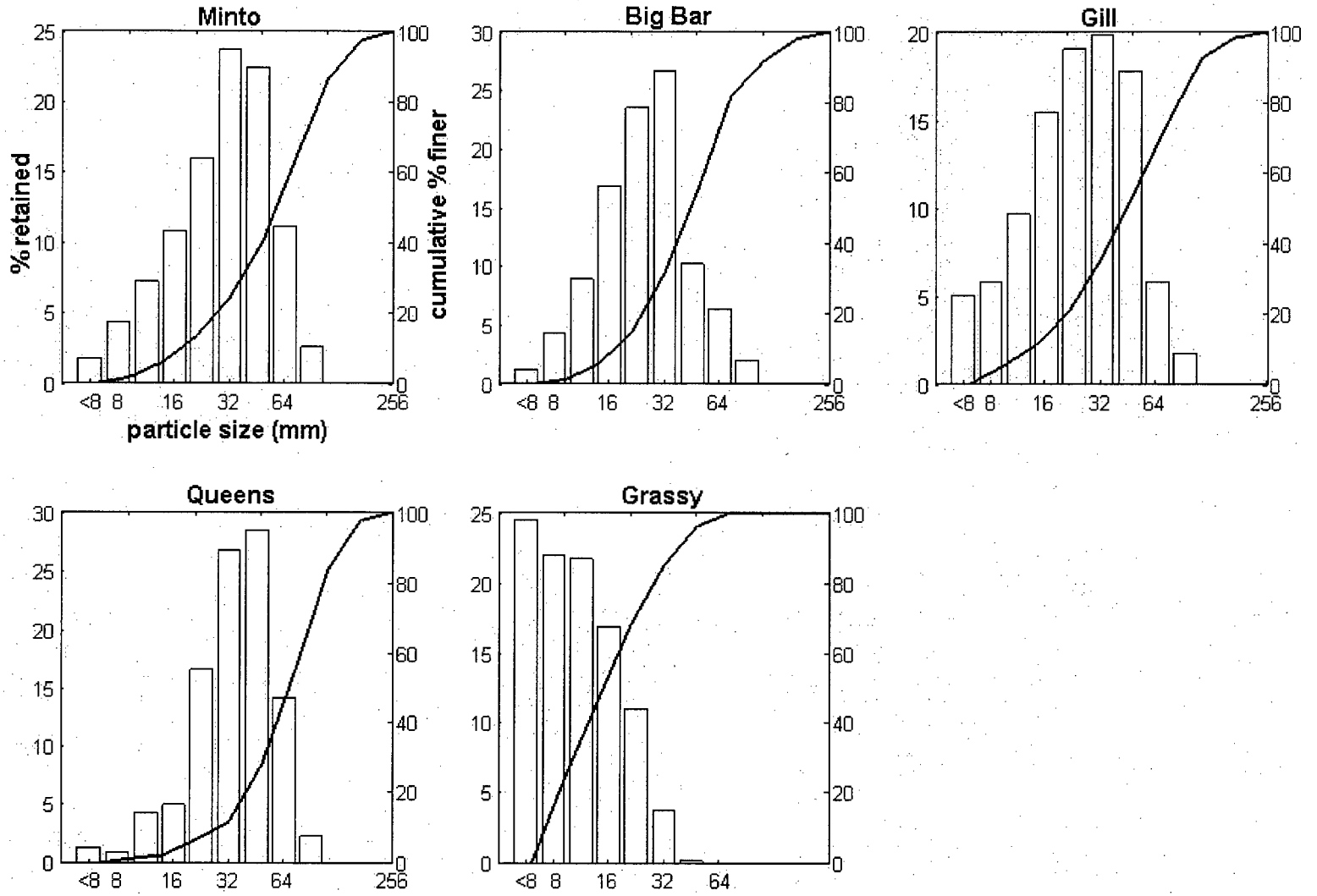

Figure B-3 Surface grain-size distributions for coarse (i.e. gravel and larger) substrates in all scaling relation sub-reaches. Note that the analyses have been truncated at 8 mm.

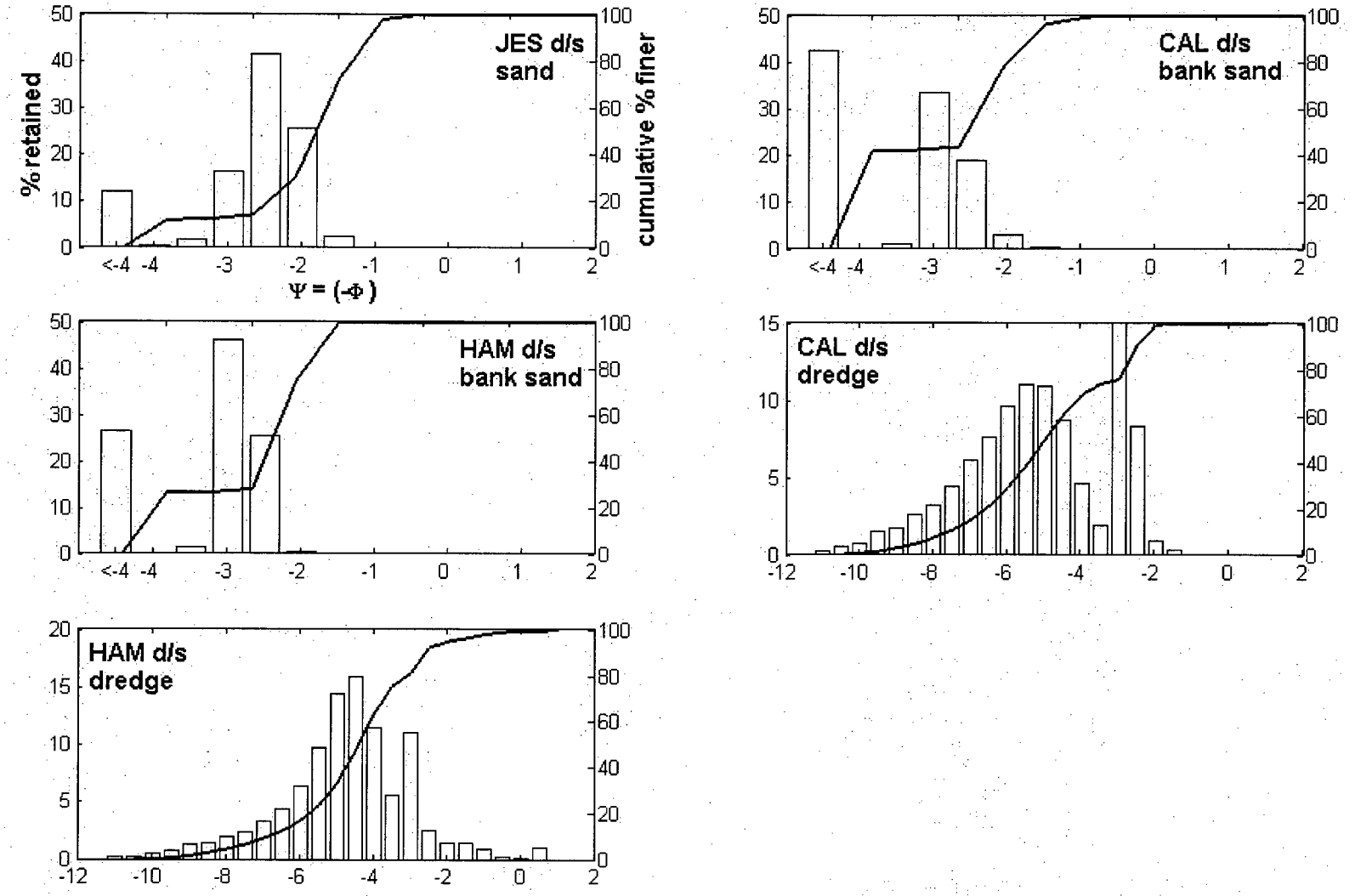

Figure B-4 Grain-size distributions for fine (i.e. sand and smaller) substrates. Note that the non-dredge sample analyses are truncated at ψ = -4 (0.0625 mm). Sedigraph analysis of dredge samples was terminated at ψ = -11 (0.5 μm).

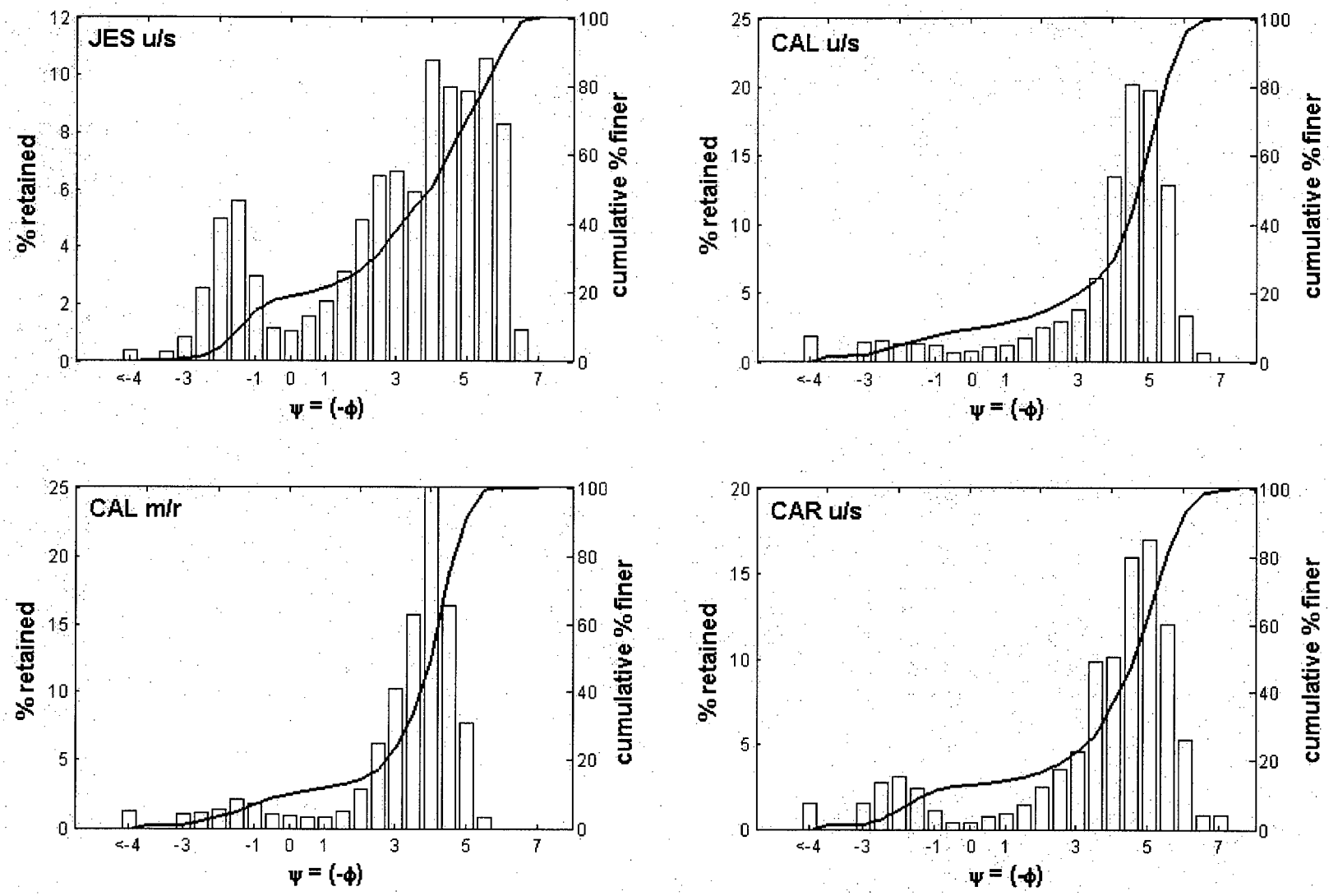

Figure B-5 Sub-surface grain size distribution for JES u/s, CAL u/s and m/r and CAR u/s. Note that the analyses have been truncated at -4Ψ (0.063 mm).

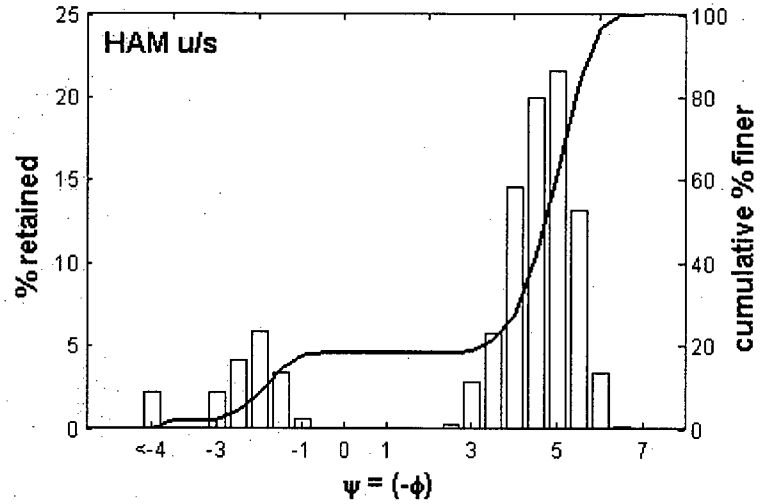

Figure B-6 Sub-surface grain size distribution for HAM u/s. Note that the analysis has been truncated at -4Ψ (0.063 mm)

Appendix C: Relation of main channel discharge to sub-reach discharge

Main-channel vs. sub-reach discharge regression results. All main channel discharge values are measured at Hope.

Table of figures: Appendix C

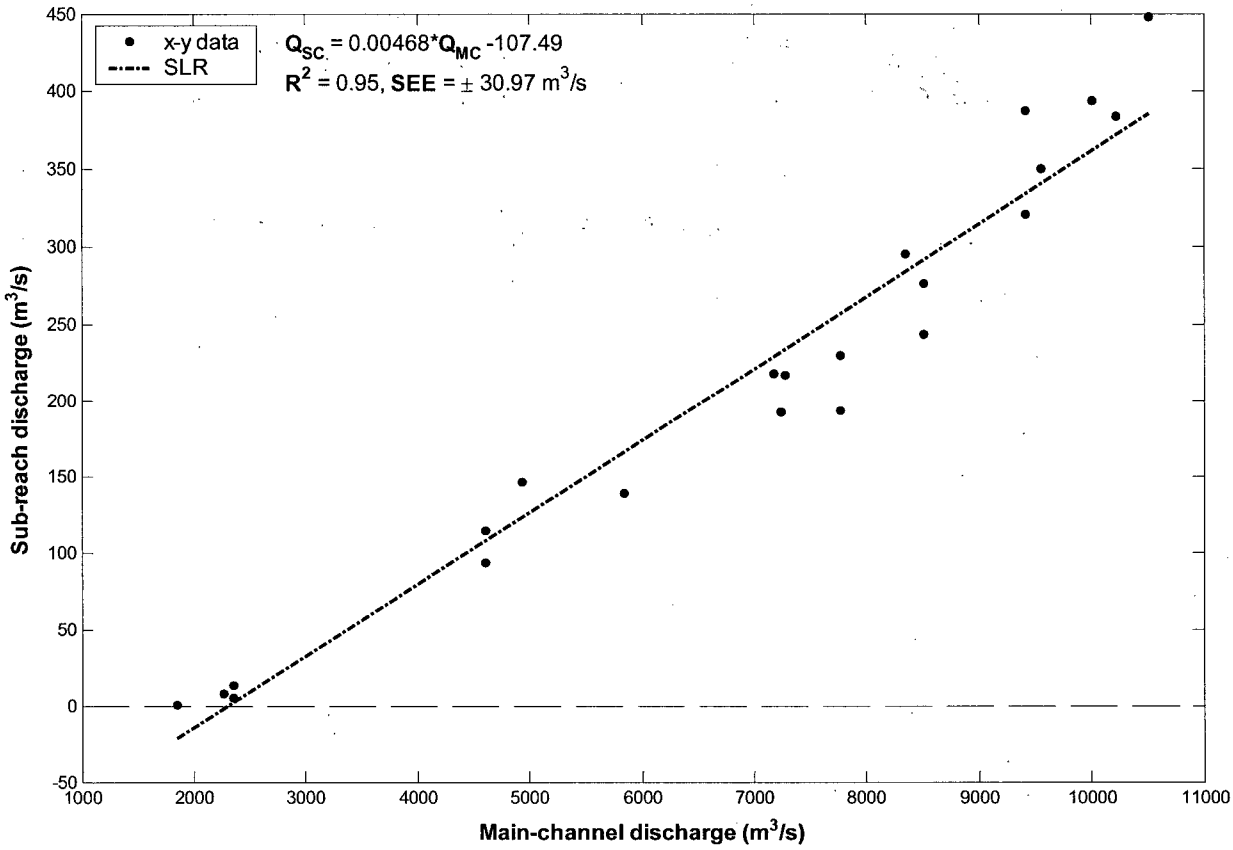

Figure C-1 Jesperson channel, all sub-reaches combined.

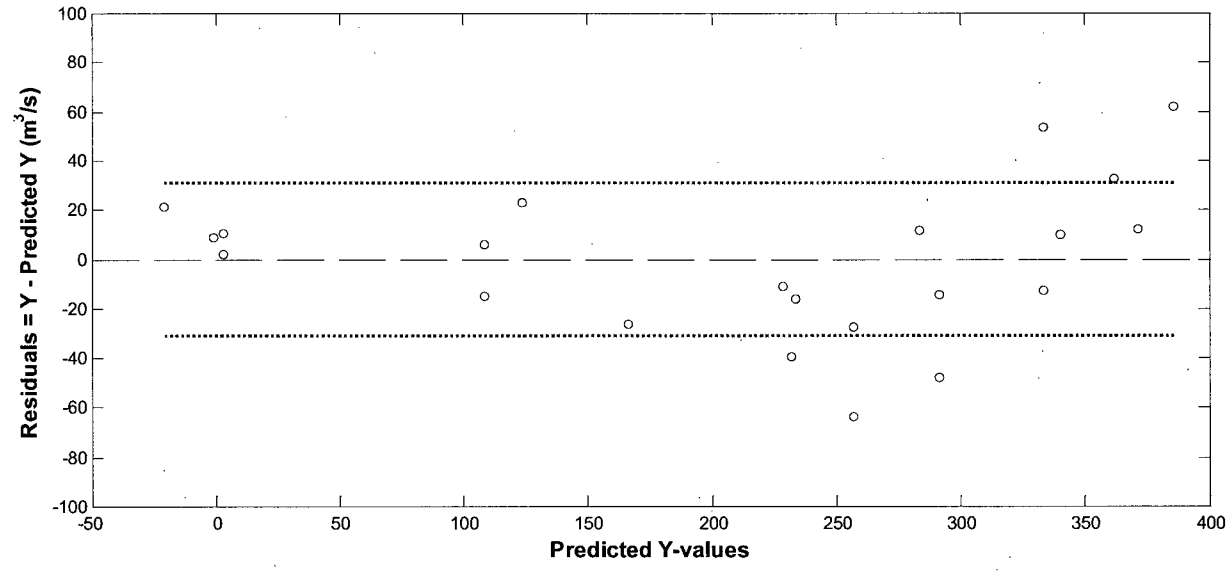

Figure C-2 Jesperson channel, all sub-reaches combined, residuals corresponding to **Figure C-1**. Dotted line indicates ± 1 SEE.

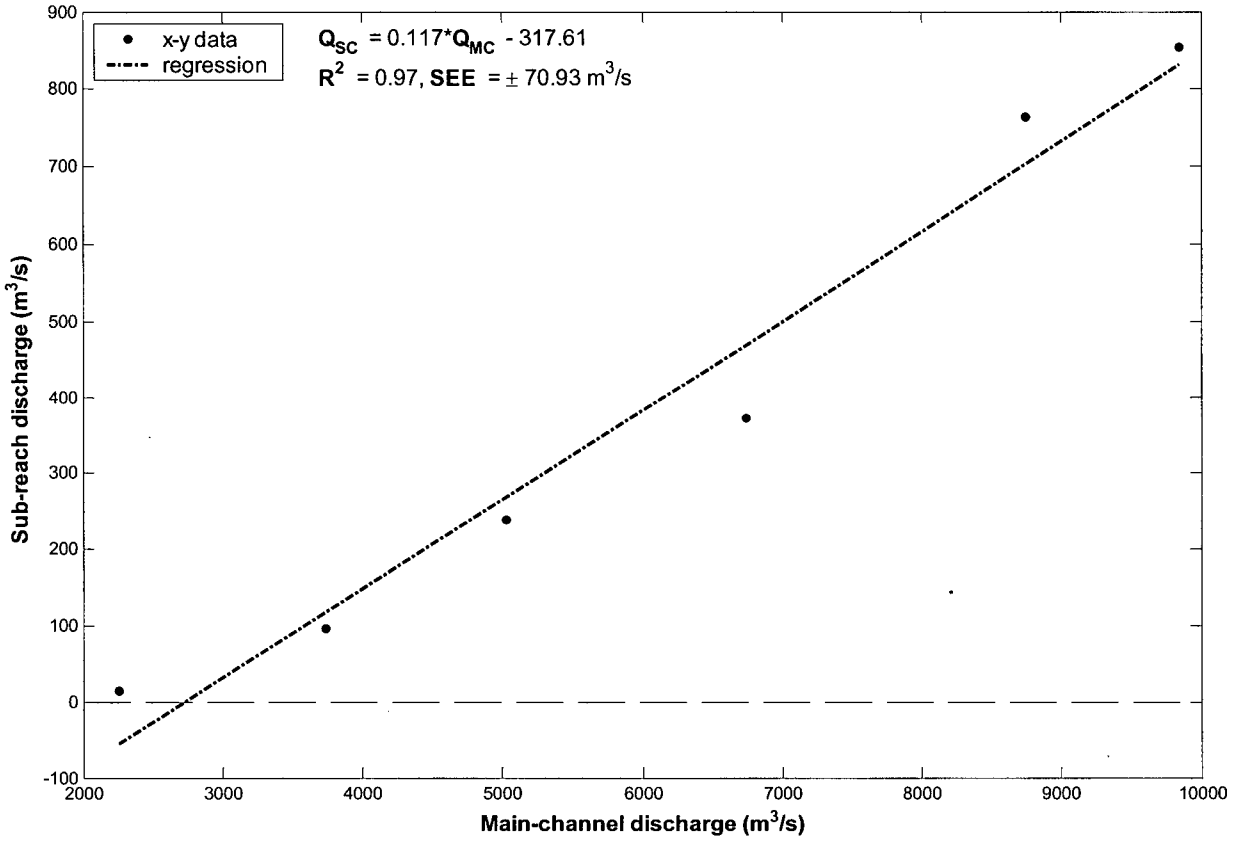

Figure C-3 Carey u/s sub-reach.

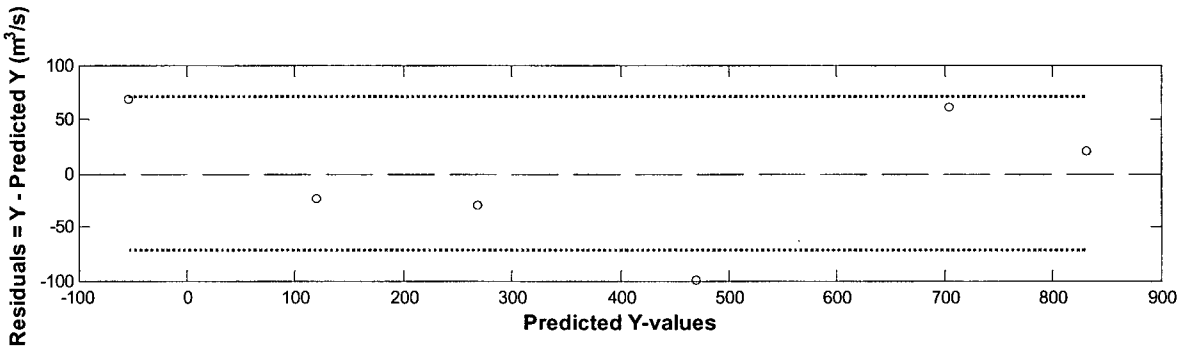

Figure C-4 Carey u/s sub-reach, residuals corresponding to **Figure C-3**. Dotted line indicates ± 1 SEE.

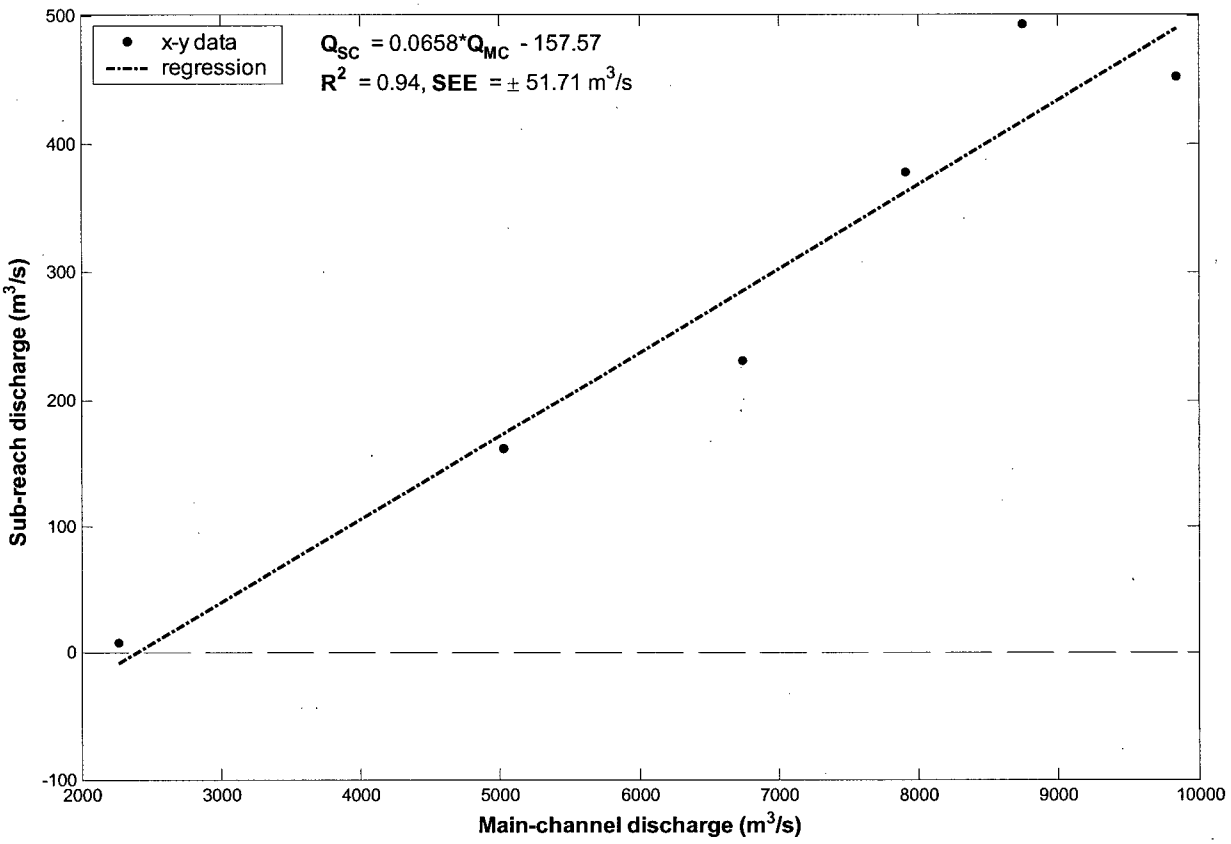

Figure C-5 Carey u/s mid sub-reach.

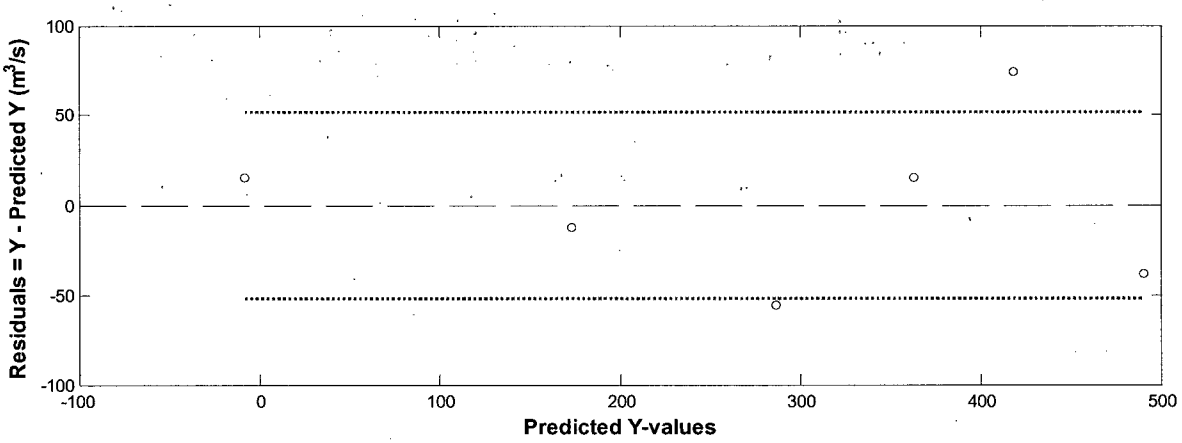

Figure C-6 Carey u/s mid sub-reach, residuals corresponding to **Figure C-5**. Dotted line indicates ± 1 SEE.

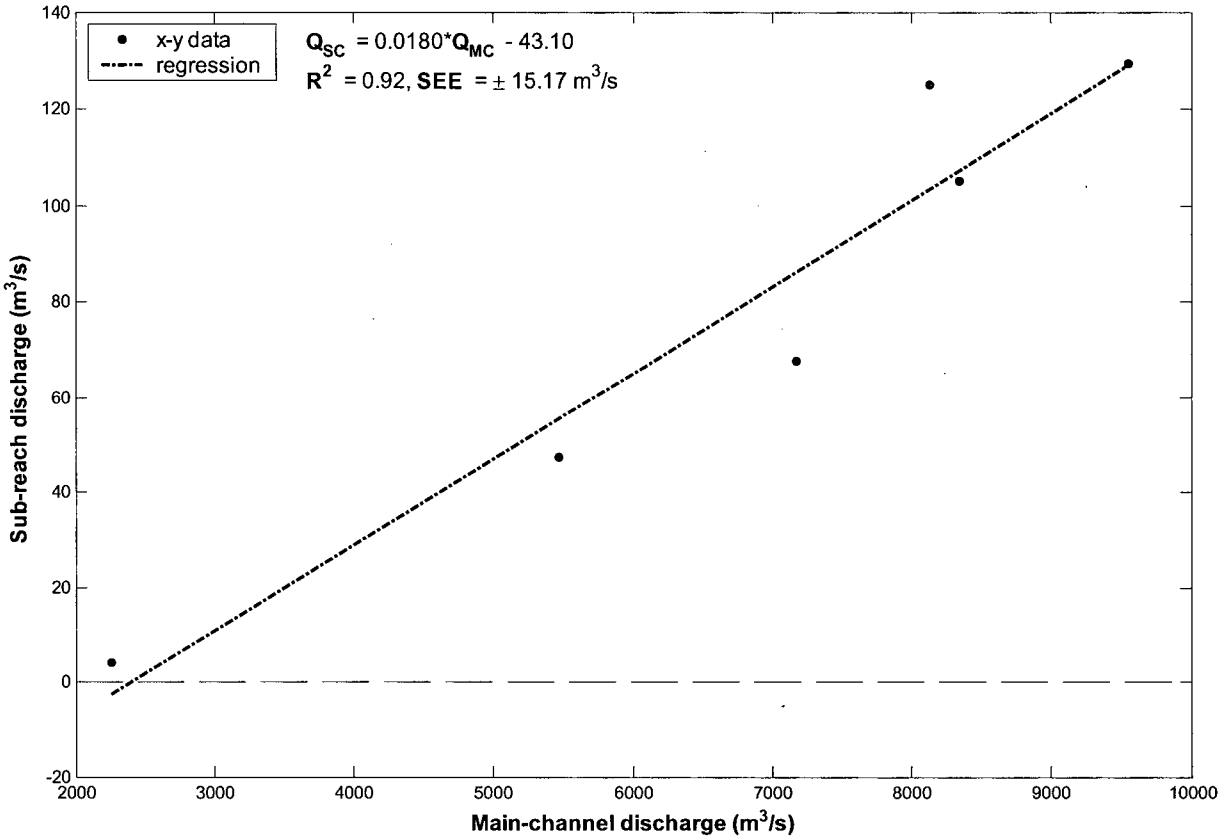

Figure C-7 Carey d/s mid sub-reach.

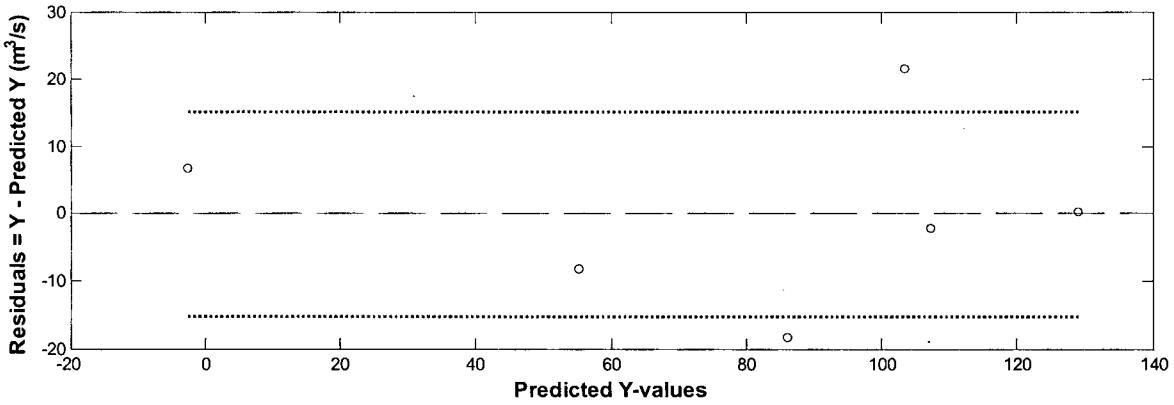

Figure C-8 Carey d/s mid sub-reach, residuals corresponding to **Figure C-7**. Dotted line indicates ± 1 SEE.

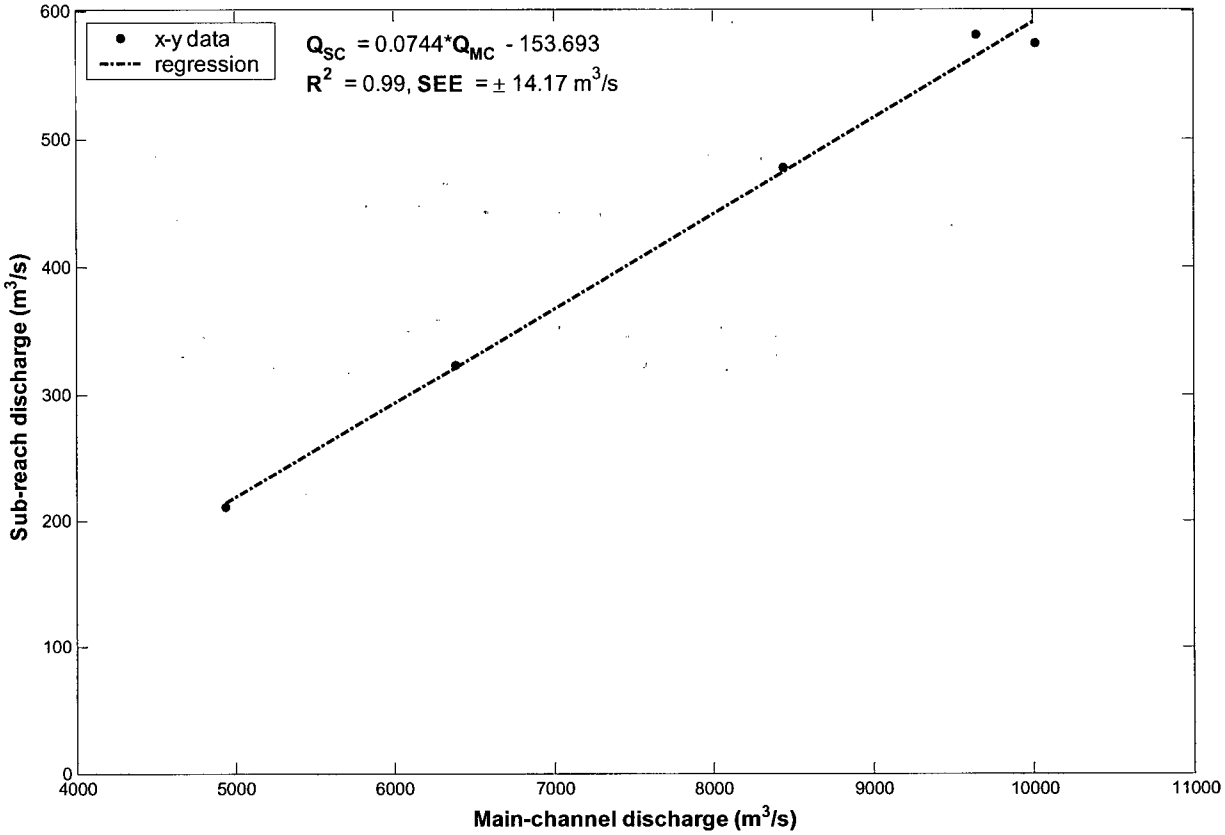

Figure C-9 Hamilton mid sub-reach.

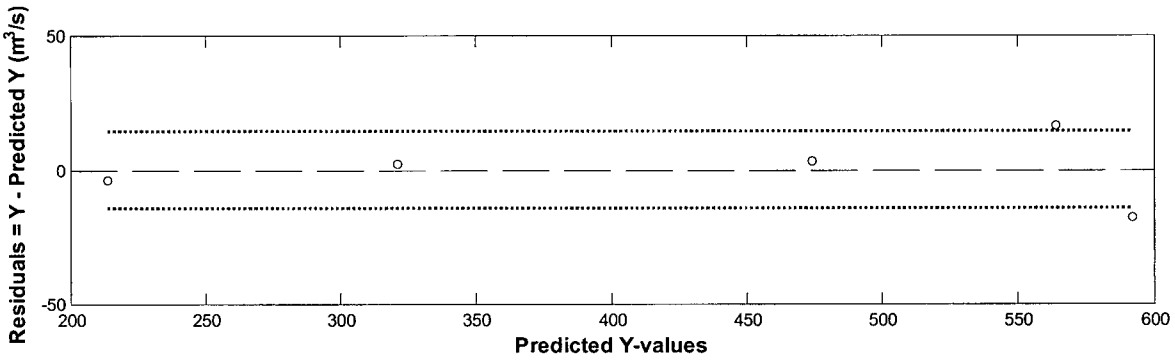

Figure C-10 Hamilton mid sub-reach, residuals corresponding to **Figure C-9**. Dotted line indicates ± 1 SEE.

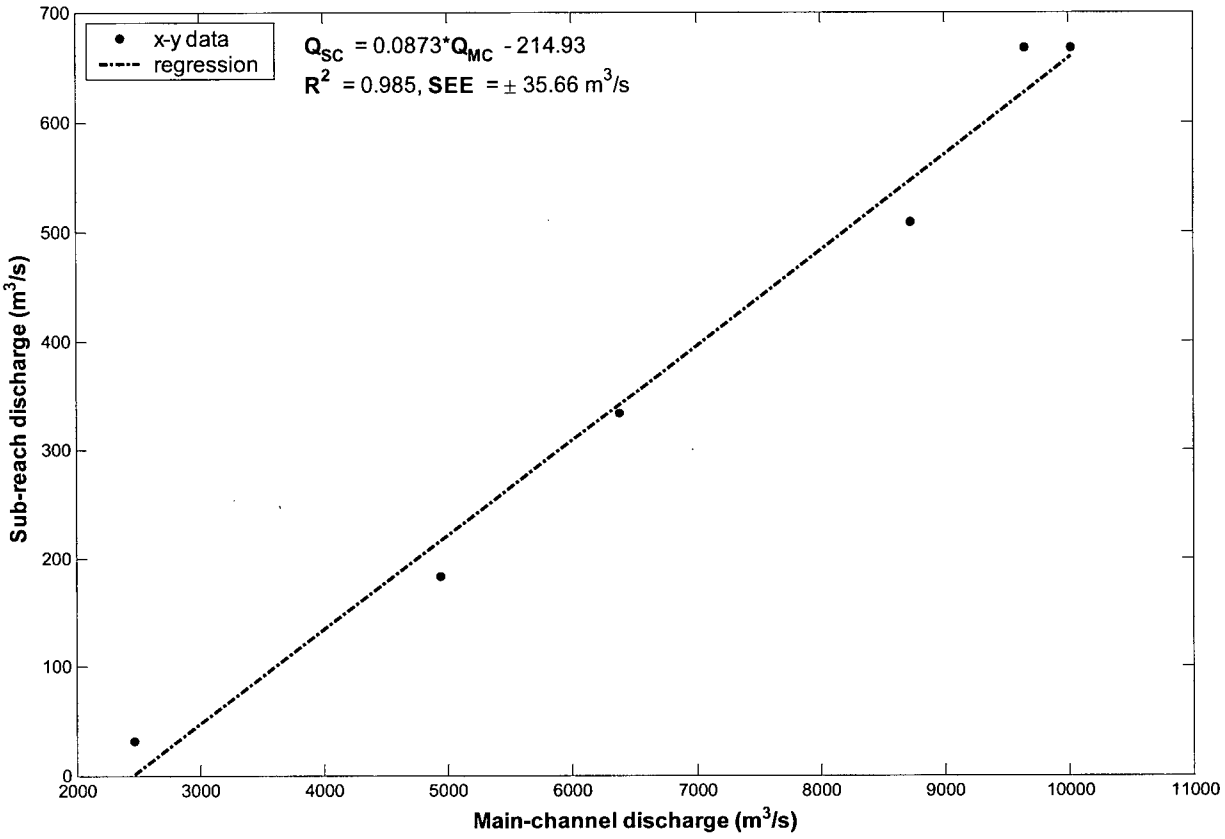

Figure C-11 Hamilton d/s sub-reach.

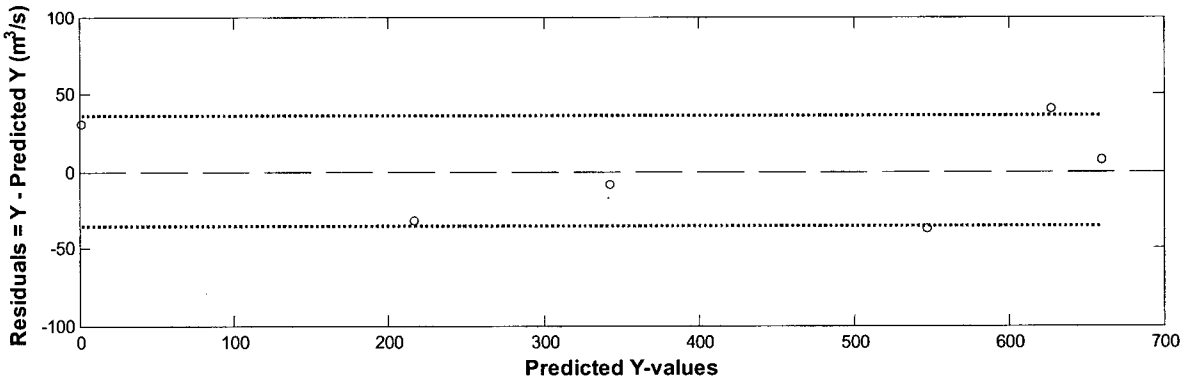

Figure C-12 Hamilton d/s sub-reach, residuals corresponding to **Figure C-11**. Dotted line indicates ± 1 SEE.

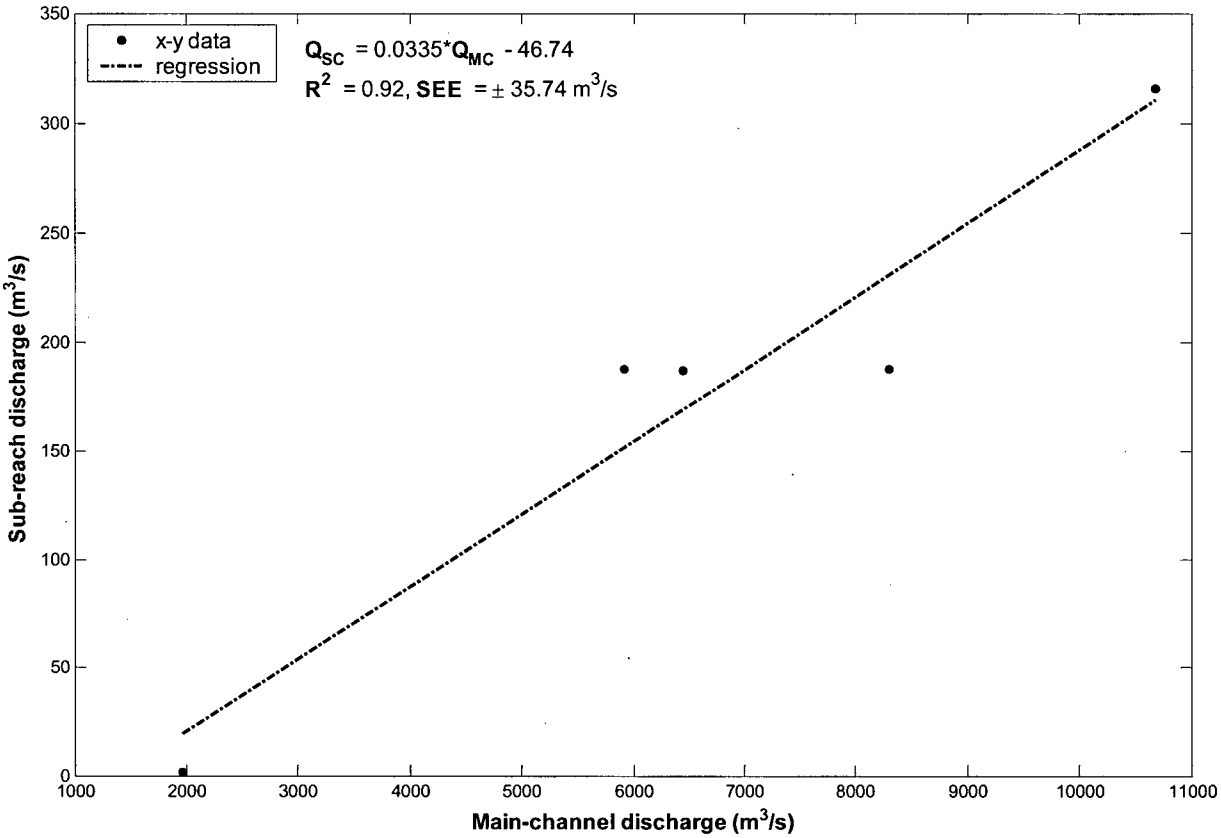

Figure C-13 Calamity u/s sub-reach.

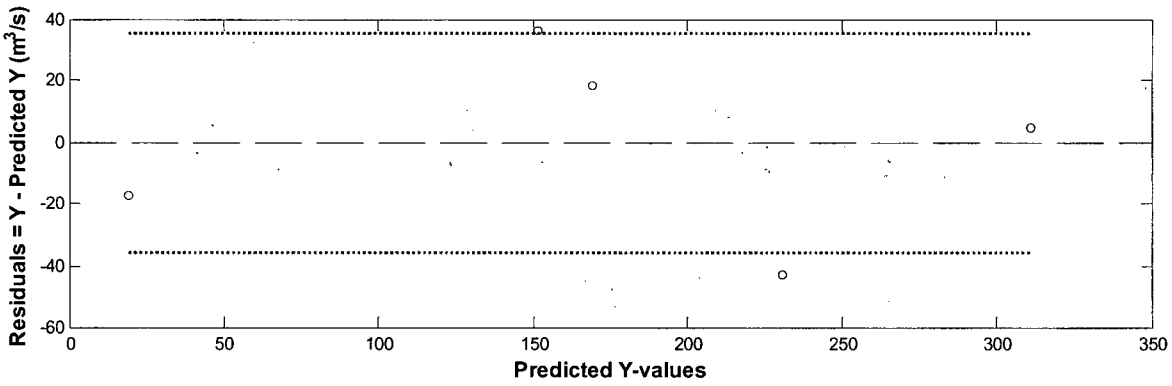

Figure C-14 Calamity u/s sub-reach, residuals corresponding to **Figure C-13**. Dotted line indicates ± 1 SEE.

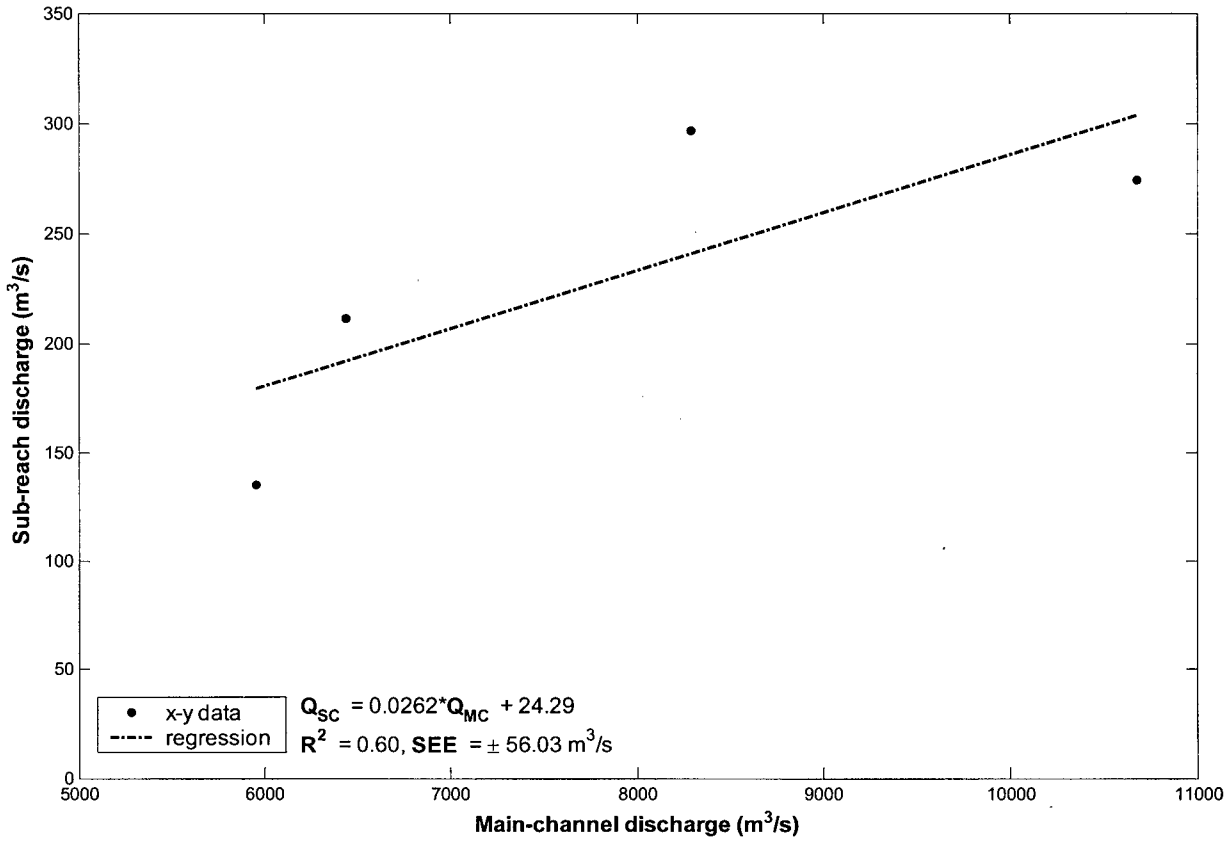

Figure C-15 Calamity mid sub-reach.

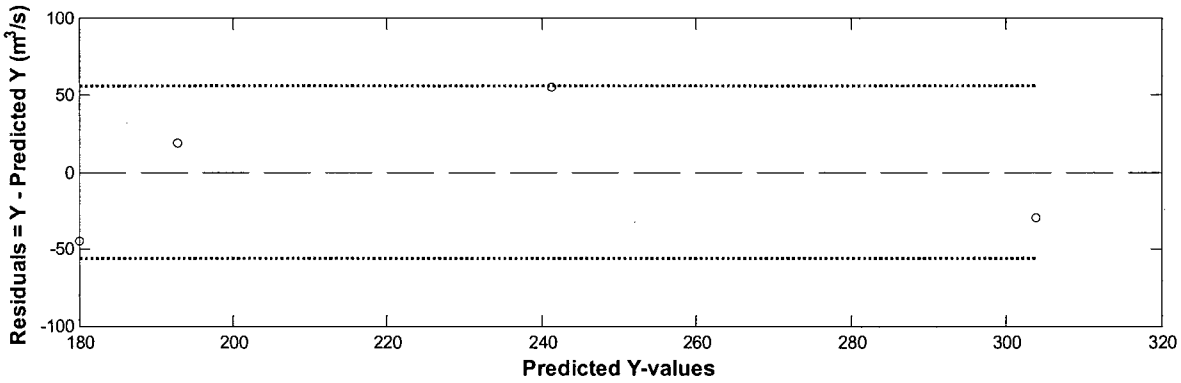

Figure C-16 Calamity mid sub-reach, residuals corresponding to **Figure C-15**. Dotted line indicates ± 1 SEE.

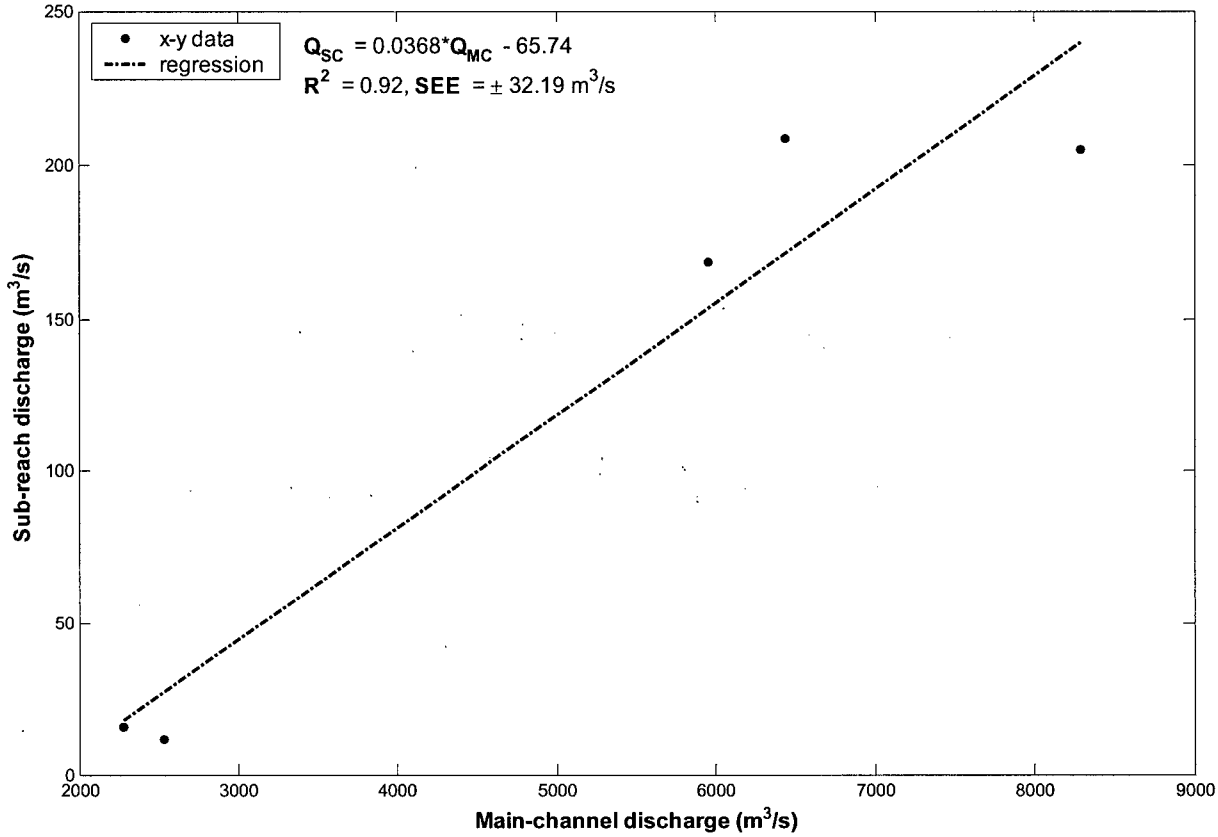

Figure C-17 Calamity d/s sub-reach.

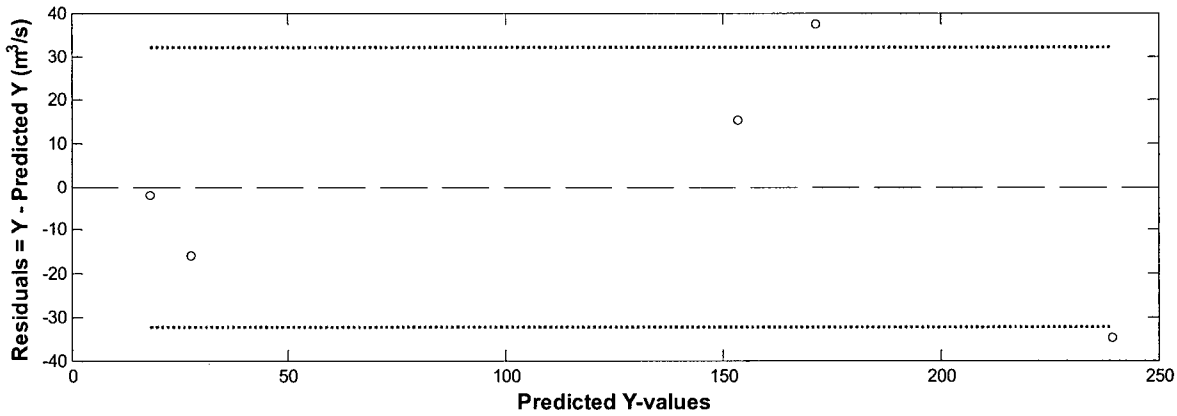

Figure C-18 Calamity d/s sub-reach, residuals corresponding to **Figure C-17**. Dotted line indicates ± 1 SEE.

Appendix D: Plots of functional scaling relations for secondary channels

Plots of functional scaling relations for secondary channels, accompanied by residual plots for the same data.

Table of figures: Appendix D

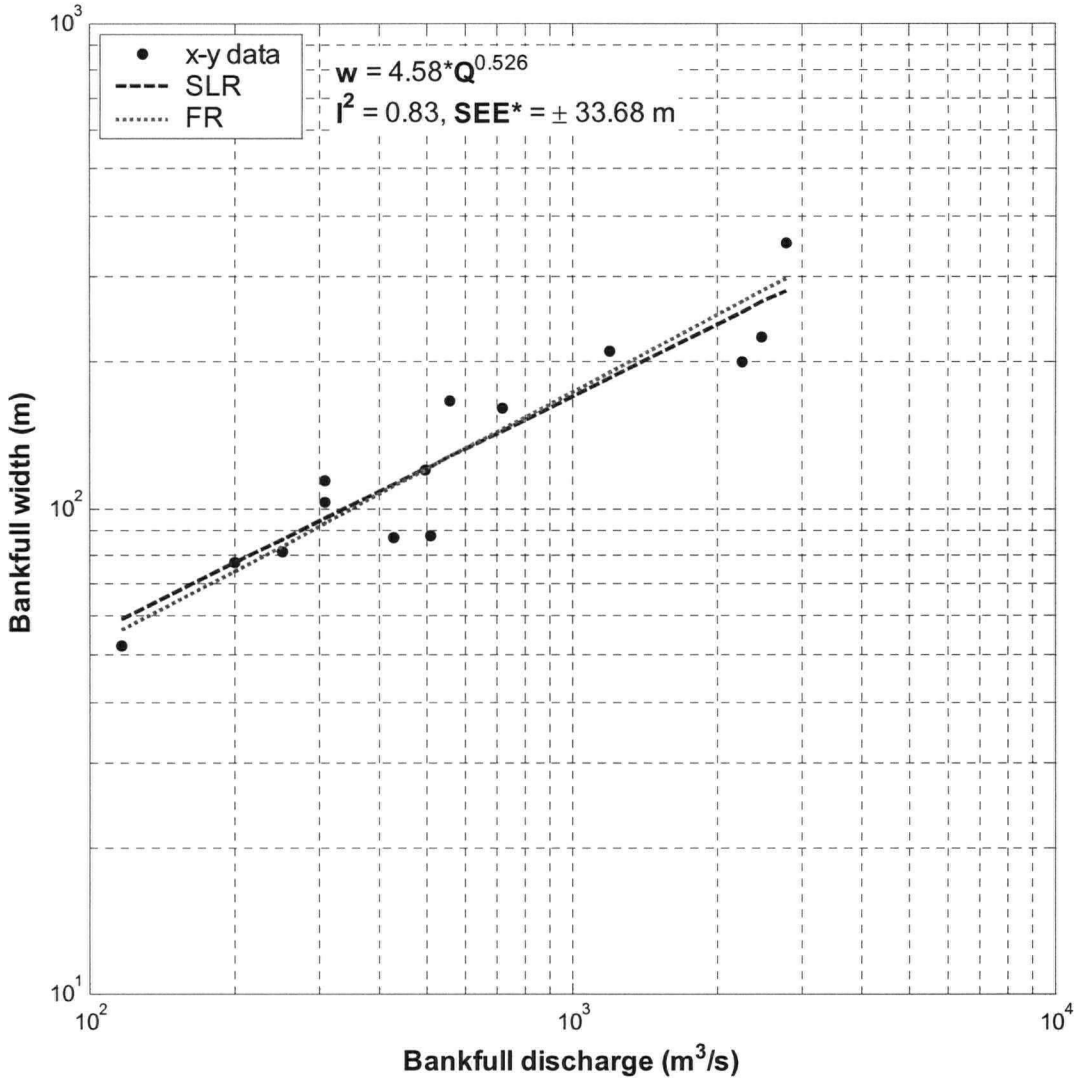

Figure D-1 Functional relation of bankfull secondary channel width to discharge, for at-a-station sub-reaches (CAL m/r excluded) and scaling relation sub-reaches.

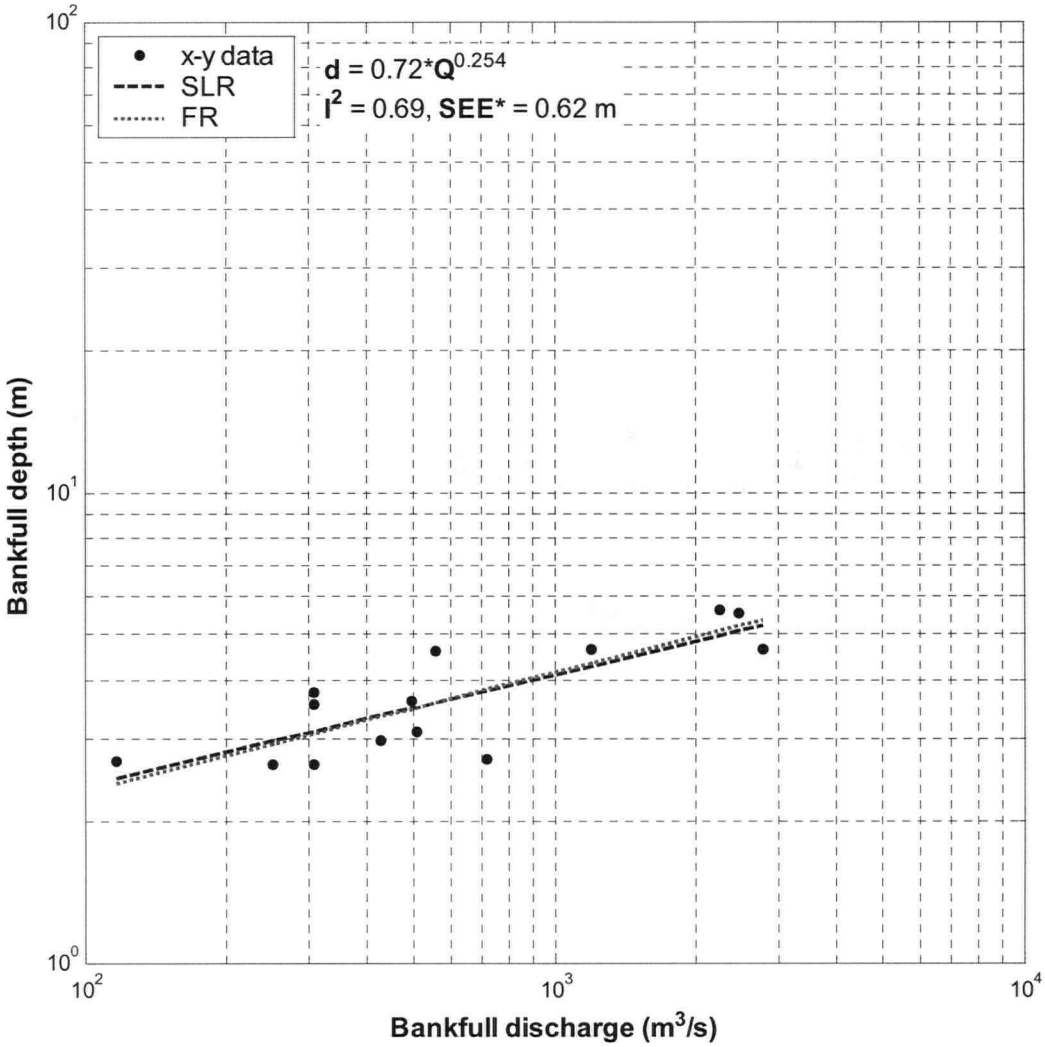

Figure D-2 Functional relation of bankfull secondary channel depth to discharge, for at-a-station sub-reaches (CAL m/r and d/s excluded) and scaling relation sub-reaches.

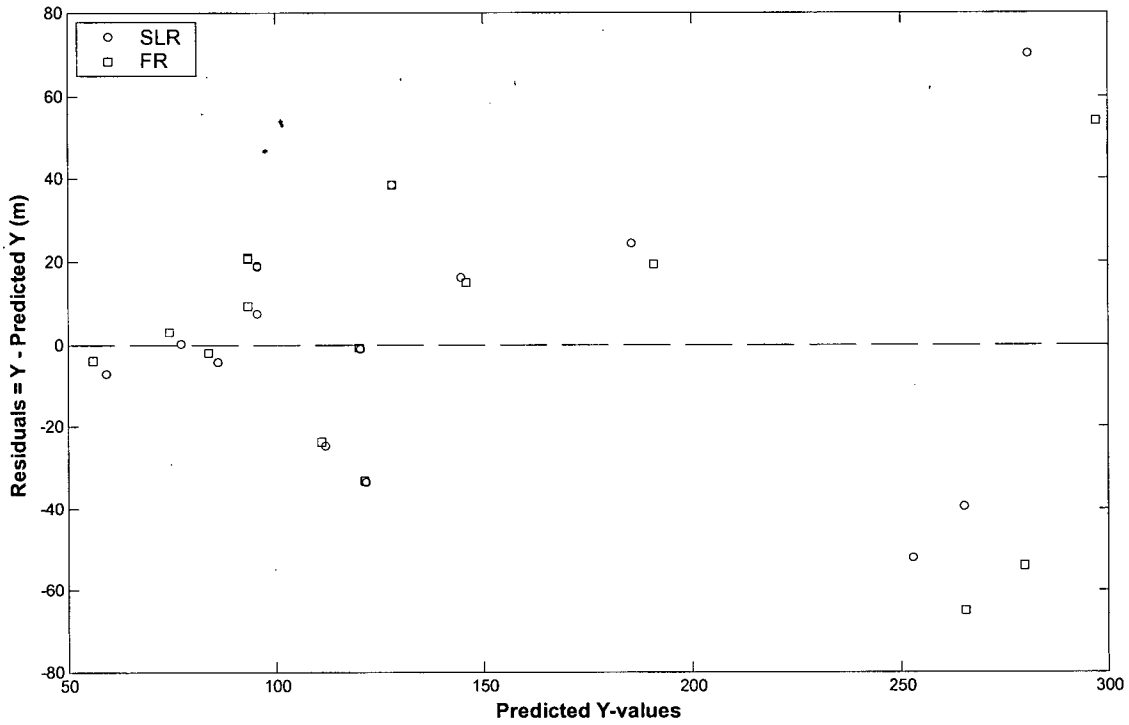

Figure D-3 Residuals for the bankfull width to discharge scaling relations (**Figure D-1**).

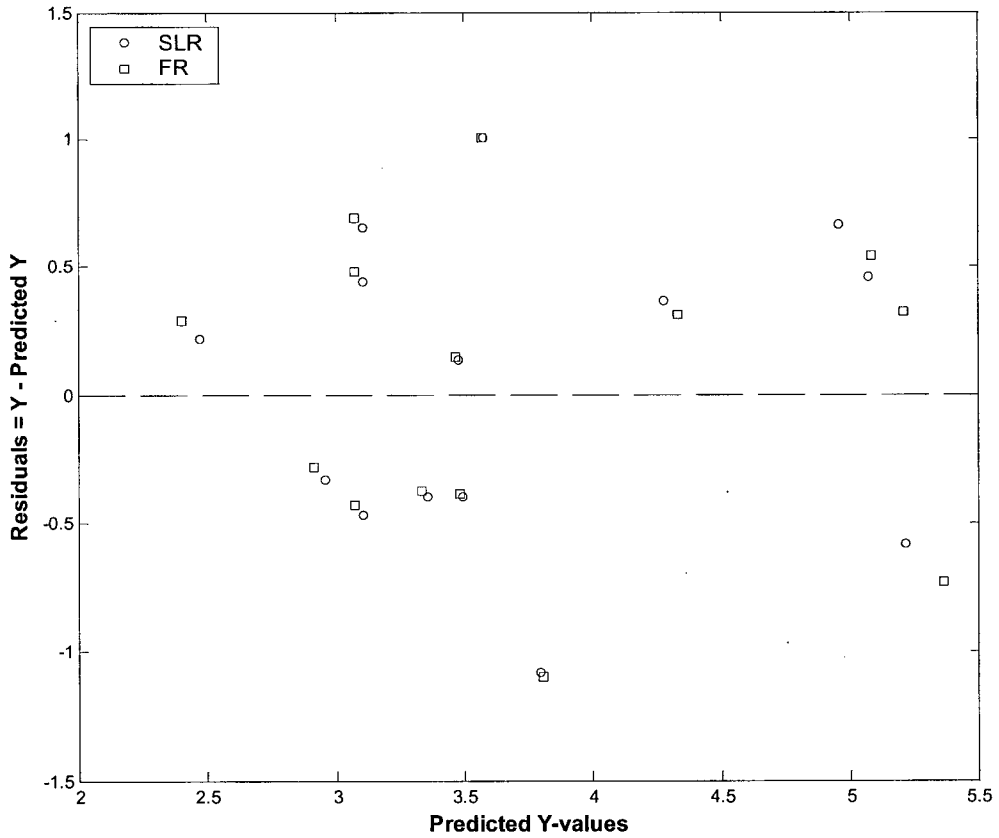

Figure D-4 Residuals for the bankfull depth to discharge scaling relations (**Figure D-2**).

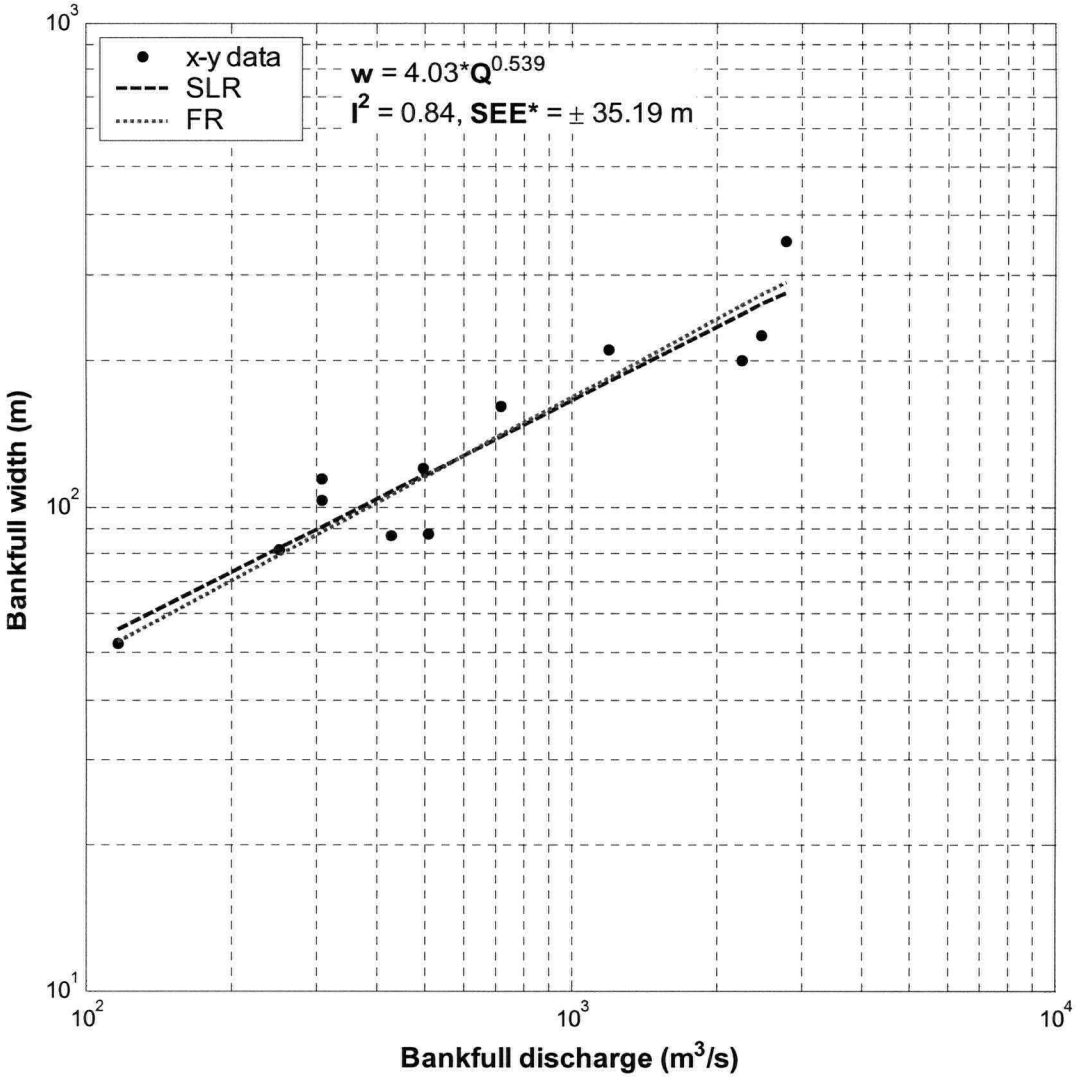

Figure D-5 Functional relation of bankfull secondary channel width to discharge, for at-a-station sub-reaches (excluding CAL m/r and all d/s sub-reaches), and scaling relation sub-reaches.

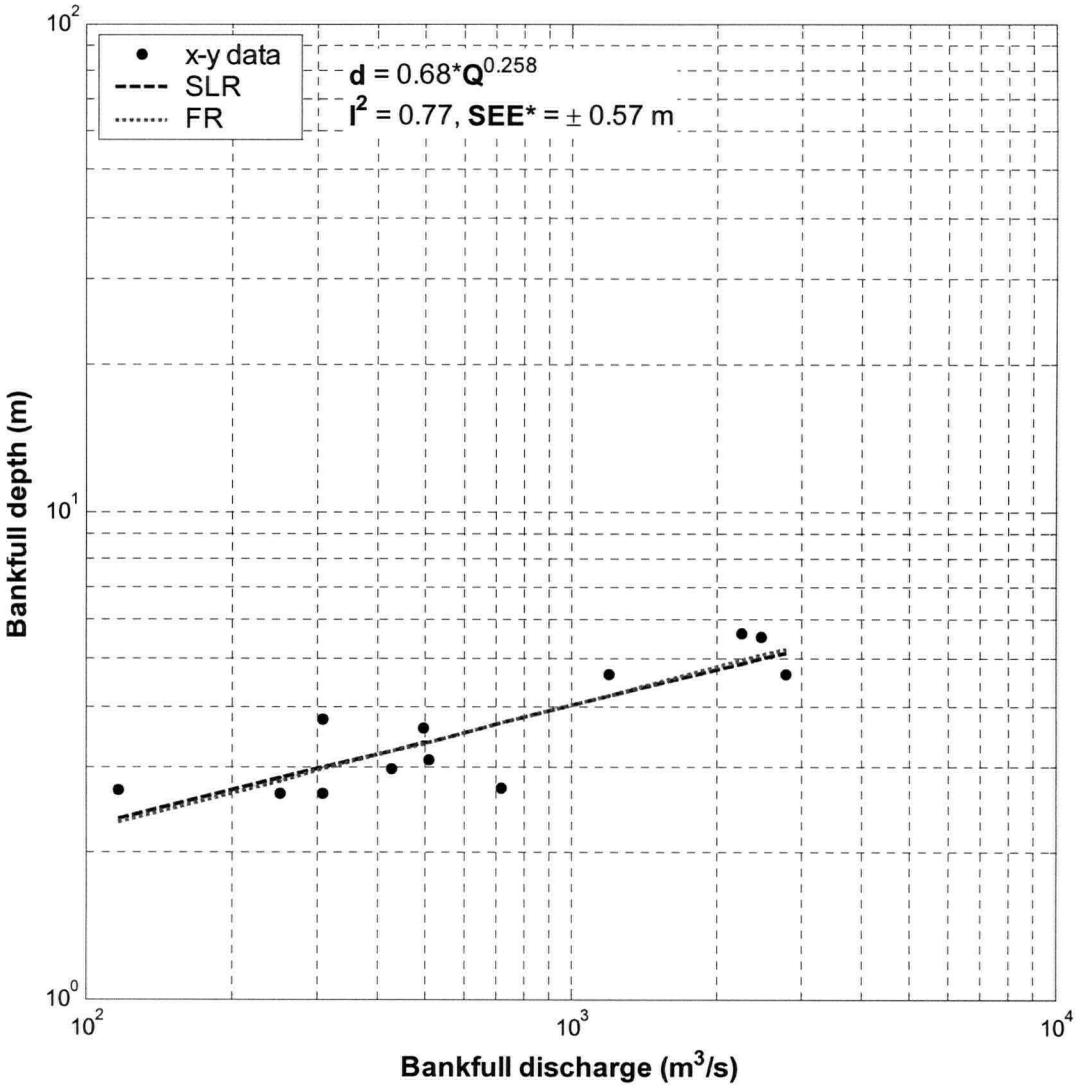

Figure D-6 Functional relation of bankfull secondary channel depth to discharge, for at-a-station sub-reaches (excluding CAL m/r and all d/s sub-reaches), and scaling relation sub-reaches.

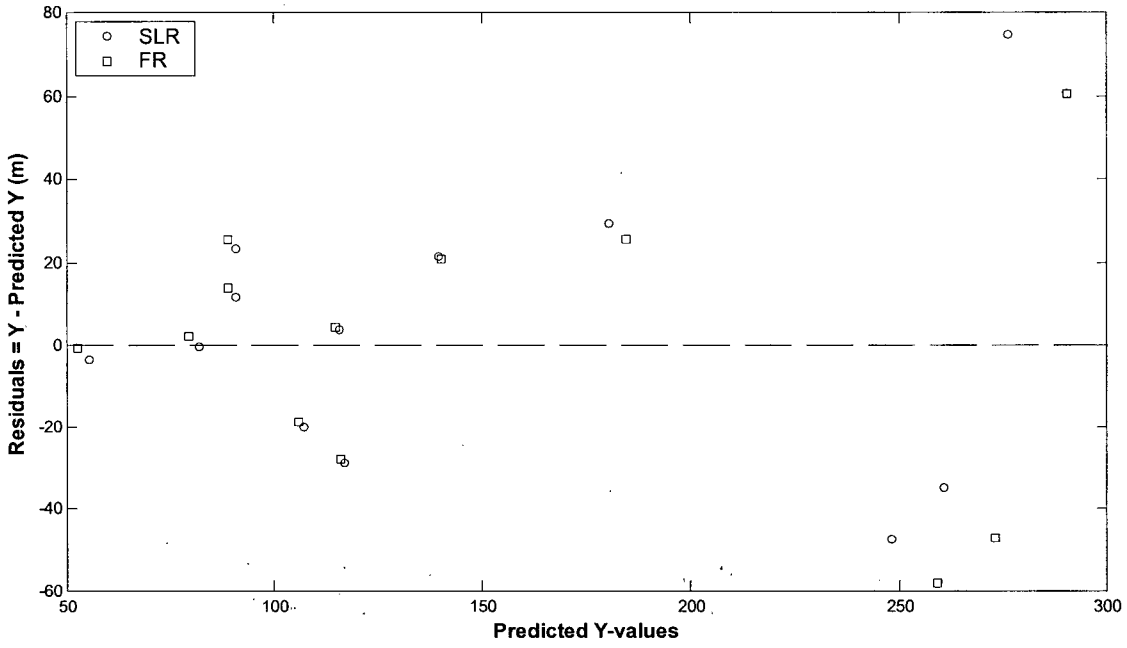

Figure D-7 Residuals for the alternate bankfull width to discharge scaling relations (**Figure D-5**).

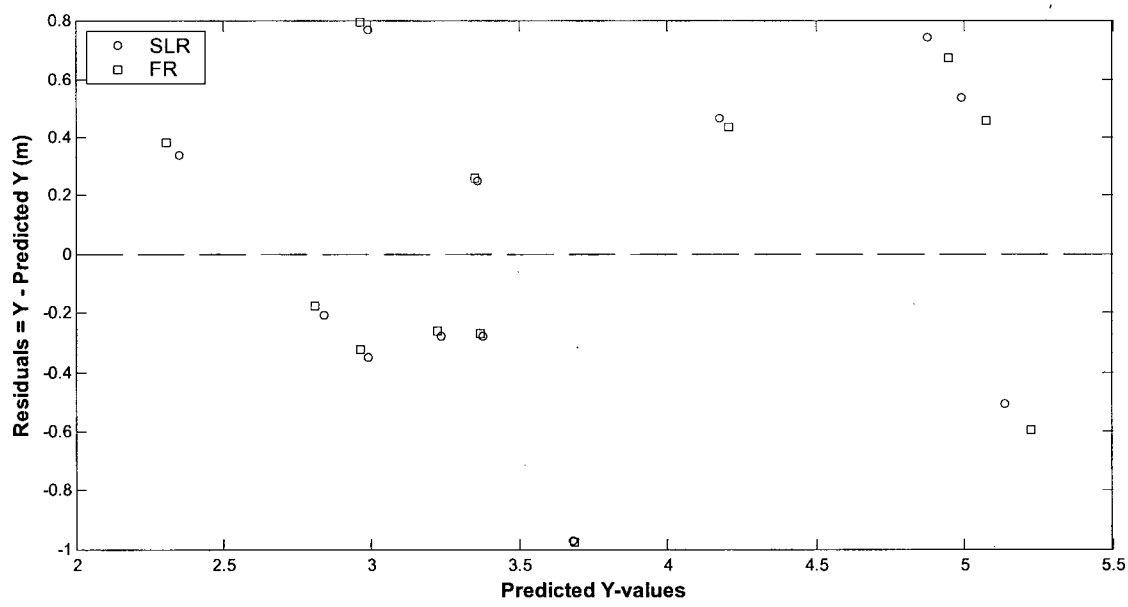

Figure D-8 Residuals for the alternate bankfull depth to discharge scaling relations (**Figure D-6**).